

From Golgi to Lipid droplet—  
Understanding of Organelle Homeostasis

**Eunjoo Lee**

Doctorate of Philosophy

Faculty of Medicine  
Department of Anatomy and Cell Biology  
McGill University  
Montreal, Quebec, Canada

This thesis is submitted to McGill University in partial fulfillment of the requirements for the degree of Doctorate of Philosophy.

October 2016

©Copyright Eunjoo Lee 2016

# From Golgi to Lipid droplet— Understanding of Organelle Homeostasis

Table of Contents .....	II
Abstract .....	VI
Resumé .....	VIII
Acknowledgement.....	X
Contribution of Authors .....	XII
Original Contributions to Knowledge .....	XIII
Ethics Statement .....	XIV
List of Abbreviations.....	XV
List of Figures .....	XVII

## Chapter 1: Literature Review

1.1. Background of Golgi research.....	2
1.1.1. How Golgi maintains its homeostasis .....	2
1.1.2. History of Golgi research around CPM and VTM .....	4
1.1.3. The anterograde trafficking.....	6
<i>COPII vesicles</i> .....	7
<i>ER-Golgi Intermediate Compartment</i> .....	8
1.1.4. The retrograde trafficking .....	9
1.1.4.a. Golgi resident enzymes.....	9
1.1.4.b. The retrograde Trafficking from Golgi to ER .....	10
1.1.4.c. COPI-mediated transport .....	11
<i>Characteristics of COPI vesicles</i> .....	13
<i>Arf and coatamer recruitment</i> .....	13
<i>Cargo recognition</i> .....	14
<i>Sorting of cargos</i> .....	15
<i>Membrane fission</i> .....	16
<i>Coat uncoating</i> .....	17
1.1.4.d. Rab6 dependent retrograde pathway .....	18
1.1.5. Extended views of the early secretory pathway .....	19
1.1.5.a. Other models.....	19
1.1.5.b. Ongoing debates in Golgi research.....	20

1.1.6. Challenges in studying ultrastructural localization of proteins in Golgi .....	22
<i>Size constraints</i> .....	22
<i>Short lifetime of carriers</i> .....	23
<i>Non-physiological probes</i> .....	23
1.1.7. <i>in vivo</i> Correlative Microscopy .....	25
1.1.7.a. GFP recognition after bleaching.....	25
1.2. Lipid Droplet .....	26
1.2.1. LD formation.....	27
<i>LD structure</i> .....	27
<i>LD proteins</i> .....	27
<i>LD formation</i> .....	28
1.2.2. LD breakdown.....	30
1.2.2.a. Lipid breakdown by lipolytic pathway.....	30
1.2.2.b. Lipid breakdown by lipophagy.....	31
1.2.2.c. Lipophagy through Kiss-and-Run .....	32
1.2.2.d. Omega-3 fatty acid Eicosapentaenoic acid (EPA) .....	33
1.2.3. Non-Alcoholic Fatty Liver Disease.....	33
1.2.4. Endophilin family of proteins.....	34
1.2.4.a. Domains and structures .....	35
1.2.4.b. Mitochondrial morphology.....	37
1.2.4.c. Clathrin-mediated endocytosis .....	38
1.2.4.d. Clathrin-independent, Fast Endophilin-Mediated Endocytosis (FEME) .....	40
1.2.5 Autophagy .....	41
1.2.5.a. Role of endophilin B1 in macroautophagy.....	42
<i>Endophilin B1 in lipid metabolism</i> .....	43
1.2.5.b. Microautophagy.....	44
1.2.5.c. Chaperone-mediated autophagy .....	45
1.3. Rationale of the study .....	45
1.3.1. New generation of probes to study Golgi.....	45
1.3.2. Functional elucidation of endophilin B1 as a novel lipid droplet protein .....	46

## **Chapter 2: Materials and methods**

2.1. Reagents and antibodies .....	48
<i>Reagents</i> .....	48
<i>Antibodies</i> .....	49
<i>Preparation of Eicosapentaenoic Acid</i> .....	50
2.2. Cell culture, transfection, and generation of inducible cells .....	50
<i>Cell culture</i> .....	50
<i>Transfection</i> .....	51

<i>Induction of LD formation</i> .....	51
<i>Generation of stable and inducible cells</i> .....	51
Table 2-1: Primer sequences for siRNA .....	52
2.3. Fusion Antibody Construction .....	52
2.4. Knockdown by siRNA .....	53
2.5. Tandem affinity purification of fusion antibody .....	53
2.6. Indirect immunofluorescence and confocal microscopy .....	54
<i>Confocal microscopy</i> .....	55
<i>Fluorescent microscopy</i> .....	55
2.7. Mass spectrometry, generation of heat map and staging .....	55
2.8. Bio-ID .....	56
2.9. Determination of LD size and number .....	58
2.10. Relative triacylglycerol levels by Thin Layer Chromatography .....	58
2.11. Determination of Kiss-and-Run .....	58
2.12. Western Blot .....	59

### **Chapter 3: New generation of probes to study retention and recycling of Golgi resident enzymes**

3.1. Construction of fusion antibody and expression in different cell types .....	62
3.2. Fusion antibody is made specifically for its respective glycosyltransferase .....	67
3.3. Fusion antibody does not affect cell viability or cause ER stress .....	74
3.4. Fusion antibody can be used to highlight antigens of non-transfected cells .....	77
3.5. Fusion antibody can be used as a tool to monitor protein cycling from the cell membrane .....	87
3.6. GalT cycles through plasma membrane before lysosomal degradation .....	90

### **Chapter 4: Endophilin B1: a novel lipid droplet protein essential for EPA mediated lipophagy**

4.1. Endophilin B1 is located on lipid droplet surface of human fatty liver tissue .....	97
4.2. Endophilin B1 is involved in lipid breakdown .....	104
4.3. Endophilin B1 is involved in EPA mediated lipophagy .....	122
4.4. Endophilin B1 acts on a pathway different from macroautophagy and lipolysis .....	127
4.5. Lipophagy by endophilin B1 involves LD-Lysosome relationship .....	134
4.6. Endophilin B1 binds with proteins involved in Kiss-and-Run lipophagy .....	142

### **Chapter 5: Discussions**

5.1. Development of tools to understand how Golgi maintains its homeostasis .....	156
5.1.1. Full characterization and advantages of fusion antibody .....	156
5.1.2. Potential to use fusion antibody to highlight another cells' antigen .....	158
5.1.3. Fusion antibody as a tool to study protein internalization .....	159
5.1.4. Visualization of glycosyltransferase with fusion antibody .....	163

5.1.5. Fusion antibody as a biosynthetic cargo and a Golgi-resident .....	164
5.2. Functional elucidation of endophilin B1 in specialized LD breakdown .....	169
5.2.1 Endophilin B1 participates in lipid droplet breakdown.....	169
5.2.2. Endophilin B1 is essential for EPA mediated lipophagy .....	171
5.2.3. Endophilin B1 mediated lipophagy is distinct from macroautophagy or lipolysis .....	173
Mechanism of cellular TAG degradation by endophilin B1 .....	175
Mechanism of EPA in lipophagy .....	178
5.2.4. Role of endophilin B1 in Kiss-and-Run lipophagy .....	180
Potential interactors of endophilin B1 .....	185
<b>Chapter 6. General conclusions</b> .....	<b>190</b>
<b>Chapter 7. References</b> .....	<b>193</b>

## Abstract

Organelles within eukaryotic cells are membrane-bound compartments that ensure the localized control of specific cellular activities. Organelles are essential to the organization and function of eukaryotic cells; therefore, it is important to understand organelle homeostasis—how organelles are formed and maintained in steady-state conditions. Organelles are unique in that they differ in their cellular function and homeostasis.

The Golgi apparatus is a self-organizing organelle that maintains its structural integrity in the face of an enormous flux of lipid and proteins. A large number of proteins and processes have been identified in order to maintain the Golgi's highly dynamic structural equilibrium. However, the mechanisms by which biosynthetic proteins and Golgi-resident enzymes traverse the Golgi have been debated for many decades. To elucidate how proteins and enzymes are transported through the Golgi, we have designed and fully characterized a novel antibody-based probe able to highlight endogenous Golgi enzymes *in vivo*. 'Fusion antibodies' constructed this way are significantly smaller than conventional antibodies, and they can be engineered to highlight cellular events. Furthermore, affinity purified fusion antibodies retain their characteristics of antigen recognition. Together with fusion antibodies and correlative microscopy, dynamic trafficking of endogenous Golgi-resident enzymes can be monitored. Results from this study will contribute to finding mechanisms of retention and recycling of Golgi-resident enzymes in the early secretory pathway.

The lipid droplet (LD) is known for its function in excessive lipid storage. However, the LD is a highly dynamic and regulated organelle with many more functions such as cholesterol regulation and prevention of lipotoxicity. Formation and breakdown of lipid droplets are crucial for the cell and body as a whole because the abnormal accumulation of lipids may contribute to

the development of metabolic diseases such as Non-Alcoholic Fatty Liver Disease (NAFLD). For this reason, it is crucial to understand how lipids are broken down and released from lipid droplets. In this thesis, we uncovered a novel lipid droplet protein, endophilin B1, which contributes to lipid droplet breakdown via non-canonical lipophagy. The results presented may further provide a novel therapeutic approach for the treatment of NAFLD.

## Resumé

Les organelles dans les cellules eucaryotes sont des compartiments membranaires qui assurent le contrôle localisé des activités cellulaires spécifiques. Les organelles sont essentielles pour l'organisation et la fonction des cellules eucaryotes. Il est donc important de comprendre l'homéostasie des organelles : comment sont-elles créées et entretenues dans des conditions stables. Chaque organelle diffère dans sa fonction cellulaire et son homéostasie.

L'appareil de Golgi est une organelle d'auto-organisation qui conserve son intégrité face à l'énorme afflux de lipides et de protéines. Grand nombre de protéines et de processus ont été cernés afin de maintenir les structures hautement dynamiques et l'équilibre de l'appareil de Golgi. Toutefois, le mécanisme par lequel les protéines biosynthétiques et les enzymes qui résident dans l'appareil de Golgi et qui le traversent est débattu depuis de nombreuses décennies. Afin d'élucider la manière dont les protéines et enzymes sont transportées à travers l'appareil de Golgi, nous avons conçu et entièrement caractérisé une nouvelle sonde fondée sur les anticorps qui peut mettre en lumière des enzymes de Golgi endogène in vivo. 'les anticorps de fusion' construits de cette façon sont considérablement plus petites que les anticorps conventionnels, et ils peuvent être conçus pour mettre en évidence les événements cellulaires. En outre, l'anticorps de fusion purifié par l'affinité conserve sa spécificité d'antigène. Avec les anticorps de fusion et la microscopie corrélative, les traits dynamiques des enzymes résidentes dans le Golgi endogènes peuvent être surveillées, et les résultats de cette étude contribueront à trouver des mécanismes de la rétention et du recyclage des enzymes qui résident dans la voie sécrétoire précoce de l'appareils de Golgi.

La Gouttelette lipidique est connue pour sa fonction de stockage des lipides excessifs. Toutefois, La Gouttelette lipidique est un milieu extrêmement dynamique et réglementé ayant beaucoup plus de fonctions comme la réglementation de cholestérol et la prévention de la lipotoxicité. La formation et la ventilation des gouttelettes lipidiques sont cruciales pour la cellule et le corps tout entier puisque l'accumulation anormale de lipides peuvent contribuer au développement des maladies métaboliques (la stéatose hépatique non alcoolique (SHNA)). Ainsi, il est extrêmement important de comprendre de quelle façon les lipides sont ventilées et libérées des gouttelettes lipidiques. Dans cette thèse, nous avons découvert une nouvelle protéine de gouttelettes de lipides endophilin B1, qui contribue à l'éclatement de gouttelettes de lipides via la lipophagie non-canonique. Les résultats présentés dans cette thèse fourniront également une nouvelle approche thérapeutique pour la stéatose hépatique non alcoolique.

## Acknowledgement

First and foremost, I would like to thank my supervisor Dr. Tommy Nilsson for accepting me as a graduate student and for supporting me in many ways so I could complete six fulfilling years in research. His guidance and constructive criticism, all of which have been invaluable in helping me succeed in this endeavor.

Next, I would like to thank Dr. Robert Scott Kiss for teaching me dedication for research, and perseverance to pull through. I would also like to give my sincere gratitude for his advice on revising this thesis.

I would like to acknowledge my advisory committee members, Dr. Chantal Autexier and Dr. John Presley for their endless advice and care. I would also like to thank members of Department of Anatomy and Cell Biology for their support.

I wish to thank Transplant Quebec, donors and their families and patients consenting to liver resection. I would like to thank Dr. Fariba Kalantari and Ali Fazel for preparing subcellular fractionations from human tissue samples. I would like to thank Dr. Sarita Negi and Dr. Husam Alamri for cryosections of human liver samples.

I would like to thank Dr. Fariba Kalantari for her constant inspiration and true friendship. She taught me not only skills for carrying out perfect experiments but also all the organizational skills that kept me on track during the graduate studies and for life. I would not have survived the graduate studies without her. I would also like to thank Shi Bo Feng for putting heads together for troubleshooting, interpreting odd results, and all other science discussions. I would also like to thank her for all the late nights and weekends (and all the snacks in the secret drawer). I would

like to acknowledge all other past and present lab members for invaluable friendship and help in revising this thesis.

I would like to thank my best friend Cyntia Bratan for her wittiness and endless support that I am fortunate for. She has been my safeguard in times of crisis.

Most of all, I would like to thank my loving parents and brother for all their supports, valuable advice and guiding me to pursue what my heart desires. Their love and dedication helped me shape who I am today.

Lastly, I would like to thank my dear husband Dr. Seun Jeon for keeping me sane and teaching me all skills that help me survive this journey. I am truly thankful to have him as a life companion and a soul mate.

## **Contribution of Authors**

Fusion antibody experiments were designed under the supervision of Dr. Tommy Nilsson, and endophilin B1 project was designed with advice from Dr. Tommy Nilsson and Dr. Robert Scott Kiss.

For Chapter 3, Novoprotein performed constructing fusion antibodies, sequencing of the mouse hybridoma cell line, and sub-cloning variable fragments into pCDNA 3.1.

Dr. Jarred Chicoine carried out the initial construction of T-REx Hek293 cells for fusion antibody study. Myself performed cloning and construction of all T-REx HeLa and Hek293 cells for endophilin B1 study.

For identification of LD proteins located in the human fatty liver, following researchers have been involved: Dr. Peter Metrakos coordinated resection of the human fatty liver; Dr. Fariba Kalantari and Ali Fazel carried out subcellular fractionation; Dr. Sarita Negi and Dr. Hussam Alamri cryo-sectioned human fatty liver.

Maryse Kochoedo performed thin layer chromatography.

For Bio-ID experiments, I subcloned T-Rex HeLa BirA cells and performed biotinylation before homogenization. Capturing biotinylated proteins, and in-gel trypsin digestions for mass spec analysis were also done by myself. Dr. Nilsson performed LC-MS/MS, and Dr. Alexander Mazur performed subsequent bioinformatics analysis.

Finally, I acquired all images and carried out all other experiments.

## **Original Contribution to Knowledge**

Work in Chapter 3 represents a novel probe construction that can be used internally within a cell. Construction and full characterization described in this chapter open up another avenue for *in vivo* probe design. Similarly, results from *in vivo* correlative microscopy with fusion antibody will help understand the early secretory pathway.

Work in Chapter 4 presents a novel lipid droplet protein for an understanding of non-canonical lipophagy. It provides the first evidence of endophilin B1 for its involvement in non-canonical lipophagy. Additionally, these findings provide additional support for non-canonical lipophagy while implicating that endophilin B1 may be a key component in finding therapeutic approaches for Non-Alcoholic Fatty Liver Disease.

## **Ethics Statement**

All handling and use of human patient and donor material was performed under IRB ethics approved protocols: "Liver Disease – Biobank" # 11-066-SDR and "Human Hepatic Tissue Organellar Isolation and Characterization" # 11-196-SDR filed at the McGill University Health Centre, Montreal, Canada in the name of Dr. Peter Metrakos. Patient and donor consent was obtained in written form for all human samples collected.

## List of Abbreviations

AC	Anterograde Compartment
Atg	Autophagy-related genes
ATP	Adenosine triphosphate
Baf	Bafilomyin A1
BAR	Bin/Amphiphysin/Rvs-homology
BFA	Brefeldin A
BIG	BFA inhibited GEF
BSA	Bovine serum albumin
CE	cholesteryl-ester
CHX	Cycloheximide
CMA	Chaperon mediated autophagy
CME	Clathrin-mediated endocytosis
CMPM	Cisternal Maturation/Progression Model
COPI	Coat Protein complex I
COPII	Coat Protein complex II
DAB	3,3'-diaminobenzidine
DG	diacylglycerol
DMEM	Dulbecco's Modified Eagles Medium
DMSO	Dimethyl sulphoxide
Drp1	Dynamin-related protein-1
DTT	Dithiothreitol
EGFP	Enhanced green fluorescent protein
EPA	Eicosapentaenoic acid
ER	Endoplasmic reticulum
ERES	ER Exit Site
ERGIC	ER-Golgi intermediate compartment
FA	Fatty Acid
FBS	Fetal bovine serum
FEME	Fast Endophilin-Mediated Endocytosis
FFA	Free Fatty Acid
FKRB	FK506 binding protein
FRB	FKBP12-Rapamycin Binding
GalNacT2	N-acetylgalactosaminyltransferase 2
GalT	beta-1, 4-galactosyltransferase
GBF1	Golgi-associated BFA-resistant protein
GlcNAc	N-Acetylglucosamine
GlcNAcT1	N-Acetylglucosaminyltransferase 1
GRAB	GFP recognition after bleaching

GUV	giant unilamellar vesicle
HCC	hepatocellular carcinoma
HSL	hormone-sensitive lipase
KD	Knockdown
LC3	Microtubule-associated proteins 1A/1B light chain 3A
LD	Lipid droplet
LIR	LC3 Interacting Region
LPAT	Lysophosphatidic acid acyltransferase
MG	monoacylglycerol
MGL	monoacylglycerol lipase
mTOR	mammalian Target of Rapamycin
N-BAR	N-terminal BAR domain
NAFLD	Non-Alcoholic Fatty Liver disease
NASH	Non-Alcoholic Steatohepatitis
OA	Oleic acid, oleate
PBS	Phosphate buffered saline
PC	phosphatidylcholine
PE	phosphatidylethanolamine
PI3KC3	Class III phosphatidylinositol 3-kinase
PLA2	Phospholipase A2
PLD2	Phospholipase D2
PRR	proline-rich regions
SH3	Src-homology-3 domain
SiaylT	Siayltransferase
siRNA	Small interfering RNA
SNAREs	SNAP receptors
TAG	Triacylglycerol
Tet	Tetracycline
TGN	Trans Golgi Network
UPR	Unfolded protein response
UVRAG	UV radiation resistant-associated gene
VSV-G	Vesicular Stomatitis Virus glycoprotein
VTM	Vesicular Transport Model
WT	Wild type

## List of Figures

<b>Illustration 1:</b> Overview of the early secretory pathway .....	3
<b>Illustration 2:</b> COPI vesicle formation.....	12
<b>Illustration 3:</b> Rapamycin-induced dimerization .....	24
<b>Illustration 4:</b> Domains and structures of the endophilin family .....	35
<b>Illustration 5:</b> Schematics of membrane curvature driven by endophilin .....	37
<b>Illustration 6:</b> Endophilin in endocytosis.....	40

### Chapter 3: New generation of probes to study retention and recycling of Golgi resident enzymes

<b>Figure 3-1:</b> Fusion antibody is constructed from single chain variable fragment of a monoclonal antibody.	
a. Overview of the fusion antibody construction .....	63
b. Construction of the mTurquoise-tagged fusion antibody.....	63
<b>Figure 3-2:</b> Fusion antibody is expressed and fluorescent .....	66
<b>Figure 3-3:</b> Fusion antibody is specifically made for its respective glycosyltransferase..	68
<b>Figure 3-4:</b> Fusion antibody is specific for Golgi enzyme.....	70
<b>Figure 3-5:</b> Fusion antibody behaves as Golgi enzyme.	
a. Live cell imaging of mTurq-FSAB- $\alpha$ -GalNacT2-SBP transfected cells after BFA treatment.....	71
b. Live cell imaging of EGFP-FSAB- $\alpha$ -GalT transfected cells after BFA treatment ...	72
c. Live cell imaging of RFP-FSAB- $\alpha$ -GalT transfected cells after BFA treatment .....	73
<b>Figure 3-6:</b> Fusion antibody does not affect the cell viability or increase ER stress.	
a. Percent cell viability measured by Trypan blue exclusion assay .....	76
b. Degree of ER stress examined by the expression of HERP .....	77
<b>Figure 3-7:</b> Fusion antibody can be used to highlight antigens of non-transfected cells.	
a. Experimental design for conditioned media.....	79
b. Immunofluorescence showing transfected cells and non-transfected cells.....	79
<b>Figure 3-8:</b> Conditioned medium from fusion antibody cells is a source of fusion antibody.	
a. T-Rex Hek293 EGFP-FSAB-GalT-RGS6His3FLAG cells inducibly expressing fusion antibody .....	81
b. Western blot probed by FLAG antibody.....	81
c. Conditioned media from T-Rex Hek293 cells can stain non-transfected cells .....	82
<b>Figure 3-9:</b> Conditioned media from T-Rex cells can be used to stain fixed and permeabilized HeLa cells .....	84
<b>Figure 3-10:</b> Affinity purified fusion antibody retains ability to recognize Golgi enzyme.	

a. Tandem-affinity purification of fusion antibody .....	86
b. Tandem-affinity purified fusion antibody can stain non-transfected cells .....	86
<b>Figure 3-11:</b> Fusion antibody can be used as a tool to observe protein internalization from the cell surface.	
a. Affinity purified fusion antibody is internalized .....	89
b. Internalization of fusion antibody is specific .....	90
<b>Figure 3-12:</b> Fusion antibody uptake to Golgi/endosomal/lysosomal compartment .....	92
<b>Figure 3-13:</b> Internalization of fusion antibody .....	
a. Internalization of affinity purified fusion antibody is blocked by bafilomycin A1 ....	94
b. Quantification of relative FLAG band intensity over GAPDH.....	94

## **Chapter 4: Endophilin B1—A novel lipid droplet protein essential for EPA mediated lipophagy**

<b>Figure 4-1:</b> Endophilin B1 is enhanced in lipid droplet fraction of human fatty livers.	
a. Heat map of endophilin B1 distribution in fatty liver subcellular fractions .....	99
b. A number of tissues with a high level of endophilin B1 .....	100
c. Western blot analysis of LD fractions from liver #4, #10, and #14 .....	100
d. Indirect immunofluorescence of human fatty liver #14 .....	100
e. Endophilin B co-localize with perilipin 1 on human fatty liver .....	101
<b>Figure 4-2:</b> Endogenous endophilin B1 is localized on LD in autophagy conditions.....	103
<b>Figure 4-3:</b> Endophilin B1 expression decreases lipid droplet size.	
a. Immunofluorescence of T-REx HeLa EndoB1-EGFP cells.....	105
b. Western blot analysis shows expression of EndoB1-EGFP .....	105
c. Bar graph showing LD diameter decrease with endophilin B1's expression.....	106
<b>Figure 4-4:</b> Endophilin B1 is involved in lipophagy.	
a. Immunofluorescence of knockdown of endophilin B1 increases LD size .....	107
b. Western blot of endophilin B1 knockdown.....	107
c. Quantification of endophilin B1 western blot relative band intensity.....	107
<b>Figure 4-5:</b> Endophilin B1 decreases cellular triacylglycerol.	
a. Average CMPA/mg protein for all time points .....	109
b. TAG change after 8 hours of endophilin B1 induction .....	109
<b>Figure 4-6:</b> Endophilin B1 moves to lipid droplet in response to eicosapentaenoic acid .	111
<b>Figure 4-7:</b> EPA treatment causes lipid droplet to decrease in size.	
a. Immunofluorescence showing EPA decreases LD diameter.....	112
b. Quantification of LD diameter .....	113
<b>Figure 4-8:</b> Time course expression of endophilin B1 and EPA causes LD breakdown.	
a. Endophilin B1-EGFP moves progressively to lipid droplet .....	114

b. Histogram for a percentage of LD diameter.....	115
<b>Figure 4-9:</b> Endophilin B1 and EPA decrease cellular triacylglycerol.	
a. Endophilin B1 and EPA decrease cellular lipids.....	117
b. Time course EPA treatment decreases cellular triacylglycerol.....	117
<b>Figure 4-10:</b> Overexpressing endophilin B1 or EPA treatment does not affect cell viability.....	119
<b>Figure 4-11:</b> EPA increases autophagosome fusion with acidic compartments.	
a. Immunofluorescence of HeLa cells showing autophagosome fusion .....	120
b. Quantification of mRFP/eGFP ratio.....	121
<b>Figure 4-12:</b> Endophilin B1 is involved in EPA mediated lipophagy.	
a. Immunofluorescence of Torin1 or EPA treated endophilin B1 KD cells.....	123
b. Quantification of LD diameter changes in Torin1 treated cell .....	123
c. Quantification of LD diameter changes in EPA treated cell .....	123
d. Western blot of endophilin B1 knockdown .....	123
<b>Figure 4-13:</b> Endophilin B1 knockdown blocks EPA mediated lipophagy.	
a. Immunofluorescence of endophilin B1 KD after EPA treatment.....	125
b. Western blot of endophilin B1 KD.....	125
c. Percentage of LDs greater than 2.5µm in diameter .....	126
d. Quantification of LD number for EPA treated endophilin B1 KD cells.....	126
<b>Figure 4-14:</b> Endophilin B1 is involved in a lipophagy distinct from the macroautophagy.	
a. Endophilin B1 decreases LD diameter regardless of Atg5 KD.....	129
b. Quantification of LD diameter .....	129
c. Western blot of Atg5 knockdown.....	130
d. Quantification of Atg5 western blot band intensity .....	130
<b>Figure 4-15:</b> Lipophagy by endophilin B1 is independent of ATGL.	
a. Immunofluorescence of T-REx EndoB1-EGFP cells after Atglistatin .....	132
b. Quantification of LD diameter .....	132
<b>Figure 4-16:</b> Atglistatin does not displace ATGL from LD.....	133
<b>Figure 4-17:</b> Endophilin B1 colocalizes with LAMP1 on human fatty liver #14 .....	135
<b>Figure 4-18:</b> Endophilin B1 KD abolishes LD-LAMP1 association in EPA treated cells.	
a. Immunofluorescence of endophilin B1 KD after Torin1 .....	137
b. Immunofluorescence of endophilin B1 KD after EPA .....	138
c. Number of LAMP1 associated LD per cell.....	139
<b>Figure 4-19:</b> Association of LD-LAMP1 is independent of macroautophagy and ATGL.	
a. Immunofluorescence of Atg5 KD cells and ATGL inhibition.....	140
b. Number of LAMP1 associated LD per cell.....	141
<b>Figure 4-20:</b> Endophilin B1 associates with Rab7 in EPA mediated lipophagy.....	143

**Figure 4-21:** EPA increases lipid droplet-lysosome association.

- a. Time-lapse series of HeLa cells expressing YFP-Rab7 ..... 146
- b. Time-lapse series of HeLa cells expressing mCherry-FYVE ..... 146
- c. Average number of overlapping pixels per cell per minute ..... 147
- d. Number of Kiss-and-Run events per cell per minute ..... 147
- e. Time-lapse series of T-Rex HeLa EndoB1-EGFP expressing CFP-Rab7 ..... 148
- f. Number of Kiss-and-Run events per cell per minute..... 148
- g. Average number of overlapping pixels per cell per minute ..... 149

**Figure 4-22:** Interacting partners of endophilin B1 in EPA mediated lipophagy.

- a. T-REx HeLa cells inducibly expressing endophilin B1-BirA ..... 151
- b. T-REx HeLa cells inducibly expressing FLAG-BirA ..... 152
- c. Potential interactors of endophilin B identified by Bio-ID ..... 152

## Chapter 5: Discussions

**Figure 5-1:** Expected observations in the early secretory pathway ..... 166

**Figure 5-2:** Possible mechanisms of endophilin B1 ..... 184

## **Chapter 1: Literature Review**

## 1.1. Background of Golgi research

After thorough ER quality control, newly translated and folded proteins reach the Golgi apparatus where glycosylation, sorting, and processing occur. This organelle, comprised of flattened membranous stacks called cisternae, has been a fascinating subject of study for many decades because of its unique structure. All eukaryotic proteins destined for secretion, export to the plasma membrane or the endosome/lysosome system must go through the Golgi processing in order to reach their final destination. Yet, the mechanisms of how biosynthetic cargo moves through the Golgi have not yet been clearly demonstrated. So far, several mechanisms of intra-Golgi transport have been proposed where the most accepted models are the cisternal maturation/progression model (CMPM) and the vesicular transport model (VTM).

### 1.1.1. How Golgi maintains its homeostasis

Properly folded biosynthetic materials leave the ER via ER-derived vesicles. It is generally thought that these transport vesicles coalesce to form an intermediary structure that later becomes an early part of Golgi, called the *cis*-cisterna (See section 1.1.3.). Through the cisternal progression, biosynthetic materials undergo processing by Golgi-resident enzymes. This maturation continues as the cisterna reaches *medial* and finally the *trans* Golgi, where the cisterna is taken apart and then fed into the secretory pathway (Illustration 1).

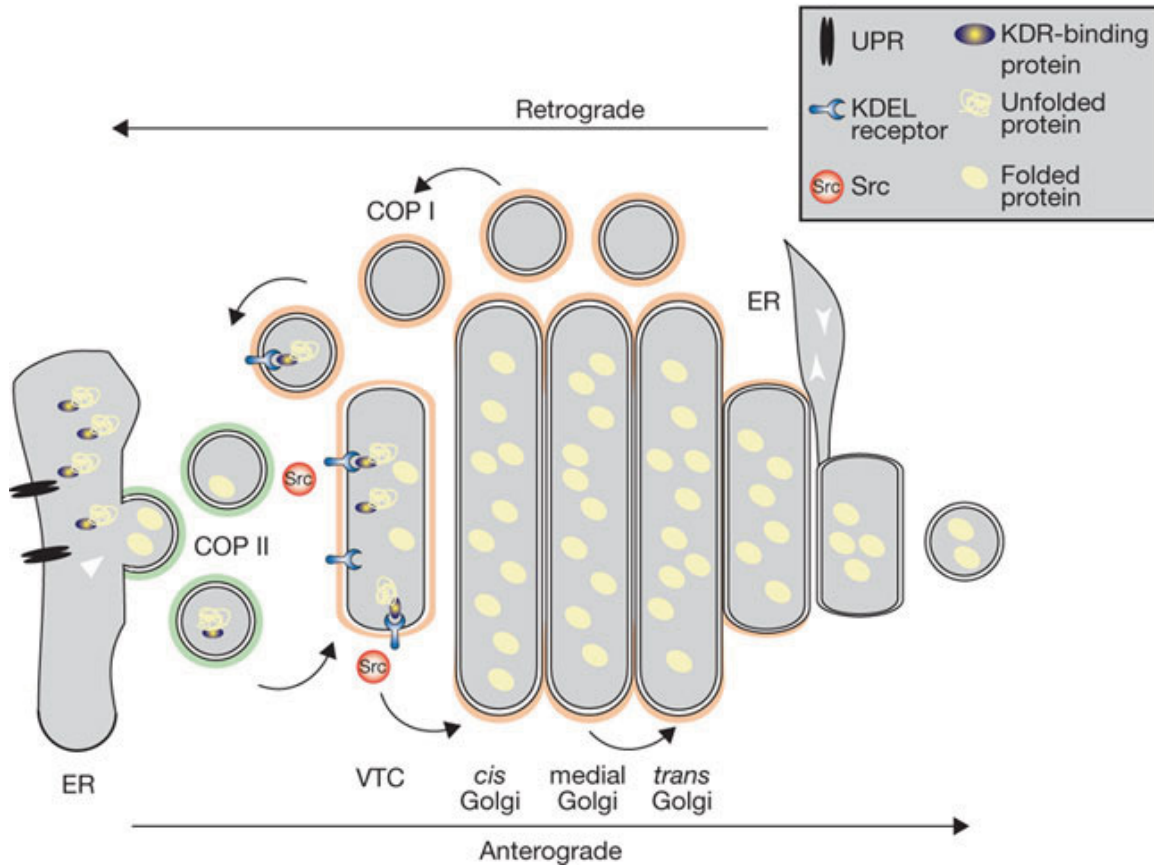


**Illustration 1:** Overview of the early secretory pathway

Biosynthetic materials leave the ER by ER-derived COPII coated vesicles. It is believed that COPII vesicles coalesce to form VTC (vesicular-tubular clusters). VTC differentiates and becomes a part of Golgi cisternae. As Golgi-resident enzymes process the biosynthetic materials, cisternal maturation occurs concurrently. Finally, when cisterna reaches the *trans* side, and the maturation is completed, cisterna is taken apart, and biosynthetic materials are delivered to their final destination. As the cisternae move in the anterograde direction, Golgi resident enzymes and KDEL receptor recycle to the precedent cisterna and to ER by COPI-coated vesicles, and this retrograde movement of the enzyme keeps the integrity of Golgi because otherwise Golgi enzymes would be lost at the *trans* side. There is also COPI-independent pathway called GERL, and it is presented as an ER tail at the right side of the illustration.

*Reprinted by permission from Macmillan Publishers Ltd: Nature Cell Biology (Asp and Nilsson, 2008)*

While being subjected to continuous flux of biosynthetic materials from the ER and disassembly of cisternae at the *trans* side, the Golgi must keep its resident proteins and structural

integrity. To do this, each cisterna must communicate with the other. The mechanism of communication of intra-Golgi trafficking is a subject of long-standing debate.

In the VTM, the Golgi is considered as a set of stable compartments. This model suggests that the Golgi enzymes that modify biosynthetic molecules reside within the fixed cisternae; whereas biosynthetic molecules move from *cis*- to *trans*- cisternae via Golgi-derived COPI (COatomer Protein complex I) vesicles in an anterograde direction. In accordance with this model, the cisternae do not change their positions or compositions.

The CMPM, on the other hand, suggests that there is continual cisternal turnover such that *cis*- cisterna progresses to become mature *trans*- cisterna. After reaching the most distal (*trans*-) cisterna, biosynthetic molecules are sorted into vesicles, and the cisterna is taken apart. The CMPM postulates that as cisternae mature, Golgi enzymes cycle backward through the stacks via COPI vesicles. This process is meant to maintain Golgi-resident enzymes in place during the continual cisternal turnover. Simultaneously, this retrograde trafficking of Golgi-resident enzymes accommodates for biosynthetic materials in a newly formed cisterna.

### **1.1.2. History of Golgi research around CPM and VTM**

Protein transport in the secretory pathway was first proposed from electron microscopic images of highly stacked Golgi and nearby vesicles (Grasse, 1957). Based on the fenestrated appearance of Golgi, the CPM was formulated. It was postulated that Golgi stacks were assembled at the *cis* side and disassembled at the *trans* side. Consequently, this model necessitated a constant input of biosynthetic cargo from the ER. However, when new protein synthesis was shown to be independent of the intracellular transport (Jamieson and Palade, 1968), this view was questioned: there was no distinguishable loss of Golgi morphology upon the

inhibition of protein synthesis (Jamieson and Palade, 1968). For this reason, the CMPM was largely abandoned. The alternative model, VTM, then hypothesized that biosynthetic cargo traversed the Golgi by moving from one cisterna to the next via vesicular carriers while Golgi-resident enzymes stayed static within fixed cisternae. This model was strengthened by an *in vitro* transport assay whereby purified Golgi membranes from N-acetylglucosaminyltransferase I (GlcNAcT1) deficient CHO cells were incubated with Golgi membranes from the wild-type cells. Then, <sup>3</sup>H-N-acetylglucosamine (GlcNAc) was transferred onto N-linked oligosaccharide of Vesicular Stomatitis Virus temperature sensitive mutant (VSV-G<sup>ts045</sup>), suggesting that somehow VSV-G<sup>ts045</sup> from one Golgi and GlcNAcT1 from the other became united (Balch et al., 1984). Subsequent experiments using this assay (Serafini et al., 1991; Söllner et al., 1993; Waters et al., 1991) and yeast genetics studies (Kaiser and Schekman, 1990) supported the movement of biosynthetic cargo through vesicles and identified the necessary elements for vesicle formation. A shortfall of the VTM was in its failure to explain how macromolecules, too large to fit within small transport vesicles, move through the secretory pathway: Indeed, immuno-EM as well as immunofluorescence studies indicated that procollagen I and algae scales traversed the Golgi without leaving the Golgi lumen (Bonfanti et al., 1998; Melkonian et al., 1991). Albumin, a biosynthetic cargo, was also shown to be distributed uniformly in Golgi, and it did not enter transport vesicles (Dahan et al., 1994). When the transport of a small, freely diffusing protein (VSV-G) and a larger protein aggregate (procollagen I) were monitored together within a transport-synchronized cell, these proteins were shown to move through the Golgi at indistinguishable rates, and they did not enter Golgi vesicles during their transport (Mironov et al., 2001). High-speed three-dimensional confocal microscopy, independently carried out by two laboratories, demonstrated that in yeast Golgi-resident membrane proteins moved in a *cis* to

*trans* direction, reflecting cisternal maturation (Losev et al., 2006; Matsuura-Tokita et al., 2006). Similarly, GTP hydrolysis by Arf1 was shown to be a prerequisite for active sorting of enzymes into budding COPI vesicles (Lanoix et al., 1999). In this experiment, biosynthetic cargo, polymeric Ig receptor, was left out of the vesicles. Indeed, these COPI vesicles generated *in vitro* showed preferential incorporation of Golgi-resident glycosyltransferases (Lanoix et al., 1999, 2001). With the advent of proteomics, the protein profile of COPI vesicles and Golgi was investigated in detail, and COPI vesicles generated *in vitro* were shown to preferentially carry Golgi-resident enzymes (Gilchrist et al., 2006). These *in vitro* experiments and proteomics results strongly support the CMPM, resurrecting this as a model for intra-Golgi transport. Nonetheless, there are subpopulations of the transport vesicles that transport the biosynthetic cargo or Golgi-resident enzymes (Lanoix et al., 2001; Malsam et al., 2005; Orci et al., 1997), and other researchers proposed different models for the early secretory pathway (Griffiths, 2000; Lavieu et al., 2013; Orci et al., 2000; Pelham and Rothman, 2000). Thus, cell biology community demands further *in vivo* evidence to reconcile with different observations and models (Emr et al., 2009).

### **1.1.3. The Anterograde trafficking**

Properly folded biosynthetic cargo leaves the ER via COPII (COat Protein complex II)—an ER-derived vesicle. Soluble cargos *en route* to Golgi are recruited into COPII vesicles (Barlowe et al., 1994), and these vesicles coalesce to form intermediate compartments.

### *COPII vesicles*

COPII vesicles initiate budding processes from the ER for ER-to-Golgi transport. COPII coats consist of two heterodimers: Sec23p/Sec24p heterodimer and Sec13p/Sec31p heterotetramer (Bickford et al., 2004; Barlowe et al., 1994). GTPase Sar1p is the main protein in the initiation of COPII vesicle budding, and its activity is regulated by Sec12, which is a Guanine nucleotide exchange factor (GEF) (Futai et al., 2004). Once Sar1p is bound to the membrane and coat complexes are recruited, cargo destined for Golgi membrane is sorted into an emerging vesicle. During cargo packaging into COPII vesicles, some proteins are selectively recruited (Barlowe, 2003). The sorting of transmembrane molecules are governed by COPII coatomers (Mancias and Goldberg, 2008). Conserved di-acidic motifs, such as DxE found in VSV-G, is required for direct or indirect binding to Sec23-Sec24 coatomers (Barlowe, 2003). Soluble molecules require receptors such as ERGIC-53 (Hauri et al., 2000; Appenzeller et al., 1999), p24 (Dominguez et al., 1998), and Erv families (Otte and Barlowe, 2002). For ERGIC-53 and p24 receptor proteins, di-hydrophobic or di-aromatic amino acid motifs such as Phe-Phe, Tyr-Tyr, and Phe-Tyr, are required, and for Erv receptor protein, a Leu or Ile containing motif is found (Kappeler et al., 1997; Otte and Barlowe, 2002). Shortly after COPII vesicles are detached, they are uncoated and fuse with each other to form the ER-Golgi Intermediate Compartment (ERGIC) or tubular clusters (Hauri and Schweizer, 1992; Mironov et al., 2003). Whether ERGIC is a stable compartment or a transitory element moving towards Golgi is a matter of debate (Ben-Tekaya et al., 2005).

### *ER-Golgi Intermediate Compartment (ERGIC)*

First discovered as vesicular-tubular clusters or pre-Golgi intermediates, ERGIC was proposed to be a specialized domain (Schweizer et al., 1990). This compartment was first seen in a live cell as an intermediate compartment that transported VSV-G<sup>ts045</sup> from ER Export Site (ERES) to the Golgi by microtubules (Presley et al., 1997). This compartment was observed to be less than 1µm in diameter, and it may fuse with each other to form *cis*- Golgi or fuse with pre-existing cisternae (Presley et al., 1997). However, one drawback of this model is that at steady-state, this compartment was located closer to ERES than the Golgi. Also, ERGIC-53, the ERGIC marker, did not travel towards Golgi as expected. Instead, large anterograde compartments (ACs) containing signal-sequence-tagged-dsRed segregated from ERGIC and traveled to the Golgi (Ben-Tekaya et al., 2005). To accommodate these observations, it was postulated that there is an ERGIC that forms from fusion of COPII vesicles and ACs containing VSV-G<sup>ts045</sup>, and dsRed separates from the ERGIC (Appenzeller-Herzog and Hauri, 2006).

The current understanding of the ER to Golgi transport is that there is short-range travel from ERES to ERGIC through COPII, and long-range travel from ERGIC to Golgi through the AC. While movement of anterograde compartment towards the Golgi is microtubule dependent, a fusion of anterograde compartment either with each other or with existing *cis*- Golgi is Rab1 dependent. TRAPP1, GEF of Rab1, activates Rab1 in ERGIC, where activated Rab1 recruits large coiled-coil domain containing proteins p115, GM130, GRASP65, and giantin. Coordinative actions of p115, Rab1, GM130, and GRASP65 cause tethering of COPII to ERGIC and/or AC to *cis*-Golgi (Appenzeller-Herzog and Hauri, 2006).

## 1.1.4 The retrograde trafficking

### 1.1.4.a. Golgi-resident enzymes

Within the Golgi, enzymatic reactions take place near its membrane surfaces where different Golgi-resident enzymes are anchored. Many processes are governed by these enzymes including post-translational modifications, glycosylation, and phosphorylation (Stanley, 2011). Synthesis of N-linked glycan will be discussed in this section. It is a co-translational process which begins in the ER and continues in the Golgi. After dolichol-linked precursor oligosaccharide is synthesized, it is transferred to a nascent protein in the ER. Oligosaccharyltransferase in the ER recognizes the consensus sequence and mediates the transfer of the precursor glycan. Three of the terminal glucose molecules are removed from the precursor by glucosidase I and II, and this process occurs in only properly folded proteins: otherwise, chaperones bind to the unfolded (or improperly folded) proteins, preventing translocation to the Golgi. In the Golgi, Golgi-resident enzymes continue the addition and removal of sugar residues. For the N-linked glycan, four of the mannose residues in the  $\alpha$ -1, 2, linkage are removed by mannosidase. Next, N-acetylglucosaminyltransferase I (GlcNAcT1) transfers a N-acetylglucosamine (GlcNAc) residue, initiating the synthesis of a hybrid and complex N-glycan. Whereas N-linked glycosylation initiates on the amino group of asparagine in the ER, there is also O-linked glycosylation, which occurs on the hydroxyl group of serine or threonine (Stanley, 2011). In this thesis, the following enzymes will be used as antigens for the probe design.

N-acetylgalactosaminyltransferase 2 (GalNAcT2) is an O-glycosylation enzyme that transfers N-acetylgalactosamine (GalNAc) residue to the hydroxyl group of serine and threonine residues. Although it is widely distributed among the Golgi stacks, it is mostly found in the *medial-trans* Golgi cisterna (Röttger et al., 1998).

$\beta$ -1, 4-galactosyltransferase (GalT) enzyme, found mostly in the *trans* Golgi, catalyzes the transfer of galactose from UDP-galactose to the hydroxyl group at the 4-position of GlcNAc of a biosynthetic cargo. GalT has two splice variants: long (wild type) and short forms. Although both variants retain galactose-transferring activity, the short form is 13 amino acids less than the WT (wild type). WT travels to the plasma membrane, and then it may be endocytosed back into the cell interior via caveolae-mediated endocytosis (Hathaway et al., 2003). It is well known that GalT is present on the cell surface of germ cells as a receptor for gamete recognition (Miller et al., 1992). Cell surface glycoprotein modification by GalT has also been observed in cells that make up mammary glands. In transgenic mice with elevated levels of WT GalT, proper morphogenesis of mammary glands was inhibited (Steffgen et al., 2002). There was excessive branching of mammary glands in WT GalT null mice, and this was due to altered expression of laminin chains (Steffgen et al., 2002). Therefore, extracellular matrix expression and deposition may require GalT, and proper functions of WT GalT may be required for branching morphogenesis of mammary glands (Steffgen et al., 2002). WT GalT may also be related to cancer because level of WT GalT was elevated in highly metastatic lung cancer cells compared to less metastatic cells (Zhu et al., 2005). Knockdown of GalT or introduction of truncated GalT inhibited cell adhesion on laminin and invasive potential *in vitro* (Zhu et al., 2005).

#### **1.1.4.b. The retrograde trafficking from Golgi to ER**

Numerous studies have observed Golgi enzyme recycling to the ER. So far, there are two pathways for Golgi proteins to travel to the ER: 1) the KDEL receptor and Rer1p; 2) Rab6-dependent pathway. The KDEL receptor retrieves escaped ER resident proteins (Cosson and Letourneur, 1994; Cosson et al., 1998). This pathway is dependent on COPI vesicles and the

small GTPase Arf1 (Bremser et al., 1999). The Rab6-dependent pathway is different in that it utilizes tubules rather than vesicles (Girod et al., 1999; White et al., 1999; Smith et al., 2009; Majeed et al., 2014) (See section **1.1.4.d**).

How do Golgi proteins choose the retrograde pathway? The answer may lie within their affinity towards the COPI or Rab6-dependent pathway. Indeed, the work by Park and colleagues demonstrated that Golgi proteins compete with CDC42 (cell division control protein 42 homolog) for coatamer binding (Park et al., 2015). In this study, constitutively active CDC42 inhibited vesicular transport, whereas knockdown (KD) of CDC42 enhanced it. CDC42 possesses a di-lysine motif that binds to COPI coatamers, and by binding to the KDEL receptor's tail, GTP-CDC42 prevented coatamer from binding to the KDEL receptor, but not from VSV-G (Park et al., 2015). In this way, COPI coatamers were unable to mediate retrograde trafficking of the KDEL receptor, and consequently, anterograde tubular transport was promoted (Park et al., 2015). Similarly, Fossati and colleagues suggested that the balance between the two signal-mediated events that predict the protein's fate in the secretory pathway; a signal that drives retrograde back to ER, as well as a signal for export through the Golgi (Fossati et al., 2014). In fact, they proposed that proteins with DxE signals (the export signal for binding to the Sec24 subunit of COPII, causing recruitment to ER exit sites) be actively excluded from entering into the Golgi for ER retrograde trafficking (Fossati et al., 2014).

#### **1.1.4.c. COPI-mediated transport**

COPI-coated vesicles transport soluble and membrane-bound proteins including Golgi-resident enzymes (Cosson and Letourneur, 1994; Gilchrist et al., 2006). It is evident that these vesicles mediate retrograde trafficking from the *trans*- to the *cis*- cisternae; although it may not

be the sole mode of retrograde trafficking. Here, the mechanism of COPI-mediated transport is summarized (Illustration 2).

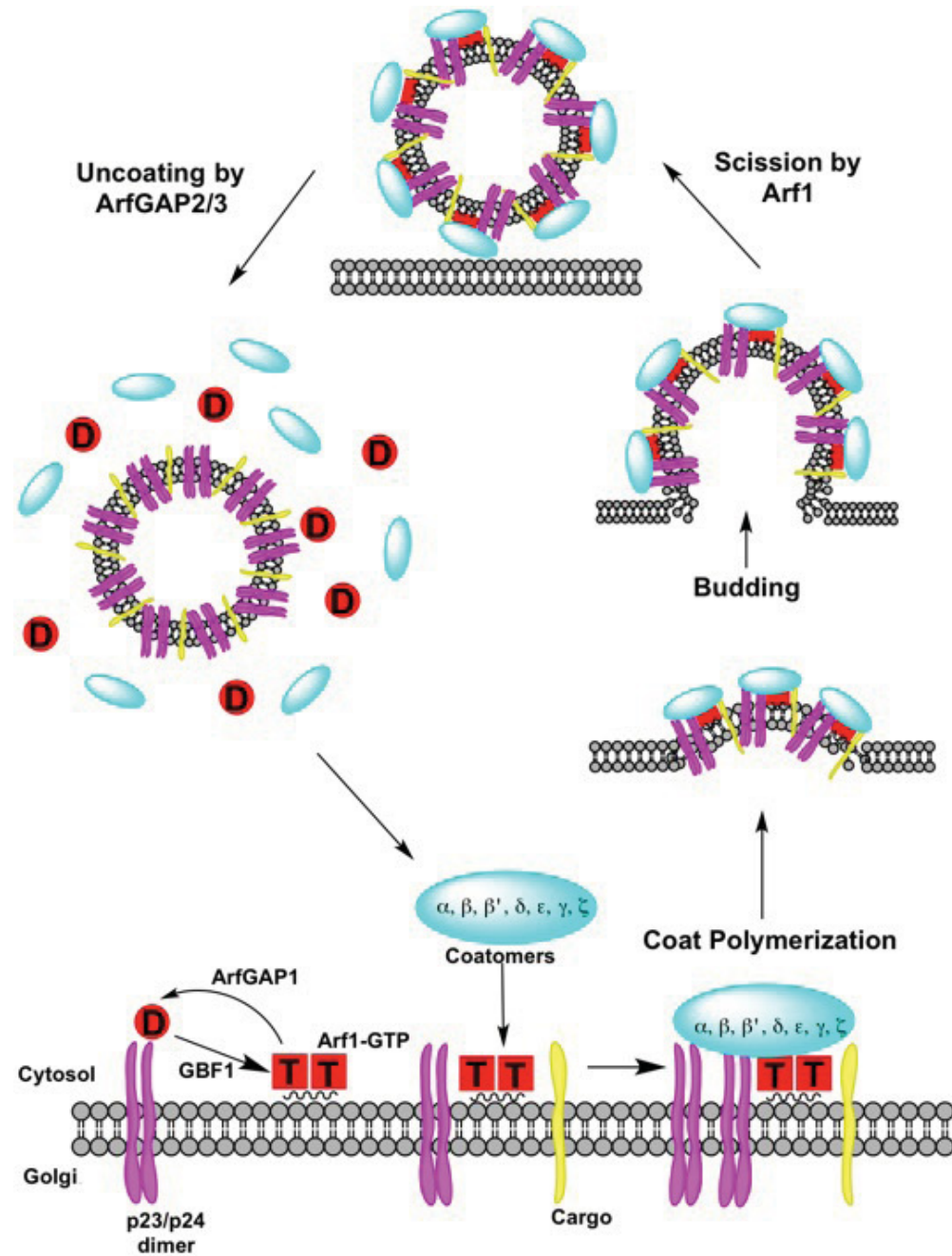


**Illustration 2:** COPI vesicle formation

Arf1 is essential in COPI vesicle formation. It binds to Golgi membrane through p23/p24 dimer. GDP of Arf1 is exchanged to GTP by GBF1. When ArfGAP1 hydrolyzes Arf1-GTP, coatomers are recruited. Coatomers recognize certain cargo motifs, and as coat polymerizes, vesicle buds off. Subsequently, upon scission by Arf1 and coat uncoating by ArfGAP, vesicle is ready to

travel to its destination.

### *Characteristics of COPI vesicle*

COPI vesicles are formed by seven different coatomer subunits:  $\alpha$ -,  $\beta$ -,  $\beta'$ -,  $\gamma$ -,  $\delta$ -,  $\epsilon$ -,  $\zeta$ -COP. Once the assembly is completed, they are 50–60nm in diameter. They form at the cytosolic side of Golgi membrane, and they are found at multiple locations around the Golgi: ERGIC (Martinez-Alonso et al., 2013); *cis*- and lateral Golgi (Oprins et al., 1993); *trans*- Golgi and TGN (Martinez-Menarguez et al., 1996); and lateral rims of cisternae (Rizzo et al., 2013). Arf GTPase mediates COPI vesicle assembly. There are five Arfs associated with the Golgi, each of which most likely mediates different steps of the transport (Volpicelli-Daley et al., 2005). The intrinsic GTPase activity of Arf is low, so conversion of GTP to GDP depends on the Arf GTPase-activating protein, ArfGAP. There are 3 ArfGAPs associated to COPI vesicle formation, and they function in COPI formation, fission, and dissociation of coatomers (Asp et al., 2009; Kartberg et al., 2010).

### *Arf and coatomer recruitment*

The molecular mechanism of COPI vesicle formation has been well characterized. It consists of coat recruitment, uptake of cargo, budding, membrane scission, and coat uncoating steps. Arf1-GDP is first recruited to the membrane by a dimeric complex p23/p24 and is activated by a guanine-nucleotide exchange factor (GEF). The specific GEFs for ARF1 are GBF1 (Golgi-associated BFA-resistant protein) at the ERGIC and Golgi membranes (Kawamoto et al., 2002, Garcia-Mata et al., 2003), and BIG1 and BIG2 (BFA inhibited GEF) at TGN and endosomes (Ishizaki et al., 2008). Activated Arf1-GTP undergoes a conformational change to

expose its N- terminal amphipathic and myristoylated helix. This conformational change allows insertion into the lipid bilayer, securing membrane anchorage (Antonny et al., 1997). A recent structural study on Arf1 suggested that the myristoylated helix might bind perpendicularly to the bilayer (Liu et al., 2010).

Arf1-GTP recruits coatomers to the membrane (Presley et al., 2002), and cargos are then recognized by these coatomers. The  $\alpha$ - and  $\beta$ -COP recognize proteins that have di-lysine motifs at their C- termini (Cosson and Letourneur, 1994). The p24 proteins interact with  $\gamma$ -COP via the di-lysine motifs (Béthune et al., 2006). ER proteins with KDEL sequences are recognized by the KDEL receptor that acts as an adaptor for the coatomers. KDEL receptors have cytosolic di-lysine motifs for coatomer interaction, and its luminal receptor domain interacts with ER resident proteins bearing KDEL sequences (Semenza et al., 1990). As a result, KDEL proteins are incorporated into COPI vesicles, transported to the ER where they dissociate from the KDEL receptor.

### *Cargo recognition*

Other than the C- terminal di-lysine motifs that p24 proteins possess, there are various types of di-lysine motifs recognized by coatomers. KKXX motifs interact with WD40 domains within  $\alpha$ -COP, and K(X)KXX motifs bind to  $\beta$ -COP (Eugster et al., 2004). The arginine based motif,  $\Phi/\Psi/R-R-X-R$ , is recognized by  $\beta$ - and  $\delta$ -COP (Michelsen et al., 2005). The aromatic “ $\delta$ L” motif binds to  $\beta$ -COP (Cosson et al., 1998), and a FXXXXXXXFXLL motif has been suggested to interact with  $\gamma$ -COP (Bermak et al., 2002).

Aside from coatomer recognition motifs, the surrounding sequences also have a substantial effect on recognition. Subtle differences in sequence can alter the strength of each

trafficking signal (Zerangue et al., 2001). For example, using either lysine- or arginine-based ER retention signals can generate a broad spectrum of signals that have different coatomer binding capacities, and hence different efficiencies for trafficking (Zerangue et al., 2001). Zerangue and colleagues suggested that these characteristics of surrounding sequences may help achieve an appropriate steady-state distribution of proteins within the Golgi (Zerangue et al., 2001).

Golgi-resident enzymes do not have COPI coatomer recognition motifs (Tu et al., 2008) yet they are well retained in the Golgi. Vps74 was found to act as an adaptor as it binds simultaneously to coatomer and cytosolic tails of *cis*- and *medial*- glycosyltransferases (Tu et al., 2008). Deletion of this domain (therefore the interaction) results in loss of Golgi localization of mannosyltransferases (Schmitz et al., 2008). The N-terminal 66 amino acids of Vps74p are required for glycosyltransferase retention and glycoprotein processing (Hsu et al., 2013).

### *Sorting of cargos*

For sorting and concentration of cargos, GTP hydrolysis by ArfGAP is essential as non-hydrolyzable GTP (GTP $\gamma$ S) and hydrolysis-deficient Arf1 Q71L mutant inhibited the incorporation of Golgi-resident enzymes (Lanoix et al., 1999). ArfGAP1 senses diacylglycerol (DAG) for tubule formation (Asp et al., 2009), and it possesses an ArfGAP1 Lipid Packing Sensor that forms an amphipathic helix on highly curved membranes (Bigay et al., 2005). ArfGAP1 directly promotes the binding of cargo proteins by forming coatomer complexes (Lee et al., 2005b). Arf1, activated by ArfGAP1, binds selectively to SNAREs (Soluble NSF Attachment protein Receptors), which allows it to stabilize its localization to the Golgi membrane in preparation of its function (Lee et al., 2005b).

### *Membrane fission*

After cargos are packaged into growing COPI buds, the membrane between the bud and Golgi must undergo fission. For this process, the membrane undergoes dynamic processes, which involve a number of factors. Arf1-GTP is able to bind to membranes regardless of coatomer, resulting in tubulation of giant unilamellar vesicles (GUVs) *in vitro* (Bek et al., 2008, Krauss et al., 2008, Lundmark et al., 2008). Dimerization of Arf1 is critical in membrane binding and vesicle scission because non-dimerizing mutant showed virtually no free vesicles (Beck et al., 2011). In a growing bud, Arf1's interaction with the membrane becomes energetically favorable. As the bud becomes more complete, a neck forms at the side of Arf1, which results in a local high-energy state. This high negative curvature is no longer favorable for Arf1 binding; therefore, to prevent Arf1 from escaping, adjacent membranes in the neck must fuse, and this causes membrane separation. (Popoff et al., 2011)

For membrane fission, BARS (Brefeldin A ADP-ribosylated Substrate) or endophilin are required, which is cell type specific (Yang et al., 2005, 2006). Yang and colleagues suggested that there are two stages in the fission process: There is an earlier stage where BARS and other COPI components are required for the neck constriction. Then, there is a later stage where fission requires phosphatidic acid (generated from phospholipase D2 activity, not acyltransferase activity of the BARS) (Yang et al., 2008). Phosphatidic acid allows binding of BARS to liposomes, and inhibition of phospholipase D2 (PLD<sub>2</sub>) leads to accumulation of COPI buds with constricted necks at the ERGIC compartment. Additionally, the phosphatidic acid may be a source of DAG since it has been proposed to be important in COPI fission due to its recruitment of ARFGAP1 to the Golgi (Gannon et al., 2014). In clathrin-dependent endocytosis, endophilin

has been shown to recruit dynamin for membrane fission and does not act as a lysophosphatidic acid acyltransferase (LAAT) (Gallop et al., 2005) (See section **1.1.4.**).

### *Coat uncoating*

For COPI vesicles to fuse with a target membrane, the coatomer must be uncoated. Although hydrolysis of Arf1-GTP is essential for active cargo selection, it is also implicated in coatomer shedding: Hydrolysis of Arf1-GTP renders the coat unstable, causing coatomers to shed (Tanigawa et al., 1993). ArfGAP2 and ArfGAP3 may also play a role in coat shedding because siRNA KD of these proteins caused a phenotype similar to when vesicle uncoating is inhibited: Golgi unstacks and cisternae shorten (Kartberg et al., 2010). Recently, J-domain chaperone auxilin has been proposed to mediate COPI and COPII coatomer uncoating (Ding et al., 2015). COPI vesicles may uncoat either while in the cytosol or while being fused with the target membrane (Trahey and Hay, 2010).

There is a retrograde transport pathway independent of COPI (Girod et al., 1999), and certain populations of COPI vesicles may participate in anterograde transport across the Golgi (Orci et al., 1997, 2000; Park et al., 2015). Also, COPI may contribute to the formation of tubule rather than vesicle (Park et al., 2015). Owing to numerous isoforms (Popoff et al., 2011), there may be different subpopulations of COPI vesicles that mediate transport in various directions, or preferentially mediate the transport of certain Golgi enzymes.

#### **1.1.4.d. Rab6 dependent retrograde pathway**

Rab6, a Golgi-associated GTPase, regulates the dynamics of transport carriers. It has been shown that Rab6 participates in a number of cellular transport pathways including post-Golgi transport, intra-Golgi transport, and Golgi to ER retrograde transport. Splice variants of Rab6 (Rab6A, Rab6A') interact with myosin II to regulate fission of transport carriers from the Golgi (Miserey-Lenkei et al., 2010). Depletion of either Rab6 splice variants impaired membrane fission because long tubules remained attached to the Golgi (Miserey-Lenkei et al., 2010).

For tubular membrane formation, the activity of PLA<sub>2</sub> has been demonstrated to be important (Ha et al., 2012). Membrane tubules may be generated by the opposing action of PLA<sub>2</sub> and lysophosphatidic acid acyltransferase (LPAT). PLA<sub>2</sub> generates inverted conical phospholipids (lysophospholipids), while LPAT introduces conical lipids (Ha et al., 2012). PLA<sub>2</sub> generates positive curvature by introducing inverted conical phospholipids, which can subsequently result in tubule formation (Ha et al., 2012). The opposing action of LPAT will turn lysophospholipids back to phospholipids, resulting in tubule shortage. In fact, tubular clusters have been observed in transporting SiaylT-FRB-EGFP from Golgi to cell peripheral ER, which is governed by Rab6 and PLA<sub>2</sub> (Sengupta et al., 2015) (More of FRB fragment in **1.1.6**).

It is plausible that the Rab6 dependent pathway involving tubules is a rapid form of transport compared to the coordinated actions required for the COPI-dependent pathway (Sengupta et al., 2015). Also, it is probable that different enzymes utilize different modes of retrograde trafficking to the ER.

## **1.1.5. Extended views of the early secretory pathway**

### **1.1.5.a. Other models**

Indeed, mechanisms of the early secretory pathway are not mutually exclusive. They would depend on the type of cargo, pathophysiological conditions, cell types, and or perhaps the trafficking steps being examined. The following models add a new perspective to existing models, and combinations of these models may arise.

The rapid partitioning model attempts to explain differential distribution of Golgi enzymes from the context of lipid bilayer characteristics. It proposes that transmembrane cargos entering the Golgi are quickly dispersed throughout the Golgi before being differentially partitioned between the two membrane environments: the processing domain that is BFA-sensitive; and the export domain that is BFA-resistant (Patterson et al., 2008). This model postulates the following: Glycerophospholipids give rise to the processing domains, and this would be a place where transmembrane Golgi enzyme accumulate; the export domain is comprised of cholesterol and glycosphingolipids, and transmembrane proteins would reside only within this domain. This model explains that gradient distribution of Golgi enzyme is merely due to their affinity for different lipids: Golgi enzymes with shorter transmembrane domains have a high affinity for thinner bilayers; and those with longer transmembrane domains prefer thicker bilayers (Patterson et al., 2008). For movement of larger biosynthetic cargos, this model incorporates the cisternal movement of the Golgi. Larger biosynthetic cargo too big to fit in vesicles or tubules would gain an affinity for export domain lipids so that they would be transported within the maturing cisternae. These export domain lipids would partition around the large cargo aggregates and form a transport carrier for the export (Patterson et al., 2008).

The COPI-independent pathway for recycling Golgi-resident enzymes has been suggested, and it is through tubular connections. These tubules were observed at 15°C, which blocks the ERGIC site such that the export from the Golgi was inhibited (Martínez-Alonso et al., 2007). These tubules were transient in nature, as they were extending toward the cell periphery and retracting back to the Golgi vicinity before disappearing. Devoid of proteins necessary for ER-Golgi transport (Sec22, membrin, Rab1, and Rab2) and biosynthetic cargos (VSV-G), these tubules were found to carry Golgi enzymes, SNAREs, Rab6, and GS15 (Martínez-Alonso et al., 2007). The formation of tubules was dependent on microtubules, but independent of BFA or cycloheximide (CHX) treatment (Martínez-Alonso et al., 2005).

Shown by Smith and colleagues, there is also a novel Rab6/COG3/COPI dependent pathway that mediates retrograde trafficking of Subtilase cytotoxin (SubAB) (Smith et al., 2009). SubAB, which hijacks the retrograde pathway, moved much slower to the *cis*- Golgi when COG 3, Rab 6, and  $\beta$ -COP were knocked down. (Smith et al., 2009).

#### **1.1.5.b. Ongoing debates in Golgi research**

Discussions on the mechanism of intra-Golgi transport are amplified, and this is partially because experiments with similar conditions have resulted in contradicting outcomes.

Previously, two premier electron microscopy laboratories independently examined the distribution of the Mannosidase II (MannII) enzyme in NRK cells using a highly characterized and specific polyclonal antibody. Surprisingly, one group showed that MannII was incorporated in peri-Golgi vesicles (Martínez-Menárguez et al., 2001) while the other group revealed the opposite (Cosson et al., 2002). These contradicting results on the distribution of MannII enzyme

may be explained by assuming a limitation in immuno-EM: specifically, the ability to reveal antigens present in small structures like peri-Golgi COPI vesicles.

Inducible aggregation of reporter protein allowed for probing these processes at will, which introduces the least perturbation in the early secretory pathway. The  $F_M$  domain is a mutant of FKBP (FK506-binding protein) that spontaneously dimerizes (Rollins et al., 2000). This dimerization and subsequent oligomerization could be disassembled by a reversible drug (Rollins et al., 2000). Two groups have used this unique  $F_M$  domain to study the behavior of membrane-bound secretory cargo and Golgi-resident enzyme, and their findings are summarized below.

Lavieu and colleagues fused four copies of  $F_M$  domains with the integral membrane protein CD8 (Cluster of Differentiation 8). When polymerized, the construct formed aggregates that spanned the cisternal lumen. After analysis using various temperature blocks, these aggregates or 'staples' were restricted in their movement, allowing the researchers to observe their localizations. When polymerization was induced in the *cis*-Golgi by shifting temperature from 37°C to 16°C, the staples were unable to traffic to the *trans*-Golgi, and they were positioned in the flattened, stacked regions of the cisternae. On the other hand, the soluble aggregates were found in the dilated rims of cisternae. When the temperature was shifted to 20°C, which blocks the exit from TGN, these staples were found throughout the Golgi. The assumption was that if Golgi moves according to the CPM, staples would be found within the Golgi. Collectively, these researchers concluded that the Golgi follows a novel rim progression model, whereby cisternae within the stacks are static, and rims of cisternae that contain soluble cargos move in an anterograde direction (Lavieu et al., 2013). However, these researchers failed to demonstrate how Golgi-resident enzymes move through the cisternae. Also, they did not

comment whether or not these staples introduced any intrusions that block the Golgi enzyme's movement.

Contrary to Lavieu's approach, Rizzo and colleagues used the  $F_M$  domain to fuse with the membrane-spanning domain of Mannosidase I, a Golgi-resident enzyme that is normally found within the *cis*- to *medial*-Golgi. In the absence of a disaggregating drug, AP12998, the engineered protein aggregated and 'plaques' formed at the centers of the *cis*-cisternae. These plaques were blocked from entering the peri-Golgi vesicles and tubule carriers. Instead, they were translocated to *trans*-cisternae, reflecting that the *cis*-cisternae containing the plaques were maturing. After being depolymerized, MannI- $F_M$  became concentrated at cisternal rims, then moved to peri-Golgi vesicles/tubules, before finally returning to *cis*-Golgi from the *trans*-Golgi within a few minutes. At the same time, the number of peri-Golgi vesicles/tubules increased (Rizzo et al., 2013). Collectively, the findings of this group support CPM.

The disparity in these two experiments involving  $F_M$  domains may be due to differences in size, topology, and orientation of the artificial proteins (Morriswood and Warren, 2013). At the same time, the two proteins used in both studies are engineered, and certainly, they do not provide a true representation of how endogenous Golgi enzymes traverse the cisternae.

### **1.1.6. Challenges in studying ultrastructural localization of proteins in Golgi**

#### *Size constraint*

Given the dynamics of the Golgi and minutely sized vesicle carrier, it is challenging to observe what truly happens within the secretory pathway. Earlier observations on Golgi enzymes have been based on using gold-conjugated secondary antibodies for immuno-EM. However, this approach often has misled the localization of Golgi enzymes due to the small size of transport

vesicle (~50nm) versus the relatively large size (~25nm) or the orientation of primary and secondary antibodies (Martínez-Menárguez et al., 2001; Cosson et al., 2002).

#### *Short lifetime of carriers*

Carriers of Golgi proteins may be short-lived or less abundant. For example, tubules observed by shifting the temperature to 15°C would not form as quickly, and they randomly fragment at physiological temperature (Martínez-Alonso et al., 2007). Also, the half-life of COPI vesicles, relative to their speed of formation and consumption, is unknown. This makes it difficult to determine to what extent COPI vesicles affect the trafficking within the Golgi (Gannon et al., 2011).

#### *Non-physiological probes*

An ER trapping assay enabled by using an oligomerizing FKBP-rapamycin-FRB complex has demonstrated the relationship between ER and Golgi proteins (Pecot and Malhotra, 2006; Sengupta et al., 2015). The FKBP and FRB domain of the mTOR make a tertiary complex in the presence of an immunosuppressant drug, rapamycin (Illustration 3). Rapamycin binds simultaneously to the two proteins, inducing a dimerization system. Therefore, when FRB and FKBP are fused with proteins of interest, rapamycin would cause an association between these proteins. The unique property of this dimerizing probe attracted many researchers to incorporate it into their system to study Golgi to ER transport (Pecot and Malhotra, 2006; Sengupta et al., 2015; Jenkins et al., 2012; Bentley et al., 2015). Sengupta and colleagues utilized this rapamycin-induced dimerizing probe to demonstrate that Golgi enzymes constitutively cycle

through the ER. They demonstrated that this transport is mediated by long tubules that are governed by Rab6 and PLA<sub>2</sub> activity (Sengupta et al., 2015).

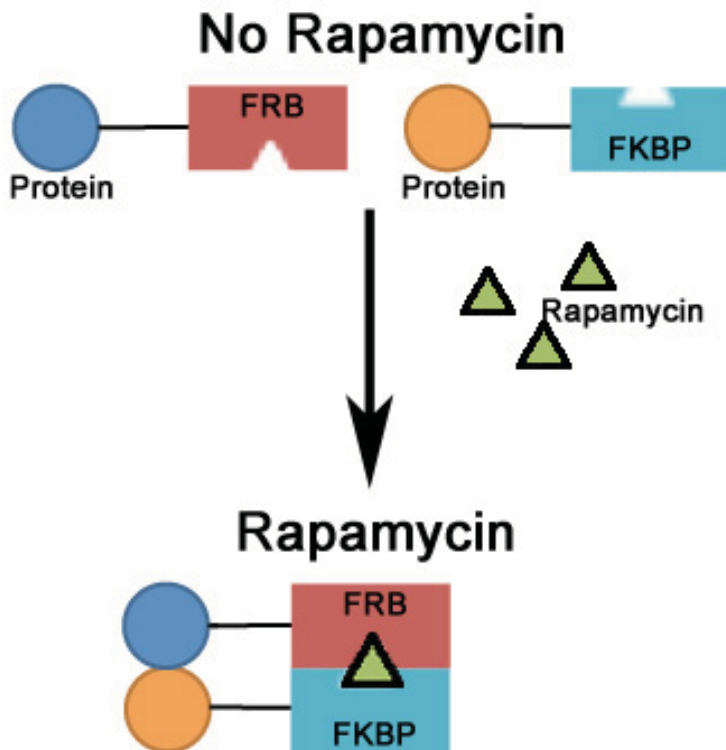


**Illustration 3:** Rapamycin-induced dimerization

FRB and FKBP bind to each other through rapamycin. This characteristic can be used to study protein interaction and localization. When FRB and FKBP are fused with proteins of interest, these proteins can be brought together within seconds after rapamycin addition. Blue and red circles may be fluorescent probes or protein of interest.

Although observations made using these probes may be valid, there may be non-desirable consequences when overexpressing these non-physiological probes. FRB is a subunit of mTOR, which is a master regulator of many essential processes within a cell, whereas rapamycin that causes the dimerization of FRB and FKBP blocks mTOR activity. Even at a low concentration (250nM), rapamycin may trigger many unwanted processes (adverse effects of mTOR inhibition). Functions of the probes cannot be ignored, as FKBP is an isomerase that acts as a

chaperone for proteins with proline residues. Negative effects of overexpressing these probes were never discussed. Sengupta and colleagues utilized this probe to highlight the interaction of the FKBP-ER protein and FRB-Golgi enzyme, and they assumed the binding of the two probes upon rapamycin addition was representative of the intrinsic movement of the Golgi enzyme to the ER (Sengupta et al., 2015). However, if rapamycin only triggers the two to bind, why can't ER protein-Golgi protein be visualized without rapamycin? It seems plausible that rapamycin is triggering the trafficking or there is a rapamycin derived carrier formation that induced the FRB-Golgi enzyme to travel.

Including these experiments, previous *in vitro* experiments so far have used engineered proteins, which are inevitably expressed at a high level compounded by the fact that the cell's steady-state is disturbed. It is, therefore, critical to develop tools that accurately represent endogenous Golgi enzymes at their undisturbed, stoichiometric ratio.

### **1.1.7. *in vivo* Correlative Microscopy**

In order to study the trafficking of biosynthetic cargo and Golgi enzyme within the Golgi, many correlative light-electron microscopy (CLEM) techniques have been developed. These techniques combine fluorescent light microscopy and electron microscopy. Cells are first observed by fluorescent light microscopy and then subsequently observed via electron microscopy after immunolabeling (van Rijnsoever et al., 2008; Spiegelhalter et al., 2010; Weering et al., 2010), or diaminobenzidine photoconversion (Meiblitzer-Ruppitsch et al., 2008; Grabenbauer et al., 2005). Often, EM labeling is done after sectioning by microtome, and the localization of protein relies on overexpression of the fluorescently-tagged protein.

### **1.1.7.a. GFP recognition after bleaching**

To visualize the Golgi enzymes *in vivo*, GFP recognition after bleaching (GRAB) technique has been developed (Grabenbauer et al., 2005). This technique uses an *in vivo* correlative light microscopy technique that overcomes spatial restrictions of immuno-EM for studies of small transport vesicles like COPI vesicles. It uses 3,3'-diaminobenzidine (DAB), which upon exposure to free radicals (generated by EGFP or other fluorescent proteins), precipitates into an electron-dense product that can be revealed through transmission electron microscopy. Resulting images are of sufficient quality to reveal detailed spatial information and are applicable to EM-based tomography. Also, the amount of precipitated DAB product is linear with initial fluorescence (Grabenbauer et al., 2005). In this way, the intra-Golgi stack and intracisternal distribution of EGFP or CFP tagged N-acetylgalactosaminyltransferase-2 (Grabenbauer et al., 2005) can be visualized. However, one drawback of the GRAB method is that it is based on the overexpression of the fusion protein, and as previously stated, this can possibly affect the enzyme's stoichiometric ratios and true steady-state distributions. Thus, a new type of probe for surveying protein localization must be developed (See section 1.3.1).

## **1.2. Lipid droplet**

Cellular lipids are stored within an organelle called lipid droplet (LD). LDs vary greatly in size ranging from 20nm to 100µm depending on cell type (Guo et al., 2009). Although this organelle had been regarded as a passive fat-storing organelle, the discovery of many LD-associated proteins have demonstrated that the LD is, in fact, a highly dynamic organelle that regulates lipid metabolism and overall cellular energy homeostasis (Kalantari et al., 2010). Similarly, the formation of LDs and fat liberation from LD are tightly regulated.

### **1.2.1. LD formation**

#### *LD structure*

LDs are composed of a neutral lipid core consisting mainly of triacylglycerol (TAG) and cholesteryl-ester (CE). Each LD is surrounded by a phospholipid monolayer (Martin and Parton, 2006) where hydrophobic tails of phospholipids are facing the core and hydrophilic head groups are facing the cytosol. This unique arrangement of phospholipids allows lipids to be contained within an aqueous environment.

#### *LD proteins*

Many LD-associated proteins are involved in lipid accumulation or for lipid hydrolysis. Among them, the perilipin family of proteins that modulate lipid metabolism is the most well characterized. Perilipin 1 (PLIN1) is thought to protect LDs until lipids are broken down by a hormone-sensitive lipase (HSL) (Gandotra et al., 2011). Adipose differentiation-related protein (ADRP/PLIN2) facilitates TAG accumulation (Imamura et al., 2002; Gao and Serrero, 1999; Gao et al., 2000). Tail-Interacting Protein of 47kDa (TIP47/PLIN3) and S3-12 (PLIN4) may have a role for packaging TAG (Dalen et al., 2004; Robenek et al., 2005; Lee et al., 2009). OXPAT (PLIN5) maintains the balance between lipogenesis and lipolysis by differential binding (Wang et al., 2011; Granneman et al., 2011). Proteins involved in LD fusion and fission are also found on the LD surface (See below).

Some LD-associated proteins are transported to the LD membrane using coatomer-dependent transport machinery. For instance, knockdown of GBF1 (GTP exchange factor for Arf1),  $\beta$ -COP (coatomer for COPI) or Sec13 (coatomer for COPII) reduced the level of adipose triglyceride lipase (ATGL) found on LD surface (Soni et al., 2009). BFA treatment (inhibitor for

ER to Golgi transport), dominant-negative or constitutively active Sar1 (GTPase for COPII formation), and dominant negative Arf1 (GTPase for COPI formation) also decrease ATGL delivery to LD (Soni et al., 2009). Knockdown of COPI subunits and loss of Arf1 function by Exo1, a selective inhibitor of Arf1 activity, results in reduced lipolysis in *Drosophila* (Beller et al., 2008).

### *LD formation*

Most cells across a species can store LD. The size, number, and composition of LD are heterogeneous within the same cell type and between different cell types (Herms et al., 2013). LDs are thought to form from the ER: neutral lipids (TAG and CE) are deposited within cytosolic leaflets of the ER membrane, and this accumulation forms a bulge that continues to grow until it pinches off into the cytosol (Hapala et al., 2011). Prior to separation, it is believed that there is a structural rearrangement of the ER membrane on the cytosolic side that allows the segregation of LD proteins (Hapala et al., 2011). LDs in non-adipose tissue have various TAG-CE ratios. Excessive fatty acid administration causes TAG-rich LDs, but CE-rich LDs can also be formed when protein translation is inhibited (by cycloheximide), independent of mTOR-signaling or autophagy (Suzuki et al., 2012).

It has been shown that ER stress causes the accumulation of intracellular lipids that results in LD formation (Lee et al., 2012; Fei et al., 2009). When there is excessive unfolded, misfolded or ubiquitinated proteins, they are sequestered within LD in order to alleviate ER stress (Ploegh, 2007). Under ER stress, toxic lipids may also be sequestered into LD, preventing their accumulation within the ER membrane. In this way, LD may play a protective role against lipotoxicity (Hapala et al., 2011). ER-localized stress responsive protein CREBH (cAMP

responsive element-binding protein, hepatocyte-specific) can also regulate lipogenic programs (Zhang et al., 2012) that can ultimately result in LD formation. Similarly, lipogenic programs activated by SREBP have also shown to trigger LD formation.

Size and number of LDs are highly regulated as LDs undergo fusion and fission. It has been suggested that fusion is SNARE-dependent (Boström et al., 2007). Western blot analysis of LD fraction and immuno-EM of cellular LDs confirmed that NSF (N-ethylmaleimide-sensitive-factor),  $\alpha$ -SNAP (soluble NSF attachment protein), SNAREs (SNAP receptors), SNAP23 (synaptosomal-associated protein of 23kDa), syntaxin-5, and VAMP4 (vesicle-associated membrane protein 4) are localized onto LDs (Boström et al., 2007). Furthermore, when these proteins are knocked down individually, or a dominant-negative mutant of  $\alpha$ -SNAP was microinjected, the rate of LD fusion decreased significantly (Boström et al., 2007). LD fusion is also affected by intact microtubule and motor protein dynein: There was a lower percentage of Oil Red stained-LDs when cells were treated with nocodazole (inhibits microtubule formation) and vanadate (lowers ATPase activity of dynein) (Boström et al., 2005). Fusion of LD may also be dependent on the availability of phosphatidylcholine (PC) since the knockdown of phosphatidylcholine cytidyltransferase (CCT), a rate-limiting enzyme for PC synthesis in *Drosophila*, caused LD fusion (Guo et al., 2008).

Fission of LDs has been observed in budding yeast (Long et al., 2012) and adipocytes (Marcinkiewicz et al., 2006). During G2 phase of budding yeast cell cycle, dumbbell-shaped LD indicative of LD fission was observed (Long et al., 2012). Furthermore, phosphorylation of LD protein, perilipin A causes LD fission, an observation similar to the administration of  $\beta$ -adrenergic agonist, isoproterenol (Marcinkiewicz et al., 2006).

## **1.2.2. LD breakdown**

### **1.2.2.a. Lipid breakdown by lipolytic pathway**

Lipid hydrolases mediate the degradation of LD-sequestered TAG by the control of extracellular signaling factors such as insulin and tumor necrosis factor (TNF) (Thiele and Spandl, 2008; Kershaw et al., 2006). One of the most characterized LD proteins is adipose triglyceride lipase (ATGL/PNPLA2), which catalyzes a rate-limiting step of TAG breakdown. In adipocytes, action of ATGL is tightly controlled by coordination of CGI-58 and perilipin 1A (Sahu-Osen et al., 2015; Schlager et al., 2015; Zagani et al., 2015). Under basal conditions, perilipin 1A is bound to CGI-58, preventing interaction with ATGL. Upon activation of PKA, perilipin 1A is phosphorylated, causing CGI-58 to dissociate into the cytosol. This ultimately enables lipase co-activation (Sahu-Osen et al., 2015). Now activated ATGL translocates to the LD, which then hydrolyzes TAG to diacylglycerol (DAG). Next, hormone-sensitive lipase (HSL) catalyzes DAG to monoacylglycerol (MAG), which in turn gets hydrolyzed to FA and glycerol by monoacylglycerol lipase (MGL) in the cytosol (Kershaw et al., 2006). Another LD lipase, PNPLA5 is also important for TAG breakdown from the LD, and it has been shown to be involved in autophagy by participating in autophagosome formation (Dupont et al., 2014). FAs liberated in this way undergo  $\beta$ -oxidation in mitochondria, and may also be re-esterified back to TAG for storage (Martin and Parton, 2006). In some conditions, where energy demand is high or if nutrients are scarce, liberation of FAs may be sped up by a process called lipophagy (See section **1.2.2.b**) (Singh et al., 2009). Interestingly, lipid breakdown by ATGL may not only be mere lipolysis since ATGL requires LC3 (microtubule-associated protein 1 light chain 1A/1B) for its lipolytic activity (Martinez-Lopez et al., 2016). Recent study shows that ATGL contains a

LIR (LC3 Interacting Region) domain, which allows its binding to the autophagosome marker, LC3. Upon LIR mutation, ATGL was not able to trigger lipid breakdown from LDs even in the presence of a lysosomal inhibitor (Martinez-Lopez et al., 2016). Also, HSL co-immunoprecipitates with LC3 in LD fraction of brown adipose tissue (BAT). At the same time, a trypsin protease protection assay on BAT autophagosomes revealed that ATGL and HSL were rather present on the outer autophagosome membranes than being on the inner membrane as cargos. Indeed, ATGL interacts with LC3 for its recruitment to LD and lipolytic activity.

### **1.2.2.b Lipid breakdown by lipophagy**

In addition to the action of lipases, lipid breakdown from LD can be mediated by an autophagic pathway (Singh et al., 2009). Autophagy is an intracellular mechanism for the degradation of cellular organelles and protein aggregates, which regulates the size and number of organelles (See section 1.2.5). Recently, it was shown that autophagic machinery is used for LD-specific breakdown called lipophagy. When key autophagic proteins such as Atg5 and Atg7 were knocked down by lentivirus-mediated RNA interference, size and number of LDs were increased in untreated and oleate loaded cells. In these cells, the relative amount of TAG were decreased, and the rate of  $\beta$ -oxidation had increased (Singh et al., 2009). Moreover, autophagosome marker LC3 was located around the LD, which was visualized by immunofluorescence and immuno-EM (Singh et al., 2009). This observation suggests that the LD is surrounded by autophagosomes for degradation.

### **1.2.2.c. Lipophagy through Kiss-and-Run**

Apart from canonical lipophagy that involves autophagosome formation, there is a non-canonical pathway called the Kiss-and-Run pathway. This type of lipophagy is distinct from the canonical lipophagy because it does not involve the autophagosome. In fact, this process is manifested by the direct fusion between the lysosome and the LD, where two organelles fuse transiently and then are separated. A small GTPase called Rab7 has been demonstrated to be indispensable for this Kiss-and-Run lipophagy (Schroeder et al., 2015). Indeed, Rab7, in starving conditions, localized to a subdomain of the LD, and the LD was bombarded by multiple lysosomes. Knockdown of Rab7 by siRNA reversed this phenotype as the LDs were enlarged (Schroeder et al., 2015).

Mechanisms that bring the two organelles together for the Kiss-and-Run lipophagy have not yet been elucidated. Nonetheless, some proteins that govern the movement of lysosome and LD may be involved. For example, BORC complex, a multi-subunit complex involved in lysosomal positioning, recruits a small GTPase, Arl8b to the lysosome and is held in place (Pu et al., 2015). Subsequently, BORC couples lysosome to kinesin motor, so it is plus-end microtubule-directed (Pu et al., 2015). Later, SKIP and kinesin are recruited to this site, moving lysosome towards the LD (Pu et al., 2015), and this is probably where RAB 7-positive domains within LD makes contact with lysosomes.

This transient docking of lysosomes to the LD surface may provide a quicker release of LD contents because there is no need for autophagosome formation (Schroeder et al., 2015). This process may certainly be less energy-costly. However, the mechanism by which the two organelles comprised of a phospholipid bilayer and a phospholipid monolayer, fuse very quickly before departing is unknown.

#### **1.2.2.d. Omega-3 fatty acid Eicosapentaenoic acid (EPA)**

Omega-3 fatty acids have been shown to have beneficial effects on overall health. They have been suggested to generate neuroprotective metabolites, lower blood pressure, and improve functions of blood vessels. A recent study suggested that they reduce lipid accumulation and lower cytotoxicity (Chen et al., 2015). A research group led by Li at Zhejiang University, China, demonstrated that EPA, a polyunsaturated fatty acid (20:5), induces autophagy by down-regulating Stearoyl-CoA desaturase 1 expression in hepatocytes, thereby inhibiting lipid accumulation and apoptosis (Chen et al., 2015). However, molecular mechanism by which EPA lowers lipid accumulation has not been elucidated clearly.

#### **1.2.3. Non-alcoholic fatty liver disease**

Non-alcoholic fatty liver disease (NAFLD) is a disease that affects a significant proportion of the population: 20 to 30% of adult population in North America (Dowman et al., 2010) and 90% of obese individuals are affected (Machado et al., 2006). It is manifested by the excessive accumulation of cytoplasmic LDs in the liver. An abnormal amount of fat leads to inflammation and scarring of the liver, which progresses to become non-alcoholic steatohepatitis (NASH). As the disease persists, scar tissue replaces liver, and the liver becomes cirrhotic (Hosseini and Saeed, 2011), which is susceptible to development of hepatocellular carcinomas (HCC) (Baffy et al., 2012). Abnormal accumulation of fat is the leading cause of the NAFLD. Thus, preventing the lipid accumulation, or enhancing lipid metabolism can slow down the disease progression. For this reason, studying these mechanisms will not only help us understand the disease, but it may also contribute to the discovery of potential treatment.

First, to understand the mechanism of TAG accumulation in the human liver, we determined the total protein profile of subcellular organelles from hepatocytes isolated from human livers with NAFLD, isolated from over 100 NAFLD patients' livers. Protein contents of the subcellular fractions were analyzed by mass spectrometry, and this experiment revealed many novel proteins localized to LDs. One of the proteins that came to our interest was endophilin B1, an N-BAR domain-containing protein involved in endocytosis.

#### **1.2.4. Endophilin family of proteins**

Endophilin B1 (SH3GLB1 or Bif-1) is a member of endophilin family that is known to participate in multiple cellular processes such as the regulation of vesicle fission (See **1.1.4.c**), endocytosis, mitochondrial morphology, and autophagy. Endophilins are highly conserved across species (Illustration 4), and in humans there are five forms. Endophilin A1, the most studied, binds to synaptojanin and acts to recycle neurotransmitter vesicles (Gallop et al., 2006). Endophilin A2 is ubiquitously expressed, and it stimulates the assembly and GTPase activity of dynamin 2 (Ross et al., 2011). Endophilin A3 is found in neurons and testis (Giachino et al., 1997). Endophilin B1 gene gives rise to three splice variants: B1a is ubiquitously expressed and B1b and c are brain specific (Modregger et al., 2003).

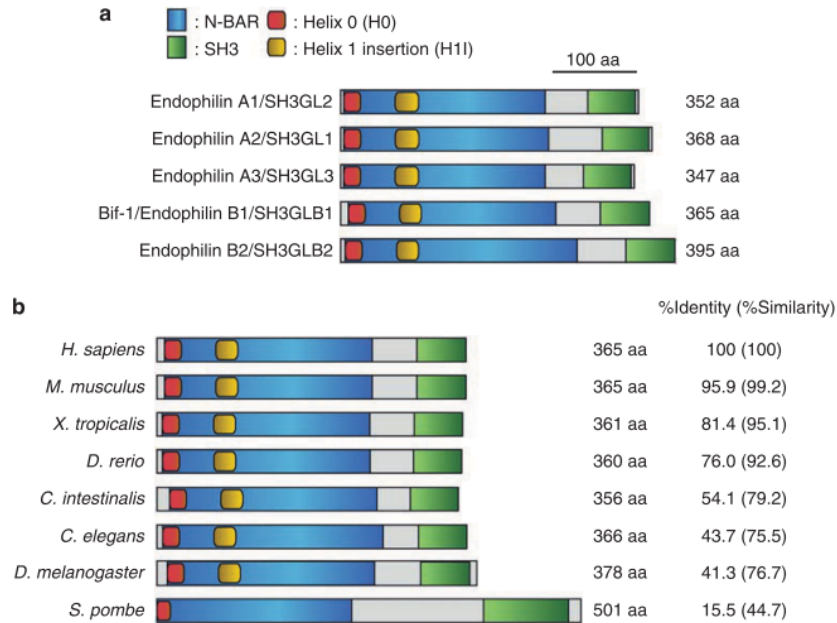


**Illustration 4:** Domains and structures of the endophilin family

There are five different isoforms of endophilin in humans (a), and endophilins are highly conserved across species (b). *Reprinted by permission from Macmillan Publishers Ltd on behalf of Cancer Research UK: Cell Death and Differentiation (Takahashi et al., 2009)*

**1.2.4.a. Domains and structures**

Structural analysis of endophilin reveals three functional regions that are essential for membrane binding *in vitro*: an N-terminal amphipathic helix (H0), an additional amphipathic helix termed insertion-helix (H1I), and a crescent-shaped region that is formed by dimerizing BAR (Bin/Amphiphysin/Rvs-homology) domains (Masuda et al., 2006a). The H0 helix is in the most N-terminal of endophilin, and the H1I helix is located within the BAR domain. The endophilin family of proteins (including A1, A2, A3, B1, and B2) shares these domains (Illustration 4).

Src-homology-3 domain (SH3) of endophilin binds to proline-rich regions (PRR) that is found in dynamin and synaptojanin. BAR domain promotes dimerization and membrane curvature generation (Illustration 4). Purified BAR domains facilitate liposome binding and tubulation *in vitro*, and cells expressing the BAR domain showed noticeable tubulation of the

plasma membrane *in vivo* (Masuda et al., 2006a). Through a liposome binding assay in the presence of variable salt concentrations, interaction between the BAR domain and the membrane was found to be electrostatic: At higher concentrations of salt (>150mM NaCl), the BAR domain falls off, but N- terminal BAR (N-BAR) domain does not (Gallop et al., 2006). Endophilin dimerizes through the BAR domain, and this rigidity of the crescent-shaped dimer is crucial for tight membrane tubulation; mutants made to form straight BAR domains creates a tube diameter greater than the wild type (Masuda et al., 2006a). Paramagnetic resonance spectroscopy showed that the H1I helix was inserted into phospholipids at a perpendicular angle (Gallop et al., 2006), and this insertion drives membrane curvature with the help of dimerized BAR main body (Gallop et al., 2006; Masuda et al., 2006a). In addition, H1I helix is responsible for liposome tubulation (Gallop et al., 2006; Masuda et al., 2006a) because its deletion in endophilin A1 resulted in only monomeric endophilin A1 *in vitro* (Gallop et al., 2006). Furthermore, the N-terminal amphipathic alpha-helix (H0) plays a role in membrane binding. Deletion of this H0 helix completely abolishes the membrane binding activity (Takahashi et al., 2011). Mutational studies revealed that dimerization through the BAR domain and the dimer's rigidity is affected by this insertion helix (Cui et al., 2009). Thus, coordinated actions of the N-terminal helix (H0), helix 1 (H1I), and the rigid crescent-shaped BAR domain together increase endophilin's membrane bending (Illustration 5). In fact, this membrane binding activity of endophilin B1 has been seen in an *in vitro* experiment of purified endophilin B1 incubated together with Bax and giant unilamellar vesicle (GUV). The results revealed that endophilin B1 binds to GUV and caused tubulation into smaller liposomes (Rostovtseva et al., 2009).

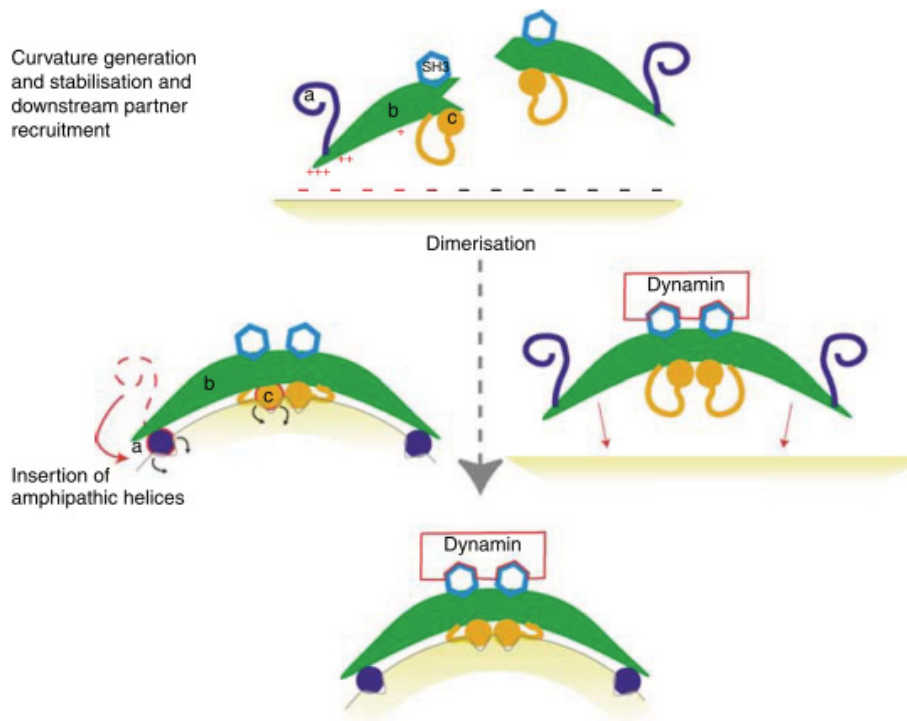


**Illustration 5:** Membrane curvature driven by endophilin

Endophilin generates membrane curvature as a dimer. Endophilin dimerizes through BAR domain, and the collective efforts of two amphipathic helices (a, c), BAR body (b), and dynamin causes the membrane to bend. *Reprinted by permission from John Wiley and Sons: The EMBO Journal (Gallop et al., 2006)*

**1.2.4.b. Mitochondrial morphology**

Interestingly, endophilin B1 has been shown to be important in the maintenance of mitochondrial morphology. Endophilin B1 is required for the regulation of mitochondrial outer membrane dynamics because siRNA knockdown of endophilin B1 and overexpression of truncated endophilin B1 resulted in profound damage to the mitochondrial network (Karbowski et al., 2004). Three distinct shapes of mitochondria have been seen when endophilin B1 is knocked down in HeLa cells; randomly broken, rounded up and peripheral, or non-tubulated and perinuclear (Karbowski et al., 2004). On many occasions, the outer mitochondrial membrane was dissociated from the matrix (Karbowski et al., 2004). In mouse primary cortical neurons,

knockdown of endophilin B1 also resulted in fragmented and depolarized mitochondria while the expression of proteins involved in mitochondrial fusion or fission remained unaffected (Wang et al., 2014). Although normally cytosolic, endophilin B1 moves to the mitochondria and forms patches around them when apoptosis is triggered by caspase inhibitors zVAD-fmk and STS (Karbowski et al., 2004). The mitochondrial network is impaired when a mutant endophilin B1 lacking the N-terminal region is overexpressed, and this observation confirms the importance of the N-terminal region (Karbowski et al., 2004). Given these observations and the fact that endophilin interacts with dynamin at SH3 domain, it is plausible that endophilin B1 coordinates mitochondrial tubulation process.

#### **1.2.4.c. Clathrin-mediated endocytosis**

Clathrin-mediated endocytosis (CME) is a process that uses receptor proteins within clathrin-coated membrane regions in the cell membrane. Nutrients, hormones, and other ligands are shuttled into small invaginations that make up small vesicles, and subsequently, they move to the cell interior. CME controls the uptake of not only receptor bound molecules, but the turnover of many membrane-bound proteins. The role of endophilin in endocytosis has been shown in mice (Milosevic et al., 2011), lampreys (Sundborger et al., 2011; Gad et al., 2000; Farsad et al., 2001), and *Drosophila* (Verstreken et al., 2002; Schuske et al., 2003).

Endophilin's function in endocytosis has been well described in lamprey neurons. Blockage of endophilin A's SH3 domain by an antibody interferes with endocytosis progression from an early to late stage (Ringstad et al., 1999). In these neurons, the number of synaptic vesicles reduced dramatically, and numerous clathrin-coated pits were found without constricted necks (Ringstad et al., 1999; Gad et al., 1998). Also, endophilin (isoform not specified) was

shown to be essential presynaptically at the neuromuscular junction of *Drosophila* because cells lacking endophilin were not able to retrieve synaptic membrane and vesicles from the presynaptic terminal (Verstreken et al., 2002). This requirement of endophilin in synaptic vesicle endocytosis may be due to its ability to recruit and stabilize synaptojanin (Schuske et al., 2003) and dynamin (Sundborger et al., 2011): In *Drosophila*, the absence of endophilin mislocalizes synaptojanin but not vice versa (Schuske et al., 2003); At lamprey synapses, endophilin A1-dynamin complex promotes budding of new synaptic vesicles (Sundborger et al., 2011). It appears that endophilin A1's SH3 domain recruits dynamin to clathrin-coated pits. The amount of dynamin recruited to clathrin-coated pits and vesicle tubulation increase in the presence of endophilin A1. Also, in another study done in lamprey, blocking the interaction of SH3 domain with dynamin resulted in un-cleaved vesicles with elongated neck (Sundborger et al., 2011). Rather than directly binding to clathrin, endophilin A1 associates with dynamin and synaptojanin. Sundborger and colleagues postulated that the endophilin A1-dynamin complex forms at the neck of emerging clathrin-coated vesicles, where endophilin A1 may guide dynamin binding. This pre-fission complex then constricts the neck to facilitate vesicle fission. Synaptojanin that is recruited earlier or at this stage may compete with dynamin for endophilin A1 binding, and it has been shown that synaptojanin plays a role in clathrin uncoating (Sundborger et al., 2011). However, deletion of endophilin did not affect the exocytosis in the abdominal neuromuscular junction of early third instar *Drosophila* larvae (Verstreken et al., 2002), suggesting that endophilin does not participate in exocytosis of synaptic vesicles. In mice, loss of three mouse endophilins impair synaptic transmission, and partial loss of endophilin causes neurological defects such as epilepsy and neurodegeneration (Milosevic et al., 2011).

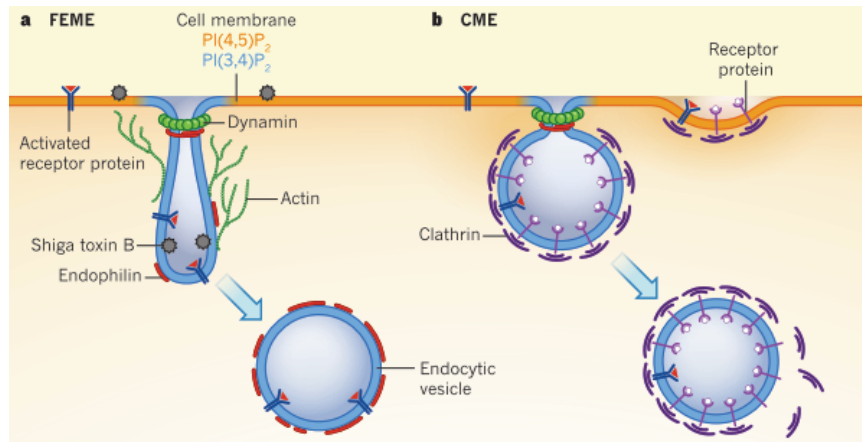


**Illustration 6:** Endophilin in endocytosis

Endophilin is involved in clathrin-independent endocytosis, FEME (a), and clathrin-mediated endocytosis, CME (b). *Reprinted by permission from Macmillan Publishers Ltd on behalf of Cancer Research UK: Nature (Haucke, 2015)*

**1.2.4.d. Clathrin-independent, Fast Endophilin-Mediated Endocytosis (FEME)**

In a recent study, endophilin A has been shown to be essential in clathrin-independent endocytosis. This pathway has demonstrated to mediate the endocytosis of growth factors, and it is termed Fast Endophilin-Mediated Endocytosis (FEME). In a study by Boucrot and colleagues, endophilin was recruited to clathrin-free membrane sites at the leading edge when  $\beta_1$ -adrenergic receptor was activated (Boucrot et al., 2014). As a result, the receptor was rapidly internalized into small vesicles and tubules. When clathrin and other partners were depleted, this process still proceeded. However, when endophilin A1, A2, and A3 were depleted, this process was abrogated. Also, the morphology of the vesicles formed in this process did not resemble other clathrin-independent pathways such as macropinocytosis. These researchers concluded that this process involving endophilin is independent of clathrin. Without endophilin, receptors ( $\beta_1$ -adrenergic receptor, proline-rich motifs within TIL of  $\alpha_{2a}$ -AR, dopaminergic receptors 3 and 4, and muscarinic acetylcholine receptor 4) did not get internalized, but rather accumulated at the PM and continued to signal. The accompanying paper by Renard and colleagues demonstrated

that bacterial toxins such as Shiga toxin B from *Shigella* hijacked this process to gain entry into the host cell (Renard et al., 2015). Endophilin A2 coats tubule-shaped membrane invaginations where Shiga toxin B binds to the cell membrane. Subsequently, endophilin A2 would work together with dynamin to detach the tubule from a growing vesicle, internalizing Shiga toxin B. Proposed mechanisms for the FEME include the following: Firstly, membrane-bound receptor proteins or bacterial toxins such as Shiga toxin B get activated, and trigger the conversion of PI(4,5)P<sub>2</sub> to PI(3,4,5)P<sub>3</sub>, which subsequently gets converted to PI(3,4)P<sub>2</sub>. Afterward, PI(3,4)P<sub>2</sub> binds to lamellipodin, which is located at the leading edge of the cell. Lamellipodin binds to endophilin, so endophilin accumulates at the leading edge. Finally, endophilin induces the formation of vesicles that become internalized, transporting their cargo to the cell interior (Boucrot et al., 2014). Cell specificity of FEME or the proportion of FEME that takes place in comparison to other types of endocytosis has not been investigated (Haucke, 2015). However, FEME may be required in neurons because they use both CME and clathrin-independent endocytosis to facilitate the internalization and release of neurotransmitter (Haucke, 2015).

### **1.2.5. Autophagy**

Autophagy is an intracellular mechanism for degradation of cellular organelles and protein aggregates, and this process thereby regulates the size and number of organelles. Interestingly, growing evidence suggests that endophilins participate in autophagy. There are different types of autophagy: macroautophagy, microautophagy, chaperone-mediated autophagy, and non-canonical autophagy. Through autophagy, defective or overly abundant organelles are also removed; Peroxisomes by pexophagy (Monastyrska and Klionsky, 2006), mitochondria by mitophagy (Kubli and Gustafsson, 2012), ER by ER-phagy (Khaminets et al., 2015), and

ribosome by ribophagy (Bąkowska-Zywicka and Tyczewska, 2009). Non-canonical autophagy for lipid droplets (LD) has been observed and is called Kiss-and-run lipophagy (Schroeder et al., 2015).

#### **1.2.5.a. Role of endophilin B1 in macroautophagy**

For macroautophagy (also called classical autophagy), an isolation membrane (phagophore) elongates to enclose cellular materials for degradation, resulting in a double-membraned organelle called an autophagosome. Once matured, autophagosomes fuse with lysosomes and become autophagolysosomes. This fusion leads to the degradation of enclosed materials along with inner membranes. In addition to basal autophagy (Seino et al., 2013), autophagy is triggered by nutrient starvation or other stress conditions.

A master regulator of cell growth, mTOR (mammalian target of rapamycin), has been shown to regulate the early steps of autophagosome formation. Upon activation, Class III phosphatidylinositol 3-kinase (PI3KC3) forms a complex with Beclin1-UVRAG, and endophilin binds to UVRAG (UV radiation resistant-associated Gene protein) through its SH3 domain during starvation-induced autophagy (Takahashi et al., 2007). Beclin1 and UVRAG play a central role in autophagy as they form a core subunit of the PI3K complex (He et al., 2013; Margariti et al., 2013). Atg9, one of the Autophagy-related gene and protein (Atg), has been shown to gather membranes from the Golgi, where the trafficking of Atg9 and fission of Golgi membranes require endophilin B1 (Takahashi et al., 2011; He et al., 2013). Endophilin's membrane binding and tubulating activity may be contributing to this process. For elongation of autophagosome membranes, there are series of Atg proteins. Atg12, the first Atg protein shown for autophagy, acts similar to ubiquitination enzymes. Atg7 is an E1-like enzyme that conjugates

Gly186 of Atg12 to Cys507 of Atg7 (Tanida et al., 1999). Then Atg12 is transferred to E2-like enzyme Atg10 (Shintani et al., 1999). Atg12 is conjugated to Lys149 of Atg5 (Mizushima et al., 1998). Now, Atg12-Atg5 conjugates to Atg16 and form dimeric complex (Fujioka et al., 2010; Kuma et al., 2002). Finally, Atg12-Atg5-Atg16 act as an E3-like enzyme, which has an important regulatory role for Atg8 (LC3) conjugation (Hanada et al., 2007; Mizushima et al., 2001). It promotes the transfer of LC3 from Atg3 to the PE substrate by stimulating the activity of Atg3 (shown *in vitro*) (Hanada et al., 2007). This PE conjugation turns LC3-I to LC3-II, and now LC3-II becomes capable of the binding membrane. Recruitment of LC3 is essential for the extension, curvature, cargo recognition (Pankiv et al., 2007), and closure of the isolation membrane to complete autophagosomes (He and Klionsky, 2009). Often, the amount or number of LC3 puncta is used as a marker for autophagosome. Finally, with the help of SNAP29/Syntaxin17/HOPS (Homotypic fusion and protein sorting) complex and VAMP8, autophagosomes fuse with lysosomes for degradation (Jiang et al., 2014; Diao et al., 2015).

#### *Endophilin B1 in lipid metabolism*

Endophilin B1 was shown to regulate lipid metabolism in a mouse model. Endophilin B1-deficient mice resulted in reduced basal rate of adipose tissue lipolysis and failed to control the size of LDs (Liu et al., 2016). Eventually, these mice developed obesity, insulin resistance, and adipocyte hypertrophy upon aging. In addition, endophilin B1 deficiency downregulated the expression of Atg9a and LAMP1 in the adipose tissue (Liu et al., 2016).

### **1.2.5.b. Microautophagy**

Microautophagy is the direct engulfment of cytosolic cargo by lysosomes, and it has been best studied in yeast. Whereas macroautophagy involves an autophagosome, microautophagy does not. Microautophagy is often regarded as a non-selective lysosomal degradation process, where the lysosome membrane is invaginated or projected to arm-like protrusions to encapsulate cytoplasmic materials. Following the encapsulation, degradation by hydrolases proceeds. Certain organelles can be degraded by selective microautophagy, and these processes are termed micromitophagy for mitochondria, micronucleophagy (piecemeal microautophagy of nucleus), and micropexophagy for peroxisomes (Mijaljica et al., 2011). Damaged, dysfunctional, or nutrient-deficient mitochondria were degraded by micromitophagy. Although some factors have been identified, direct mechanism of mitochondria recognition and involvement of cytosol have not been elucidated fully (Kiššova et al., 2007). Nitrogen, carbon starvation as well as rapamycin have been shown to promote the interaction between the vacuole and outer nuclear membrane. Eventually, a portion of the nucleus is sequestered into a vacuolar lumen (Millen et al., 2009). However, it is not clear how essential nuclear constituents are prevented from micronucleophagy. Also, the precise mechanism of how micronucleophagy proceeds is yet to be discovered (Mijaljica et al., 2011). For degradation of peroxisomes, the micropexophagy-specific membrane apparatus (MIPA) is formed, which mediates fusion between the tips of the invaginating vacuoles (Li et al., 2012). Following peroxisome engulfment, the membrane is detached, and encapsulated peroxisomes are lysed within the low pH environment. Formation of the MIPA involves a series of Atg proteins and additional pexophagy-specific factors. Whether or not these mechanisms of microautophagy are conserved in higher eukaryotes is unclear (Mijaljica et al., 2011).

### **1.2.5.c. Chaperone-mediated autophagy**

Chaperone-mediated autophagy (CMA) is a selective autophagy mediated by chaperones, lysosomal heat shock proteins, and lysosome-associated membrane glycoprotein 2A (LAMP2A). It is also called the selective lysosomal pathway, KFERQ pathway, or direct lysosomal pathway as this process involves direct recognition of substrate, and KFERQ is a recognition sequence (Kaushik and Cuervo, 2008). CMA was first proposed as a selective delivery of cytosolic proteins to lysosomal membranes.

One of the features that make CMA unique is that chaperones bind to protein substrates to assist in unfolding prior to lysosomal translocation. LAMP2A was shown to act as a receptor, mediating binding of the chaperone and substrate complex to lysosomal membranes (Cuervo and Dice, 1996). Although there are three splice variants available from a single LAMP2A gene, only one form is shown to be necessary. LAMP2A, a single-span membrane protein (type I) (Schröder et al., 2007), exists as a monomer when chaperone-substrate complex binds, but upon binding, they are multimerized into a high-molecular-weight complex that is necessary for membrane translocation (Bandyopadhyay et al., 2008).

## **1.3. Rationale of the study**

### **1.3.1. New generation of probes to study Golgi**

Indeed, the field of Golgi biology has been flooded with observations favoring either of the two well-established models. To date, there are overwhelming *in vitro* and proteomics results (Lanoix et al., 1999; Gilchrist et al., 2006) that show preferential incorporation of Golgi-resident enzymes in COPI vesicles. Despite this, the cell biology community seems reluctant to accept the CMPM, in which COPI plays major roles in the recycling of Golgi-resident enzymes. They still

challenge researchers to provide corresponding proof *in vivo*. To clarify this unsettled matter, we have developed a new generation of antibody-based probes, termed fusion antibodies. It is constructed so that it can act as a probe to represent the location of endogenous Golgi-resident enzymes *in vivo*. The fusion antibody can be expressed within the cell such that the antibody portion can bind to the endogenous Golgi enzyme, where its fluorescent protein portion enables their visualization. Therefore, I hypothesize that the fusion antibody accurately represents how endogenous Golgi-resident enzymes are retained and recycled. Additionally, unique characteristics of the fusion antibody combined with *in vivo* correlative photo-oxidation microscopy will reveal the ultrastructural location of the bound Golgi enzyme and overcome current limitations discussed earlier. Through this method, I aim to study the behavior of Golgi-resident glycosyltransferases and provide further insights and evidence to clarify intra-Golgi transport.

### **1.3.2. Functional elucidation of endophilin B1 as a novel LD protein**

Based on these studies, we propose that endophilin B1 may affect lipophagy. Indeed, our study reveals that endogenous endophilin B1 localizes onto the lipid droplet of human fatty liver frozen sections. In the presence of EPA that enhances lipophagy, endophilin B1 localizes on LD surface. Based on these preliminary observations, this study aims to elucidate functions of endophilin B1 on lipophagy. Furthermore, we hypothesize that endophilin B1 mediates lipophagy by causing LD fission and facilitating the Kiss-and-run lipophagy in the presence of EPA.

## **Chapter 2: Materials and methods**

## 2.1. Reagents and antibodies

### *Reagents*

Atglistatin (#530151) was purchased from *EMD Millipore Corporation* (California, USA). Ampicillin (#A9518), oleic acid (#O1008), Brefeldin A (#B7651), Bafilomycin A 1 (#B1793), NaCl (#BP358-1), KH<sub>2</sub>PO<sub>4</sub> (#P285-500), MgCl<sub>2</sub> (#M2670), Fish skin gelatin, Saponin (#47036), Mowiol, NH<sub>4</sub>Cl (#A9434), poly-L-Lysine (#P4707), bovine serum albumin (#A7906), bovine serum albumin fatty acid free (#A6003), Tween 20 (#P7949), HEPES (#H3375), PMSF (#P7626) anti-FLAG® M2 Affinity Gel (#A2220) and 3X FLAG® peptide (#F4799) were purchased from *Sigma-Aldrich* (Ontario, Canada). Guanidine hydrochloride (#EL200-002-3), DMSO (#D-128), glycine (#BP381-5), CaCl<sub>2</sub> (#C70-500), KCl (#BP366-500), Geneticin® (#11811098), microscope slide (#12-550-A3) and microscope cover glass (#12-545-80) were purchased from *Fisher Scientific* (Quebec, Canada). FuGENE HD Transfection Reagent, SDS (#11-667-289-001) cOmplete™, EDTA-free (#04693132001) and Tris base (#11-814-273-001) were purchased from *Roche Ltd* (Laval, Quebec, Canada). ECL detection kit (#NEL104001EA) was purchased from *Perkin Elmer* (Massachusetts, USA). Paraformaldehyde (#CAS30525-894) was from *Mecalab Ltd.* (Quebec, Canada). β-Mercaptoethanol, Protein A-HRP conjugate (#170-6222), Goat anti-mouse HRP-conjugate (#170-6216), Precision Plus Protein™ WesternC™ standards (#161-0373), ammonium persulfate (#161-0700), TEMED (#161-0800), 2-mercaptoethanol (#210006565) and Bio-Rad DC Protein Assay (#500-0116) were all purchased from *Bio-Rad* (Ontario, Canada). Nile Red (#N1142), LysoTracker Blue DND-22 (#L7525), UltraPure agarose (#16500-100), OptiMEM (#31985), Bodipy 493/503 (#D3922), Bodipy 558/568 (#D2219), 0.25% trypsin-EDTA (#25200-056), hygromycin (#10687010), Lipofectamine (#13778-150) and Blastidicin (#A1113903) were purchased from *Invitrogen*

(California, USA). Triton X-100 (#17-1315-01) was purchased from *PlusOne*. LB agar (#LBA408.500) and LB broth (#LBL405.1) were purchased from *BioShop* (Ontario, Canada). Kanamycin monosulfate (#400-145), DMEM (#319-005-CL), Penicillin and Streptomycin (#450-201-EL), were purchased from *Wisent* (Quebec, Canada). Plasmid Maxiprep (#12262) was purchased from *Qiagen* (Hilden, Germany). Gel and PCR clean-up and In-Fusion® HD Cloning Plus (#638909) were purchased from ClonTech (California, USA). Hyclone Fetal Bovine Serum (#SH30071.01) was purchased from *GE Healthcare* (Quebec, CA). Sodium phosphate dibasic (#84486-300) and sodium phosphate monobasic (#84456-380) were purchased from *Anachemia* (Quebec, Canada). E.D.T.A (#A1316) was purchased from *Research Organics* (Ohio, USA). His-Spin Protein Miniprep (#P2002) was purchased from *Zymo Research* (California, USA). Eicosapentaenoic Acid (#90110.1) was purchased from *Cayman Chemical* (Michigan, USA).

### *Antibodies*

For Western blot analysis, rabbit N11 polyclonal antibody recognizing human GalT polypeptide was used according to the protocol described previously (Watzel et al., 1991). For immunofluorescence, monoclonal purified mouse antibody against GalT was used according to the protocol described previously (Kawano et al., 1994). Rabbit polyclonal antibody recognizing myc-tag was used according to the protocol described previously ((Evan et al., 1985).  $\beta$ -Tubulin (#sc-9104), PLIN1 (#sc-67164), and Endophilin B1 (#sc-374146) used for indirect immunofluorescence were purchased from *Santa Cruz Biotechnology* (Texas, USA). Endophilin B1 (#IMG-265A) used for Western blot was purchased from *IMGENEX* (California, USA). Monoclonal Anti-FLAG M2 (F3165) was purchased from *Sigma-Aldrich*. LAMP1 (#25630) and

LC3 (#ab48394) were purchased from *AbCam* (Cambridge, United Kingdom). Atg5 (#2630) was purchased from *Cell Signaling* (Massachusetts, USA). The LC3 antibody used for indirect immunofluorescence (NB600-1384) and Western blot (NB100-2220, CZ) were purchased from Novus Biochemicals (Colorado, USA). AlexaFluor 488 (#A21206, #A21202), AlexaFluor 568, AlexaFluor 594 (#A11058, #A21235), and AlexaFluor 647 (#31573) were all purchased from *Invitrogen* (California, USA).

### *Preparation of Eicosapentaenoic Acid*

EPA was dissolved in ethanol prior to addition of 5N NaOH, which is evaporated under a stream of nitrogen gas. 150mM NaCl is added as the solution is being mixed and warmed up to 60°C. Once Na-EPA is fully dissolved, ice cold 20% BSA is added. Fully dissolved solution is filtered through 0.22µm filter and aliquoted to store at -20°C. To use, this 10mM stock EPA was diluted to 0.4mM in growth media.

## **2.2. Cell culture, transfection, and generation of inducible cells**

### *Cell culture*

HeLa cells were grown in DMEM with 10% FBS and 100U/mL penicillin and 100mg/mL streptomycin. HepG2 cells were grown in DMEM with 10% FBS, 100U/mL penicillin and 100mg/mL streptomycin, and 10mM HEPES pH 7.4. T-REx HeLa cells inducibly expressing EGFP or BirA constructs were grown in above media with the addition of 2µg/ml blasticidin and 100µg/ml hygromycin B. T-REx Hek293 cells inducibly expressing EGFP, mTurquoise or BirA were grown in above media with the addition of 10µg/ml blasticidin and

50µg/ml hygromycin B. For amino acid starvation, cells were washed with starvation media (140 mM NaCl, 1mM CaCl<sub>2</sub>, 1mM MgCl<sub>2</sub>, 5mM glucose, and 20mM Hepes, pH 7.4) before incubation with starvation media plus 1% BSA. All cells were incubated at 37<sup>0</sup>C and 5% CO<sub>2</sub>.

### *Transfection*

Cells were transfected using FuGENE HD according to the manufacturer's instructions. For all transfections, 1µg of plasmid DNA was used unless stated otherwise. Cells were transfected in 10% FBS for 16-24hours.

### *Induction of LD formation*

To induce LD formation, 0.2mM oleic acid (100mM stock prepared in ethanol) was diluted in complete media and incubated 30 minutes at 37<sup>0</sup>C water bath prior to addition.

### *Generation of stable or inducible cells*

HeLa cells stably expressing fusion antibody were generated after being selected in DMEM with 10% FBS, 100U/mL penicillin, 100mg/mL streptomycin, and 400µg/ml G418 media for four weeks. Upon picking up positive clones, the G418 concentration was reduced to 100µg/ml.

HeLa cells expressing endophilin B1\_EGFP/FLAG-BirA were generated after being selected in selection media containing 4µg/ml blasticidin and 200µg/ml hygromycin. Flp-in T-REx HeLa cell line is a gift of Dr. Stephen Taylor from Faculty of Life Sciences University of Manchester, United Kingdom. To generate cells inducibly expressing Endophilin B1-EGFP,

primers flanking pCDNA/FRT/TO were generated. Primer sequences are listed in the table below. The gene of interest was amplified with flanking ends by PCR, then it was inserted into NotI site of pCDNA/FRT/TO plasmid by homologous recombination (In-Fusion HD Cloning Kit). Endophilin B1-BirA constructs were generated the same way. Primer sequences are listed in the table below.

**Table 2-1: Primer sequences for endophilin B1**

<b>Primer</b>	<b>Primer Sequence</b>
<b>For_EGFP</b>	TGGAATTCTGCAGATATCGCCACCATGAATATCATGGACTTCAACGTG
<b>Rev_EGFP</b>	CTTGCTCACCATGATATTGAGCAGTTCTAAGTAGGTAATT
<b>For_BirA</b>	CGCGCCATAGCGGCCACCATG AATATCATGGACTTCAACGTG
<b>Rev_BirA</b>	TCCTTCATTGCGGCCGCATTGAGCAGTTCTAAGTAGGTAATT

### **2.3. Fusion antibody construction**

Fusion antibody was constructed based on Peipp et al., 2004 where murine Ig k-chain leader sequence, ScFv for CD7, GFP and 6His tags were constructed under CMV promoter (Peipp et al., 2004). The ScFv consisted of heavy chain variable region followed by a linker (GGGGS)<sub>4</sub> and a light chain variable region.

Hybridoma cells which express highly specific and efficient monoclonal antibody against GalNacT2 and GalT were sent to Novoprotein. Novoprotein extracted total RNA, purified mRNA, reverse transcribed to generate cDNA. From this, variable domains of a heavy chain and a light chain were PCR-amplified by using mouse IgG primer set. Subsequently, murine Ig k-chain leader sequence, heavy chain variable region, a linker, a light chain variable region, EGFP, and 6HIS were sub-cloned into pCDNA3.1 for expression. Design specifications regarding fusion antibody construction were delivered from our laboratory to Novoprotein.

## **2.4. Knockdown by siRNA**

Endophilin B1 siRNA was purchased from Dharmacon, (M017086-01-0005), siGENOME human SH3GLB1, SMARTpool, 5nmol. Cells were seeded on poly-L-lysine coated 35mm dish at 100,000cells/ml, and the siRNA was transfected at 50-100pmol final concentration using RNAiMAX and OptiMEM. Four hours after transfection, DMEM with 10% FBS was applied until following day. Second siRNA transfection was done at 50pmol final concentration following the manufacturer's directions. To see the effect of endophilin KD on LD, 0.2mM oleate was applied for 6 hours on the fourth day. To see the effect of endophilin KD on EPA mediated lipophagy, 0.2mM oleate was applied for 16 hours followed by 6 hours of 0.4mM EPA. Atg5 siRNA was purchased from Life Sciences (#HSS114103), Stealth RNAi. Cells were seeded at 200,000cells/ml, and 50pmol of siRNA was transfected with RNAiMAX and OptiMEM. 72 hours after transfection, 0.2mM oleate was applied for 16 hours followed by 6 hours of 0.4mM EPA.

## **2.5. Tandem affinity purification of fusion antibody**

T-REx Hek293 EGFP-FSAB-RGS6His3FLAG cells were plated at 40% confluency into 3 x 15 cm plates. Tetracycline was added at 1µg/ml for 24 hours for induction of fusion antibody. Following wash with 2x PBS, cells were scraped with 500µl cold RIPA buffer (25mM Tris pH 7.4, 100mM NaCl, 0.5% NP-40, 0.5% Na deoxycholate, 50mM NaF, 1x Complete™). Harvested cells were rotated 15 minutes at 4°C then centrifuged at 13,000rpm for 20 minutes at 4°C. The supernatant is cleared lysate. His-tagged fusion antibody was purified from the cleared lysate by using Zymo His-spin Protein Miniprep™ according to manufacturer's instructions. His-tagged fusion antibody was eluted with 30µl elution buffer. The eluate from this purification was further

purified by using anti-FLAG M2 Affinity Gel according to manufacturer's instructions. FLAG-tagged fusion antibody was eluted with 3X FLAG® peptide (100ng/μl), three times with 50μl each. To analyze, an equal volume of each sample (cleared lysate, flow-through, wash, and eluate) was taken and loaded onto 10% SDS gel. After the transfer, PVDF membrane was blotted against FLAG® antibody.

## **2.6. Indirect immunofluorescence and fluorescent microscopy**

For indirect immunofluorescence, cells were grown on glass coverslips at least 16hours prior to treatment. Seeding density differed depending on experiments: 200,000cells/ml for TLC and transfection experiments; 100,000cells/ml for knockdown and live cell experiments. Following experiments, cells were fixed using 3% formaldehyde with 0.1mM CaCl<sub>2</sub> and 0.1mM MgCl<sub>2</sub>. The rest of indirect immunofluorescence protocol was processed as described in *Gannon, PLoS one 2014*.

Human liver cryosections were cut from isopentane frozen tissue with a 6-9 micron thickness. The tissue samples were fixed using 3% formaldehyde with 0.1mM CaCl<sub>2</sub> and 0.1mM MgCl<sub>2</sub> for 20 minutes before washing in PBS. The fixed samples were submerged in 6M guanidine hydrochloride for 10 minutes before being permeabilized by 0.2% Triton x100 for 20 minutes. They were blocked using 10% goat serum for 30 minutes. Both primary and secondary antibodies were diluted in 5% goat serum at concentrations recommended by manufacturers' instructions. Primary antibodies were incubated for 60 minutes, and secondary antibodies were incubated for 45 minutes. Following PBS wash, coverslips were mounted by Mowiol.

### *Confocal microscopy*

To capture images, Zeiss LSM780 was used. For DAPI and LysoTracker blue, 405nm Diode laser was used. For Alexa 488 and Bodipy 493/503, Argon Multi-line laser was used. Alexa 568, Alexa 594, and Nile Red were excited by 561nm DPSS laser. Alexa 647 was excited by HeNe laser. For all images, 63x/1.40 oil DIC Plan-Apochromat was used. For detection of fusion antibody and endophilin B1, GaAsP detector was used.

### *Fluorescent microscopy*

Endogenous endophilin B1 was observed using Zeiss Axiovert 200M fluorescent microscope with Hal100/HBO100 illuminator and FluoArc lamp. Images were captured with AxioCam MRm camera.

To capture live cell images, Olympus IX81 Disk Spinning Unit microscope was used. Fluorophore was excited by X-Cite series 120Q EXFO excitation light source. Images were taken with QuantEM 512SC CCD camera at various exposure length and intervals.

## **2.7. Mass spectrometry, generation of heat map and staging**

Resected liver tissue or liver tissue derived from donors was processed for quantitative LC-MS/MS. Briefly, Liver homogenate (Hom) was subjected to subcellular fractionation using sucrose gradients to enrich for cytosol (Cyt), plasma membrane (PlsM), mitochondria (Mit), smooth (SER) and rough (RER) endoplasmic reticulum, nuclei (Nuc), cytoplasmic lipid droplets (CLDs) and Golgi/endosome/lysosomes (GEL). Proteins were precipitated using acetone, and

approximately 20 $\mu$ g protein was subjected to SDS-PAGE. Each gel lane was divided into 20 slices, each subjected to in-gel trypsin digestions followed by acetonitrile-based elution. Peptides were then analyzed by LC-MS/MS and, searched against the human database NeXtProt using Mascot and validated using Scaffold to ascertain statistical significance. Proteins were identified with a minimum of two independent peptides, each at >95% significance. False discovery rate for the entire dataset was < 0.01%. Proteins were quantified through the spectral count, normalized and displayed through Java TreeView. Selected protein distributions were exported from Java TreeView and imported into Adobe Illustrator for final assembly. Increasingly red indicates increasingly high protein expression level.

For staging, each liver tissue was independently scored for degree of steatosis, inflammation and fibrosis and divided into 4 categories, low NAFL (low steatosis with no fibrosis), NAFL (medium to high steatosis), inflammation (NASH) and cirrhosis as described in Kleiner et al., 2005, *Hepatology*, 41, 1313-21.

## **2.8. Bio-ID**

Protocol for the Bio-ID was adapted from Roux et al., 2012. Cells were plated in 6 x 150mm dishes per condition for 24 hours. Then, 0.2mM OA, 100ng/ml tetracycline and 50 $\mu$ M biotin was added in 20% FBS and 1% Penstrep for 20 hours. Cells were rinsed with warm PBS once before adding 0.4mM EPA and biotin in 10% FBS and 1% Penstrep. After 8hours, cells were rinsed once with warm PBS, scraped in cold PBS, and pelleted at 800rpm (140xg) for 5 minutes at 4°C. Cell pellets were snap-frozen and stored at -80°C.

All the solutions required for biotinylated protein capture were made fresh, and all plastic ware was sterilized. Sepharose beads (GE17-5113-01 Sigma Streptavidin Sepharose R High-Performance GE Healthcare) were prepared by washing with washing buffer (50mM Tris pH 7.4, 150 mM NaCl, 1% NP40, 0.1% SDS, 1mM EDTA) and spinning at 2000rpm for 30 sec for 5 times. Cell pellets were thawed on ice and lysed with RIPA (50mM Tris pH 7.4, 150 mM NaCl, 1% NP-40, 0.5% Sodium deoxycholate, 0.1% SDS, 1mM EDTA, 1mM PMSF, 62.5U/ml Benzonase R and Complete protease inhibitor). The crude lysate was sonicated for 4x 10 sec bursts at 4°C followed by centrifugation at 14000 rpm for 30 min at 4°C. Cleared lysates were mixed with the washed beads and rotated for 3 hours at 4°C. Upon centrifugation at 200 rpm at 4°C for 2 min, supernatant was removed and beads were washed 5 times with 50mM Tris pH 7.4, 150 mM NaCl, 1% NP-40, 0.5% Sodium deoxycholate, 0.1% SDS, 1mM EDTA. Beads were rinsed with 50mM ammonium bicarbonate pH 8.0 for four times. Biotinylated proteins were eluted with 75M biotin in 2x Laemmli buffer. Samples were incubated at 37°C for 15 min, 98°C for 10 min and spun at 3200g for 1 min. Final supernatant was loaded onto stacking gel for in-gel trypsin digestion. Protein bands were excised out for in-gel trypsin digestion and analyzed by LC-MS/MS summarized above.

Biotin stock was prepared by dissolving 100mg biotin in 28% NH<sub>4</sub>OH (Sigma #221228). This 200mM solution was neutralized by adding 1N HCl to obtain a 15mM stock solution. The final solution of pH 7.5- 8.0 was 0.22µm filter sterilized and kept in 4°C. Working biotin at 2mM was prepared by diluting the stock in DMEM.

## **2.9. Determination of LD size and number**

For quantification of LD, LDs were stained by Bodipy 493/503 and nucleus was stained with DAPI. For each experiment, 50-200 cells were randomly selected from DAPI (or DIC) channel and diameter of LDs was measured by generic measure function in Image J (NIH). Criteria used were following: cells were randomly chosen from DAPI (or DIC) channel and only the cells that show full lateral view were selected.

## **2.10. Relative triacylglycerol levels by Thin Layer Chromatography**

Cells were cultured with [ $^{14}\text{C}$ ] oleate, and the cellular lipids extracted with hexane. Lipids were then dried with nitrogen gas, redissolved into chloroform and resolved by thin-layer chromatography using hexane, ether, acetic acid in volumetric ratios of 65:20:1. To locate bands, stain the plate by placing into an iodine chamber for 20 minutes. TAG bands are scraped into scintillation vials and dissolved by 5ml scintillation cocktail. Radioactivity was read by Tri-Carb 2800 TR Domestic (Perkin Elmer).

## **2.11. Determination of Kiss-and-run**

To measure number of Kiss-and-run, cells were transfected with fluorescent lysosomal marker, and LDs were labeled with fluorescent lipid probes (Nile red, Bodipy 558/568, or Bodipy 493/503). Live cell images were captured every 1.25sec (for HeLa cells) or 1.5sec (for T-REx HeLa cells) for at least 1 minute. All images were processed and analyzed with ImageJ 1.45 (National Institutes of Health, USA). In all cases, background (pixel value outside the cells) was relatively low (<10% of the signal). Therefore, background subtraction was not performed to

minimize data manipulation. Firstly, images from each channel were converted to grey scale (0-255). Next, they were default-thresholded to binary by using lower limit of 0 and upper limit ranging from 20-30. Thresholded images from each channel were merged to find pixels that overlapped. Same processing was applied for all time-lapse series imaged for 1 minute. Merged images were converted to grey scale and thresholded, and this revealed only the overlapping pixels between the two channels. These pixels correspond to areas where LDs and lysosomes come together. A number of incidents where the value was greater than the average (over a minute) were considered Kiss-and-run, and these values were recorded for each cell. For each group, more than ten cells were counted. To calculate an average number of overlapping pixels, the number of overlapping pixels per each frame was averaged for a minute. This calculation was performed for more than ten cells per condition, and a standard deviation was calculated per each condition.

## **2.12. Western blot**

To harvest cells, either simple lysis buffer (PBS pH 7.4, 1x cOmplete<sup>TM</sup>, 0.1% Triton x100) or RIPA buffer (25mM Tris, 100mM NaCl, 0.5% NP-40, 0.5% Na deoxycholate, 50mM NaF, 1x cOmplete<sup>TM</sup>) was used. Lysis buffer was added to 2x PBS washed cells, and cells were incubated for 30 minutes on ice. The crude cell lysate was collected, spun at 14,000 rpm for 20 minutes at 4°C, and only the supernatant was saved. Proteins were quantified by modified Lowry method using Bio-Rad DC protein assay. For all fusion antibody related blots, 10µg of proteins were loaded in each lane. For all endophilin B1 blots, 30µg of proteins were loaded in each lane. Samples were prepared using 2-4X Laemmli buffer, boiled at 95°C for 5 minutes before spinning

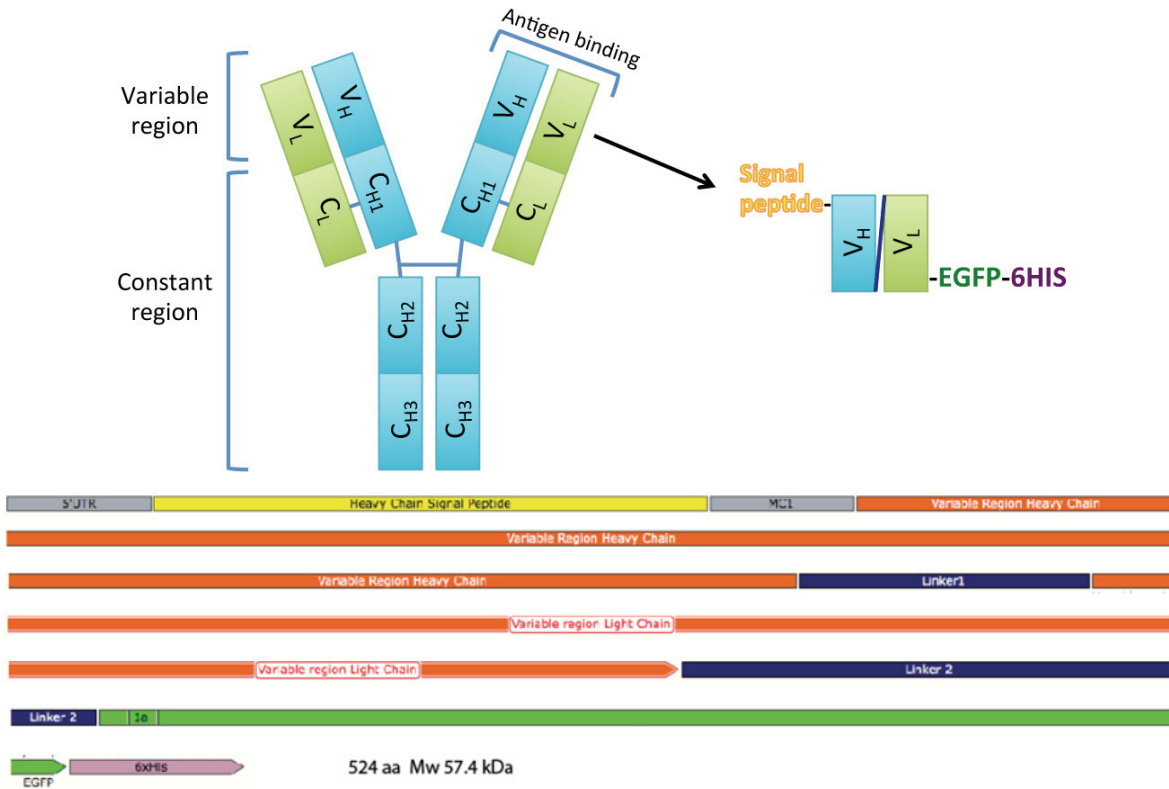
at 10,000rpm for 5 minutes at room temperature. All samples were run on 12% acrylamide gel at 25mA/gel using Hoefer apparatus. Proteins were then transferred onto PVDF membrane. Primary antibody was diluted in either 5% skim milk in PBS or 5% BSA in TBS for overnight at 4°C. Subsequently, blots were washed using either 0.3% skim milk in PBS or TBST. Goat anti-mouse HRP-conjugate or Protein A-HRP conjugate was applied for 45 minutes at room temperature. ECL was added 1 minute prior to chemiluminescence detection using ImageQuant LAS 4000 (GE Healthcare, Quebec, CA). Amount of proteins was normalized against GAPDH or tubulin, and proteins were semi-quantitated based on band intensity identified using ImageJ gel analysis option.

**Chapter 3: New generation of probes to study retention and recycling of Golgi-resident enzymes**

### **3.1. Construction of fusion antibody and expression in different cell types**

In order to observe the behavior of Golgi-resident enzymes, we decided to make a novel antibody-based probe. We took variable fragments of highly characterized monoclonal antibody and added an affinity tag to make a ‘fusion antibody’ probe. Fusion antibodies have been constructed against N-acetylgalactosaminyltransferase 2 (GalNacT2) and  $\beta$ 1, 4-Galactosyltransferase (GalT) enzymes, to which we have highly specific monoclonal antibodies. In collaboration with *Novoprotein*, we were able to sequence their variable domains based on their hybridoma cell lines, and sub-clone them into a pCDNA3.1 vector, which can be expressed in mammalian cells. Construction of these fusion antibodies is shown in Fig. 3-1.

a.



b.

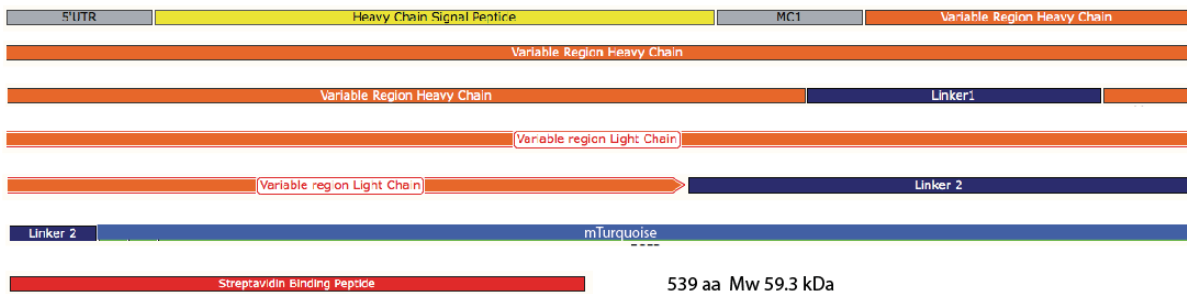


(Figure legend continues on the next page.)

**Figure 3-1:** Fusion antibody is constructed from single chain variable fragment of a monoclonal antibody

a. Overview of the fusion antibody construction. Variable fragments from the monoclonal antibody were sequenced, and fluorescent tag (EGFP) and affinity tag were added. This construct was sub-cloning into pcDNA3.1. A heavy chain signal peptide (yellow) allows the nascent protein to enter the early secretory pathway. A heavy chain and light chain

variable fragment (orange) constitute a single-chain variable fragment (ScFv). A linker (navy) in between the heavy and light chain allows correct folding. EGFP (green) and 6xHis tag (purple) allows for visualization and detection. This figure illustrates a fusion antibody design for EGFP-FSAB- $\alpha$ -GalT.

- b.** Construction of the mTurquoise-tagged fusion antibody. mTurquoise and Streptavidin binding peptide replace EGFP and His tag, respectively. In this way, two constructs were produced; mTurq-FSAB- $\alpha$ -GalNacT2-SBP and mTurq-FSAB- $\alpha$ -GalT-SBP.

We have made fusion antibodies by utilizing variable regions from two highly characterized monoclonal antibodies against GalNacT2 and GalT. These regions are single-chain variable fragments (scFv) of an antibody, and they are significantly smaller than whole antibody molecules: The antibody is composed of one Fc (Fragment constant) domain and two variable Fab domains (Fragment antigen-binding), each of which is made up of a heavy and a light chain. ScFv is smaller than one Fab domain because it is only the variable regions of the Fab domain (Fig. 3-1a). A fluorescent tag and an affinity tag were added to facilitate visualization and purification, respectively. Finally, the construct was subcloned into pCDNA3.1. We have generated four constructs: EGFP-FSAB- $\alpha$ -GalNacT2; RFP-FSAB- $\alpha$ -GalNacT2; EGFP-FSAB- $\alpha$ -GalT; and RFP-FSAB- $\alpha$ -GalT.

Additional fusion antibodies have been built with an mTurquoise tag in place of EGFP or RFP (Fig. 3-1b). The mTurquoise is the brightest and the most photo-stable cyan dye (Goedhart et al., 2010). Longer fluorescence lifetime and larger free radical generating capacity (Goedhart et al., 2010) make mTurquoise adequate for Correlative Light Electron Microscopy (CLEM), which offers the versatility of the light microscope with the resolution power of the electron microscope (See section **1.1.7.a**). Unlike EGFP, mTurquoise is a monomer, and this property prevents dimerization of the fusion antibody. In addition, Streptavidin Binding Peptide (SBP)

was added for further applications. In this way, the two fusion antibodies were constructed: mTurq-FSAB- $\alpha$ -GalNacT2-SBP; and mTurq-FSAB- $\alpha$ -GalT-SBP (Fig. 3-1b).

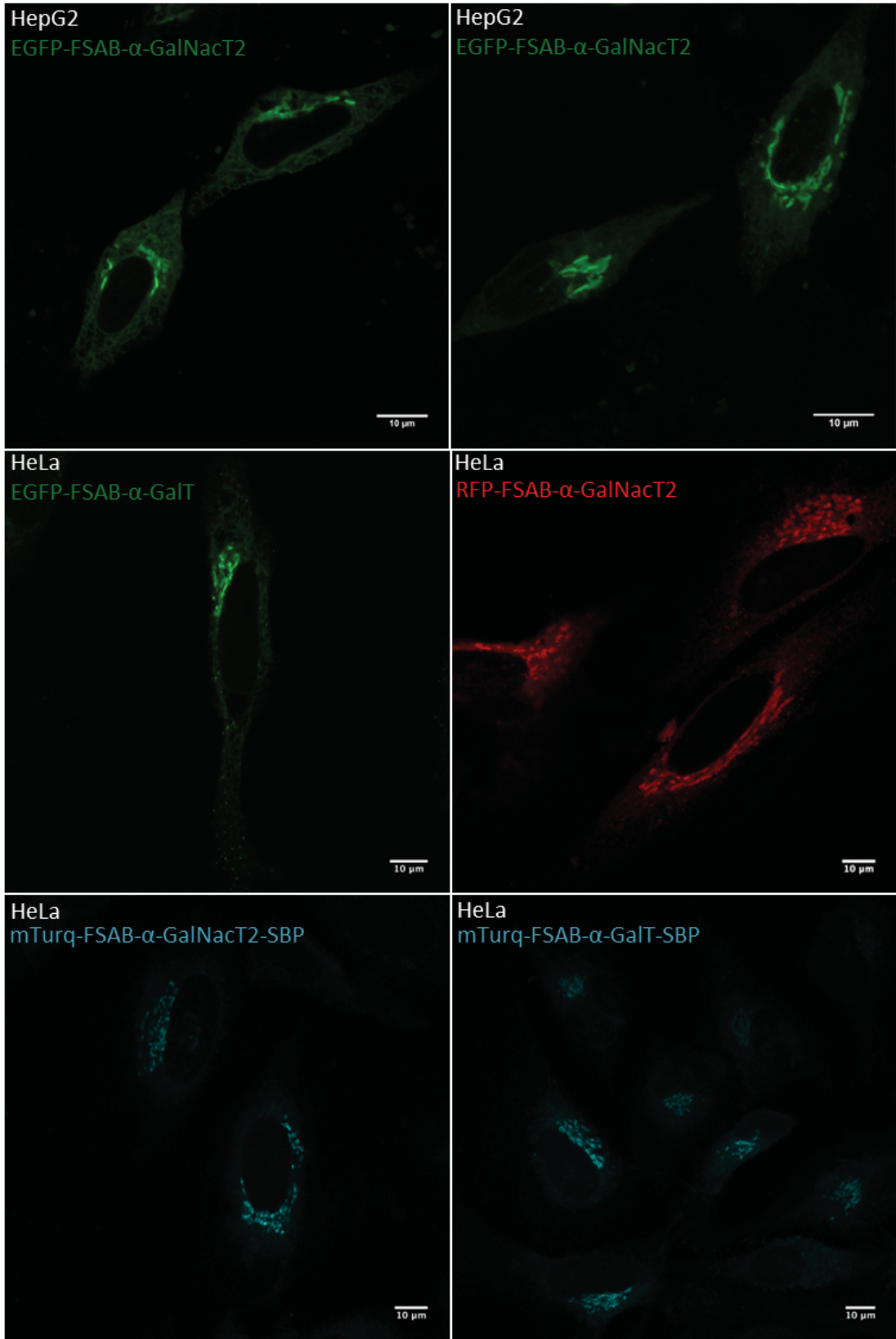


(Figure legend is found on the next page.)

**Figure 3-2:** Fusion antibody is expressed and fluorescent.

HeLa cells were seeded on coverslips at 200,000cells/ml. 24 hours after HeLa cells were seeded, they were transfected with 1 $\mu$ g fusion antibody plasmid for 16 and 24 hours. HepG2 cells were transfected as they were seeded. Upon fixation, coverslips were mounted and imaged. Scale bar is 10 $\mu$ m.

With the exception of vector construction, I carried out all the experiments included in this chapter. To determine if the fusion antibody is well expressed in a cell, HeLa and HepG2 cells were transfected with 1 $\mu$ g plasmid for 16-24 hours. When imaged on the fluorescent microscope, fusion antibodies against GalNacT2 and GalT appear fluorescent (Fig. 3-2).

### **3.2. Fusion antibody is made specifically for its respective glycosyltransferase.**

In order to verify that fusion antibody recognizes the proper antigen, we wanted to stain fusion antibody transfected cells with another antibody that recognizes a different epitope from the same Golgi enzyme. To do this, HeLa cells were plated at 200,000cells/ml, and they were transfected with mTurq-FSAB- $\alpha$ -GalT-SBP. Following fixation, cells were permeabilized and stained against GalT. Subsequently, cells were imaged. Indeed, distributions of the fusion antibody and the GalT antibody greatly overlapped, suggesting that the fusion antibody was made correctly for the corresponding antigen, GalT (Fig. 3-3).

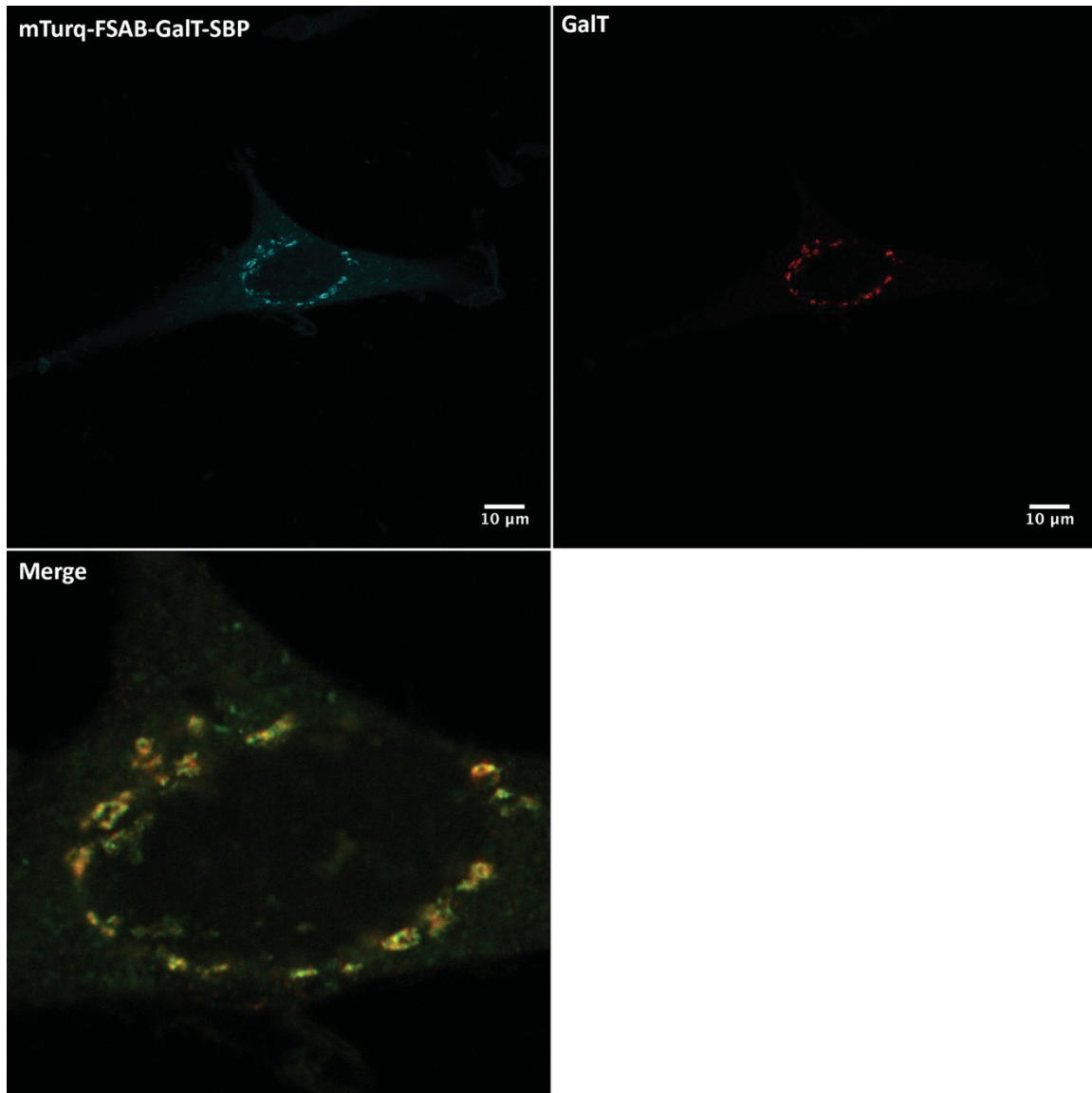


**Figure 3-3:** Fusion antibody is specifically made for its respective glycosyltransferase.

HeLa cells were seeded at 200,000cells/ml and transfected with mTurq-FSAB- $\alpha$ -GalT-SBP for 16 hours. After fixation, free fixatives were quenched with  $\text{NH}_4\text{Cl}$ , and non-specific sites were blocked with fish skin gelatin. After cells had been permeabilized with saponin, they were stained with mAb GalT and subsequently with Alexa 568 (red). Fusion antibody is shown as cyan in the upper left panel, but is pseudo coloured to green in the merge panel since co-localization with red is readily visible with green. Scale bar is 10 $\mu\text{m}$ .

So far, we have determined that fusion antibody is expressed in a cell, and it recognizes the correct antigen. However, there is a constant turnover of Golgi cisternae, and it is possible that fusion antibody in previous figures is freely floating in the Golgi as a biosynthetic molecule, rather than a probe that binds specifically to the antigen. To determine whether or not fusion antibodies remain tightly bound to their respective antigens, transfected cells were treated with 100µg/ml cycloheximide (CHX) that inhibits translational elongation. The rationale is that if fusion antibody were not bound to Golgi enzyme, then it would be removed from the Golgi as other biosynthetic cargos go through the early secretory pathway. After 16 hours of transfection, transfection media was removed, and cells were washed once with PBS. CHX was added in a new media and incubated for the indicated times (Fig. 3-4). Under these conditions, the fusion antibody against GalT remained in the Golgi for up to six hours (Fig. 3-4). The CHX treatment also removes unbound fusion antibody to some extent: ER-localized fusion antibody is removed after 2 hours of CHX treatment.

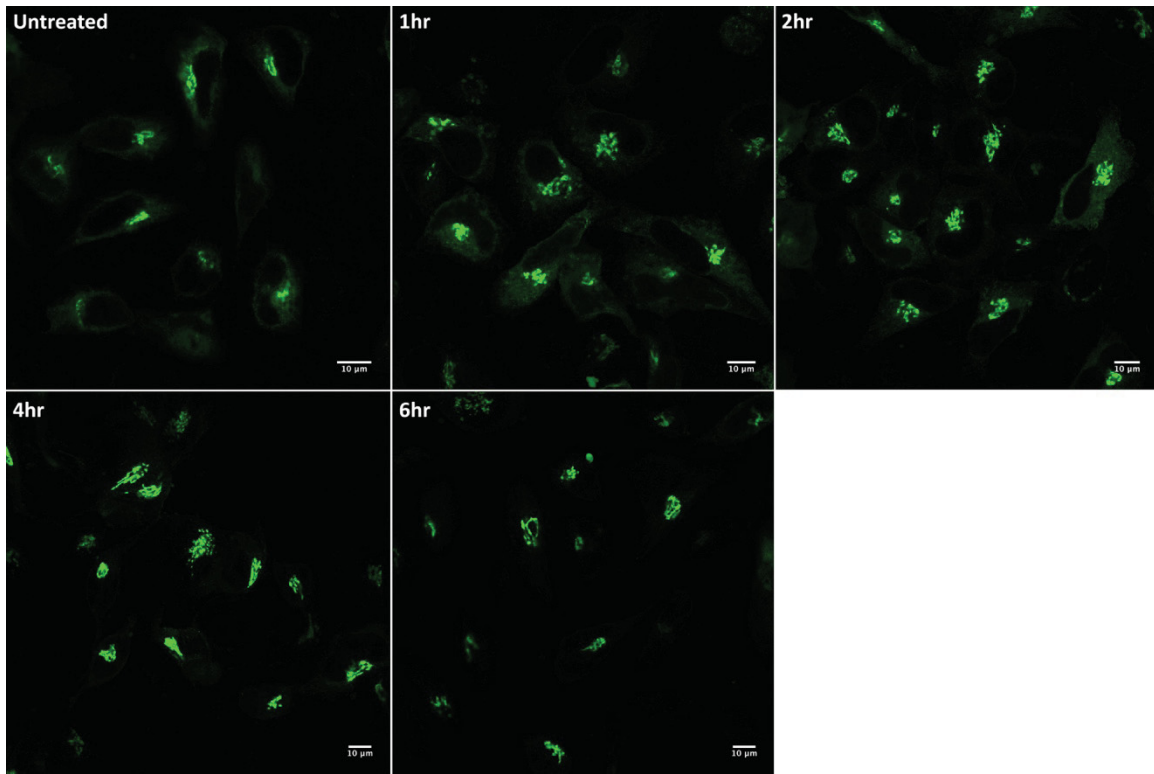


**Figure 3-4:** Fusion antibody is specific for Golgi enzyme.

HeLa cells were seeded at 200,000cells/ml and transfected with 1 $\mu$ g/ml of EGFP-FSAB- $\alpha$ -GalT plasmid for 16 hours. Following the transfection, cells were washed once with PBS before adding 100 $\mu$ g/ml cycloheximide for up to 6 hours. After indicated time points, each coverslip was fixed. After the time had elapsed, coverslips were mounted on a glass slide for imaging. Scale bar is 10 $\mu$ m.

To further characterize the fusion antibody, transfected cells were treated with Brefeldin A (BFA). BFA is a fungal metabolite that reversibly interferes with ADP-ribosylation factor (ARF). Upon BFA treatment, Arf is unable to associate coatomers to the Golgi membrane (Helms and Rothman, 1992), and therefore, Golgi-to-ER transport is blocked. As a consequence, Golgi cisternae are disassembled (Fujiwara et al., 1988). To perform this experiment, HeLa cells were plated at 200,000cells/ml on a glass-bottom dish and transfected with 1 $\mu$ g/ml of mTurq-FSAB- $\alpha$ -GalNacT2-SBP plasmid for 24 hours. Following the transfection, cells were washed once with PBS, and 1ml of normal media was added. Cells were positioned into a pre-warmed

chamber for live-cell imaging. While capturing images, 1ml of 20 $\mu$ g/ml Brefeldin A was added to 1ml of cells, and this caused final concentration to be at 10 $\mu$ g/ml. Images were captured at 5minute intervals. After fifteen-minute treatment of 10 $\mu$ g/ml BFA, Golgi was fragmented and the fusion antibody was seen in the fragmented Golgi (Fig. 3-5). These experiments shown in Fig. 3-4 and Fig. 3-5 confirm that fusion antibodies are specific for the Golgi enzymes.

**a.**

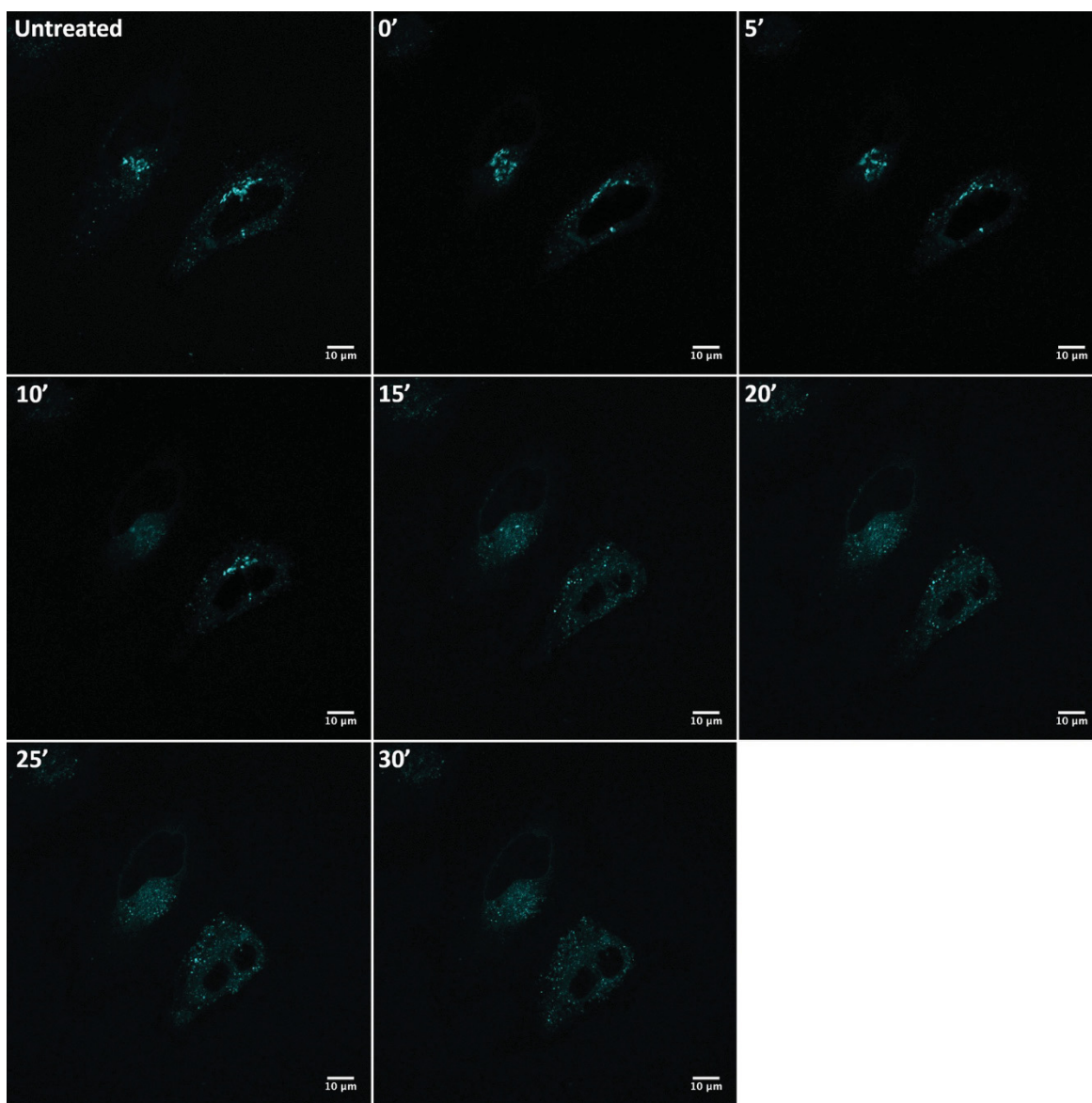


(Figure continues on the next page.)

b.

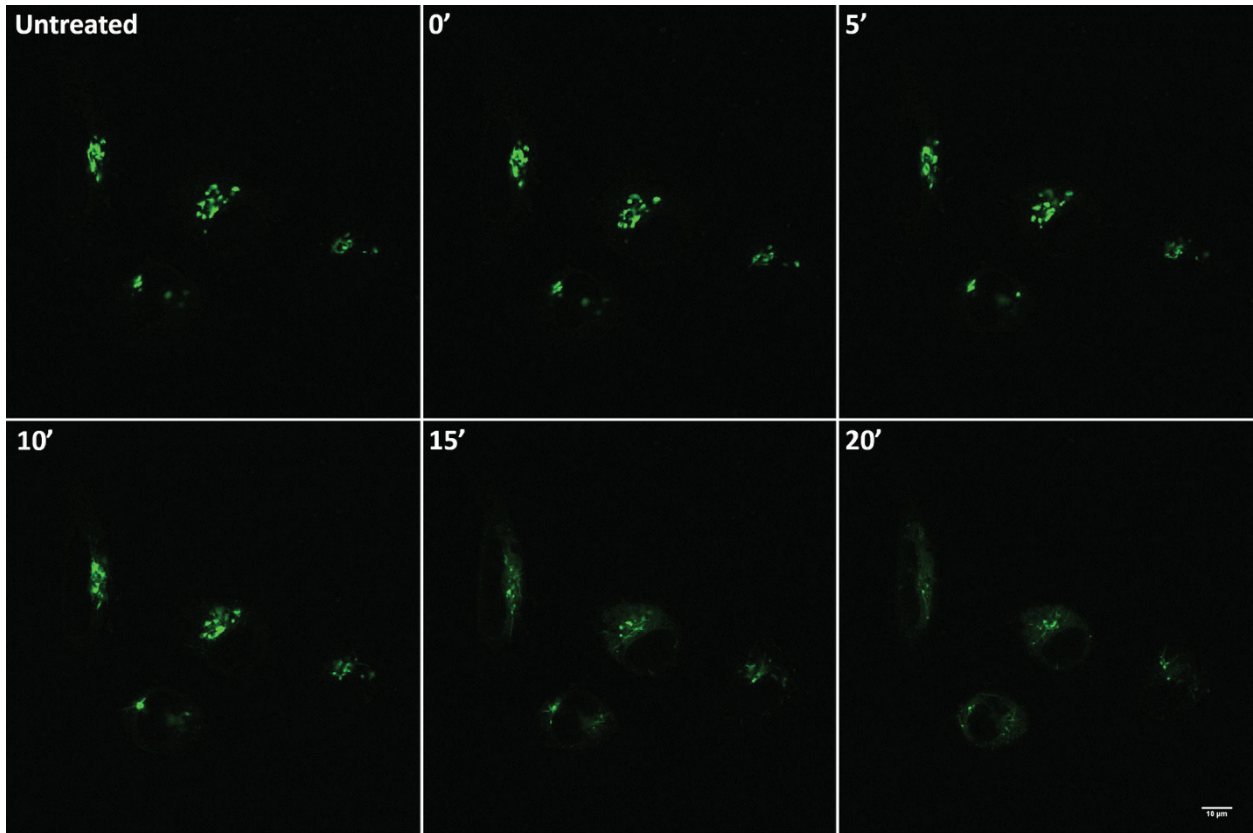


(Figure continues on the next page.)

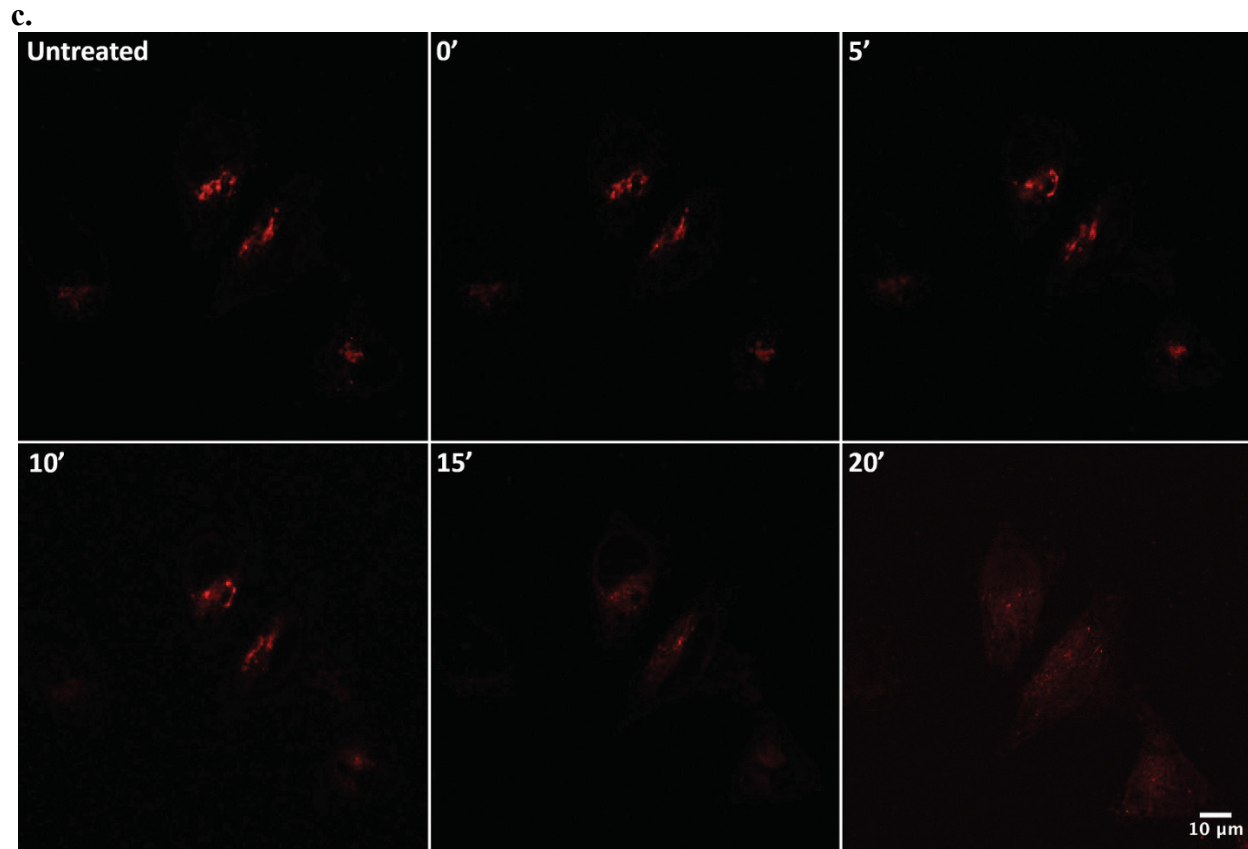


**Figure 3-5:** Fusion antibody behaves as Golgi enzyme.

- a. Live cell imaging of mTurq-FSAB- $\alpha$ -GalNacT2-SBP transfected cells after BFA treatment. Transfected cells were washed once before imaging. During imaging, 10 $\mu$ g/ml BFA was applied, and the movement of fusion antibody was monitored. Each image was captured in the 5-minute intervals. Brefeldin A treatment on mTurq-FSAB- $\alpha$ -GalNacT2 transfected cells caused Golgi fragmentation. Scale bar is 10 $\mu$ m.
- b. HeLa cells transfected with EGFP-FSAB- $\alpha$ -GalT. Cells were imaged for 20 minutes post-BFA. Scale bar is 10 $\mu$ m.
- c. HeLa cells transfected with RFP-FSAB- $\alpha$ -GalT. Cells were imaged for 20 minutes post-BFA. Scale bar is 10 $\mu$ m.

### **3.3. Fusion antibody does not affect cell viability or cause ER stress.**

Although fusion antibody is smaller than conventional antibody and it binds specifically to Golgi enzymes, it is plausible that expressing fusion antibody in a cell can cause stress, which can inevitably affect cell viability. To determine if the expression of fusion antibody affects cells' viability, HeLa cells transiently and stably expressing fusion antibody were tested for their viability (Fig. 3-6a). After cells had been plated at pre-determined density, one group of cells was transiently transfected with EGFP-FSAB-GalT construct for 24 hours while non-transfected and stably transfected cells (with EGFP-FSAB-GalT) were not. After the experiment, cells were detached, and they were mixed with trypan blue according to the manufacturer's instructions. Numbers of blue (dead) and clear (viable) cells were counted using a hemocytometer. Cells were counted for three times at three different passages, and this generated nine measurements for each cell line. Percent cell viability was calculated by dividing a number of clear cells by total cells. Then, percent cell viability from all measurements was averaged, and the standard deviation was calculated. Statistical significance was measured by using a student T-test. Percent viability was reported as a bar graph (Fig. 3-6a). There were no significant differences between non-transfected, transiently transfected and stably transfected HeLa cells ( $p=0.39$ ), confirming that expressing fusion antibody does not affect cell viability (Fig. 3-6a).

In order to carefully modulate the expression of fusion antibody, we decided to use tetracycline inducible system, T-REx™: T-REx™ cell line stably expresses tetracycline repressor protein that binds to a promoter, upstream of the gene of interest. Therefore, the gene of interest does not transcribe unless repressor is removed. When tetracycline is added, it binds to the repressor protein, releasing it from the transcript. Therefore, transcription can begin.

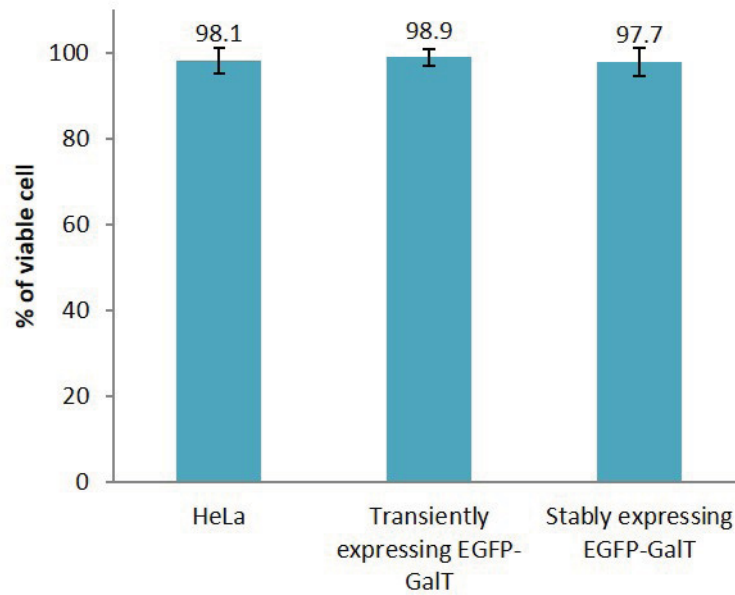
Therefore, T-REx system allows expression of protein in an inducible manner. Similarly, the amount of protein expression is dependent on tetracycline concentration.

To generate T-REx cells that can inducibly express fusion antibody, fusion antibody construct is cloned into pCDNA5/FRT/TO plasmid that contains RGS6His3FLAG, a tag that facilitates tandem affinity purification. Then, this plasmid is co-transfected with pOG44, which supplies the Flp recombinase vector, into Flp-In™ T-REx Hek293 cells that contain a single FRT site at a transcriptionally active genomic locus. As a result, pCDNA5/FRT/TO-fusion antibody-RGS6His3FLAG is stably integrated into a FRT site. Every cell has a single FRT site, and this allows a single integration of fusion antibody; As a result, all transfected cells will have homogeneous levels of gene expression. Initial construction of T-REx Hek293 fusion antibody-RGS6His3FLAG cell line was performed by Dr. Jarred Chicoine from Dr. Sladek's laboratory (McGill University). This T-REx system is widely used in this thesis (Fig. 3-6 and onwards).

Next, the degree of ER stress was measured by observing the amount of HERP expression, a protein whose expression level is correlative of the ER stress (Kokame et al., 2000). T-REx EGFP-FSAB- $\alpha$ -GalT cells were induced by increasing concentrations of tetracycline, and the amount of HERP expression was compared to the non-induced cells that were treated with thapsigargin, DTT, and tunicamycin. Thapsigargin specifically blocks ER Ca<sup>2+</sup> ATPase pump leading to the depletion of ER calcium storage. This inhibition leads to the fallout of ER chaperones like calnexin, so unfolded proteins accumulate (Samali et al., 2010; Osowski and Urano, 2011). DTT is a strong reducing agent that blocks disulfide-bond formation, leading to an increase of ER stress (Osowski and Urano, 2011). Tunicamycin inhibits N-linked glycosylation, the initial step of glycoprotein biosynthesis. Therefore, tunicamycin causes accumulation of unfolded proteins (Osowski and Urano, 2011).

To determine whether or not fusion antibody expression causes ER stress, T-REx cells were plated, and fusion antibody expression was induced with various concentrations of tetracycline. Subsequently, cell lysates were prepared, and HERP level was compared to thapsigargin, DTT, and tunicamycin-treated cells. The amount of HERP expressed in tetracycline-induced EGFP-FSAB- $\alpha$ -GalT expressing cells is negligible (Fig. 3-6b). The Same experiment was performed in T-REx Hek293-mTurq-GalT-SBP-RGS6His3FLAG cells. For all subsequent experiments, 1 $\mu$ g/ml tetracycline was used since this condition had minimal ER stress, yet yields a bright fluorescent signal (Fig. 3-7).

**a.**



<b>T-Test</b>	<b>p-values</b>
HeLa vs. Transfected	0.59
HeLa vs. Stable	0.77
Transfected vs. Stable	0.39

(Figure continues on the next page.)

**b.**

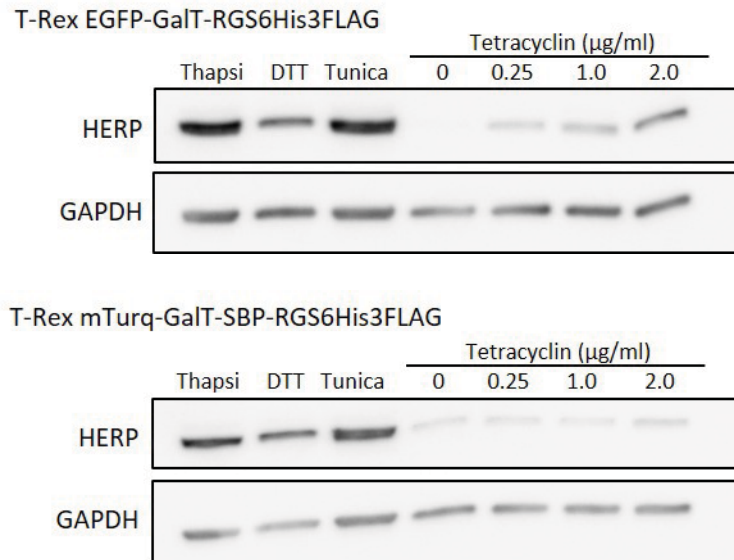


**Figure 3-6:** Fusion antibody does not affect the cell viability or increase ER stress.

- a.** Percent cell viability measured by Trypan blue exclusion assay. HeLa cells transiently expressing EGFP-FSAB-GalT and HeLa cells stably expressing EGFP-FSAB-GalT are shown. Trypan blue was used to count viable cells. Cells were counted for 3 times in 3 passages, and all measurements were calculated to percent cell viability. Average percent cell viability was represented as a bar graph, and standard deviation from each group is shown. T-test result was summarized in a table below. Differences between the three groups are not significant ( $p > 0.05$ ).
- b.** Degree of ER stress examined by the expression of HERP. T-REX Hek293 cells inducibly expressing fusion antibody were incubated with thapsigargin, DTT, and tunicamycin. Also, they were induced with indicated concentrations of tetracycline. 10µg proteins were loaded for all wells. GAPDH is a loading control.

### **3.4. Fusion antibody can be used to highlight antigens of non-transfected cells.**

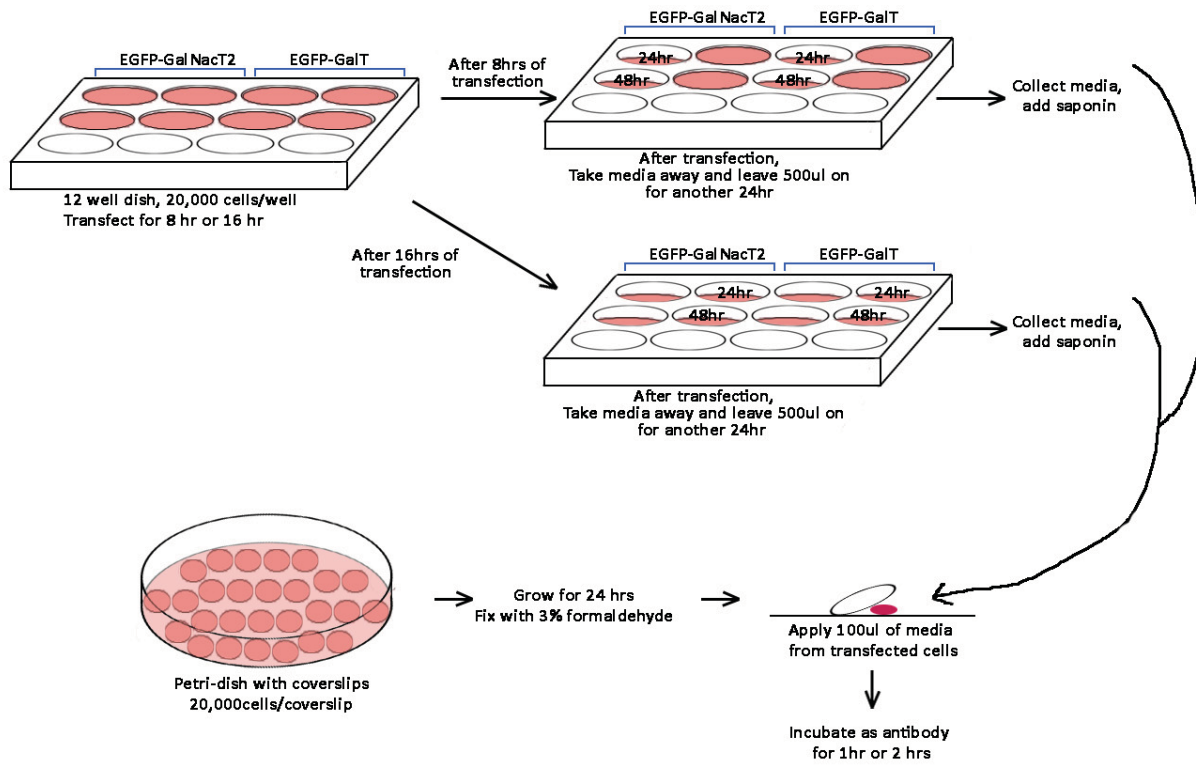
Another way to test for specificity of fusion antibody is to take the conditioned media from transfected cells and apply this to non-transfected, fixed and permeabilized cells. This experiment also tests if the secretory functions were affected because improperly folded fusion antibody would not pass through the secretory pathway. To test these rationales, cells were first

transfected, and conditioned media was collected. This experiment is summarized as an illustration in Fig. 3-7a.

Firstly, HeLa cells were seeded at 20,000cells/well density, and they were transfected for 8 and 16 hours. In order to avoid carry-over of transfection agent (or tetracycline for later experiments), transfection media was removed. Then, cells were rinsed twice with PBS before new media (500 $\mu$ l) was added for additional 24 hours (Fig. 3-7a). This conditioned medium was filtered through 0.22 $\mu$ m filter to avoid possible carry-over of transfected cells. Finally, 0.1% saponin (non-ionic detergent, used in all other indirect immunofluorescence experiments in this thesis) was added to the conditioned medium before adding to non-transfected, fixed, and permeabilized cells for 1hour labeling.

Transfected cells were imaged after additional 24-hour incubation, and non-transfected cells were imaged immediately after the staining. They show that fusion antibody is at Golgi and on the cell surface, indicating that fusion antibody is being secreted into the conditioned media (Fig. 3-7b, immunofluorescence, left panel). Non-transfected cells stained this way had strong Golgi staining, confirming that the fusion antibodies indeed recognize Golgi enzymes (Fig. 3-7b, immunofluorescence, right panel). This experiment also verified that the conditioned medium could be used to localize antigens of another cell.

a.



b.

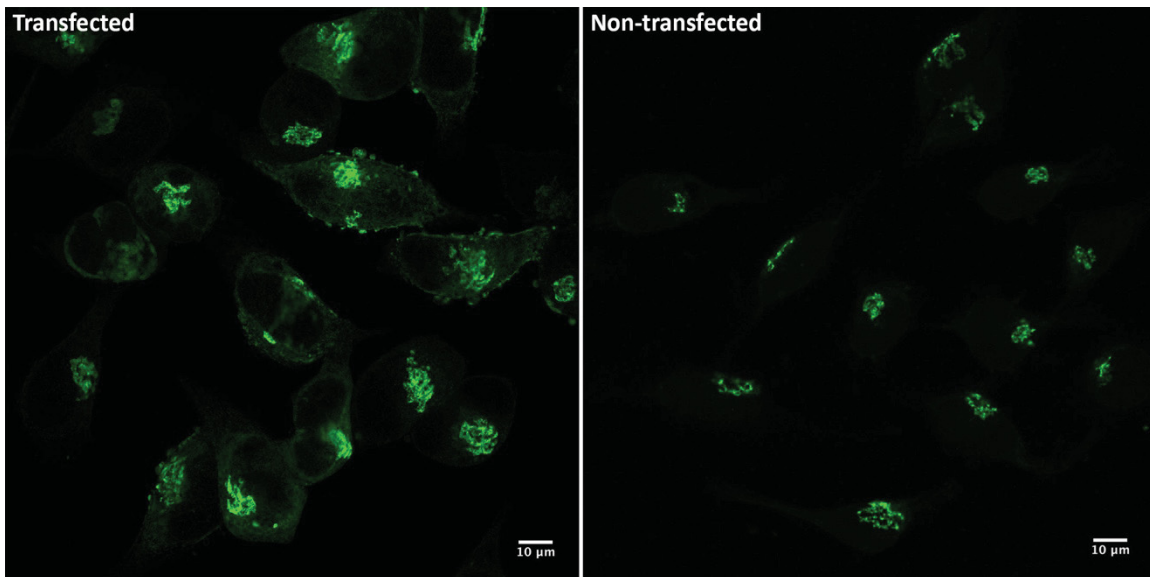


(Figure legend continues on the next page.)

**Figure 3-7:** Fusion antibody can be used to highlight antigens of non-transfected cells.

a. Experimental design for the conditioned medium experiment. One population of cells was transfected transiently with EGFP-FSAB-GalNacT2 (or GalT) while other population of cells

were seeded on a glass coverslip without transfection. After transfection, transfection medium was removed and new medium was added for 24 hours to collect fusion antibody. This conditioned medium was filtered. Non-transfected cells were fixed and permeabilized prior to incubation with conditioned medium.

- b.** Immunofluorescence images of EGFP-FSAB-GalT transfected cells and non-transfected cells stained with the conditioned medium. Scale bar is 10 $\mu$ m.

The experiment above confirmed that fusion antibody recognizes a Golgi enzyme. It also verified that conditioned medium is a source of fusion antibody. This result revolutionizes the antibody production: Highly specific, monoclonal antibody-like probe can be produced by simply harvesting a conditioned medium.

Although conditioned medium is a source of fusion antibody, this method requires continuous transfection and post-processing to ensure no carry-over of transfected cells. In order to avoid the cumbersome processes, tetracycline-inducible Hek293 cells were used: Advantage of the tetracycline inducible cells is that the expression of fusion antibody can be modulated by tetracycline addition. Indeed, these cells upon induction showed fusion antibody expression that could be observed by immunofluorescence and Western blot probed against FLAG (Fig. 3-8). First, T-REx Hek293 EGFP-FSAB-GalT-RGS6His3FLAG cells were plated at 200,000cells/ml. Expression of fusion antibody was induced with various concentrations of tetracycline ranging from 0 $\mu$ g/ml to 2 $\mu$ g/ml. After 24 hours of induction, conditioned media were saved, and the T-REx Hek293 cells were fixed. Concurrently, non-transfected HeLa cells were plated on coverslips, and they were fixed with 3% formaldehyde and permeabilized with 0.1% saponin/fish skin gelatin/PBS. Conditioned media were spun down briefly to remove cellular debris before adding 0.1% saponin. Subsequently, coverslips were incubated with the conditioned media for 1 hour. Immunofluorescence of T-REx Hek293 cells indicates that fusion antibody is produced by tetracycline induction (Fig. 3-8a). Fluorescent signals seen in cells without tetracycline (0 $\mu$ g/ml)

may be an auto-fluorescence or basal expression of fusion antibody due to tetracycline in fetal bovine serum (Fig. 3-8a, left panel). Then, expression of fusion antibody was confirmed by Western blot analysis (Fig. 3-8b). Conditioned media from T-REx Hek293 cells also contained enough fusion antibody molecules to stain non-transfected cells (Fig. 3-8c). Fusion antibody prepared in this way recognizes GalT enzyme because EGFP-FSAB-GalT co-localizes with a monoclonal antibody against GalT (Fig. 3-8c).

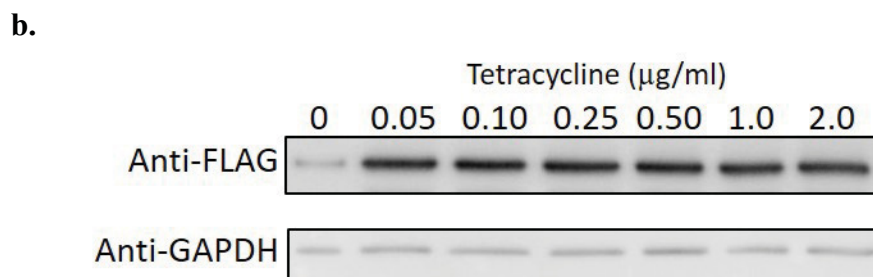
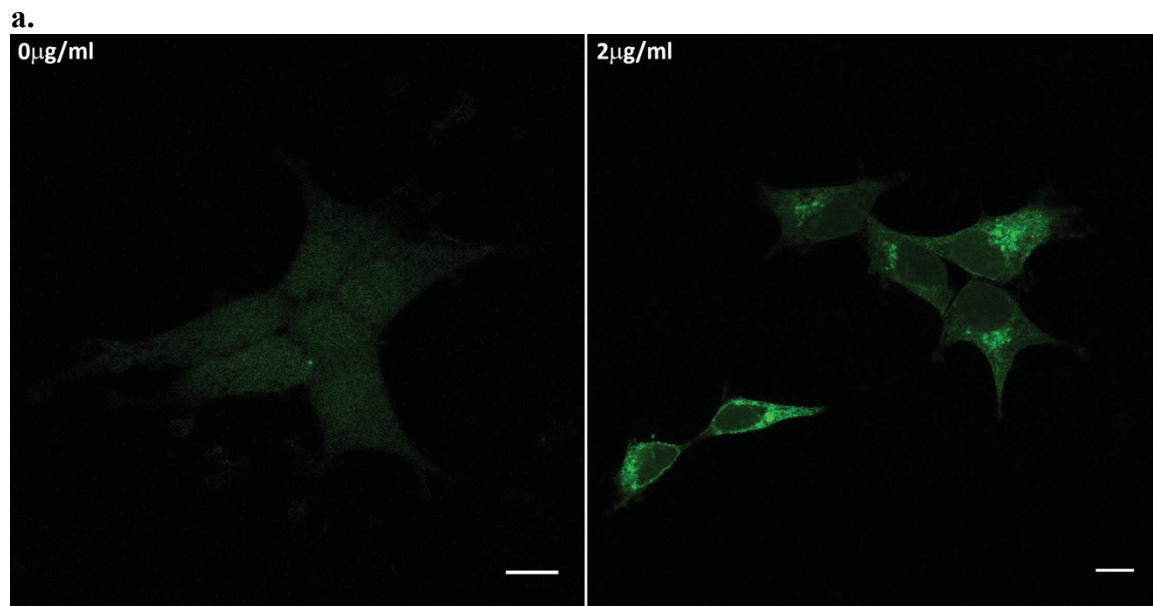


(Figure continues on the next page.)

c.

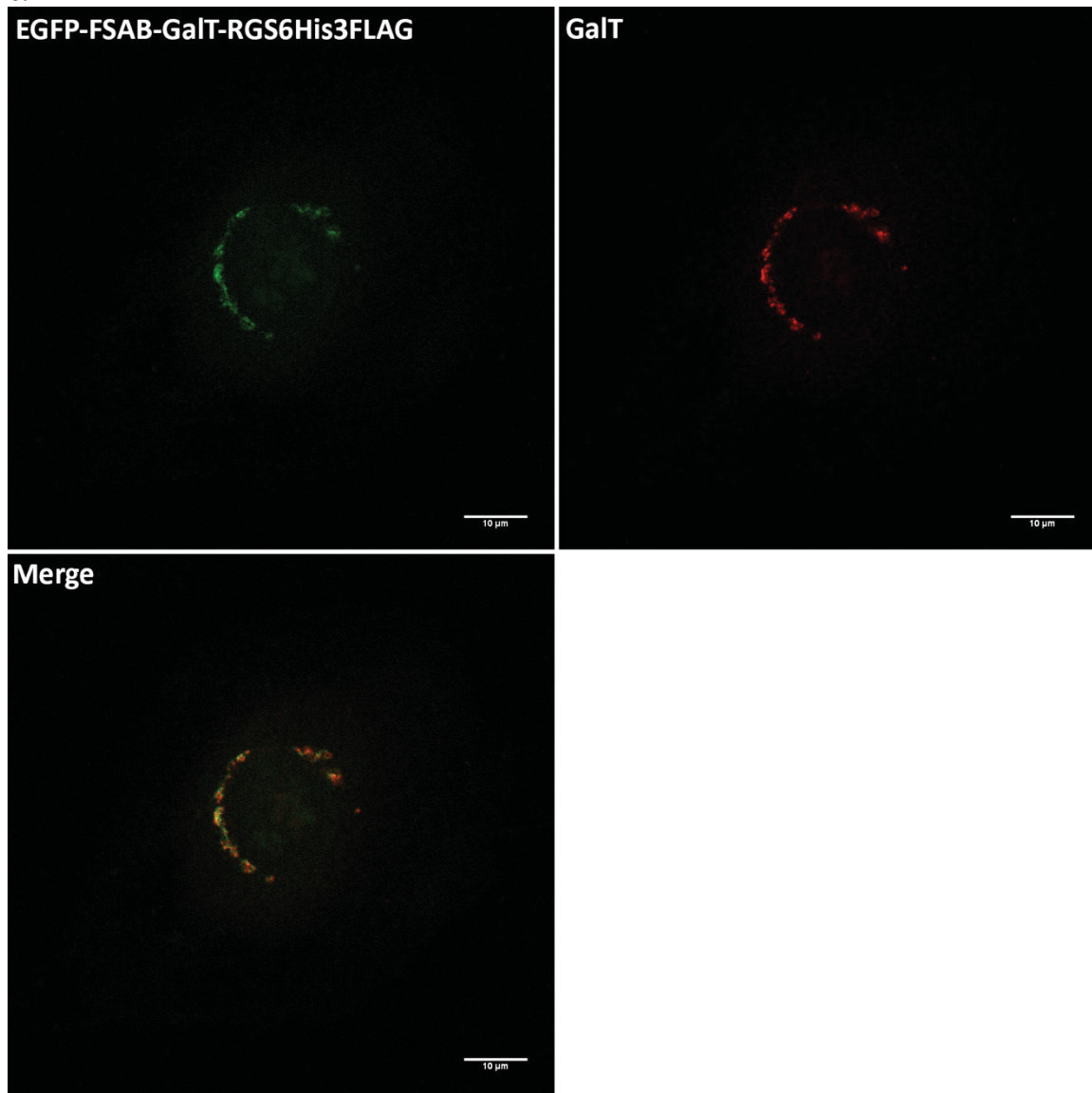


(Figure legend continues on the next page.)

**Figure 3-8:** Conditioned medium from the T-REx Hek293 cells is a source of fusion antibody.

- a. T-REx Hek293 cells inducibly expressing fusion antibody. After seeding cells at 200,000 cells/ml, expression of EGFP-FSAB-GalT-RGS6His3FLAG was induced using indicated concentrations of tetracycline for 24 hours. Upon fixation, cells were mounted with Mowiol mounting media. Scale bar is 10 μm.
- b. Western blot probed by FLAG antibody shows fusion antibody expression. T-REx Hek293 cells were induced with the indicated concentrations of tetracycline for 24 hours for EGFP-FSAB-GalT-RGS6His3FLAG expression. For each lane, 10 μg of protein was loaded. GAPDH is a loading control.

- c. T-REx Hek293 cells were induced with 0.10 $\mu$ g/ml tetracycline for inducing EGFP-FSAB-GalT-RGS6His3FLAG, and the conditioned media from these cells were used to stain fixed and permeabilized HeLa cells. These cells were co-stained with mAb GalT-Alexa 568 (Red). Scale bar is 10 $\mu$ m.

Various concentrations of tetracycline triggered expression of fusion antibody, and conditioned media from these cells can be used to stain endogenous Golgi enzyme (Fig. 3-9). As seen previously (Fig. 3-7b), fusion antibody is seen in Golgi and plasma membrane of T-REx Hek293 cells (Fig. 3-9, left row), indicating that fusion antibody is secreted.

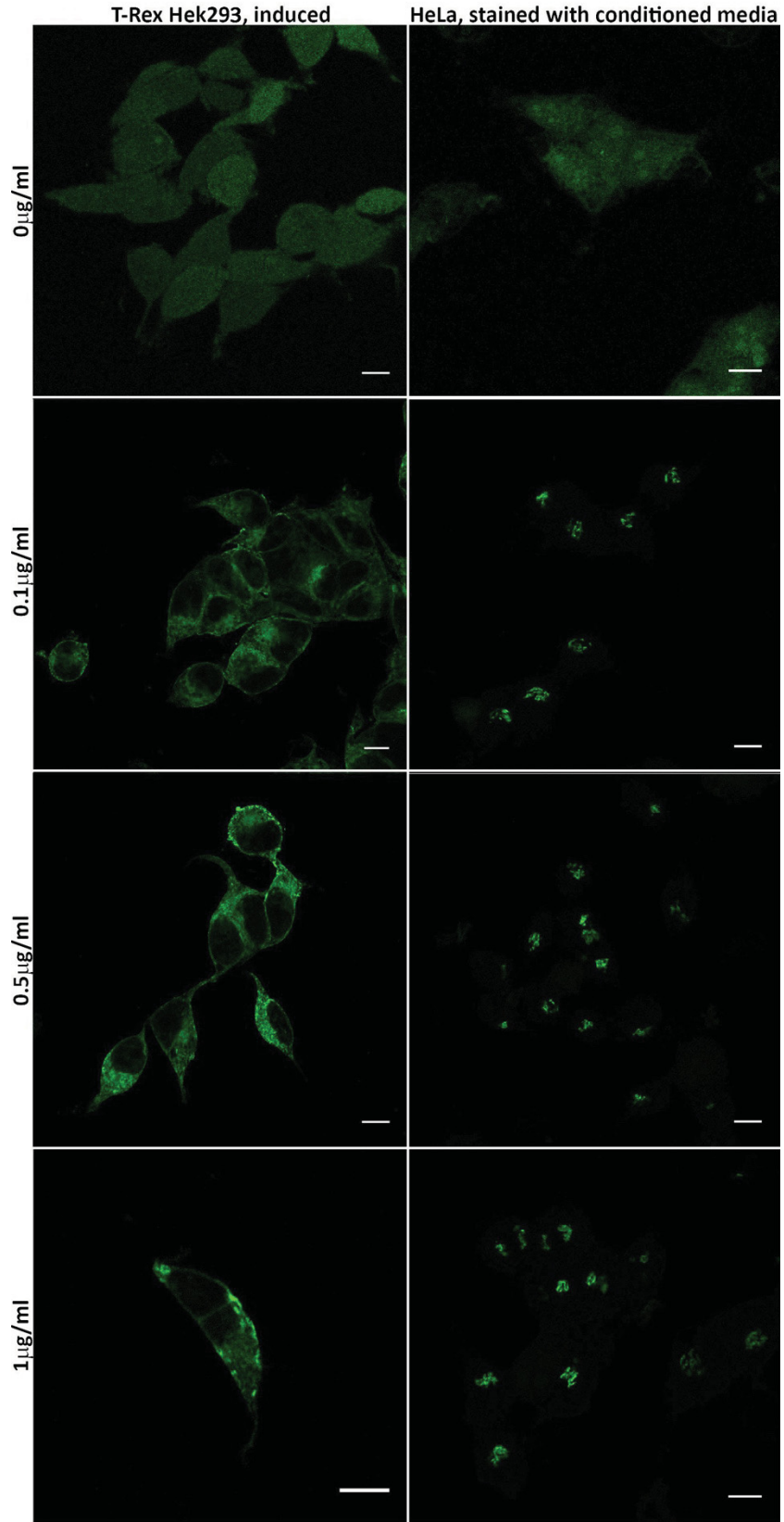


(Figure legend is found on the next page.)

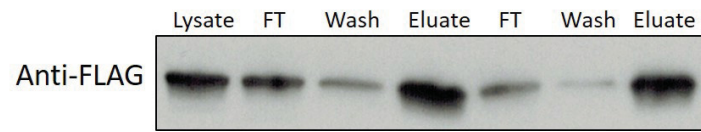
**Figure 3-9:** Conditioned media from T-REx Hek293 cells can be used to stain fixed and permeabilized HeLa cells.

Fusion antibody is secreted into the conditioned media of T-REx Hek293 cells, and it can be used to stain fixed and permeabilized HeLa cells. After seeding T-REx Hek293 cells at pre-determined density, expression of EGFP-FSAB-GalT-RGS6His3FLAG was induced using the indicated concentrations of tetracycline. Conditioned media from these cells were used to stain fixed and permeabilized HeLa cells. Scale bar is 10 $\mu$ m.

Next, we wanted to find out whether or not affinity purified fusion antibody can be used to stain endogenous Golgi enzyme. Advantage of affinity purification is that fusion antibody can be applied to live cells. Also, amount of fusion antibody can be controlled (Fig. 3-9).

To carry out this experiment, three 150mm plates of T-REx Hek293 EGFP-FSAB- $\alpha$ -GalT-RGS6HIS3FLAG cells were prepared, and they were induced with 1 $\mu$ g/ml tetracycline for 24 hours. To obtain purified fusion antibody, cleared lysate was first applied to Nickel resin to isolate HIS-tagged proteins. Followed by imidazole elution, eluate was directly applied to ANTI-FLAG® beads to purified FLAG-tagged proteins. This additional purification step ensures removal of contamination and increase of yield. In this way, fusion antibody was purified successfully (Fig. 3-10a). Fusion antibody purified in this way retains antigenic ability because it highlighted Golgi enzyme in non-transfected, fixed, and permeabilized HeLa cells (Fig. 3-10b).

a.



b.

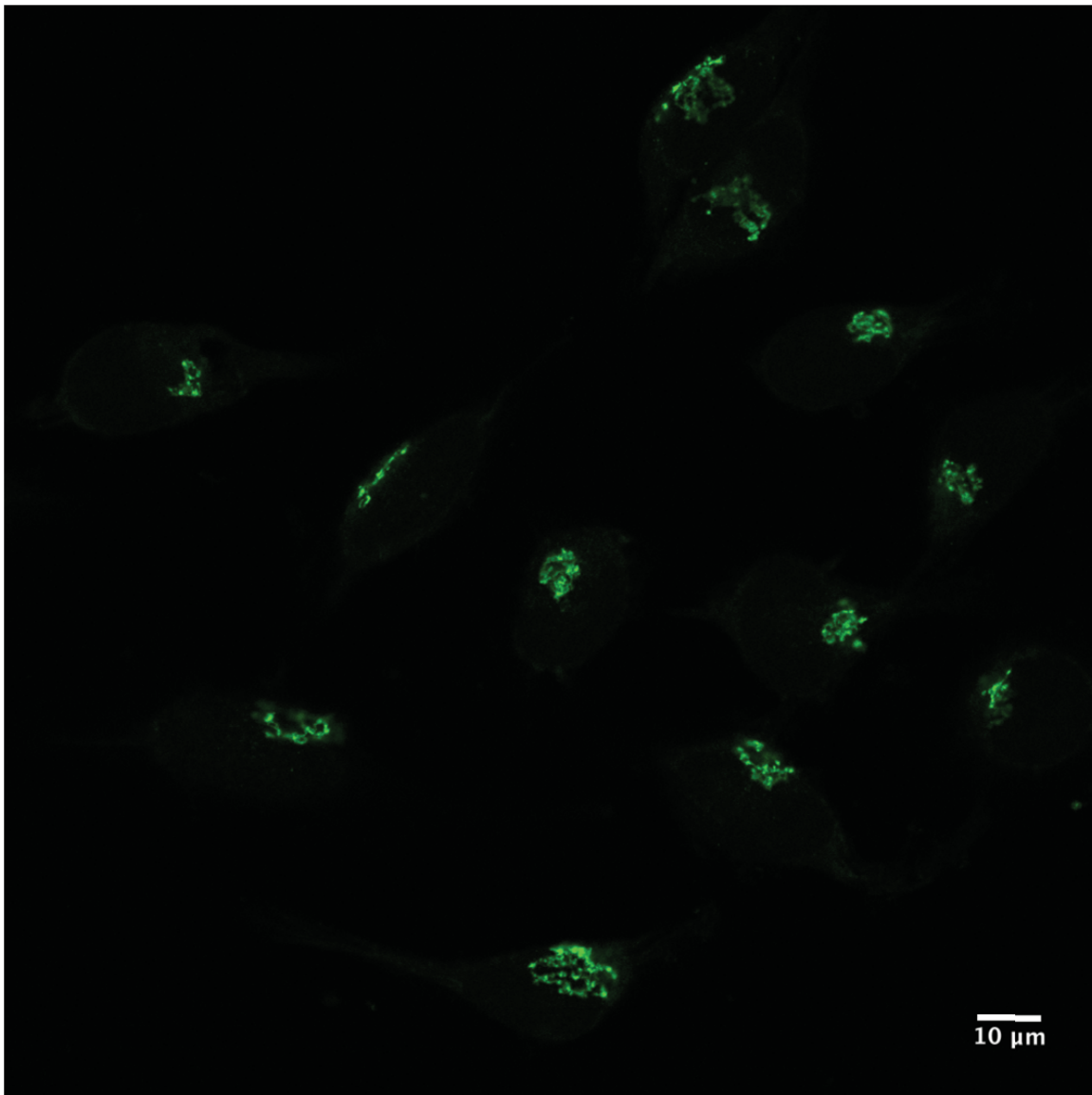


(Figure legend continues on the next page.)

**Figure 3-10:** Affinity purified fusion antibody retains ability to recognize Golgi enzyme.

- a. Tandem-affinity purification of fusion antibody. After T-REx Hek293 cells were induced with 1µg/ml tetracycline for 24 hours, cells were lysed and fusion antibody was purified by tandem-affinity purification. Lysate, flow through (FT), wash and eluate were analyzed by Western blot against FLAG. Equal volume of each fraction was loaded to verify the presence of fusion antibody.
- b. Immunofluorescence is showing non-transfected HeLa cells that are fixed, permeabilized and stained with the purified fusion antibody.

Collectively, conditioned media from fusion antibody-transfected cells and tandem-affinity purified fusion antibody from cell lysate can be used to highlight antigens of non-transfected cells. These experiments did not only fully characterize fusion antibody, but also shows a potential that fusion antibody can be used in place of traditional IgG. Ultimately, these experiments demonstrate that fusion antibody can be used to highlight behavior of endogenous Golgi enzymes.

Additionally, these fusion antibody constructs have been transfected into T-REx HeLa cells because HeLa cells are more adherent, and therefore they are more useful for future *in vivo* correlative microscopy for studying behavior of endogenous Golgi enzymes.

### **3.5. Fusion antibody can be used as a tool to observe protein internalization from the cell surface.**

So far, we were able to fully characterize the fusion antibody for its antigenic ability. We also discovered that conditioned media contains fusion antibody, which can be used to stain fixed and permeabilized cells.

In order to determine whether or not the fusion antibody could be used as a tool to monitor protein cycling from cell membrane, affinity purified fusion antibody from the T-REx

Hek293 cells were added to live cells. Non-transfected HeLa cells were incubated with 1 $\mu$ g affinity purified fusion antibody for 24 hours in 1% serum. After fixation, cells were stained with monoclonal GalT antibody. Here, GalT antibody was raised against an epitope that is different from that of the fusion antibody. Immunofluorescence images acquired from this experiment shows that fusion antibody was internalized, and it partially co-localizes with endogenous GalT (Fig. 3-11a).

In order to eliminate a possibility of non-specific internalization, HeLa cells were incubated with 1 $\mu$ g of secondary antibody (anti-rabbit Alexa 568) for 24 hours in 1% serum. While fusion antibody EGFP-FSAB-GalT-RGS6HIS3FLAG internalized to intracellular environment, there was no obvious internalization of the secondary antibody (Fig. 3-11b). Therefore, there must be a specific mechanism for uptake of fusion antibody from plasma membrane.

**a.**

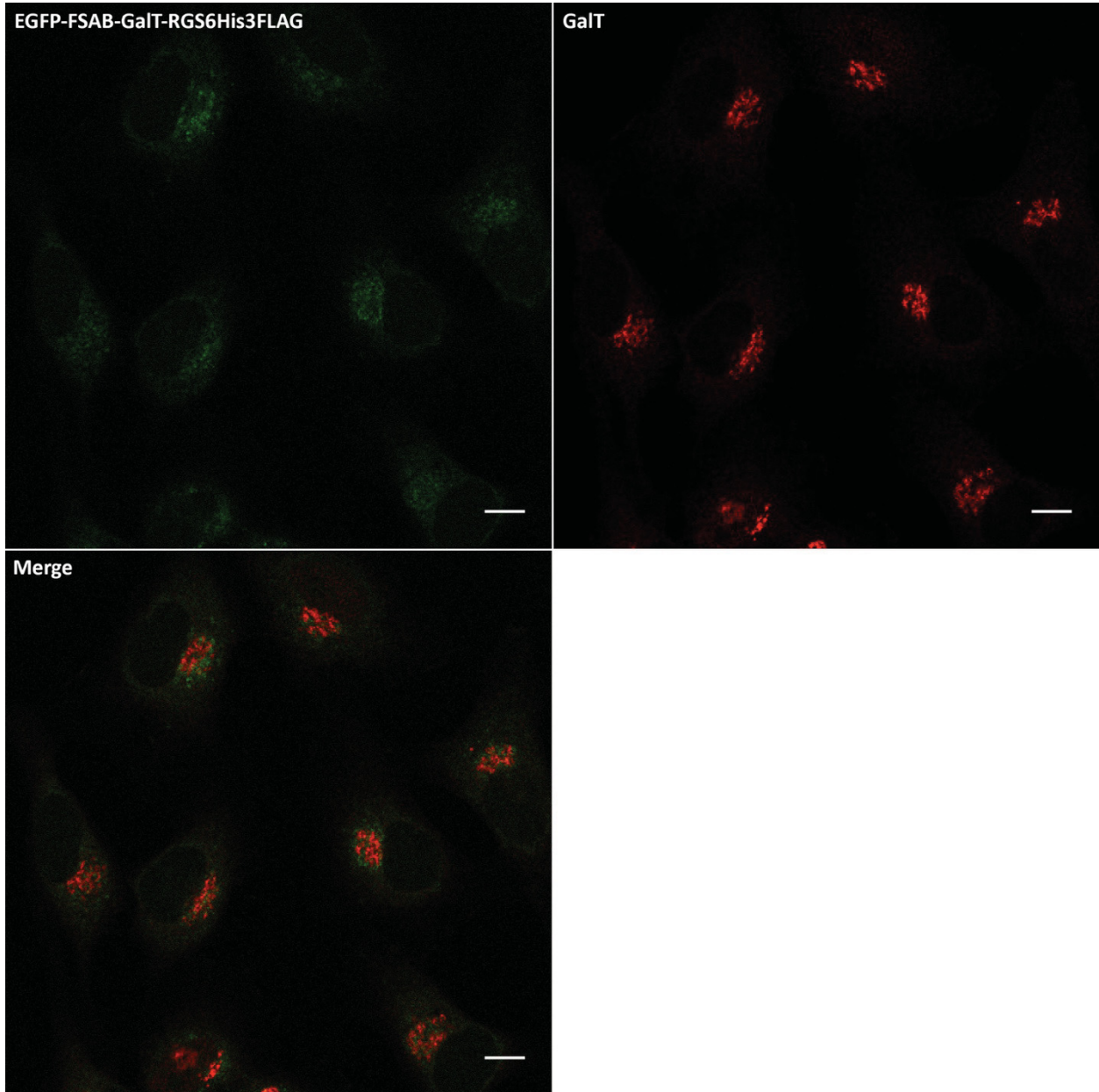


(Figure continues on the next page.)

**b.**

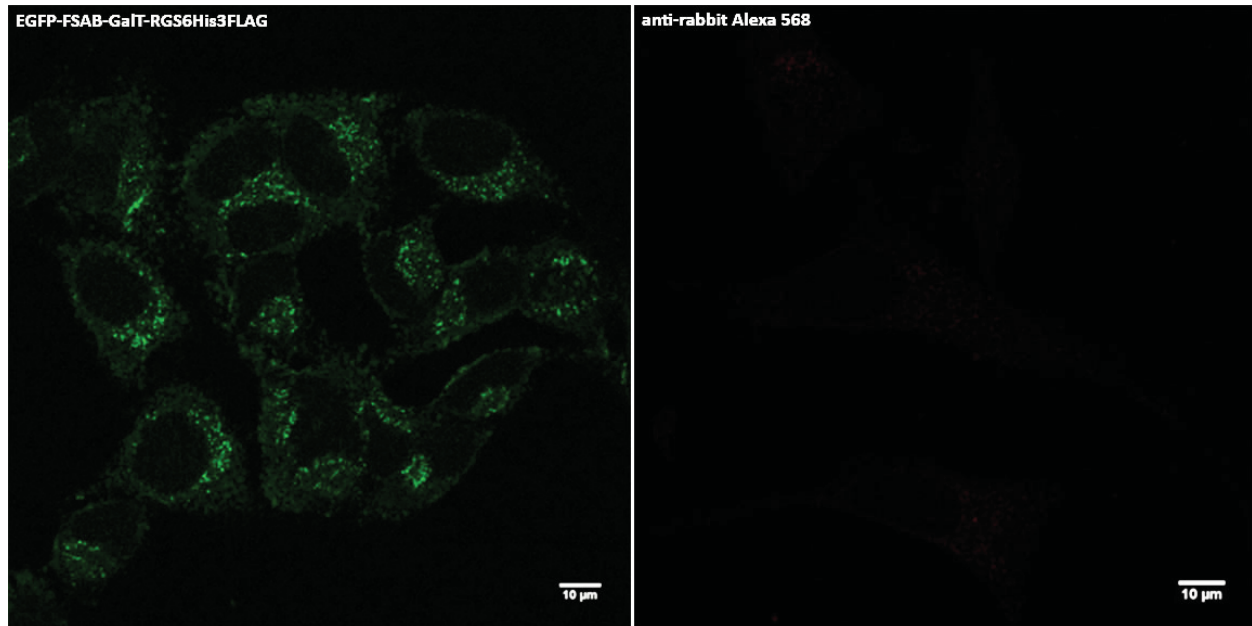


**Figure 3-11:** Fusion antibody can be used as a tool to observe protein internalization from the cell surface.

- a.** Affinity purified EGFP-FSAB-GalT-RGS6HIS3FLAG is internalized. Affinity purified fusion antibody from the T-REx Hek293 cells was added to non-transfected HeLa cells for 24 hours. Upon fixation, cells were stained with monoclonal antibody GalT (Alexa 568, red). Scale bar is 10 $\mu$ m.
- b.** Internalization of fusion antibody is specific. HeLa cells were incubated with 1 $\mu$ g of affinity purified fusion antibody (left panel) or anti-rabbit Alexa 568 (right panel) for 24hours. Subsequently, cells were fixed and mounted.

### **3.6. GalT cycles through plasma membrane before lysosomal degradation.**

GalT is post-translationally modified, where the C-terminal tail is cleaved. As a result, there are two forms of GalT enzyme: long form (wild-type) and short form (13 amino acids shorter). Previously, it was shown that the two forms of GalT are localized at different locations. Although both have galactose transferring activity, the long form (wild-type) was postulated to travel to cell membrane: Research group led by Shur postulated that the wild type (WT) travels to cell surface, and this cycling is dependent on phosphorylation (Hathaway et al., 2003). Fusion

antibody is an adequate tool for testing this hypothesis because fusion antibody is highly specific for GalT, and it can be added to live cells to monitor protein internalization. Furthermore, fusion antibody was made from a luminal domain of the GalT monoclonal antibody; therefore, it can recognize both WT and short form. Additionally, there are different populations of HeLa cells, which stably express different variants of GalT: WT GalT-myc, phosphorylation mutant (serine mutated to alanine) GalT-myc; and short GalT-myc. According to the hypothesis by Shur and colleagues, this phosphorylation mutant of GalT (SA-GalT-myc) and the short form without the cytoplasmic tail (short GalT-EGFP) would not be traveling to cell membrane. If fusion antibody can highlight GalT internalization, SA-GalT-myc will have no or little fusion antibody uptake. Similarly, there will be no internalization in short GalT-EGFP expressing cells.

In Figure 3-12, non-transfected cells were incubated with tandem-purified fusion antibody for 24 hours, and fusion antibody was shown to be partially co-localizing with GalT. Distribution of fusion antibody is not perfectly Golgi, and it resembles post-Golgi/endosomal compartment: it is plausible that fusion antibody is taken up, and it has not yet reached the Golgi. To facilitate fusion antibody uptake to Golgi, we used monensin, a reversible cationophore: It exchanges luminal  $H^+$  for  $Na^+$ , causing swollen vesicles in post-Golgi/endosomal compartments. Golgi enzymes, such as GalT and SialT ( $\alpha$  2,6-sialyltransferase1), were found in these swollen vesicles after 30-60 minute treatment (Schaub et al., 2006). Monensin is reversible; after 30-60 minutes of the washout, Golgi starts to re-integrate (Berger et al., 1993).

For this experiment, four populations of HeLa cells expressing GalT (non-treated HeLa, WT GalT-myc, and SA GalT-myc, and short GalT-myc) were plated at 200,000cells/ml. 1 $\mu$ g of affinity purified GalT fusion antibody was added directly to HeLa cells for 24 hours. In addition, 1% fetal bovine serum was used instead of 10% because GalT in the serum (Madiyalakan et al.,

1987) may cause depletion of fusion antibody reaching to cells. Then, monensin was added for 60 minutes at 2 $\mu$ M concentration, and cells were washed twice with DMEM before adding back the fusion antibody for a recovery. After 2 hours of recovery, cells were fixed and stained against GalT to determine whether or not fusion antibody has reached the Golgi. Immunofluorescence images shown in Fig. 3-12 are maximum intensity Z-projections. In all cells, fusion antibody (green) seems to have reached post-Golgi/endosomal/lysosomal compartment.

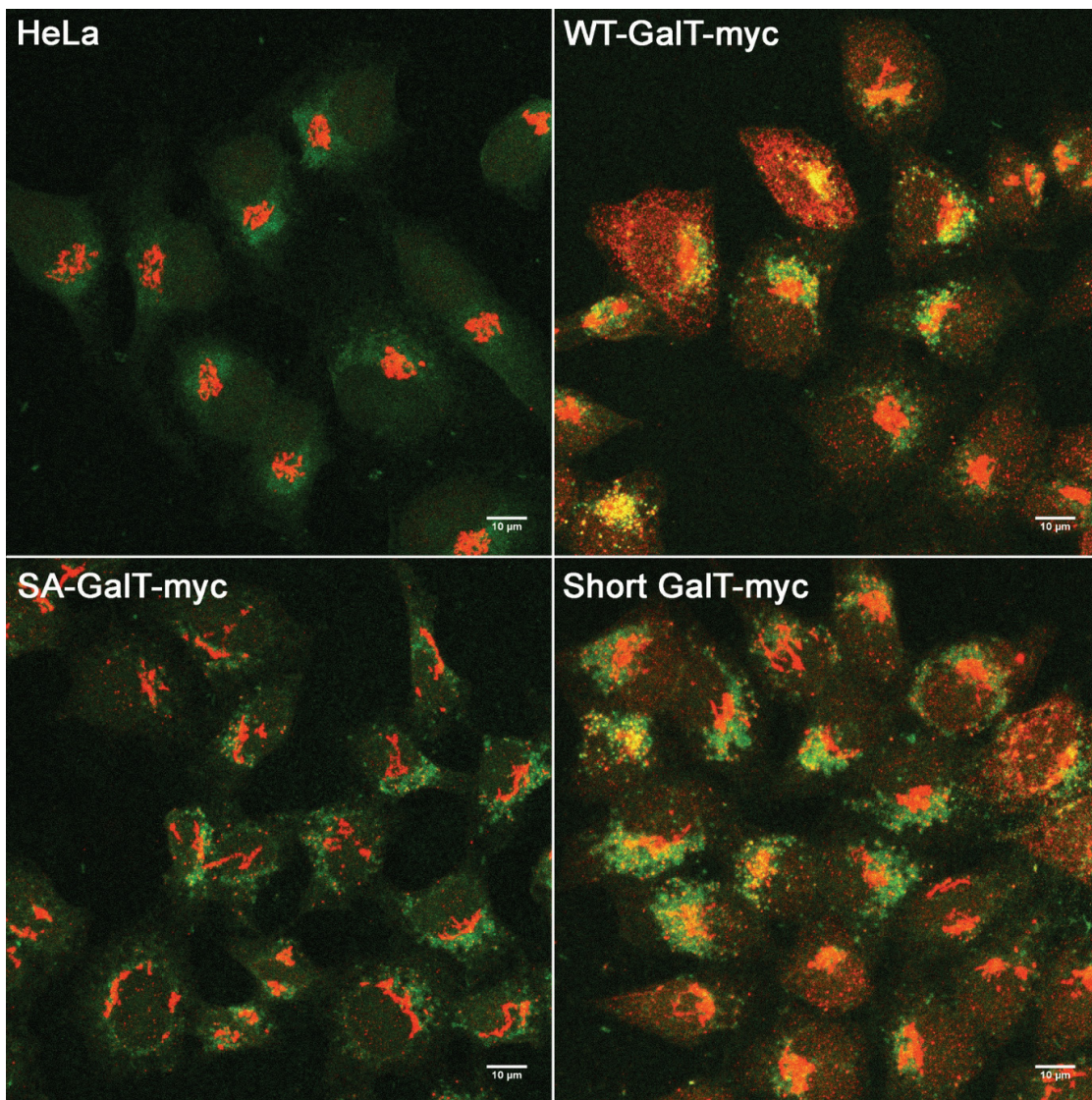


(Figure legend continues on the next page.)

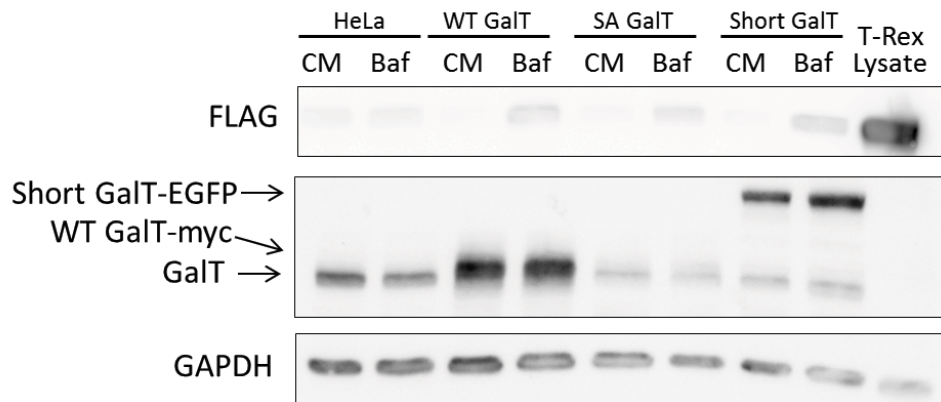
**Figure 3-12:** Fusion antibody uptake to Golgi/endosomal/lysosomal compartment.

HeLa WT GalT-myc, HeLa SA GalT-myc, and short GalT-myc were incubated with 1 $\mu$ g of affinity purified fusion antibody for 24 hours and 2 $\mu$ M monensin for 60 minutes. Cells were rinsed twice before adding back fusion antibody for 2hour recovery. After the experiment, cells were fixed, permeabilized, and stained for GalT-Alexa 568 (red). Z-sections were taken in 0.39 $\mu$ m increments from top to bottom, and max intensity projections were generated using ImageJ. Scale bar is 10 $\mu$ m.

In order to enhance the amount of fusion antibody uptake, fusion antibody concentration, and monensin concentration and treatment conditions were varied. Yet, some fusion antibody was in post-Golgi/endosomal compartment; fusion antibody did not seem to reach fully to the Golgi. It is plausible that GalT is presented on the cell surface, and not all of it cycles back to Golgi: GalT on cell surface may be degraded by endosomal/lysosomal compartments, and affinity purified fusion antibody taken from the cell surface binds to the cell surface GalT, and follows GalT for degradation. In order to test this hypothesis, bafilomycin A1, a drug that inhibits vacuolar H<sup>+</sup> ATPase, was added to stop the lysosomal acidification and degradation.

To carry out this experiment, four populations of HeLa cells expressing GalT were plated at pre-determined density and 2 $\mu$ g of affinity purified fusion antibody (EGFP-FSAB-GalT-RGS6His3FLAG) was added for 24 hours. Four hours before fusion antibody incubation was finished, 400nM Bafilomycin A1 was added. After the experiment, cells were harvested, and proteins were analyzed by Western blot. To semi-quantify the fusion antibody internalization, the blot was probed by FLAG (Fig. 3-13a).

a.



b.

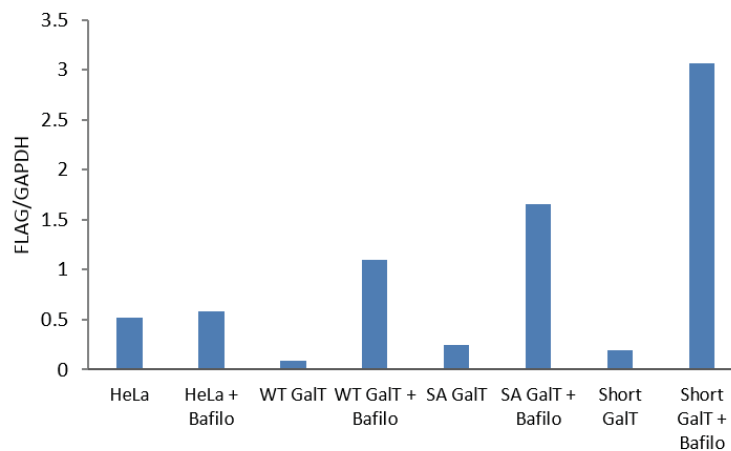


**Figure 3-13:** Internalization of fusion antibody.

- a. Internalization of affinity purified fusion antibody is blocked by bafilomycin A1. HeLa cells stably expressing WT GalT-myc, SA GalT-myc or short GalT-EGFP were incubated with affinity purified fusion antibody for 24 hours and 400nM bafilomycin A1 for 4 hours. Cell lysates with internalized fusion antibody (EGFP-FSAB-GalT-RGS6His3FLAG) were analyzed by Western blot against FLAG. Different variants of GalT were analyzed by GalT antibody, and GAPDH is a loading control. CM: control media (no Bafilomycin A1), Baf: Bafilomycin A1.
- b. Quantification of relative FLAG band intensity over GAPDH.

Interestingly, the amount of internalized fusion antibody was different, and with bafilomycin A1, there are increasing the amount of internalization (Fig. 3-13). Surprisingly, HeLa stably expressing short GalT-myc have significant amount of fusion antibody uptake, which was 2 to 7 times greater than other forms of GalT. If the fusion antibody uptake is correlated with the GalT cycling from PM, this observation suggests that the GalT lacking the cytoplasmic tail is localized on the PM and it may be internalized and degraded by lysosomes.

**Chapter 4: Endophilin B1—A novel lipid droplet protein essential  
for EPA mediated lipophagy**

#### **4.1. Endophilin B1 is located on lipid droplet surface.**

First, to understand the mechanism of TAG accumulation in the human liver, we determined the total protein profile of subcellular organelles from hepatocytes isolated from human livers. These tissues were donated from over 100 NAFLD and cirrhotic liver patients. Protein contents of the subcellular fractionations were analyzed by mass spectrometry, and results were displayed as relative protein abundance in the heat map (Fig. 4-1a). Higher intensity towards red indicates higher protein expression level. Many known LD-associated proteins and novel proteins were detected in LD fractions. For instance, LD-associated proteins PLIN1-5 are distributed over LD fractions. One of the proteins that came to our interests was endophilin B1, an N-BAR domain-containing protein involved in endocytosis. Endophilin B1 is usually present in the cytosol, plasma membrane, and Golgi. Indeed, our mass spectrometry detected endophilin B1 specific tryptic peptides in homogenate (Hom), cytosol (Cyt), rough ER (rER) smooth ER (sER), Golgi/endosome/lysosomes (GEL) and lipid droplet (denoted as cLD in this figure. Otherwise LD). A pathologist examined each liver section, which was subsequently classified as 'low NAFLD,' 'NAFLD,' 'NASH' or 'cirrhotic,' and these are denoted by green, yellow, red and blue colours, respectively (Fig. 4-1a). Note that distributions of endophilin B1 are not uniform between the livers. In order to make a better connection between the levels of endophilin B1 and the disease states, the levels of endophilin B1 in LD fractions from mass spectrometry were grouped to 'low (ND and 2x)' and 'high (5x and 10x)' (see table, Fig. 4-1b). The levels of endophilin B1 was subsequently plotted as a bar graph in Fig. 1b. Interestingly, there was a positive correlation between the expression level of endophilin B1 and the severity of fatty liver disease state (Fig. 4-1b).

To verify the relative protein level (tryptic peptide) seen by the mass spectrometry, delipidated LD fractions from livers #4, #10 and #14 were further analyzed by Western blot. High level of endophilin B1 was detected from LD fractions of liver #4 and #14 (Fig. 4-1c), and it corresponded to relative abundance seen by the mass spectrometry (10x, Fig. 4-1a). Similarly, Western blot band intensity from liver #10 was roughly half compared to livers #4 or #14, and this also corresponded to relative abundance seen by the mass spectrometry (5x, Fig. 4-1a). For subsequent experiments, liver #14 was used. To verify that endophilin B1 is present in LD fraction, cryo-sectioned human livers have been stained with Bodipy green (Bodipy 493/503) and endophilin B1 monoclonal antibody. Endophilin B1 is clearly around LD in liver #14 (Fig. 4-1d). Also, endophilin B1 co-localizes with a LD marker perilipin 1, proving the Bodipy green staining structures, which endophilin B1 is localized, are indeed LDs (Fig. 4-1e). As a negative control, liver #57 was selected due to a low level of endophilin B1 manifested by mass spectrometry (Fig. 4-1a). Furthermore, no specific endophilin B1 staining around LD was confirmed by indirect immunofluorescence (Fig. 4-1d). Western blot and immunofluorescence result shown here validate the mass spectrometry data.

a.

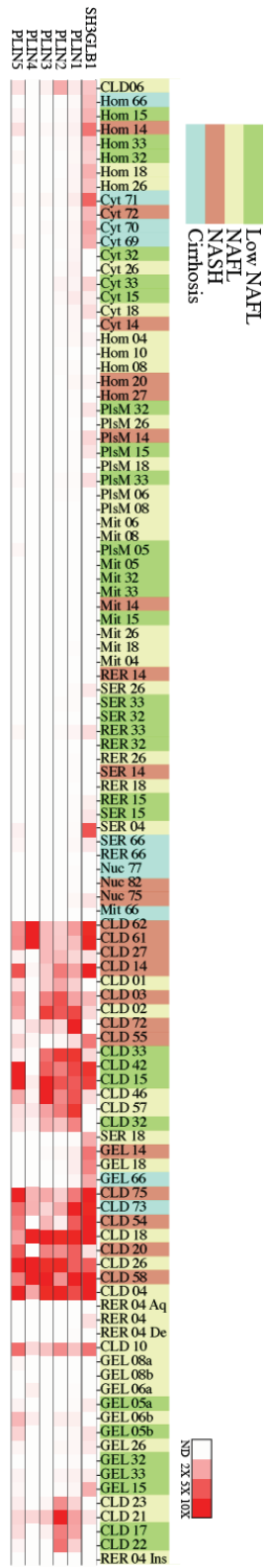
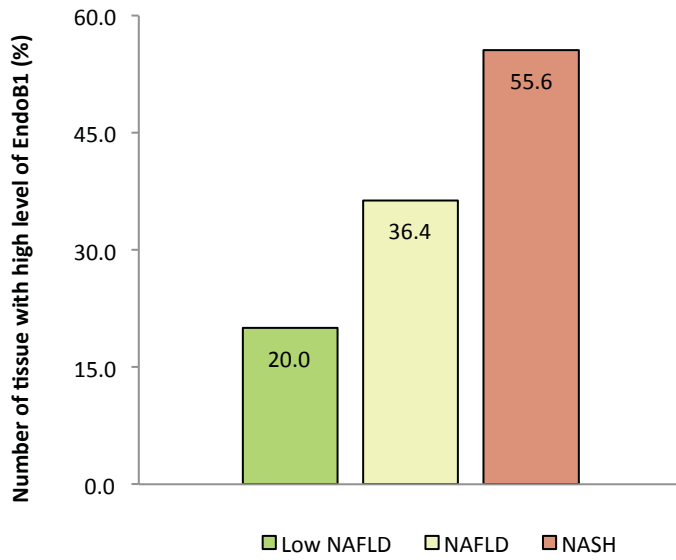
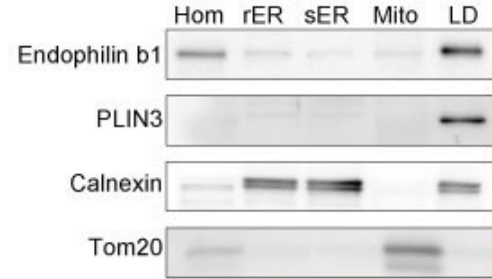


(Figure continues on the next page.)

**b.**



**c.**



Percentage (%)	Low NAFLD	NAFLD	NASH
Low EndoB1 level	80.0	63.6	44.4
High EndoB1 level	20.0	36.4	55.6

**d.**

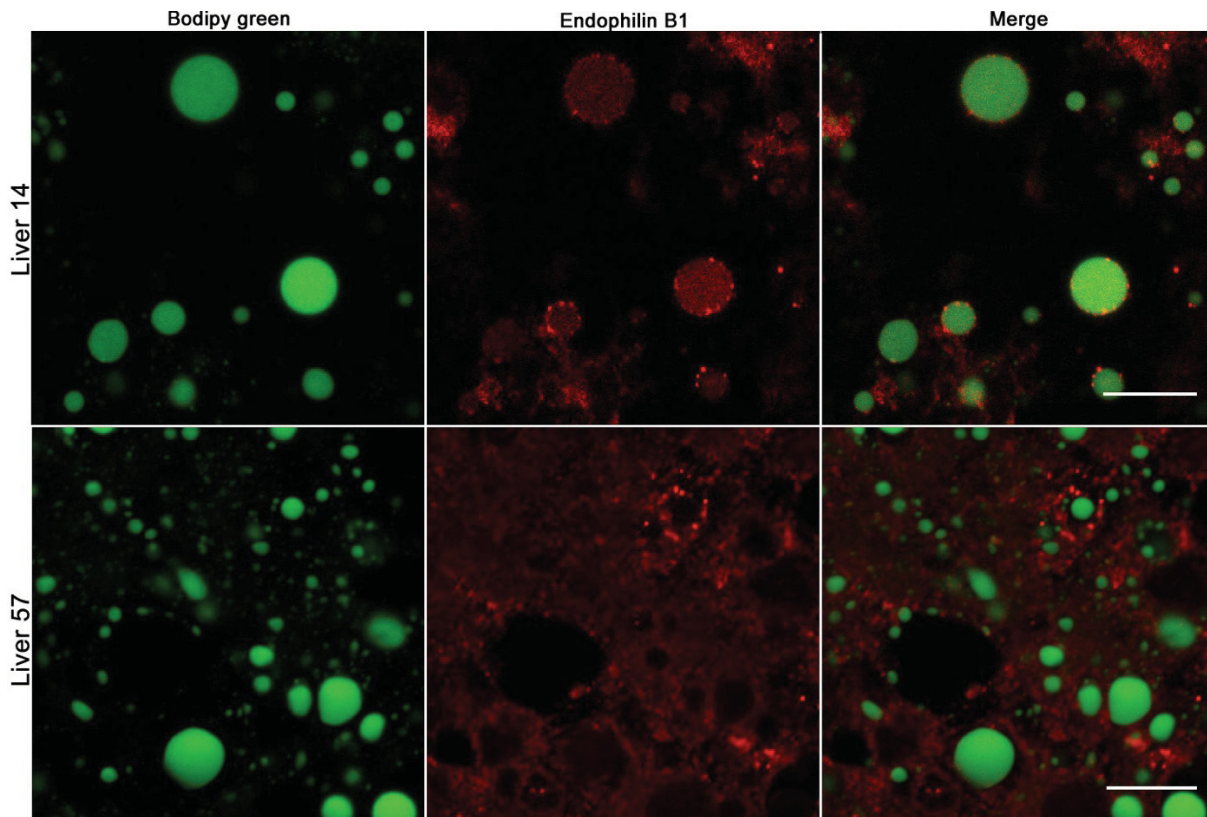


(Figure continues on the next page.)

e.

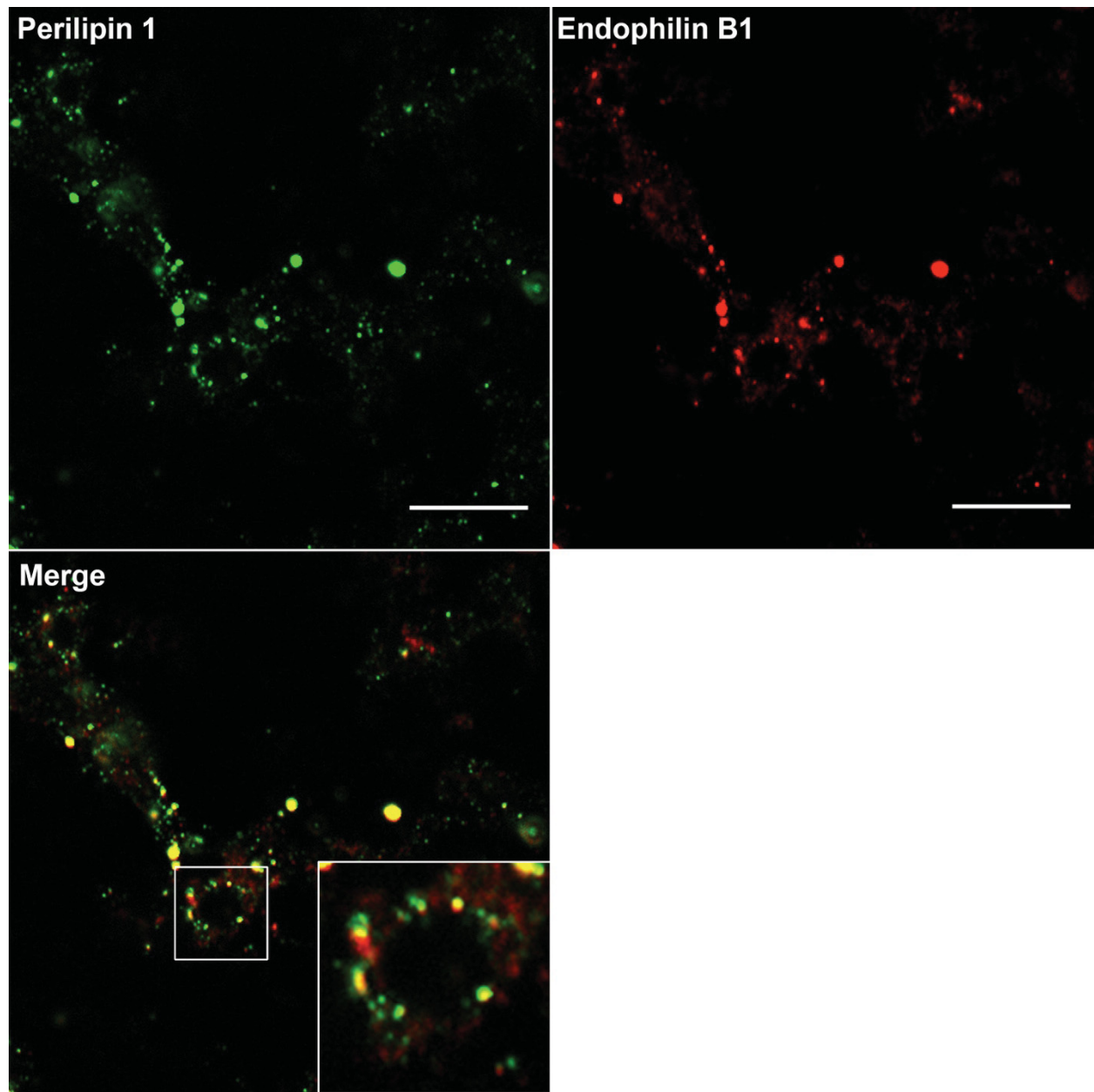


**Figure 4-1:** Endophilin B1 is enriched in LD fractions of human fatty livers.

**a.** Heat map shows that LD fractions of human fatty livers contain endophilin B1 (SH3GLB1). Endophilin B1 is detected in homogenate (Hom), cytosol (Cyt), rough ER (rER) smooth ER (sER), Golgi/endosome/lysosomes (GEL) and lipid droplet (cLD). LD-associated proteins PLIN1-5 are distributed over LD fractions. Note that distributions of endophilin B1 are not uniform between livers. Bar: Relative expression level set as not detected (ND), and times (X) relative to the lowest expression such that 1X equals eight peptides for each protein. Labels are liver homogenate (Hom); cytosol (Cyt); plasma membrane (PlsM); mitochondria (Mit); smooth (SER) and rough (RER) endoplasmic reticulum; nuclei (Nuc); cytoplasmic

lipid droplets (CLDs); and Golgi/endosome/lysosomes (GEL).

- b.** A number of tissues with a high level of endophilin B1. From a, ND and 2x were grouped as 'low,' and 5x and 10x were grouped to 'high.' These values were represented as percentages and a bar graph.
- c.** Western blot analysis with Hom, rER, sER, Mito (mitochondria) and LD fractions from Liver #14. Different organellar markers are shown: PLIN3 for LD, Calnexin for ER, Tom20 for mitochondria. It shows that LD fraction is enriched with endophilin B1.
- d.** Indirect immunofluorescence of human fatty liver #14 shows that endophilin B1 localizes on the surface of LD. Human liver cryo-sections were cut from isopentane frozen tissue with a 6-9 micron thickness. The tissue samples were fixed using 3% formaldehyde with 0.1mM CaCl<sub>2</sub> and 0.1mM MgCl<sub>2</sub> for 20 minutes before washing in PBS. The fixed samples were submerged in 6M guanidine hydrochloride for 10 minutes before being permeabilized by 0.2% Triton x100 for 20 minutes. These samples were blocked using 10% goat serum for 30 minutes. Primary antibody against endophilin B1, anti-mouse Alexa 568 (red) and Bodipy green were diluted in 5% goat serum. Primary antibody was incubated for 60 minutes, and secondary antibodies were incubated for 45 minutes. Following PBS and final wash with water, coverslips were mounted by Mowiol. Endophilin B1 (red) localizes around LD (green) of liver 14, but not of liver 57. Scale bar is 10µm.
- e.** Frozen human fatty liver section from liver #14 was stained with LD marker perilipin1 (Alexa 488, green) and anti-endophilin B1 (Alexa 568, red). Endophilin B1 localizes around LD. To prevent crosstalk of fluorescence emission, two individual lasers were used to scan the tissue sequentially, and two separate detectors were used with different filter sets. Scale bar is 10µm.

Our mass spectrometry data from subcellular fractionation shows that endophilin B1 is present in plasma membrane and cytosol, and these observations are consistent with endophilin B1's previously suggested functions in endocytosis and autophagy. Also, a novel role of endophilin B1 was proposed in lipid metabolism (Liu et al., 2016). Yet, its mechanism or localization on LD was never investigated. Therefore, we were interested to find out how and when endophilin B1 is involved in lipid metabolism. First, we observed that endogenous endophilin B1 is present on LD surface under conditions that stimulate autophagy. In Figure 4-2, HepG2 cells were treated with excess OA (0.5mM for 4hours), followed by rapamycin and bafilomycin A. Rapamycin is an inhibitor of mTOR1 and its inhibition will ultimately enhance

autophagy. That is, mTORC (of which mTOR1 is a part of) acts as a clamp for autophagy, and when it is inhibited, autophagy is promoted. Bafilomycin A is an inhibitor of lysosomal ATPase pump, and it prevents the acidification of lysosome. Eventually, in bafilomycin A treated cells autophagosomes cannot fuse with the lysosome, leading to disturbed autophagosome clearance. Using rapamycin and bafilomycin A, autophagosome can be visualized. In the images taken by wide-field fluorescent microscope, endophilin B1 stained by Alexa 488 is localized on LD (identified by LD marker PLIN2-Alexa 594). Under basal conditions (top panel), endophilin B1 is distributed in the cytosol. In contrast, when autophagy is enhanced by rapamycin and bafilomycin A, endophilin B1 rather is observed on the LD surface (Fig. 4-2, bottom two panels).

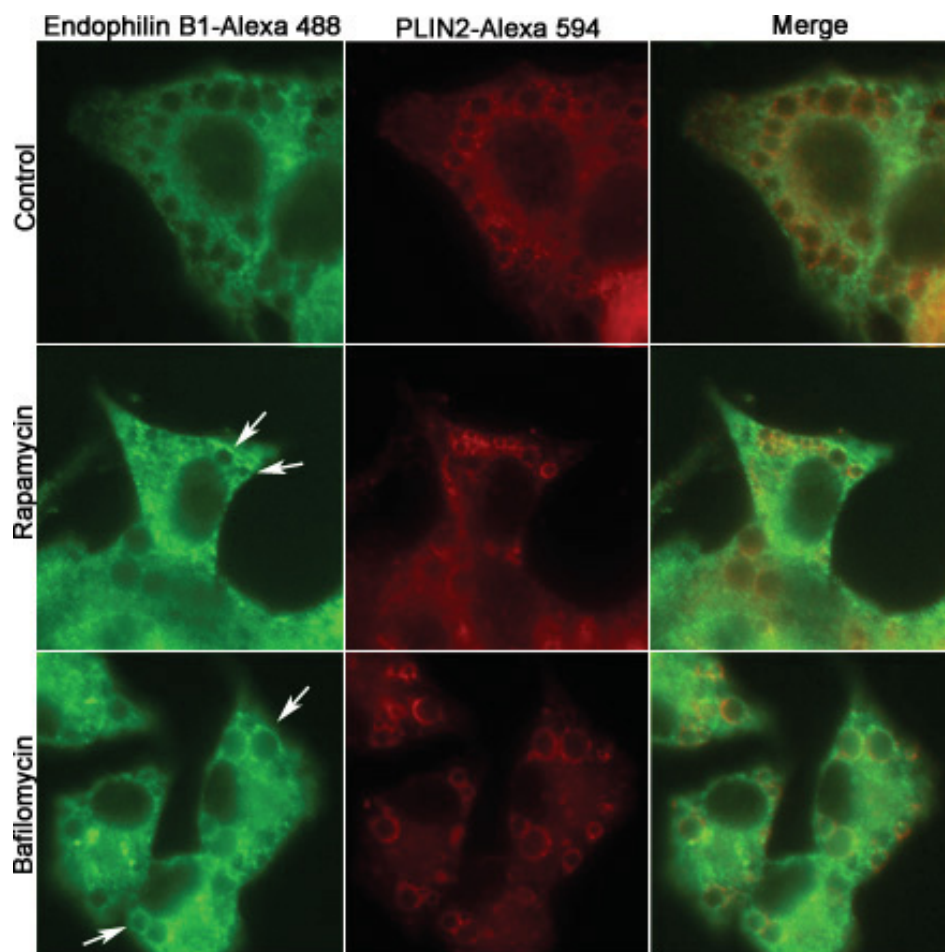


(Figure legend is found on the next page.)

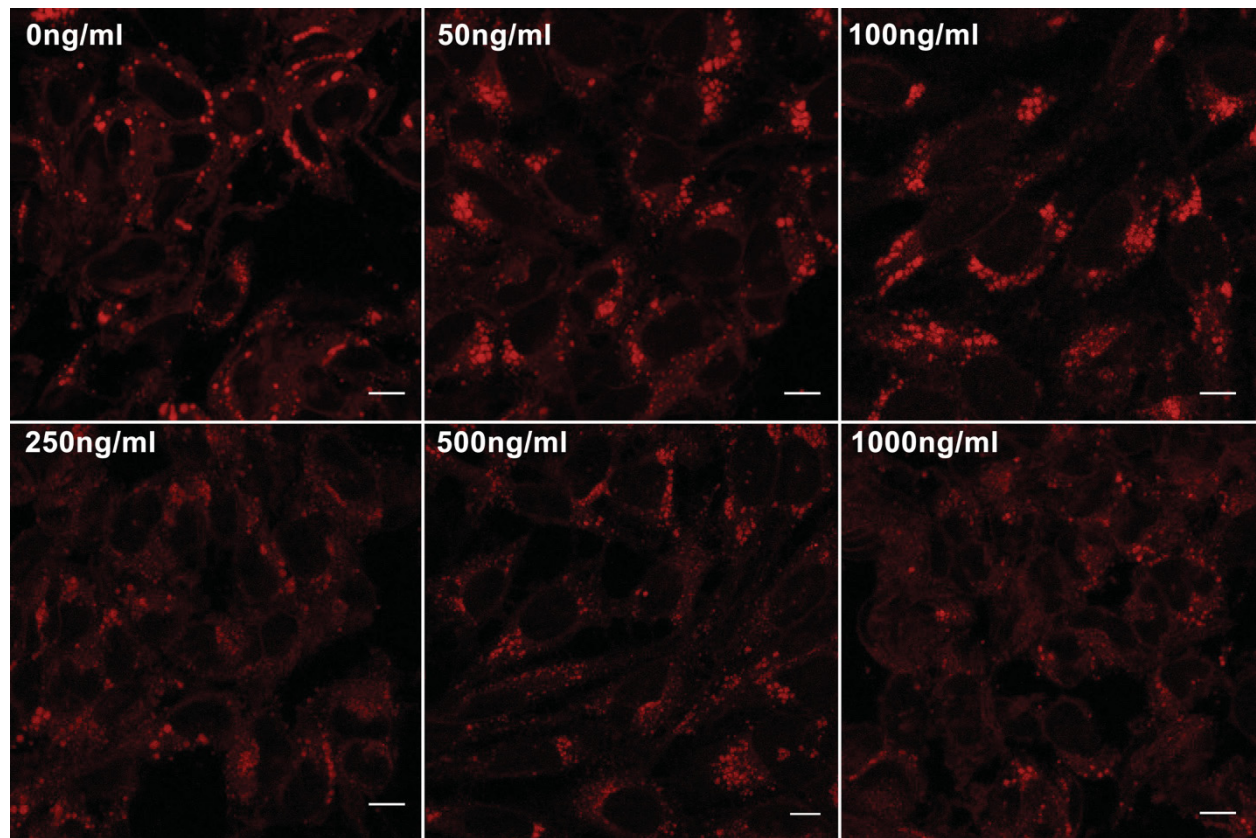
**Figure 4-2:** Endogenous endophilin B1 is localized on LD in autophagy conditions.

Immunofluorescence shows endogenous endophilin B1 moves to LD in autophagy. HepG2 cells were incubated with 0.4mM oleate for 4 hours and control media, rapamycin (5 $\mu$ M) or bafilomycin (50nM) were added for 20 hours. Upon fixation, cells were stained with endophilin B1-Alexa 488 and PLIN2-Alexa 594. Images were acquired by Zeiss Axiovert wild field microscope. Note the endophilin B1 moves to PLIN2 positive LDs in rapamycin and bafilomycin-treated cells. In control cells, endophilin B1 shows a global distribution.

## **4.2. Endophilin B1 is involved in lipid breakdown.**

Although functions of the endophilin family of proteins have been implicated in endocytosis and autophagosome formation, endophilin B1 has never been seen on LD, nor the role of endophilin B1 in lipid metabolism was elucidated. Here, in order to reveal functions of endophilin B1 on LD, endophilin B1 was first overexpressed. To enhance endophilin B1 expression in an inducible manner, we have generated T-REx HeLa cell line that inducibly expresses endophilin B1-EGFP in the presence of tetracycline. The advantage of this inducible system was that the amount of endophilin B1-EGFP could be carefully modulated depending on the tetracycline concentration. This tetracycline-inducible system was widely used in this chapter. After plating the cells, various concentrations of tetracycline were added for 24 hours. Subsequently, oleic acid (OA) was also added for 16 hours at 0.2mM concentration. Upon fixation, cells were stained with Nile red to highlight and assess LD size. Finally, cells were also harvested for protein analysis. As expected, cells that were not induced of endophilin B1-EGFP expression had the largest LDs with an average size of 1.30 $\mu$ m in diameter whereas cells that were expressing the most endophilin B1-EGFP produced the smallest LDs of 0.94 $\mu$ m in diameter (Fig. 4-3).

**a.**



**b.**

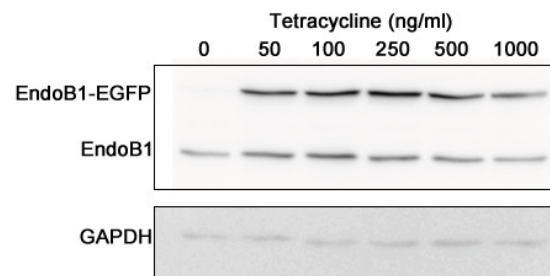


(Figure continues on the next page.)

c.

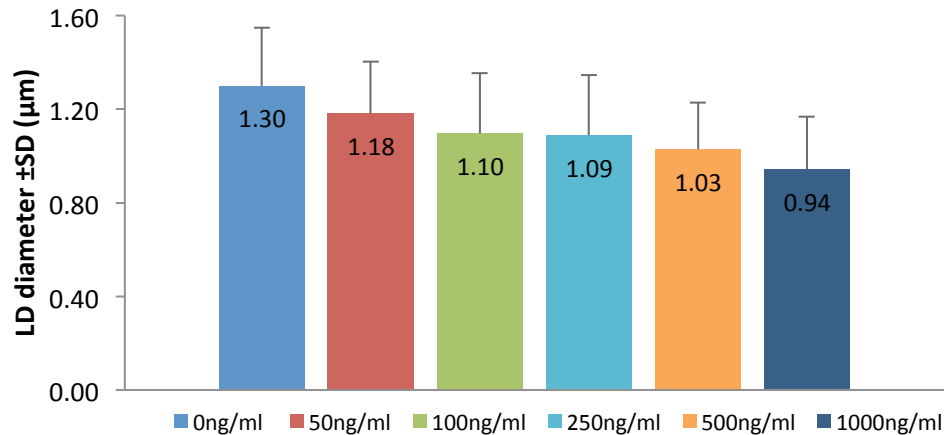


**Figure 4-3:** Endophilin B1 expression decreases LD size.

In order to investigate whether expressing the greater amount of endophilin B1 causes LD breakdown, T-Rex HeLa EndoB1-EGFP cells were incubated with the indicated amount of tetracycline for 24 hours and oleate was added for the last 16 hours.

- Immunofluorescence of T-Rex HeLa EndoB1-EGFP cells. After the experiment, cells were fixed and stained with Nile Red. Note that LDs becomes smaller progressively with more endophilin expression (correlates with tetracycline concentration). Scale bar is 10µm.
- Western blot analysis shows expression of endophilin B1-EGFP and endogenous endophilin B1. Increase in the tetracycline concentration correlates with the amount of endophilin B1-EGFP expression. GAPDH shows equal loading of proteins in all lanes.
- Bar graph showing LD diameter (µm). The diameter of LD decreases from 1.30µm to 0.94µm as tetracycline concentration is increased from 0ng/ml to 1000ng/ml. Difference between 0ng/ml and 1000ng/ml is significant ( $p=1.21e-10$ ). Error bar is the standard deviation. More than ten cells and 500 LDs were counted per condition.

To better understand the function of endophilin B1 on LDs, endophilin B1 was knocked down. After plating cells at pre-determined density, cells were transfected with 50pM of endophilin B1 specific siRNA for two successive days. Then, OA was added at 0.2mM concentration for 6 hours to induce LD formation. Following fixation and staining LDs with Bodipy green, the effect of endophilin B1 KD on LD was observed. Interestingly, KD of

endophilin B1 resulted in enlarged LD in both cultured hepatocytes (HepG2) and cervical cancer cells (HeLa) (Fig. 4-4).

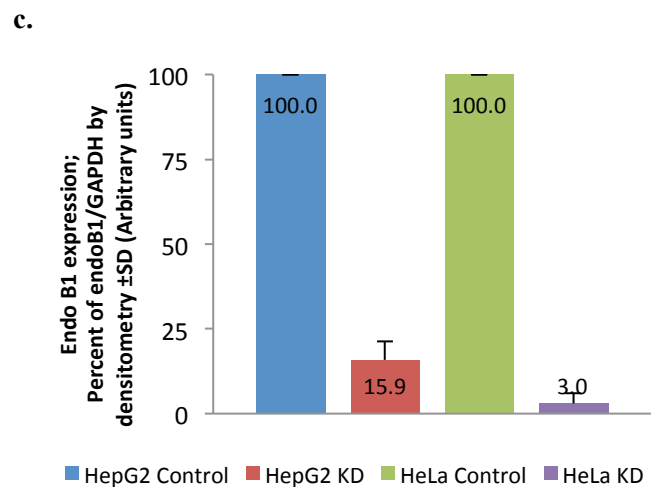
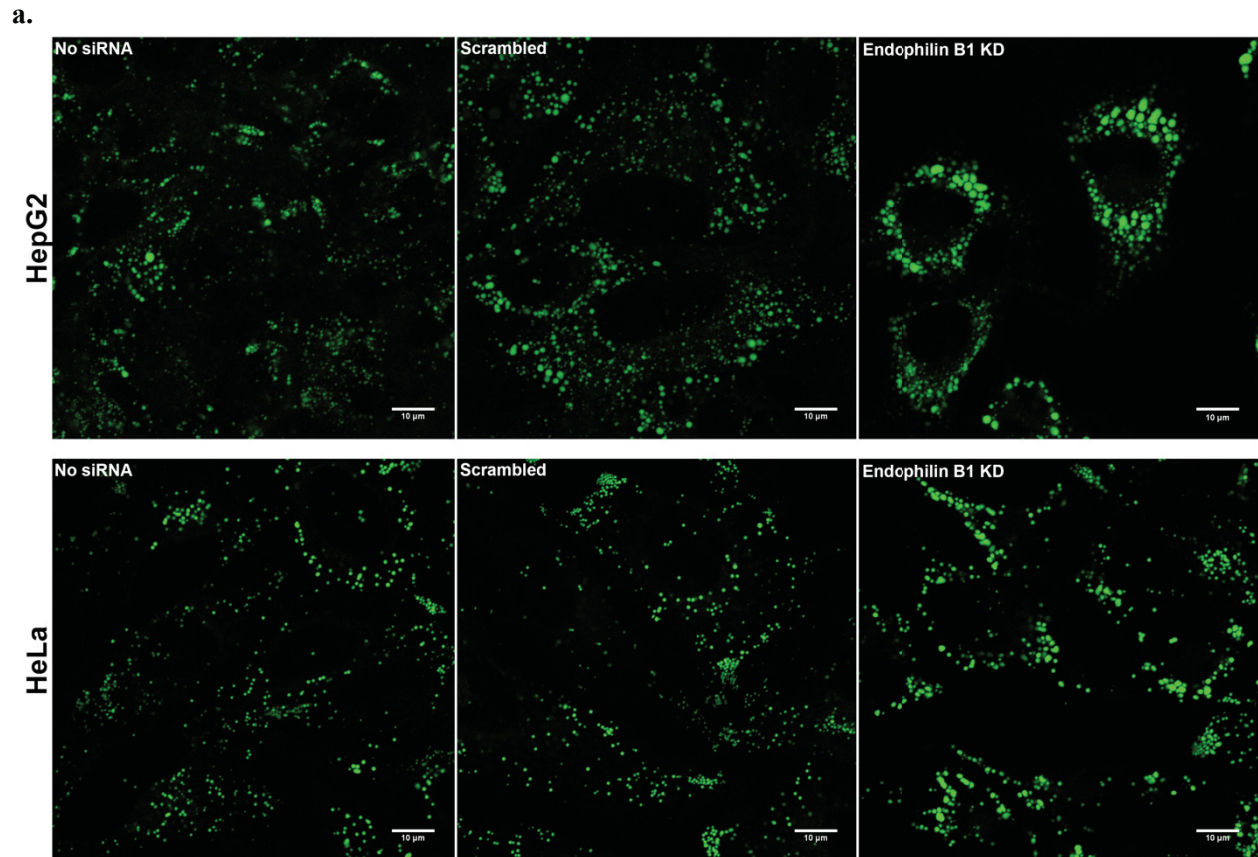


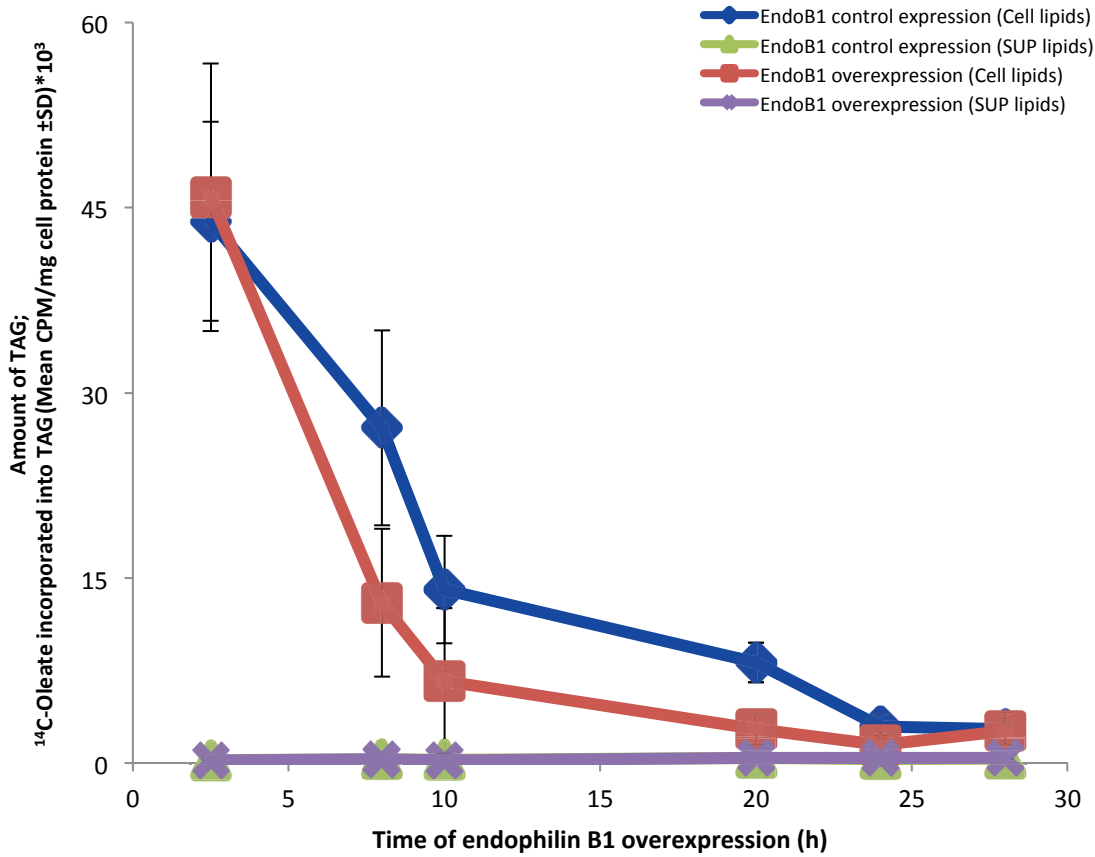
(Figure legend continues on the next page.)

**Figure 4-4:** Endophilin B1 is involved in lipophagy

- a.** When endophilin B1 is knockdown in HepG2 and HeLa cells, the size of LD becomes greater. Following siRNA transfection, oleate was added for 6 hours. Upon fixation, cells were stained with Bodipy green. Scale bar is 10 $\mu$ m.
- b.** Western blot shows endophilin B1 was successfully knocked down in both HepG2 (84.1%) and HeLa (97%) cells. GAPDH is a loading control.
- c.** The relative intensity of each band was quantified and presented as a bar graph on the right. Band intensities for no siRNA and scrambled were averaged and denoted as Control.

Enlarged LDs in endophilin B1 KD cells might be due to endophilin B1's LD tubulating activity. In fact, endophilin B1 has a unique N-BAR domain that inserts into the membrane to cause membrane tubulation (Gallop et al., 2006; Masuda et al., 2006b). Similarly, recombinant endophilin and Bax causes vesiculation of giant unilamellar vesicle (GUV) in a cell-free system (Rostovtseva et al., 2009). If endophilin B1 causes mere LD fission, the amount of cellular triacylglycerol, a major component of LD, would be similar regardless of endophilin B1's presence. To clarify this hypothesis, the amount of cellular triacylglycerol (TAG) was measured after various hours of endophilin B1 expression. First, T-REx HeLa endophilin B1-EGFP cells were plated. After 24 hours, 0.2mM OA and 1 $\mu$ Ci/ml [<sup>14</sup>C]-oleate were added to trigger LD formation. To induce endophilin B1 expression, tetracycline was added for 2.5, 8, 10, 20, 24 and 28 hours. Following the experiment, radiolabeled lipids were extracted from the cells and analyzed by Thin Layer Chromatography (TLC). Radioactivity from media was also measured. Results show that cellular TAG is decreased drastically as endophilin B1 is expressed (Fig. 4-5a). Notably, the amount of TAG after 8 hours of endophilin B1 expression was at least two-fold lower than the control (Fig. 4-5b). Comparably, radioactivity in the media after the above treatment was extremely low (Fig. 4-5a), precluding the possibility of FFA export (see discussion for more detail). Therefore, endophilin B1 does not only localize onto LDs of human fatty liver and cultured cells, but it also reduces cellular TAG.

a.



b.

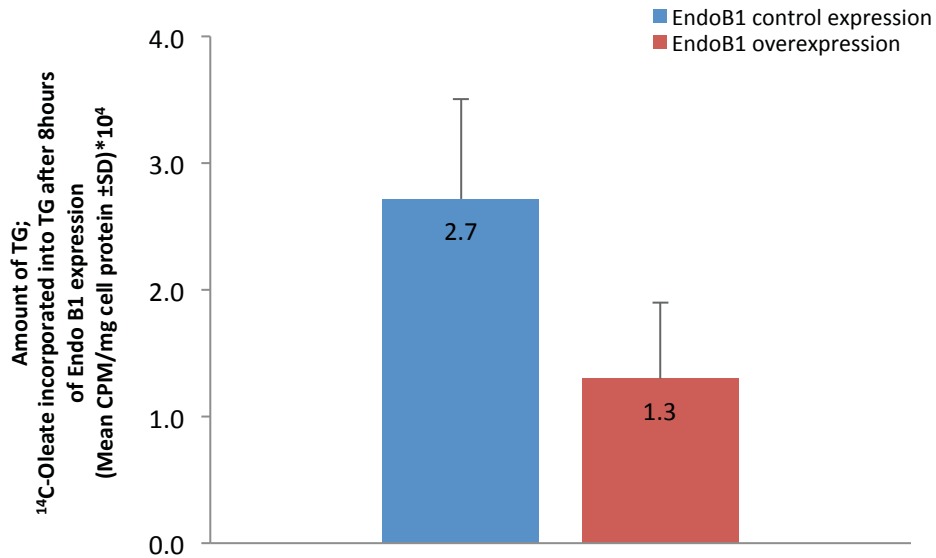


(Figure legend continues on the next page.)

**Figure 4-5: Endophilin B1 decreases cellular triacylglycerol.**

Inducing endophilin B1 expression in T-REx HeLa cells caused a reduction of cellular TAG level. To investigate whether endophilin B1 expression causes lipophagy, cells were incubated with 0.2mM [<sup>14</sup>C]-oleate for 16 hours. Then tetracycline was added for the indicated time to induce endophilin B1 expression. After all the time has elapsed, radiolabeled lipids were extracted and analyzed by TLC. Radioactivity from media was also measured to determine whether or not lipids were exported (SUP lipids). Counts per minute from each sample were normalized by miligram of protein. All conditions were performed in quadruplicate.

- a. Average CMPA/mg protein for all time points.
- b. TAG change after 8 hours of endophilin B1 induction.

It has been previously shown that endophilin B1 is involved in macroautophagy as it binds to essential autophagy triggering proteins such as UVRAG and Beclin1. By doing so, it has been postulated that endophilin B1 gathers membranes necessary for autophagosome formation. LD breakdown that is seen in our experiment may be due to this membrane gathering activity that eventually leads to autophagosome formation around LD. Similarly, endogenous endophilin B1 moved to LD surface upon treatments that favored autophagosome formation (Fig. 4-2). In order to observe how endophilin B1 behaves in an environment that enhances lipid breakdown, T-REx HeLa Endophilin B1-EGFP cells were treated with eicosapentaenoic acid (EPA) (Fig. 4-6). EPA is an omega-3 fatty acid that has been shown to reduce cellular TAG and lipotoxicity (Chen et al., 2015). After seeding cells at pre-determined density, cells were incubated with 250ng/ml tetracycline and 0.2mM OA for 24 and 16 hours, respectively. Then cells were washed once with PBS before adding EPA for 8 hours. After the EPA treatment, endophilin B1-EGFP moved to LD (see arrow in Fig. 4-6).

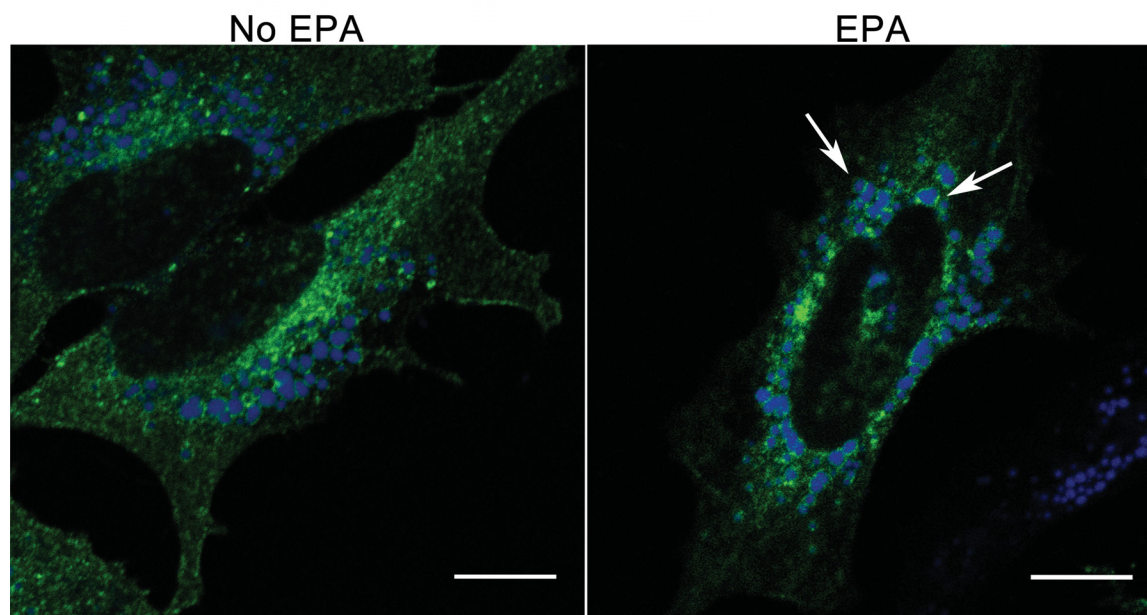


**Figure 4-6:** Endophilin B1 moves to lipid droplet in response to eicosapentaenoic acid (EPA).

EndoB1-EGFP moves to LD when cells are treated with EPA. T-REx HeLa EndoB1-EGFP cells were firstly incubated with tetracycline and oleate for 24 and 16 hours, respectively. Cells were washed once with PBS before adding EPA for 8 hours. Upon fixation, coverslips were stained with Nile red (pseudo coloured to blue) and were mounted on a glass slide for imaging. Cellular LDs are visible in blue. EndoB1-EGFP moves to LD after EPA (arrow). Scale bar is 10 $\mu$ m.

EPA has been shown to decrease cellular lipids, so we wanted to investigate what role endophilin B1 plays in the presence of EPA. Firstly, we tested EPA's lipid breakdown activity by adding it to oleate loaded HepG2 cells for various time points. As seen in Fig. 4-7, EPA gradually makes LD size smaller, where its effect was the most evident upon 6 hours. This phenotype confirms previous findings and, hence, we will use EPA to highlight endophilin B1's behavior in subsequent experiments.

a.

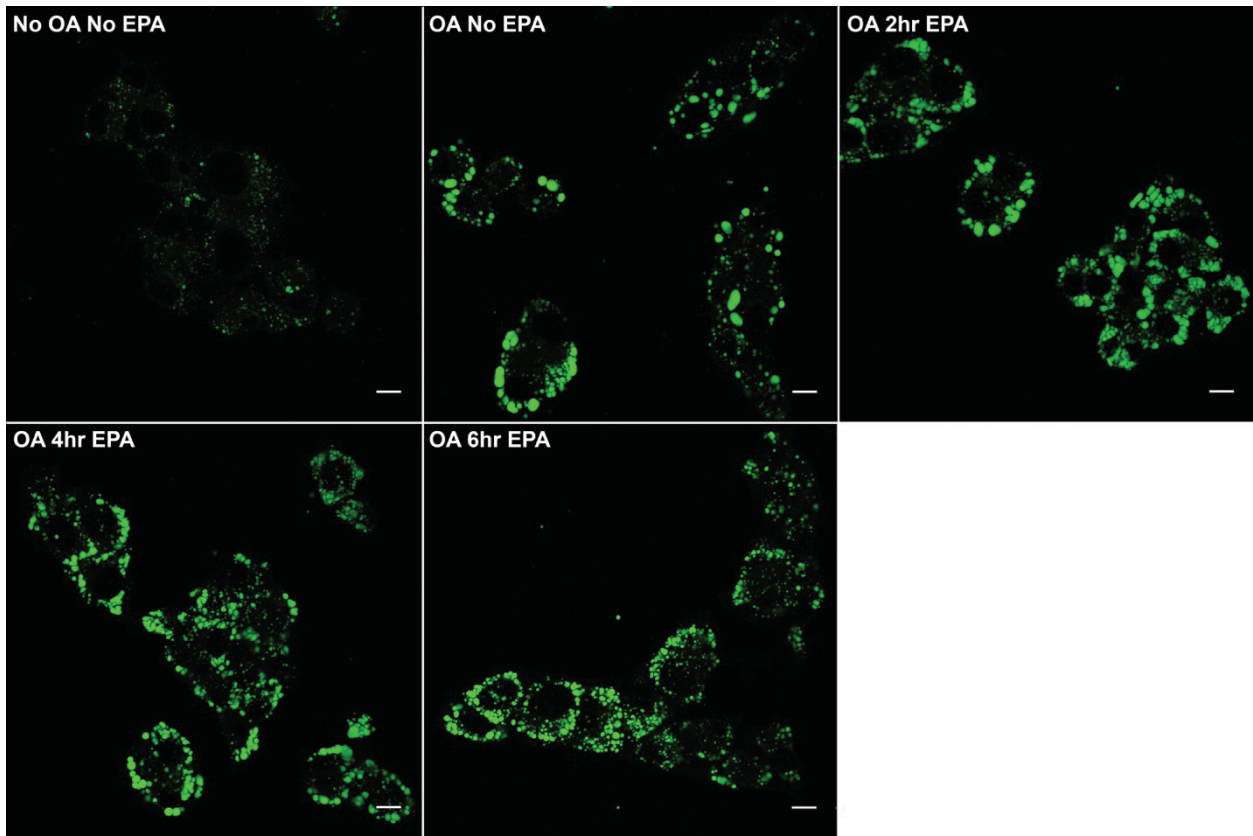


(Figure continues on the next page.)

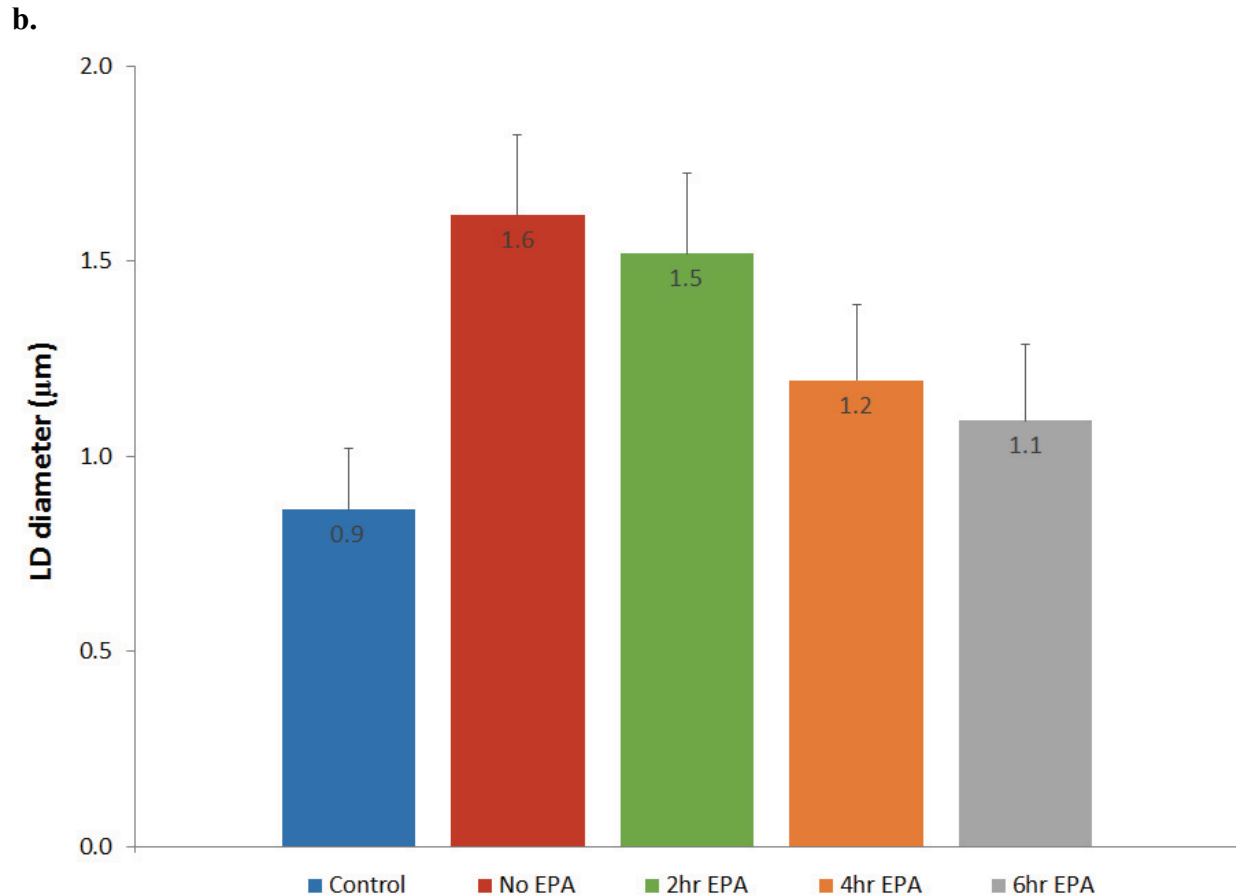


**Figure 4-7:** EPA treatment causes lipid droplet to decrease in size.

- a.** In HepG2 cells, EPA causes LD to decrease in size progressively. Cells were incubated with OA for 16 hours followed by EPA for the indicated times. Upon fixation, cells were stained with Bodipy green. Scale bar is 10µm.
- b.** Bar graph shows LD diameter (µm). For each condition, more than 200 cells were counted. The difference between Control and 6 hour EPA is significant ( $p=1.70e-60$ ).

It is already known that endophilin B1 is involved in the macroautophagy and starvation-induced autophagy (Takahashi et al., 2011). Our results show that endophilin B1 translocated from the cytosol and/or Golgi to LD when autophagy was enhanced (by Torin1 and amino acid starvation), and these results correspond to the previous finding. However, the function of endophilin B1 has never been illustrated in EPA-treated cells. To determine if endophilin B1-mediated LD breakdown is related to EPA, endophilin B1 expressing cells were treated with

EPA. Indeed, upon induction of endophilin B1-EGFP expression, endophilin B1-EGFP translocates progressively to LD surface (Fig. 4-8a). Moreover, increasing hours of EPA treatment progressively decreases LD diameter. After 6 hours of EPA treatment, a significant percentage of LDs falls below 0.5 $\mu$ m in diameter (Fig. 4-8b).

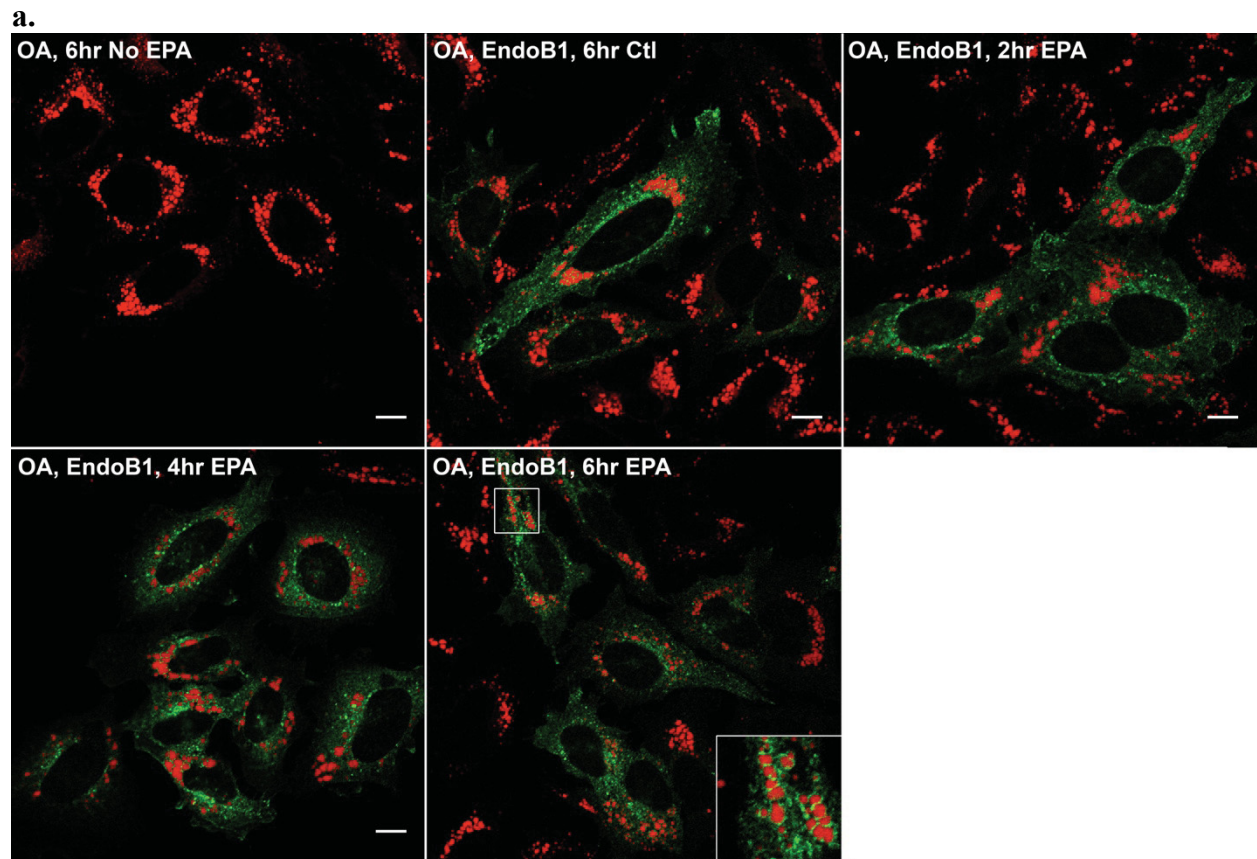


(Figure continues on the next page.)

b.

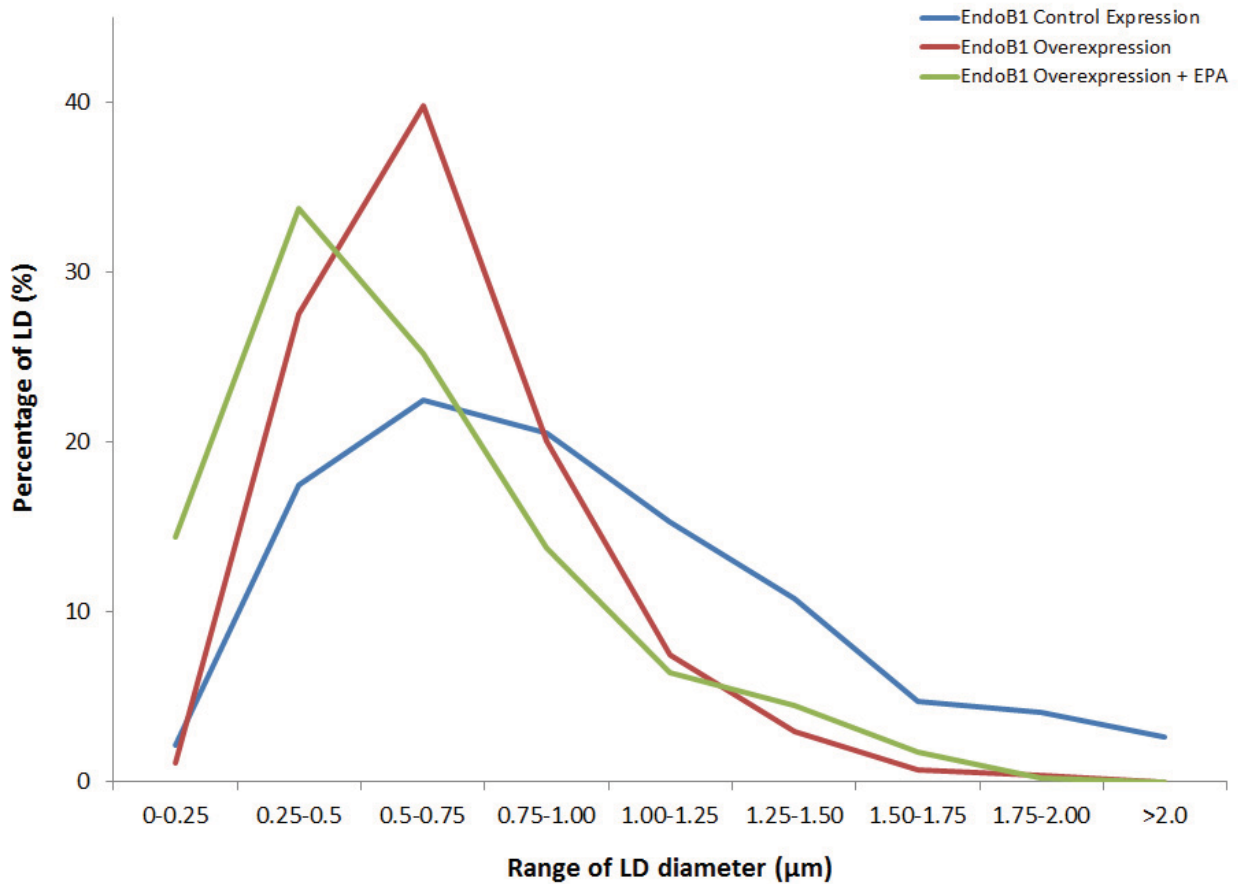
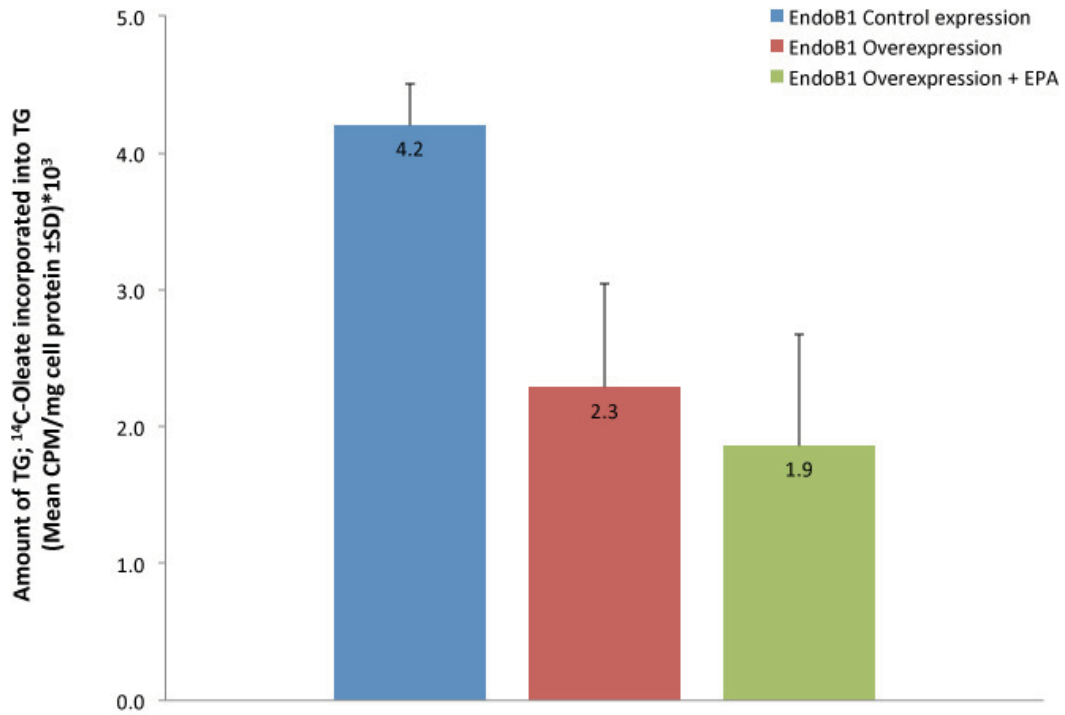


**Figure 4-8:** Time course expression of endophilin B1 and EPA causes LD breakdown.

- a. Endophilin B1-EGFP in T-REx HeLa cells moves progressively to LD (See inset). Expressing endophilin B1 (Tet) and EPA treatment cause LD size to decrease progressively. After endophilin B1-EGFP expression had been induced by tetracycline, OA was added for 16 hours followed by EPA treatment for 6 hours. Upon fixation, cells were stained with Nile Red.
- b. Histogram for a percentage of LD diameter. The bin is described as a range of LD diameter, and it is 0.25μm. When endophilin B1 is overexpressed (Tet, red graph), the graph is skewed to the right, and this denotes a decrease of LD size. Note that 39.8% of endophilin B1 overexpressing cells' LDs are 0.5-0.75μm in size. When EPA is added (Tet, EPA, green graph), the graph is strongly skewed to the right. Peak size shifts from 0.5-0.75μm to 0.25-0.5μm. More than 500 LDs were counted, and experiments were performed for six times.

It seems that endophilin B1 does not only decrease LD diameter in response to EPA, but also it speeds up lipophagy because total level of TAG decreases with endophilin B1 expression and EPA treatment (Fig. 4-9a). To observe time course response of EPA treatment in endophilin B1 expressing cells, cells were incubated with radioactive OA (0.2mM OA and 1 $\mu$ Ci/ml [<sup>14</sup>C]-oleate) for 24 hours and tetracycline (100ng/ml) to induce endophilin B1 expression. Followed by PBS wash, EPA was added for 2.5, 8, 10, 20, 24 and 28 hours. Media was also collected to determine whether or not radiolabeled lipids were exported. Radioactive lipids were extracted from the cell with hexane and analyzed by TLC. Compared to cells that only had OA and tetracycline (endophilin B1 expression), EPA loaded cells had lower TAG (Fig. 4-9b). Media from each well was centrifuged at 10,000rpm for 5 minutes, and 100 $\mu$ l of it was measured. Compared to cellular lipids, there is a minuscule amount of radioactivity (Fig. 4-9b, SUP lipids). This observation suggests that EPA does not increase lipid exocytosis.

a.



b.

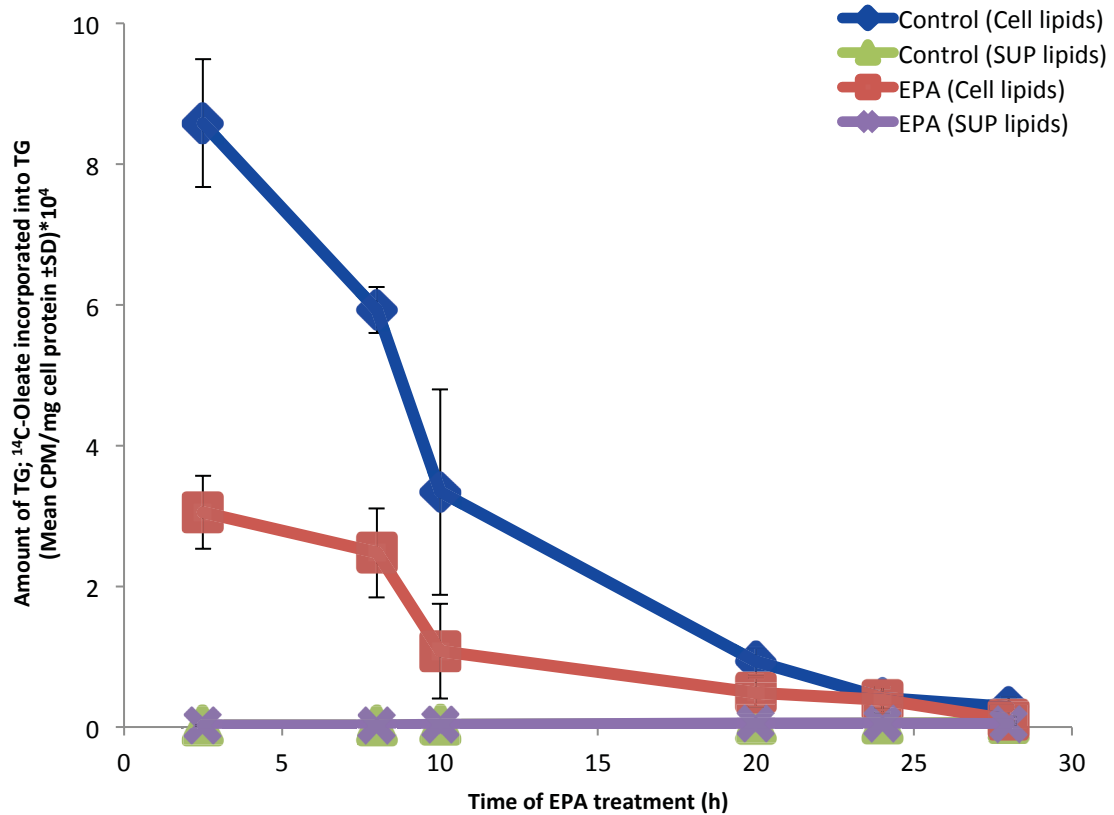


**Figure 4-9:** Endophilin B1 and EPA decrease cellular triacylglycerol.

- a.** Endophilin B1 and EPA decrease cellular lipids. Inducing endophilin B1 expression in T-REx HeLa cells causes a reduction of total TAG level. Upon induction by tetracycline, [<sup>14</sup>C]-Oleate was added for 16 hours followed by 8 hour EPA incubation. Radiolabeled lipids were extracted and measured. Counts per minute from each sample were normalized by microgram of protein. The experiment was repeated two times.
- b.** Time course EPA treatment decreases cellular triacylglycerol. Inducing endophilin B1 expression in T-REx HeLa cells caused a decrease of cellular TAG level. To observe the lipophagic effect of EPA and endophilin B1, cells were incubated with [<sup>14</sup>C]-oleate and tetracycline for 24 hours. Then EPA was added for the indicated time. After all the time has elapsed, radiolabeled lipids were extracted and analyzed by TLC. Counts per minute from each sample were normalized by protein concentration. All conditions were performed in quadruplicate.

Endophilin B1, as Bif-1, has been shown to bind BAX, initiating apoptosis. However, the involvement of endophilin B1 in the apoptosis does not seem intuitive; while overexpression of endophilin B1 leads to the initiation of apoptosis, knockdown does not affect apoptosis. In order to test whether the conditions used in this thesis affect the cell viability, T-REx HeLa endophilin B1-EGFP cells were seeded at a pre-determined density and were tested for cell viability using trypan blue exclusion counts. One population of cells was not incubated with OA or tetracycline, and this population represents control endophilin B1 expression. Other populations were either tetracycline added (to induce endophilin B1 expression), OA loaded (to induce LD formation), or EPA supplemented for 6 hours (to induce lipophagy). In these conditions, average percent cell viability was 96.9%, 95.6%, 94.4%, and 95.5% with p-value greater than 0.33. Therefore, cell viability was not affected by overexpression of endophilin B1, OA, or EPA.

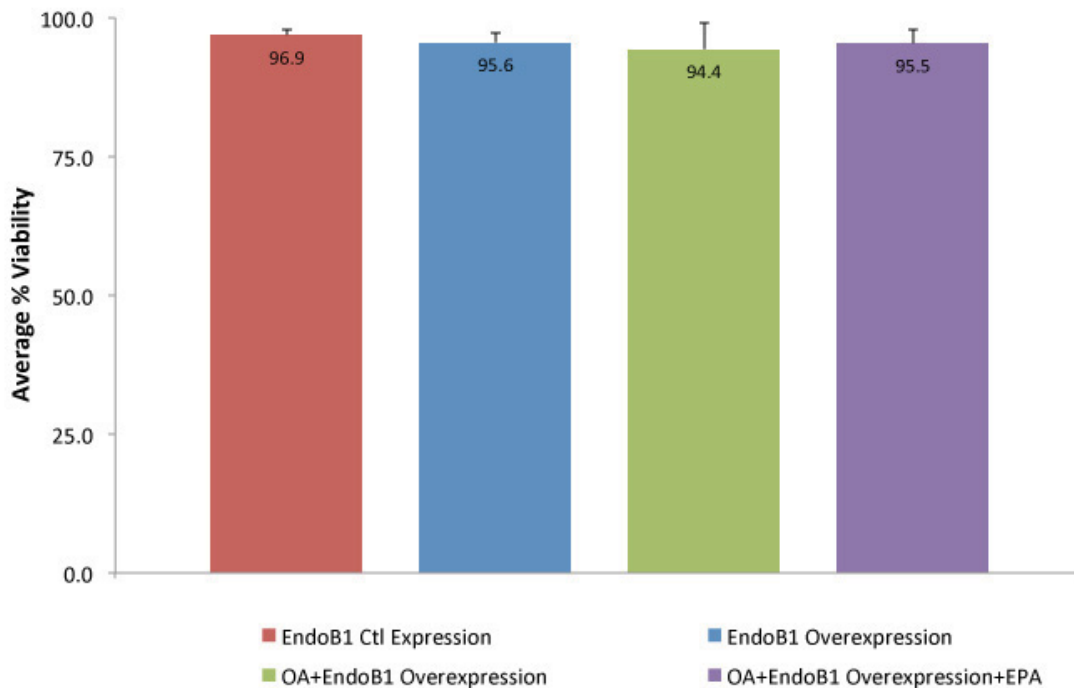


**Figure 4-10:** Overexpressing endophilin B1 or EPA treatment does not affect cell viability.

Bar graph showing average percent cell viability. T-REx HeLa endophilin B1-EGFP cells were counted after mixing appropriate volumes of cells and trypan blue assay according to the manufacturer's instructions. Clear cells were marked viable, and blue cells were marked dead. To overexpress endophilin B1, 100ng/ml tetracycline was added for 24 hours (Blue, green and purple bars). To induce LD formation, 0.2mM OA was added for 16 hours (Green and purple bars). To stimulate lipophagy, 0.4mM EPA was supplemented for 6 hours (Purple bar). Endophilin B1 control expression (red bar) is without induction, OA or EPA. Differences between the conditions are not significant as  $p > 0.33$ . Measurements are in triplicate.

A Recent study showed that EPA reduces lipid accumulation within the liver cells, lowering cytotoxicity (Chen et al., 2015). This group has also demonstrated that prolonged incubation of EPA increased LC3 turnover. In order to see if we could replicate this finding, we transfected HeLa cells with eGFP-RFP-LC3 plasmid, which allows visualization of lysosome-fused autophagosomes (autophagolysosomes). The rationale is that this eGFP is pH-sensitive,

and it does not fluoresce at low pH. On the other hand, mRFP is pH-insensitive. Therefore, mRFP remains visible whereas eGFP is lost when autophagosome fuses with the lysosome. HeLa cells transfected with this construct were incubated with or without EPA for 6 hours and were observed by live cell imaging. Series of Z-stack images were captured with z distance of 0.2~0.4 $\mu$ m. All images were projected to one plane to count the total number of eGFP and mRFP puncta per cell (Fig. 4-11a, b).

**a.**

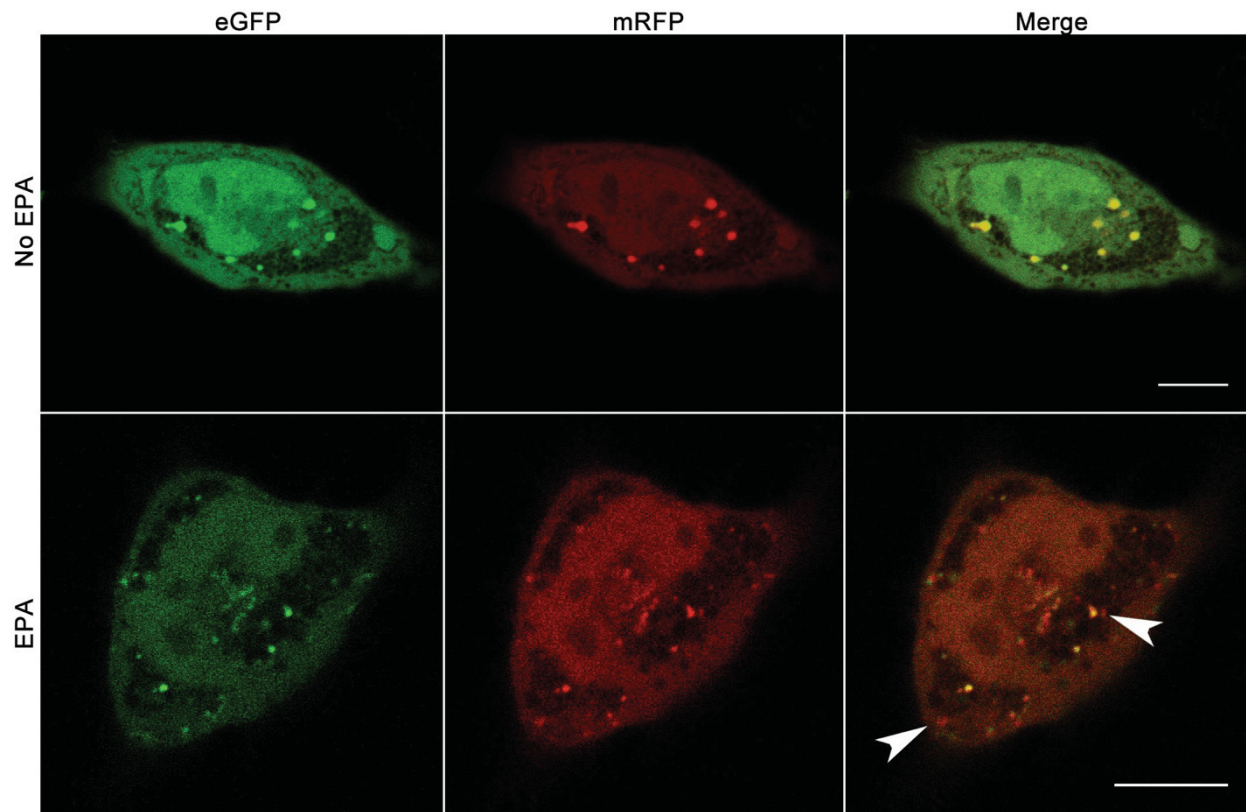


(Figure continues on the next page.)

**b.**

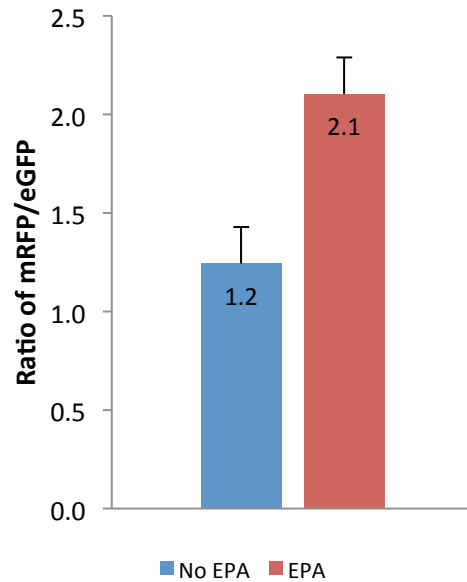


**Figure 4-11:** EPA increases autophagosome fusion with acidic compartments.

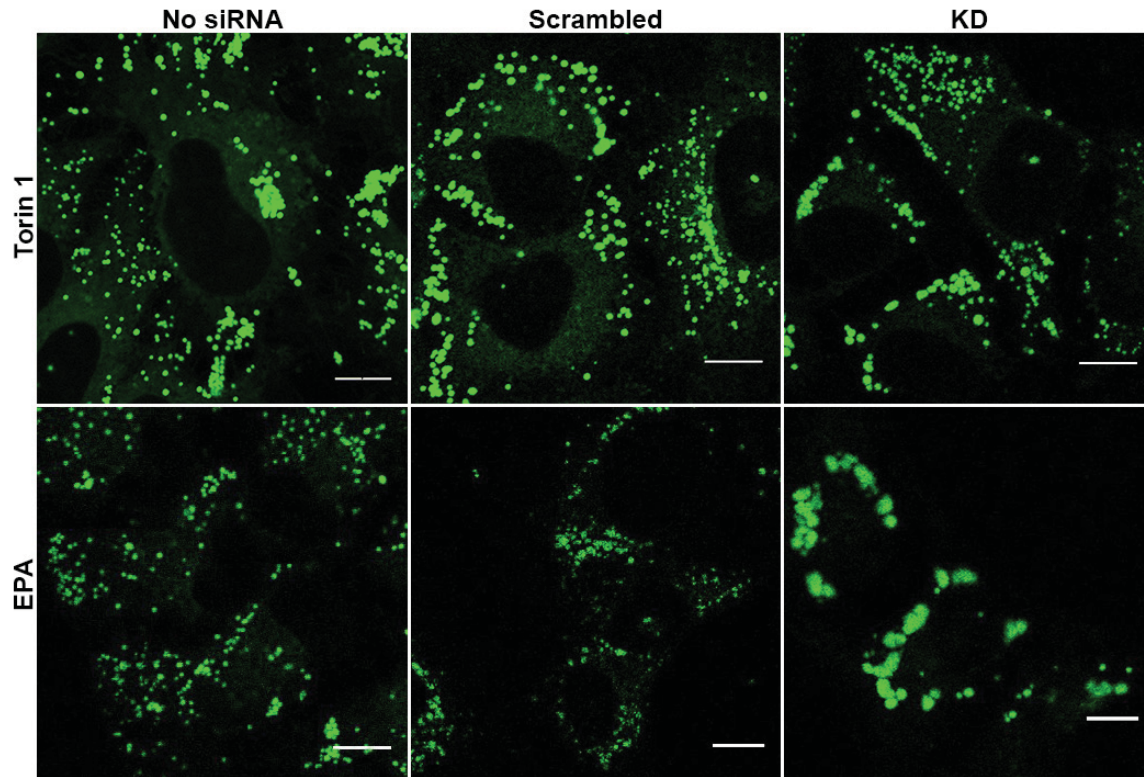
- a.** Immunofluorescence of HeLa cells showing autophagosome fusion. HeLa cells were seeded on glass bottom dish for 16 hours. Then, cells were transfected with 1 $\mu$ g of eGFP-mRFP-LC3 construct for 24 hours and loaded with 0.2mM OA for 16 hours. Cells were washed once with PBS before adding 0.4mM EPA for 6 hours. Following the incubation, EPA media was removed, and cells were imaged with live cell imaging. All images were taken from top to bottom of the cell with 0.2-0.4 $\mu$ m Z-distances. Images shown here are one plane amongst all Z-stacks. Scale bar is 10 $\mu$ m.
- b.** Quantification of mRFP/eGFP ratio. All eGFP and mRFP puncta were counted, and mRFP/eGFP ratio was calculated for each cell. All mRFP/eGFP ratios were averaged and presented as a bar graph. For each condition, more than ten cells per experiment were counted, and this experiment was repeated for four times.

Collectively, these results in Figure 4-9 and 4-11 suggest that EPA treatment increases autophagosome (monitored by LC3) and that it cooperates with endophilin B1 to reduce cellular TAG.

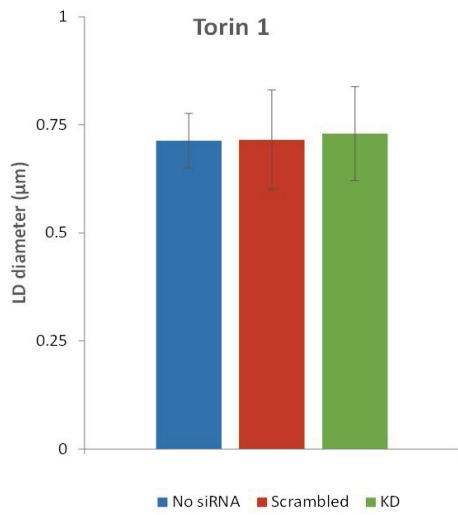
### **4.3. Endophilin B1 is involved in EPA mediated lipophagy.**

In order to determine what steps within lipophagy endophilin B1 is involved in, endophilin B1 was knocked down in HeLa cells, and subsequently Torin1 or EPA was loaded for 6 hours. Coverslips were fixed and stained with Bodipy green to assess the size of LD. Cell lysates were also prepared for Western blot analysis. Surprisingly, endophilin B1 knockdown did not have any effect on LD size in Torin1. However, in EPA treated endophilin B1 KD cells, LDs remained extremely large (Fig. 4-12a). The diameter of LDs was measured from immunofluorescence images and summarized as bar graphs (Fig. 4-12b, c). It is evident that knockdown of endophilin B1 did not affect the Torin1 treatment as Torin1 continues to enhance macroautophagy in the form of LD breakdown (or lipophagy). However, KD of endophilin B1 seems to block the lipophagy by EPA. From these observations, it is clear that the mechanism of LD breakdown by EPA is different from that of Torin1. Similarly, the role of endophilin B1 in macroautophagy (inhibited by Torin1) and in EPA mediated lipophagy is different.

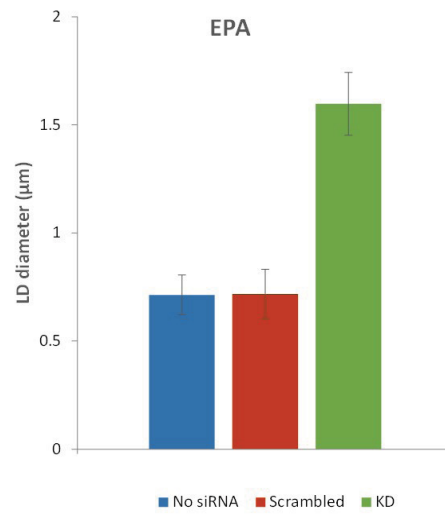
a.



b.



c.



d.

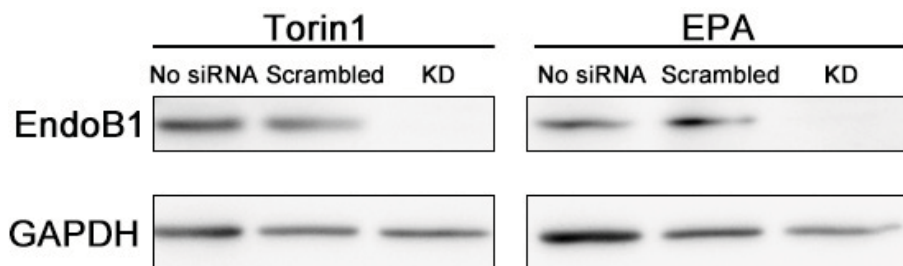
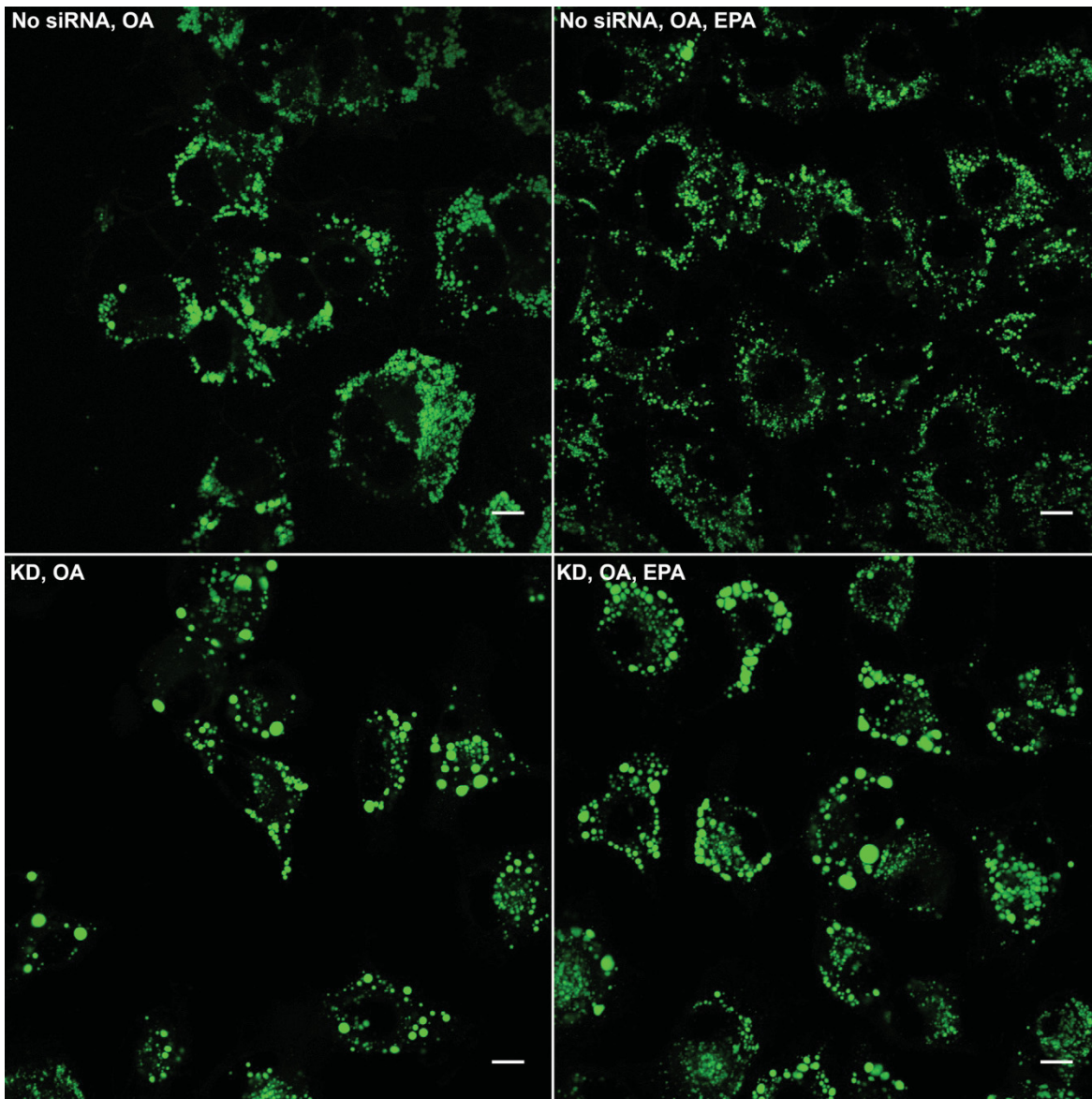


**Figure 4-12:** Endophilin B1 is involved in EPA mediated lipophagy.

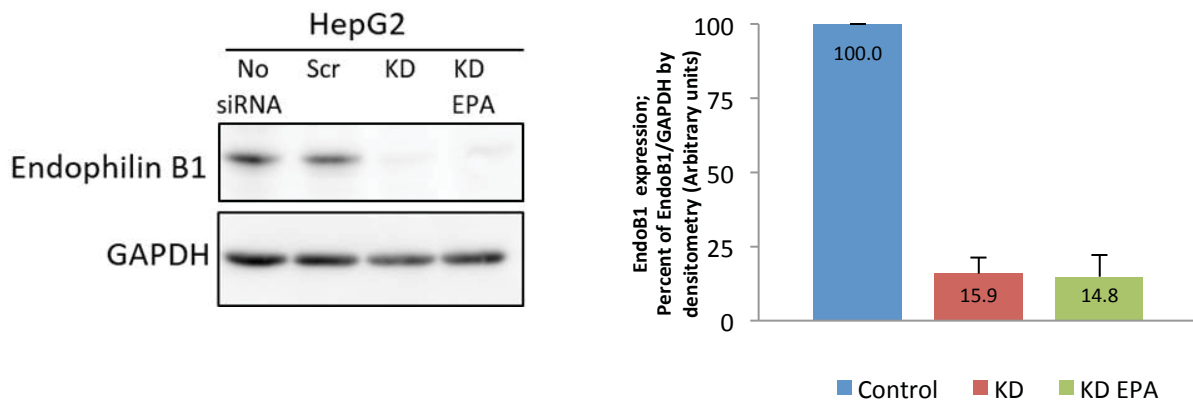
- a.** Immunofluorescence of Torin1 or EPA treated endophilin B1 KD cells. When endophilin B1 is knockdown in HeLa cells, the size of LD becomes greater. Following siRNA transfection, oleate was added for 16 hours and subsequently, either Torin1 or EPA was added for 6 hours. Amino acid starvation media was added for 1.5hours. Upon fixation, cells were stained with Bodipy green. Scale bar is 10 $\mu$ m.
- b.** Quantification of LD diameter changes in Torin1 treated cell. The size of LDs was measured and presented as bar graphs. There is negligible difference in Torin1 treated cells ( $p>0.11$ ). Average LD diameter for each group is 0.71 $\mu$ m, 0.72 $\mu$ m, and 0.73 $\mu$ m for No siRNA, scrambled and KD, respectively.
- c.** Quantification of LD diameter changes in EPA treated cell. In EPA-treated cells, differences between No siRNA and KD, scrambled and KD were both significant as p values are 3.86e-60 and 4.30e-46, respectively. Average LD diameter for each group is 0.71 $\mu$ m, 0.72 $\mu$ m, and 1.60 $\mu$ m for No siRNA, scrambled and KD, respectively.
- d.** Western blot shows endophilin B1 was successfully knocked down in all three conditions. GAPDH is a loading control.

In order to clarify the role of endophilin B1 in EPA-mediated lipophagy, HeLa and HepG2 cells were knocked down for endophilin B1 and then they were treated with EPA. EPA continues to trigger lipophagy in control cells, but not in endophilin B1 knockdown cells (Fig. 4-13a-d). Moreover, endophilin B1 knockdown decreased the number of LDs per cell compared to control (Fig. 4-13e). Yet, EPA treatment did not change the number of LDs per cell although LDs became even larger than KD condition alone (Fig 4-13e). These observations suggest that endophilin B1 participates in LD fission, where EPA trigger LD shrinkage. Collectively, these results imply that endophilin B1 is essential for EPA mediated lipophagy.

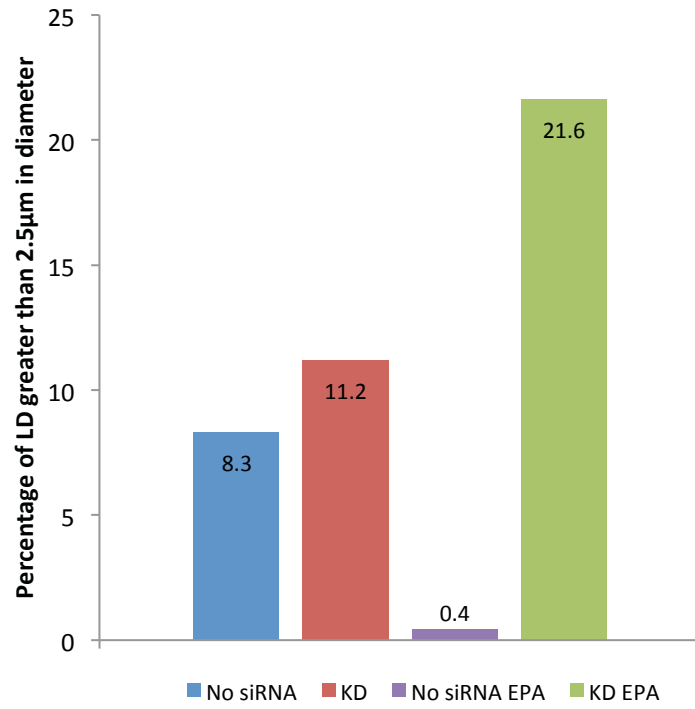
a.



b.



c.



d.

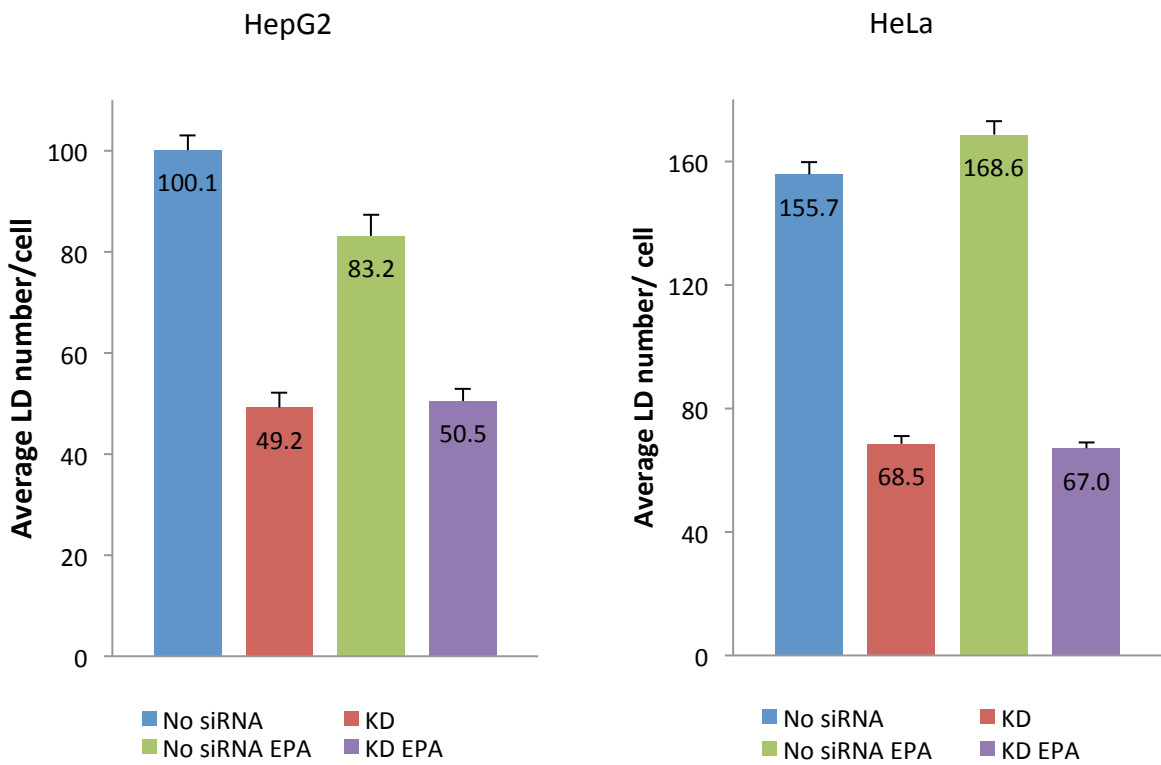


(Figure legend continues on the next page.)

**Figure 4-13:** Endophilin B1 knockdown blocks EPA mediated lipophagy.

- a.** Immunofluorescence images of endophilin B1 KD cells with or without EPA. Following the transfection with endophilin B1 specific siRNA, 0.2mM OA was added for 16 hours. Cells were washed once with PBS before adding 0.4mM EPA for 6 hours. Cells were fixed before being stained by Bodipy green. Scale bar is 10 $\mu$ m.
- b.** Western blot analysis shows endophilin B1 knockdown was successful (84.1% for KD, 85.2% for EPA treated KD). The relative intensity of each band was quantified and presented as a graph on the right. Band intensities for no siRNA and scrambled were averaged and denoted as Control.
- c.** Percentages of LDs greater than 2.5 $\mu$ m in diameter are following: No siRNA is 8.3%, KD is 11.2%, No siRNA EPA is 0.4%, and KD EPA is 21.6%. The p-value between No siRNA vs. KD is 1.90e-06. The p-value between No siRNA vs. No siRNA EPA is 5.43e-03. The p-value between KD and KD EPA is 1.17e-02. And p-value between No siRNA EPA and KD EPA is 8.19e-08. For each group, more than 50 cells were counted over three experiments.
- d.** Endophilin B1 KD decreases LD number in both HeLa and HepG2 cells. For HepG2, average LD number per cell for No siRNA is 100.1, KD is 49.2, No siRNA EPA is 83.2, and KD EPA is 50.5. The p-value between No siRNA vs. KD is 7.14e-5, and the p-value between No siRNA EPA vs. KD EPA is 9.06e-5. For HeLa, average LD number per cell for No siRNA is 155.7, KD is 68.5, No siRNA EPA is 168.5, and KD EPA is 67.0. The p-value between No siRNA vs. KD is 2.11e-19, and the p-value between No siRNA EPA vs. KD EPA is 2.88e-16. For each group, more than 50 cells were counted over three experiments.

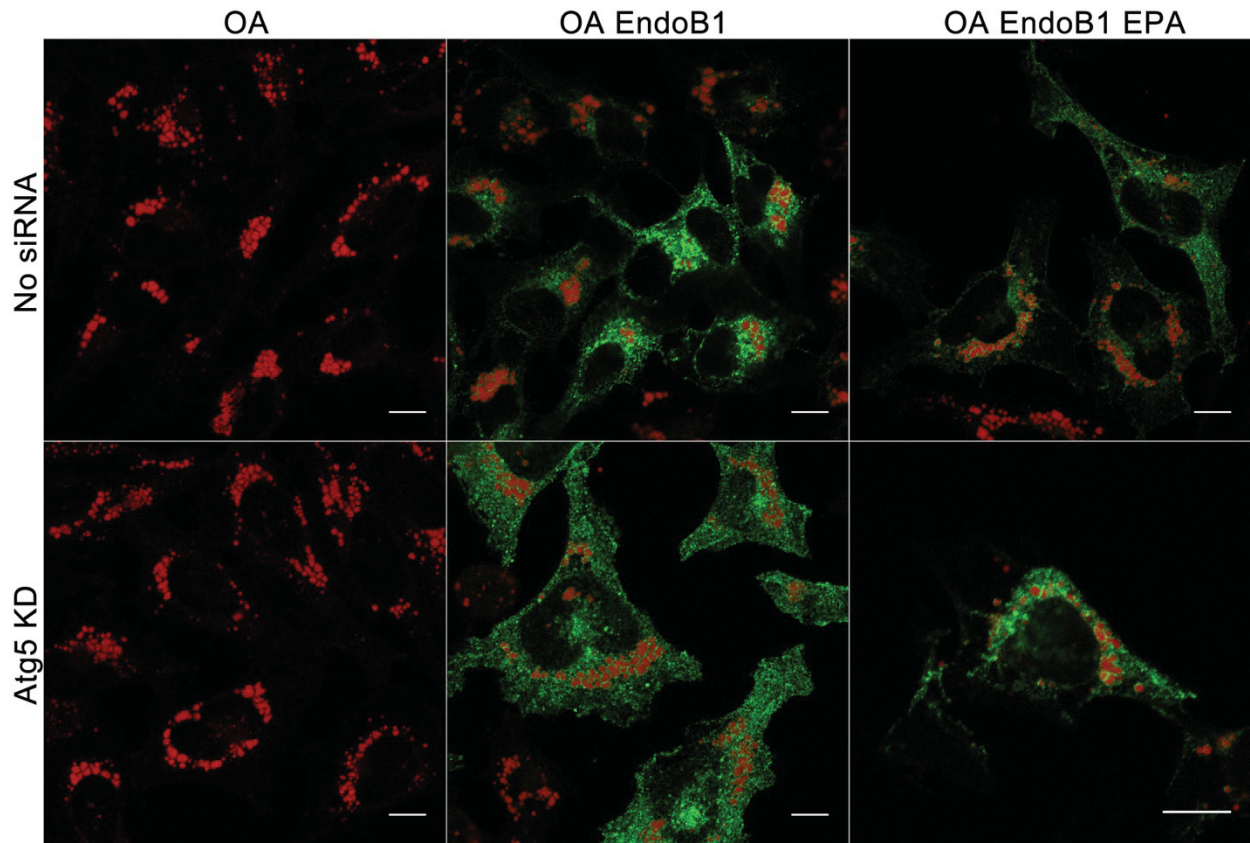
#### **4.4. Endophilin B1 acts on a pathway different from macroautophagy and lipolysis.**

Atg 5 is a key protein for autophagosome elongation as it is required for lipidating LC3-I to LC3-II (Otomo et al., 2013). Therefore, Atg5 is essential for macroautophagy. Knockdown of Atg5 showed enlarged LDs, and this observation has led to the discovery that lipophagy requires autophagic components (Singh et al., 2009). It is known that endophilin B1 is involved in macroautophagy, especially in supplying membranes to contribute to autophagosome formation (Takahashi et al., 2011). If EPA-mediated lipophagy is through macroautophagy machinery,

knockdown of Atg5 would remove endophilin B1 from LD. This observation will also lead to inhibition of EPA-mediated lipophagy.

To verify whether observations we have seen with endophilin B1 were due to mere macroautophagy, Atg5 was knocked down by siRNA and cells were loaded with EPA. After T-REx HeLa endophilin B1-EGFP cells had been plated in pre-determined density, siRNA specific for Atg5 was transfected at 50 pM for 24 hours. Subsequently, 250ng/ml tetracycline and 0.2mM OA were added for 16 hours. Cells were rinsed with PBS prior to 8 hours of EPA treatment. After fixing cells and staining for LDs (Nile red), localization of endophilin B1-EGFP and diameter of LDs were observed. Similarly, lysates were prepared to access protein level. In conditions where Atg5 is successfully knocked down (Fig. 4-14c, d), endophilin B1 remains tightly associated with the LD (Fig. 4-14a Ctl/OA/EndoB1 vs. Atg5KD/OA/EndoB1). Similarly, endophilin B1-EGFP is localized on to the LD surface even in cells that were treated with EPA, regardless of Atg5 KD (Fig. 4-14a Ctl/OA/EndoB1/EPA vs. Atg5KD/OA/EndoB1/EPA). As well, endophilin B1 and EPA continues to drive LD breakdown as LD diameter decreases regardless of Atg5 KD (Fig. 4-14b). It is plausible that lipophagy by endophilin B1 and EPA compensates for the macroautophagy defects. Together, these observations suggest that endophilin B1 participates in a pathway that is different from macroautophagy.

a.



b.

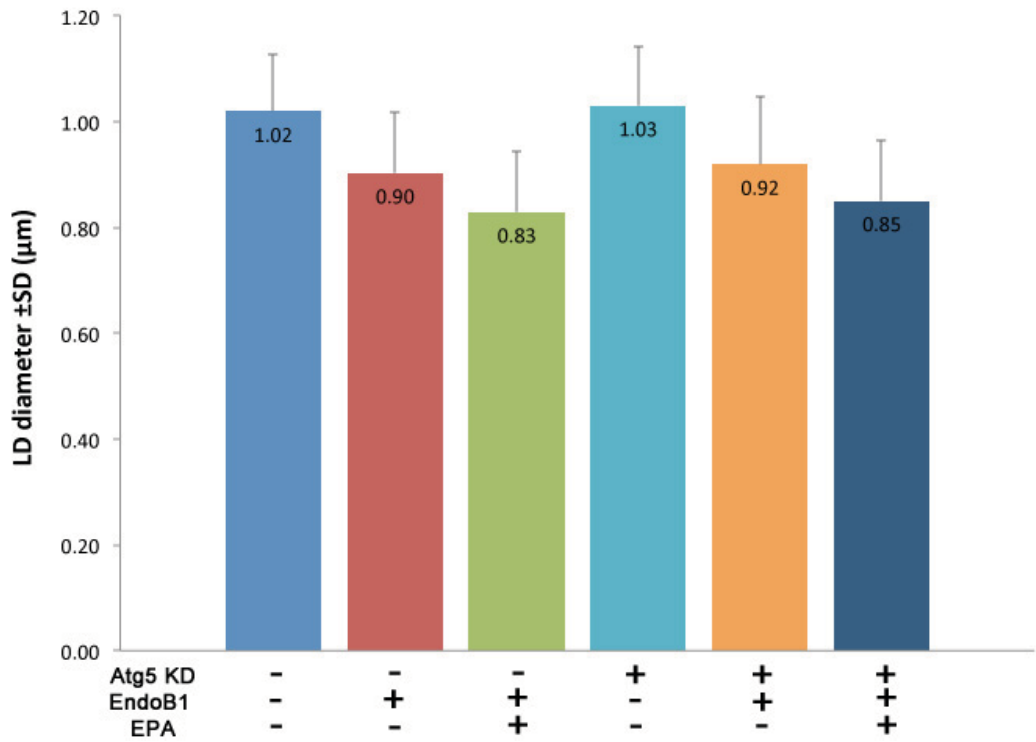
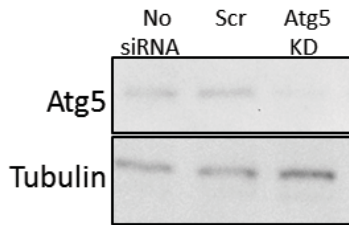


(Figure continues on the next page.)

c.



d.

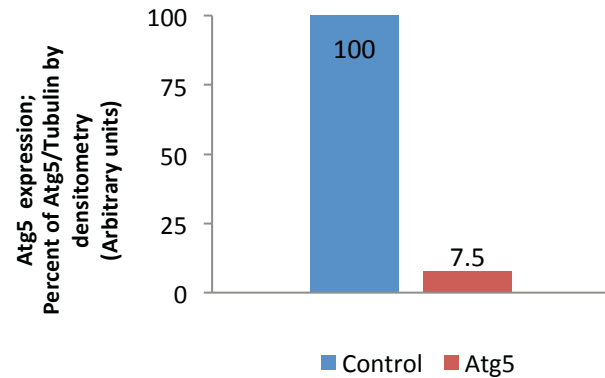


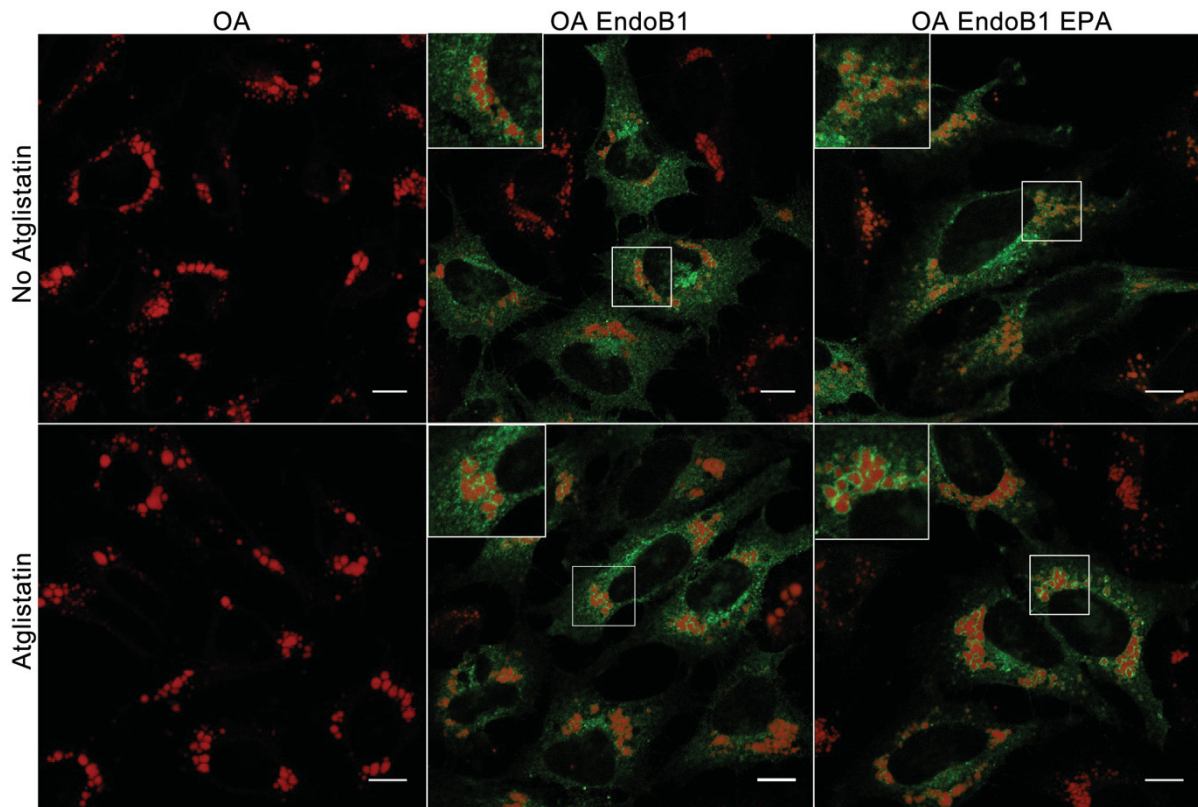
**Figure 4-14:** Endophilin B1 is involved in a type of lipophagy distinct from macroautophagy.

- a. Endophilin B1 decreases LD diameter regardless of Atg5 KD. After transfection with Atg5-specific-siRNA, T-REx HeLa EndoB1-EGFP cells were incubated with oleate for 16 hours followed by EPA for 8 hours. Upon fixation, cells were stained with Nile red to visualize LD. Scale bar is 10 $\mu$ m.
- b. Quantification of LD diameter ( $\mu$ m) in Control and Atg5 KD cells. In Control condition, expression of EndoB1 continues to decrease LD diameter as seen in previous figures (p-value between No siRNA OA (blue bar) and No siRNA OA EndoB1 (red bar) is 0.00863, p-value between No siRNA OA EndoB1 (red bar) and No siRNA OA EndoB1 EPA (green bar) is 0.02308). In Atg5 KD condition, expression of EndoB1 and addition of EPA still result in LD breakdown (p-value between Atg5 KD OA (light blue bar) and Atg5 KD OA EndoB1 (orange bar) is 0.009032, p-value between Atg5 KD OA EndoB1 (orange bar) and Atg5 KD OA EndoB1 EPA (navy bar) is 0.047996).
- c. Western blot analysis shows successful Atg5 knockdown.
- d. Western blot band intensity was quantified and reported as a bar graph.

Aside from macroautophagy or lipophagy, cellular LDs can be metabolized by lipases such as ATGL. ATGL initiates the degradation of TAG from LD, where it cleaves FA from TAG. A DAG formed in this way is quickly degraded to glycerol and FFAs. Subsequently, FFAs are released into energy through beta-oxidation in mitochondria. It is plausible that LD breakdown after endophilin B1 and EPA treatment was through actions of ATGL. In order to test this possibility, the lipolytic pathway was blocked by Atglistatin. Atglistatin competitively inhibits ATGL activity, but it does not displace ATGL from LD of adipocytes or interfere with ATGL's

binding to CGI-58 (Mayer et al., 2013; Zagani et al., 2015). In addition, treatment of Atglistatin at 50 $\mu$ M concentration for 8 hour does not affect cell viability (Mayer et al., 2013). For our experiments, T-REx HeLa endophilin B1-EGFP cells were plated at pre-determined density, and 250ng/ml tetracycline and 0.2mM OA were added for 24 and 16 hours, respectively. After washing cells once with PBS, cells were treated with 50 $\mu$ M Atglistatin for 8 hours, and cells were fixed and stained for LDs. Immunofluorescence images were taken and size of LDs was measured (Fig. 4-15). Firstly, LDs from OA/Atglistatin condition has slightly larger LD than OA condition (Fig. 4-15b,  $p=8.03e-05$ ), confirming that Atglistatin works to inhibit ATGL activity. Note that ATGL does not leave LD after Atglistatin treatment (Fig. 4-16), verifying previous findings on ATGL localizations. Secondly, when endophilin B1 expression was induced in the presence of Atglistatin, endophilin B1 did not fall off from the LD. Instead, it remained tightly bound to LD (Fig. 4-15a). On the other hand, the size of LDs did not increase, suggesting that endophilin B1 may be compensating for the loss of lipolysis (Fig. 4-15b, EndoB1 (red bar) vs. EndoB1/Atglistatin (orange bar),  $p>0.05$ ). When EPA was added along with Atglistatin, however, LDs did not decrease in size. In fact, LDs increased in size from 0.79 $\mu$ m to 0.97 $\mu$ m (Fig. 4-15b, EndoB1/EPA (green bar) vs. EndoB1/EPA/Atglistatin (navy bar)). These observations show that endophilin B1 may be compensating for the loss of ATGL activity, but EPA may not. It is possible that ATGL plays a role in the EPA mediated lipophagy as well as the macroautophagy (see discussion **5.2.3**). However, it should be noted that endophilin B1-EGFP remains tightly on the surface of LD even when ATGL activity is blocked.

a.



b.

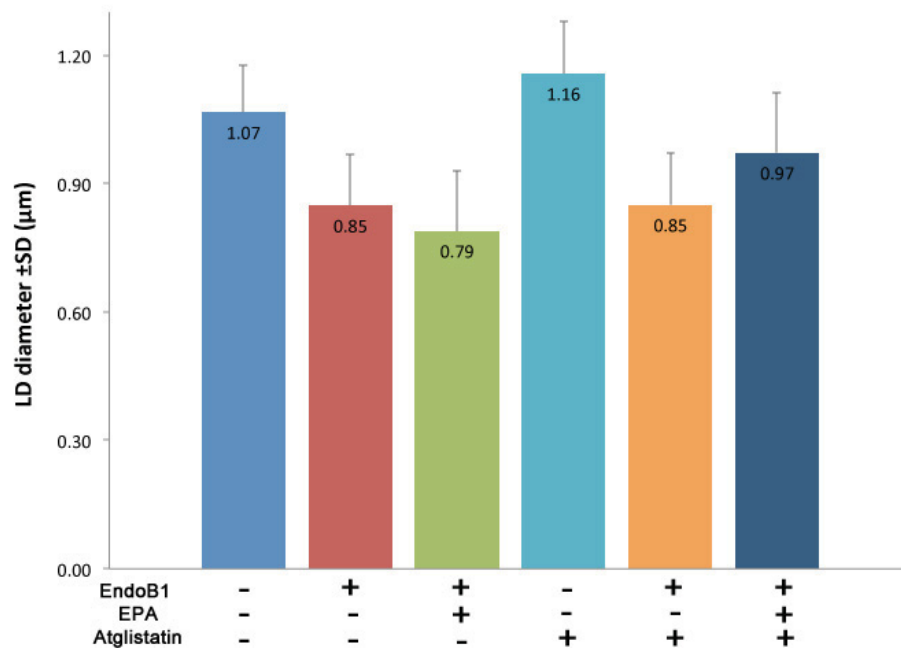


(Figure legend continues on the next page.)

**Figure 4-15:** Lipophagy by endophilin B1 is independent of ATGL.

- a.** Immunofluorescence of T-REx HeLa EndoB1-EGFP cells after Atglistatin treatment. A diameter of LD continues to decrease with tetracycline (EndoB1 expression) and EPA treatment regardless of Atglistatin treatment (except OA EndoB1 EPA Atglistatin. See text for details). Note that association of LD and endophilin B1 is not affected by ATGL activity (See inset). To induce EndoB1-EGFP expression and LD formation, tetracycline was added for 24 hours and oleate was added for 16 hours. To prevent ATGL activity, 50 $\mu$ M Atglistatin was added (in no serum media) for 8 hours. Upon fixation, cells were stained with Nile red. Scale bar is 10 $\mu$ m.
- b.** Lipophagy by endophilin B1 is not affected by ATGL inhibition. The diameter of LD in all conditions was measured and reported as bar graph shown here. The addition of Atglistatin increased the LD size, confirming the effect of ATGL inhibition (with and without Atglistatin,  $p=8.03e-05$ ). Differences between all groups are significant ( $p<2.24e-03$ ). All cells were loaded with OA. See texts for more details.

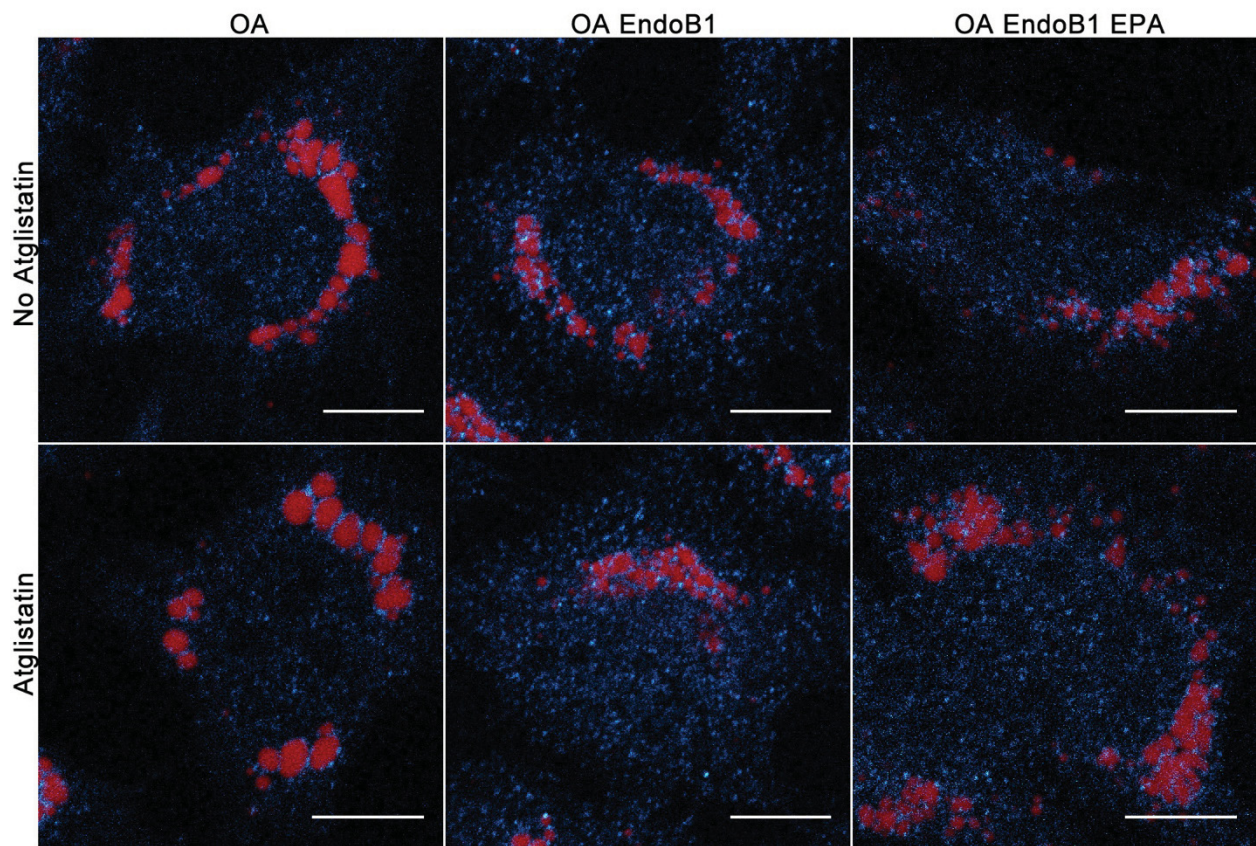


(Figure legend continues on the next page.)

**Figure 4-16:** Atglistatin does not displace ATGL from LD

T-REx HeLa endophilin B1-EGFP cells were treated with Atglistatin to inhibit ATGL function. To induce EndoB1-EGFP expression and LD formation, tetracycline was added for 24 hours and oleate was added for 16 hours. To prevent ATGL activity, 50 $\mu$ M Atglistatin was added (in no serum media) for 8 hours. Upon fixation, cells were stained with Nile Red and ATGL-Alexa 647 (pseudo coloured to cyan). Scale bar is 10 $\mu$ m.

#### **4.5. Lipophagy by endophilin B1 involves LD-Lysosome relationship.**

So far, we have determined that endophilin B1 participates in a novel type of LD breakdown mediated by EPA and in this kind of lipophagy endophilin B1 acts differently than in macroautophagy or lipolysis. To clarify such mechanism, we investigated into what organelles LDs associate when EPA is added. Previously, it has been shown that making direct contact with lysosomes may result in LD break down (Schroeder et al., 2015). This non-canonical type of lipophagy indicates that lysosome directly fuses with LD, and there is no necessity for autophagosome involvement. There is a quick sampling of cargo into lysosome; therefore, physical interaction of the two organelles is the key. In fact, one LD may be bombarded by multiple lysosomes, and this LD-lysosome relationship is referred to as Kiss-and-run (Schroeder et al., 2015). We enquired whether endophilin B1 and EPA make this type of lipophagy. To do so, cryosection of human fatty liver #14 was stained with endophilin B1 and a lysosome marker LAMP1. It is clearly shown that subdomains of endophilin B1 around LD co-localize with LAMP1 (Fig. 4-17), proposing that certain proportion of LDs in the human fatty liver may undergo Kiss-and-Run lipophagy and endophilin B1 may be involved in this process.

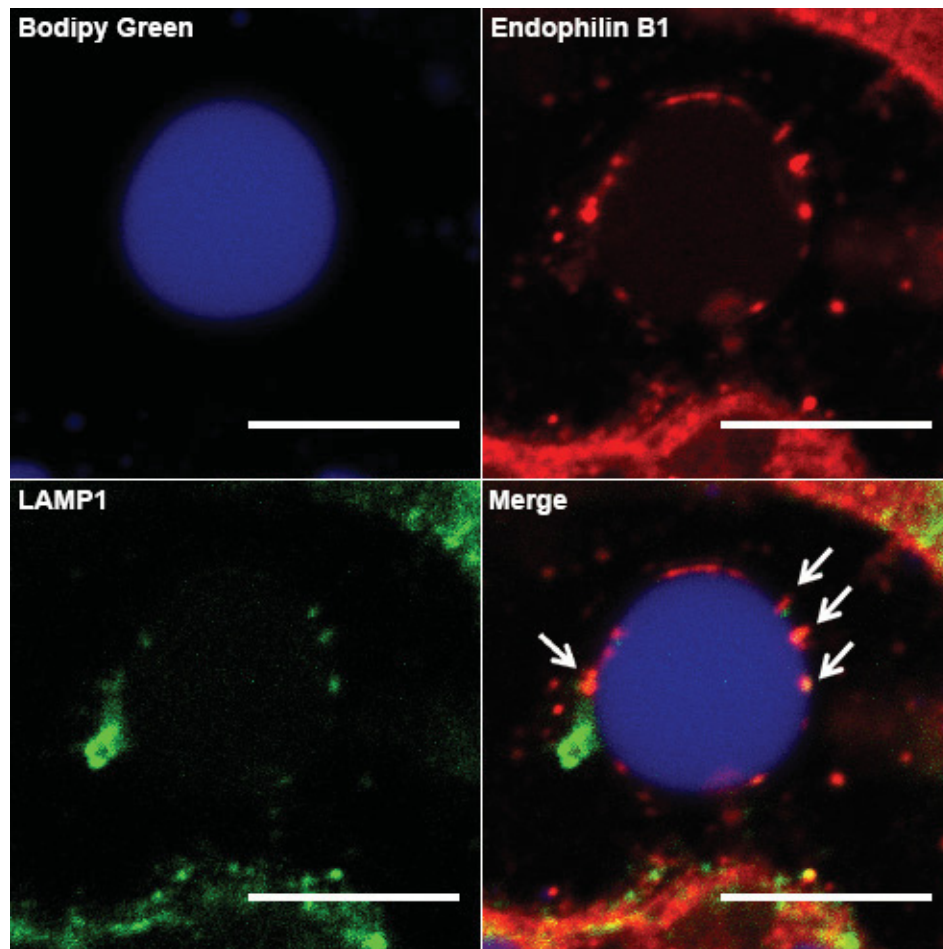


**Figure 4-17:** Endophilin B1 colocalizes with LAMP1 on human fatty liver #14. Frozen human fatty liver section was stained with Bodipy green (pseudo coloured to blue), anti-endophilin B1 (Alexa 568, red) and anti-LAMP1 (Alexa 647, green). Arrows indicate endophilin B1 colocalizing with LAMP1. Scale bar is 10 $\mu$ m.

To investigate what happens to the LD-lysosome relationship when endophilin B1 is absent, the expression of endophilin B1 has been silenced using siRNA. Upon seeding cells at pre-determined density, cells were transfected with 50pM endophilin B1 siRNA in two successive days. Then, OA was added for 16 hours followed by EPA or Torin1 treatment for 6 hours. Coverslips were fixed, and cell lysates were prepared. Upon fixation, cells were stained to highlight endogenous LAMP1 (red) and LC3 (pseudo coloured to magenta). LDs were stained with Bodipy green. Immunofluorescence images shown are a single plane from the z-stack

acquisition, and the number of LAMP1 associated LDs were counted from max projected z-stacks. Interestingly, Torin1 and EPA-treated cells in control conditions (No siRNA) showed many LDs positioned next to or entirely co-localizing with LAMP1 staining lysosomes (See arrow, Fig. 4-18a, b). There were 5.32 and 5.35 LDs associated with LAMP1 in each cell of Torin1 and EPA-treated cells, respectively (Fig. 4-18c). However, when endophilin B1 was knocked down, this LD-LAMP1 association decreased drastically. Especially, EPA-treated cells did not have any LAMP1 associated LDs (Fig. 4-18 b). Notice that endogenous LC3 is globally localized in Torin1 treated cells regardless of endophilin B1's presence. However, endogenous LC3 is around LD in EPA treated endophilin B1 KD cells, and this indicates that cell is utilizing the macroautophagy machinery in an attempt to compensate for the loss of Kiss-and-run although there is no reduction in LD size (Endophilin B1's absence renders cell unable to form autophagosome). Collectively, these observations strongly support that EPA mediates a lipophagy in Kiss-and-run manner and that endophilin B1 plays a crucial role in LD-lysosome relationship.

a.

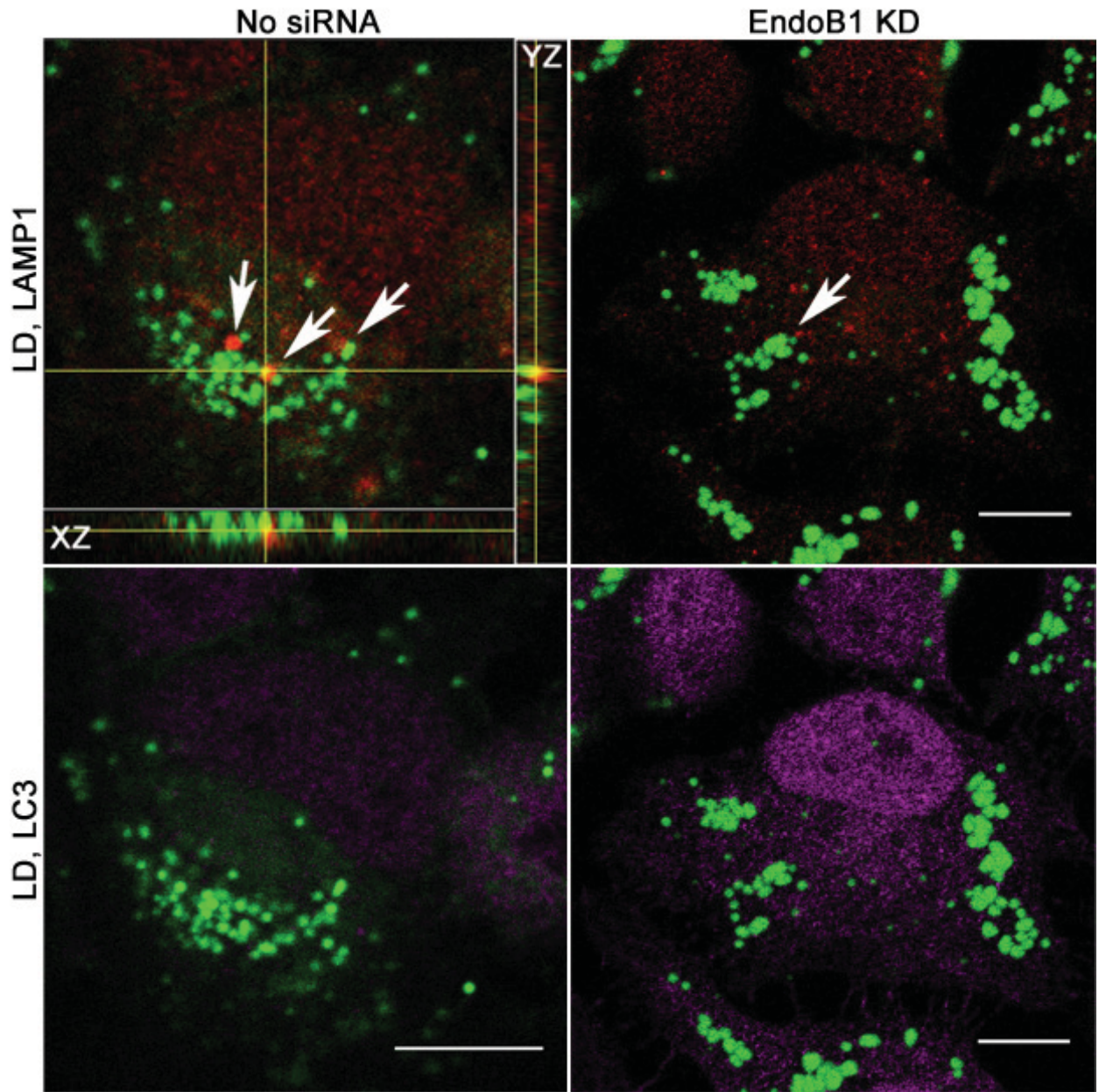


(Figure continues on the next page.)

b.

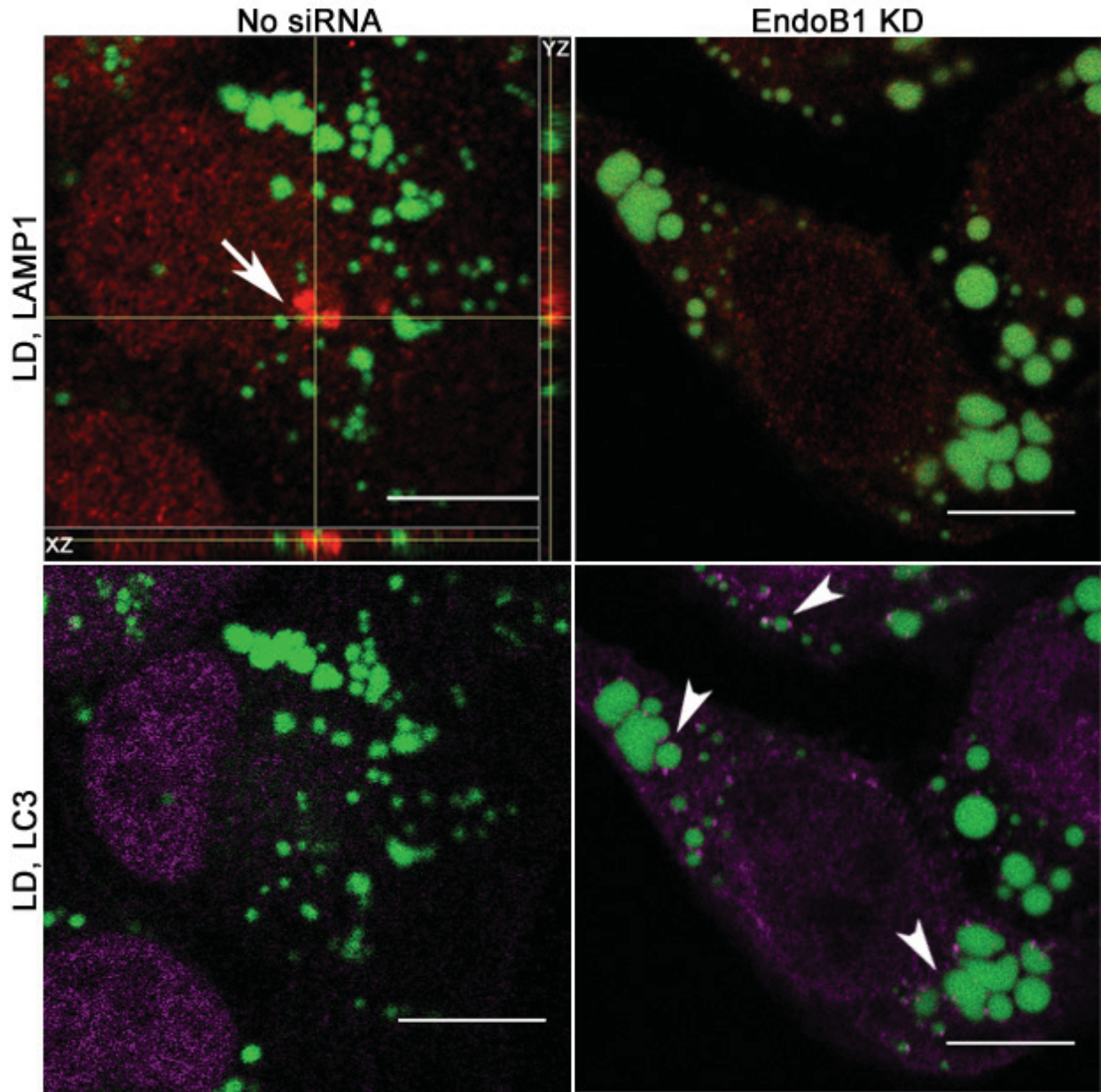


(Figure continues on the next page.)

c.

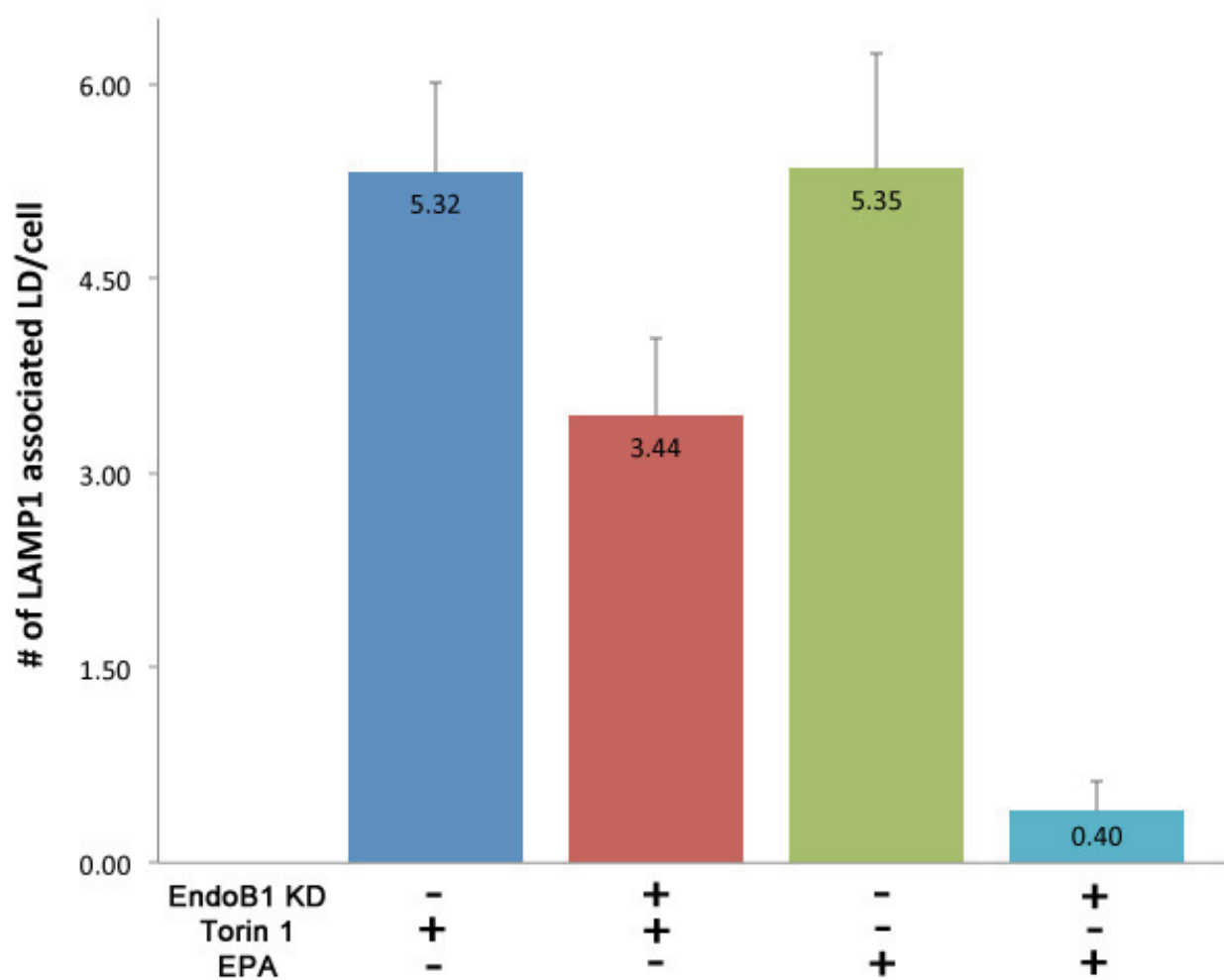


**Figure 4-18:** Endophilin B1 KD abolishes LD-LAMP1 association in EPA-treated cells.

- Immunofluorescence of EndoB1 KD cells after Torin1 treatment. After transfection with siRNA, cells were incubated with OA for 16 hours followed by Torin1 for 8 hours. Upon fixation, cells were stained with Bodipy green. LAMP1 was labeled with Alexa 568 (red), and LC3 was labeled with Alexa 647 (magenta). Arrows indicate an LD-LAMP1 association. Arrowhead shows LAMP1 remote from LD. Scale bar is 10 $\mu$ m.
- Immunofluorescence of EndoB1 KD cells after EPA treatment. The experiment was done in the same way as in **a**.
- The number of LAMP1 associated LD per cell is denoted as a bar graph.

In order to preclude macroautophagy and lipolysis from the Kiss-and-run, macroautophagy was blocked through Atg5 KD and Atglistatin treatment. Subsequently, the

effect of macroautophagy and lipolysis block was observed on LD-LAMP1. After cells had been transfected with 50pM Atg5 specific siRNA, 250ng/ml tetracycline and 0.2mM OA was added for 24 and 16 hours, respectively. After washing cells once with PBS, 50μM Atglistatin was added with or without EPA. Immunofluorescence images clearly show that LD continues to associate with LAMP1 regardless of Atg5 KD or Atglistatin (Fig. 4-19). This observation strongly suggests that Kiss-and-run lipophagy by endophilin B1 and EPA is distinct from macroautophagy or lipolysis.

**a.**

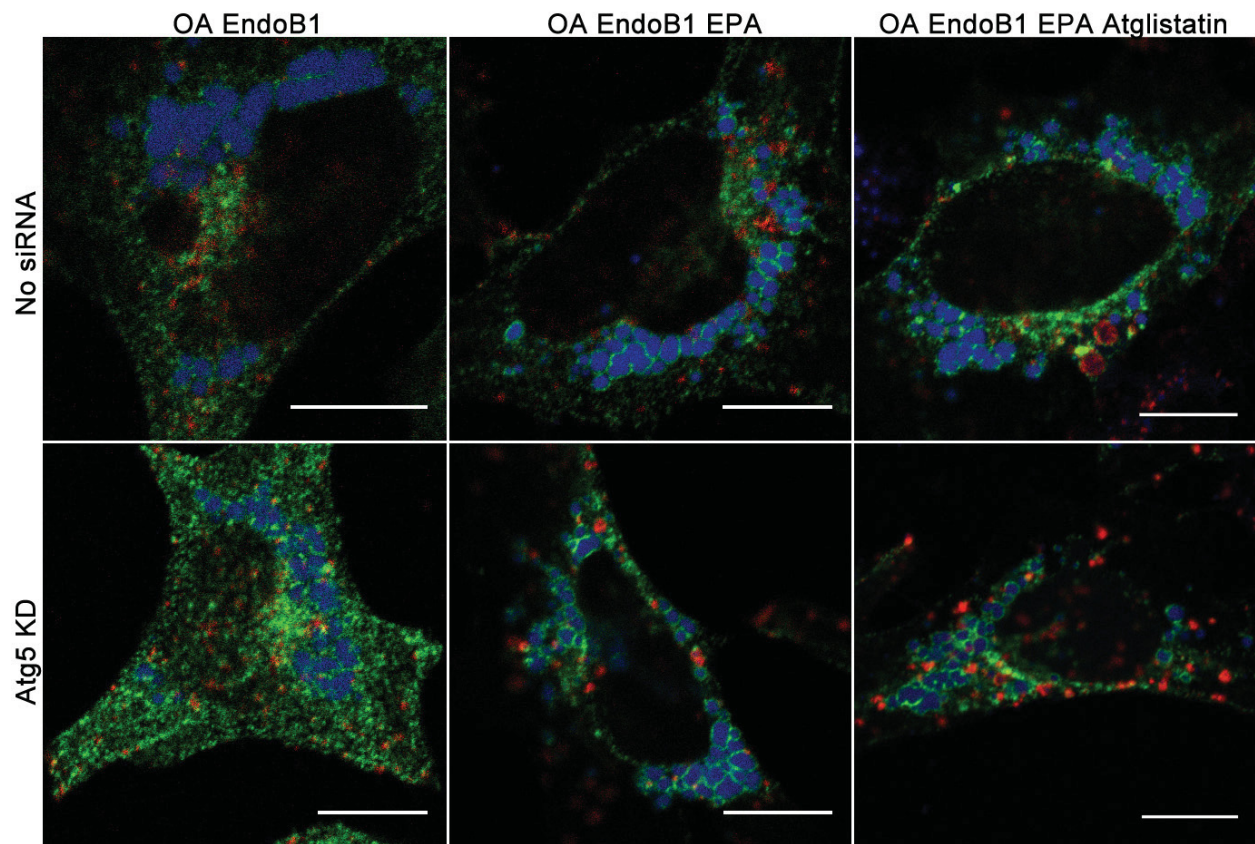


(Figure continues on the next page.)

b.

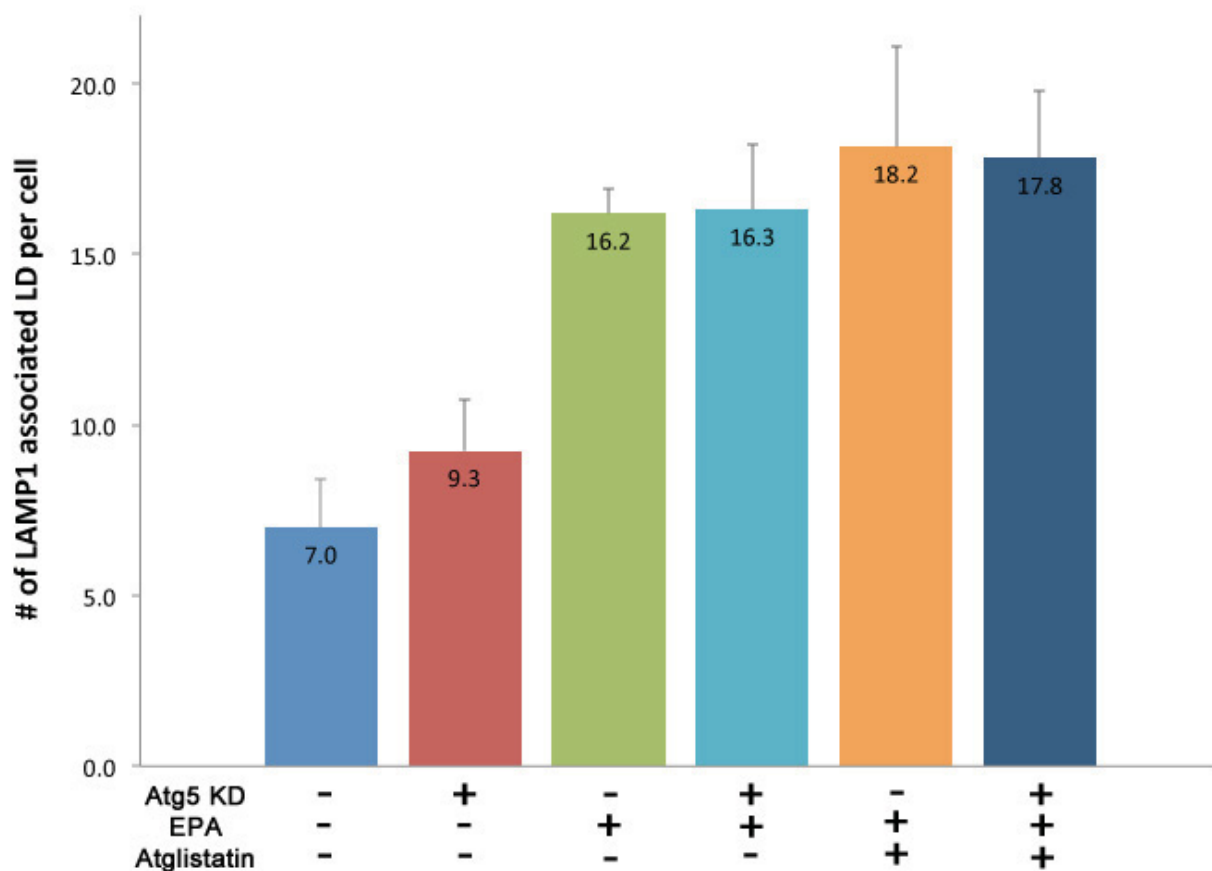


**Figure 4-19:** Association of LD-LAMP1 is independent of macroautophagy and ATGL.

- a. Immunofluorescence of T-REx HeLa EndoB1-EGFP cells after Atg5 KD and ATGL inhibition. After transfection with siRNA, endophilin B1 expression was induced with tetracycline for 24 hours. Then cells were incubated with OA for 16 hours followed by EPA and/or Atglistatin for 8 hours. Upon fixation, cells were stained with Nile red for LD (pseudo coloured to blue), and LAMP1-Alexa647 (pseudo coloured to red). Note that LD and LAMP1 associate regardless of Atg5 KD and ATGL inhibition. Scale bar is 10 $\mu$ m.
- b. Number of LD-LAMP1 association per cell. From No siRNA to Atg5 KD, a number of LAMP1 associated LDs does not change significantly ( $p > 0.052$ ). The addition of EPA in both No siRNA and Atg5 KD conditions increases the number of LAMP1 associated LDs ( $p < 4.77e-04$ ). For each group, more than 20 cells were counted. This experiment was repeated for three times.

#### **4.6. Endophilin B1 binds with proteins involved in Kiss-and-Run lipophagy.**

Recently, Rab7 has been shown indispensable for lipophagy in hepatocytes (Schroeder et al., 2015). Under starvation conditions, Rab7 is highly active, and this activation is shown to be essential for the transient interaction between the LD and lysosome referred to as Kiss-and-run lipophagy (Schroeder et al., 2015). If endophilin B1 participates in Kiss-and-Run lipophagy, it may interact with Kiss-and-Run proteins such as Rab7. First, cells were transfected with 1.0 $\mu$ g of CFP-Rab7 plasmid for 24hours, and subsequently, tetracycline and OA were added for endophilin B1-EGFP induction and LD formation, respectively. Indeed, Rab7 localized onto the lysosome (colocalizes with LAMP1) and onto the LD (Fig. 4-20). Moreover, in conditions where EPA is added, Rab7 localizes on LDs that endophilin B1 is located (Fig. 4-20). These observations support that endophilin B1 is involved in Kiss-and-Run lipophagy.

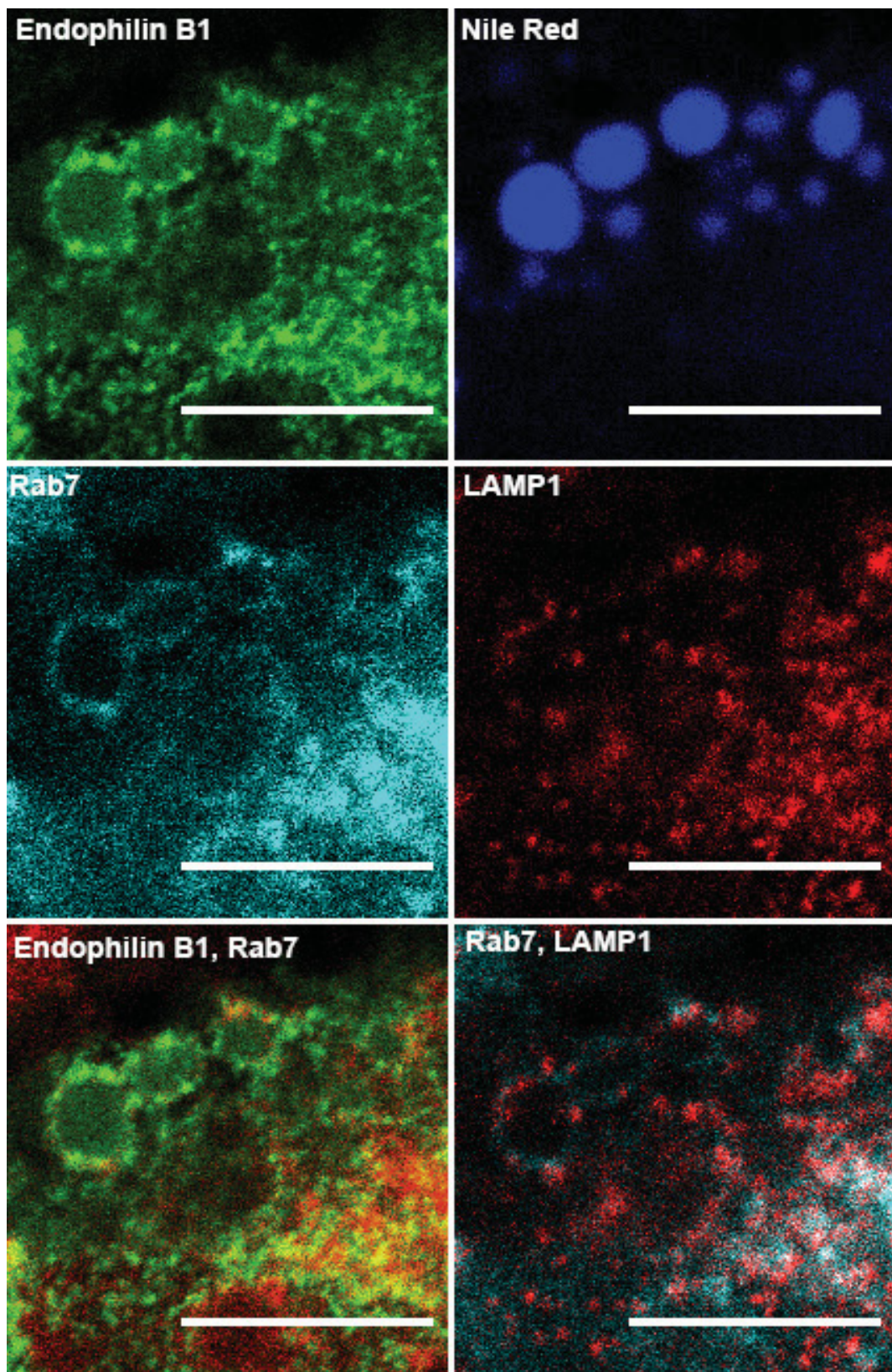


(Figure legend found on the next page.)

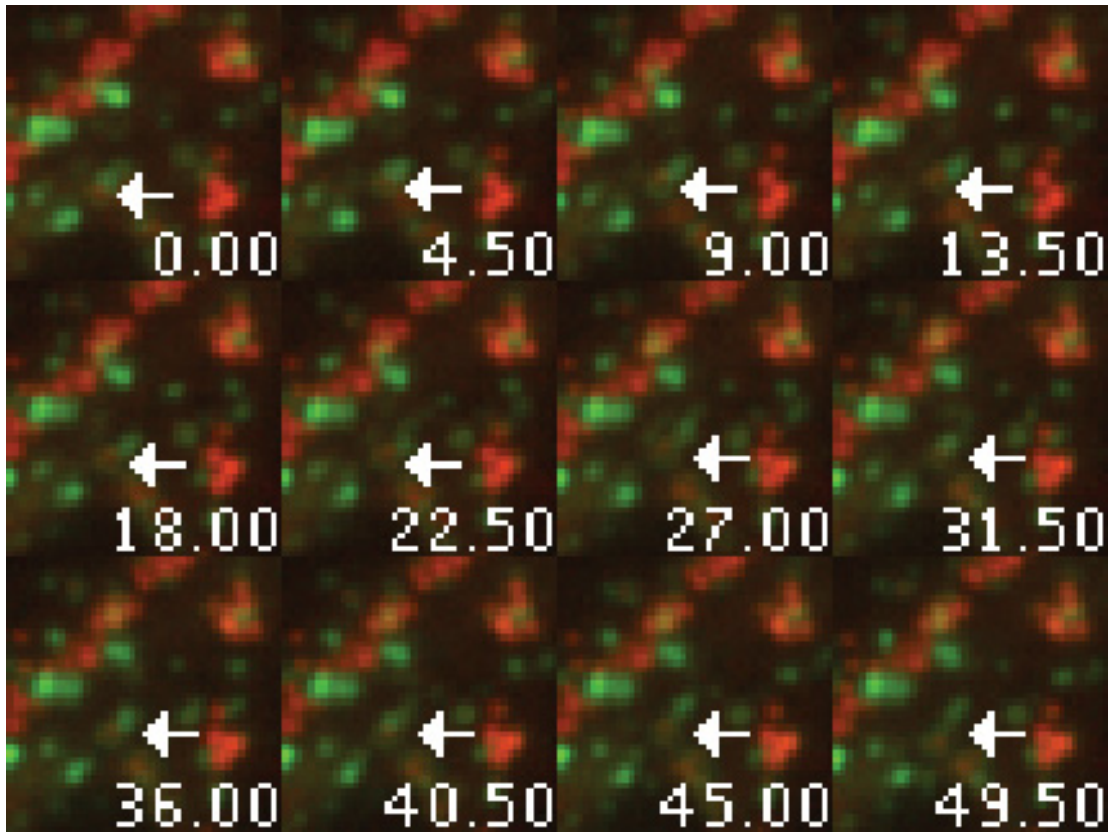
**Figure 4-20:** Endophilin B1 associates with Rab 7 in EPA mediated lipophagy.

After induction of endophilin B1-EGFP, CFP-Rab7 was transfected for 24 hours. Cells were then incubated with oleate for 16 hours followed by 8 hours EPA treatment. After fixation, cells were stained with Nile red (pseudo coloured to blue), and LAMP1-Alexa 647 (pseudo coloured to red). For merge with endophilin B1, Rab7 is shown in red. Scale bar is 10 $\mu$ m.

In order to visualize Kiss-and-run lipophagy, which is characterized by transient docking of lysosome to LD surface, cells were observed by time-lapse microscopy using spinning disk microscope, and images were acquired at 1.25sec (or 1.50) intervals for at least 1 min. Firstly, cells were plated on a glass-bottom dish, and they were transfected with Rab7, a central regulator of Kiss-and-run lipophagy that localizes on lysosome and LD surface (Schroeder et al., 2015). Next, 0.15mM OA was added for 16 hours to induce LD formation. Followed by PBS wash, EPA was added at 0.4mM for 6 hours. Images were acquired in 37°C live cell chamber. For HeLa cells, images were acquired for every 1.25s for at least 1 minute, and this corresponds to 48 frames. In these cells, many Rab7-positive lysosomes were in close proximity to LDs, and there were many occasions where LD and lysosome come together and separate. Schroeder and colleagues demonstrate that Rab7 localizes in sub-domain of LD, and lysosomes contact these domains for Kiss-and-run lipophagy (Schroeder et al., 2015). In Fig 4-21a, LD (red) is surrounded by Rab7 (green) (see arrow), and Rab7-positive lysosome comes in proximity, and finally merges with LD at 31.50s. After a brief encounter, the two organelles disjoin at 49.50s. Notice, Rab7-positive LD stains faintly with Bodipy. HeLa cells were also transfected with mCherry-FYVE, a domain found in Fab1, YOTB, Vac1, and EEA1. It binds to PtdIns3P, and it is involved in vacuolar protein sorting and endosome function (Lee et al., 2005a). In EPA treated HeLa cells, FYVE-positive organelle (green) associated with LD (red) (Fig. 4-21b). When the number of Kiss-and-run was counted per cell per minute, Rab7-EPA-treated cells had 4.25

whereas no-EPA cells had 3.49 incidents. Similarly, FYVE-EPA-treated cells had a higher number of overlapping pixels and more Kiss-and-run event than no-EPA cells (Fig. 4-21c, d). T-REx HeLa endophilin B1-EGFP cells were also imaged to determine number Kiss-and-run/cell/min. Cells were transfected with CFP-Rab7, and tetracycline was added to induce endophilin B1-EGFP expression. Subsequently, EPA was added for 6 hours. In Fig. 4-21e, LDs are shown in red, and Rab7 is shown in green. In EPA added cells, Rab7-positive lysosome and LD come close to each other and are joined at 43.5sec (Fig. 4-21e). In these cells, the number of overlapping pixels (Fig. 4-21f), and numbers of Kiss-and-run were quantified as earlier (Fig. 4-21g). In Rab7-transfected cells, the presence of endophilin B1 did not make a noticeable difference in the number of Kiss-and-run (2.22 vs. 2.20) (Fig. 4-21g). However, by adding EPA, the number of Kiss-and-run increased (2.20 vs. 2.98). It is clear that EPA treatment enhances the LD-lysosome association per cell, and this strongly supports the Kiss-and-run lipophagy.

a.



b.

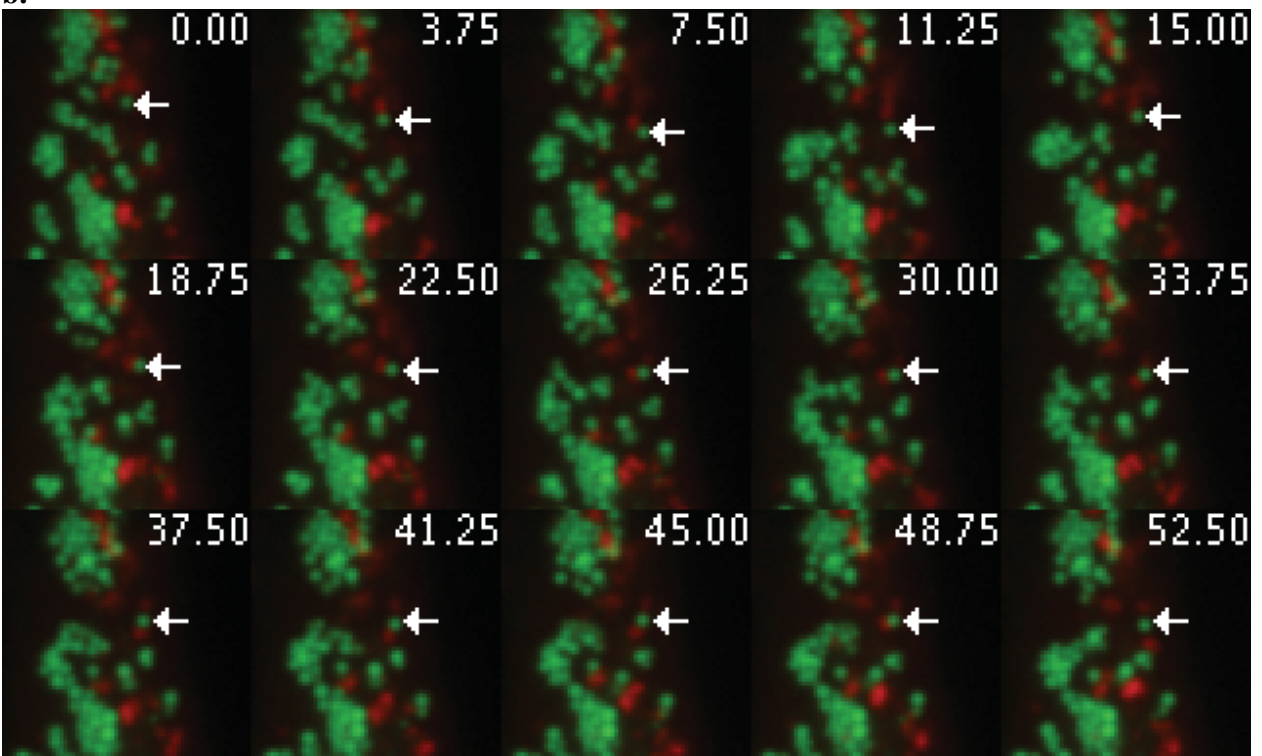
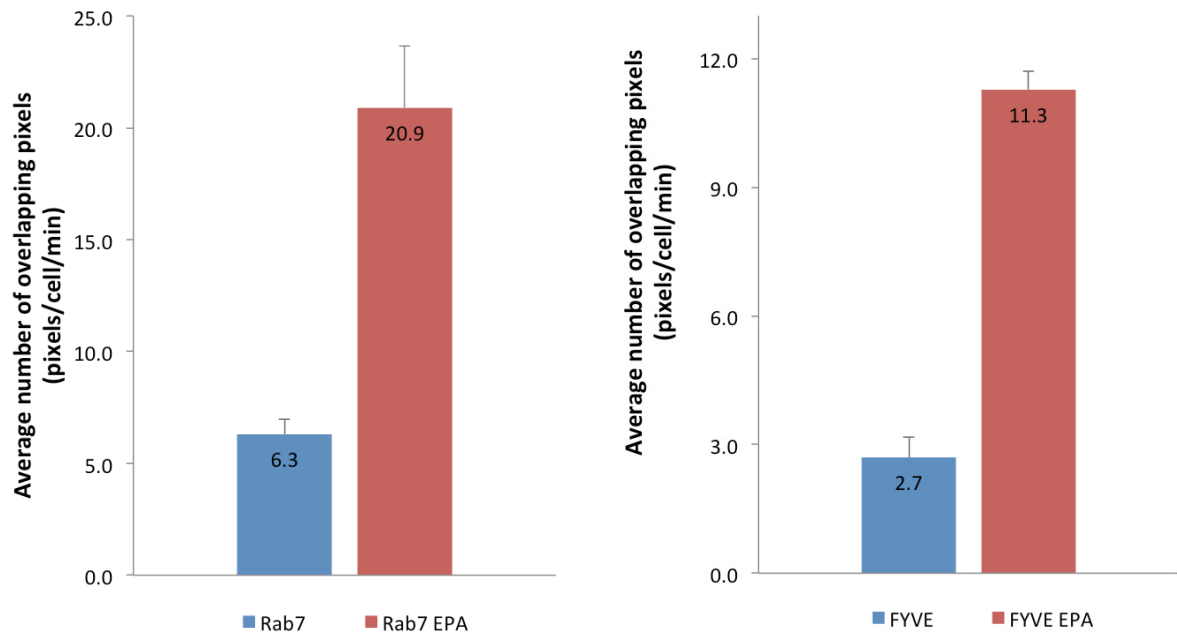


(Figure continues on the next page.)

c.



d.

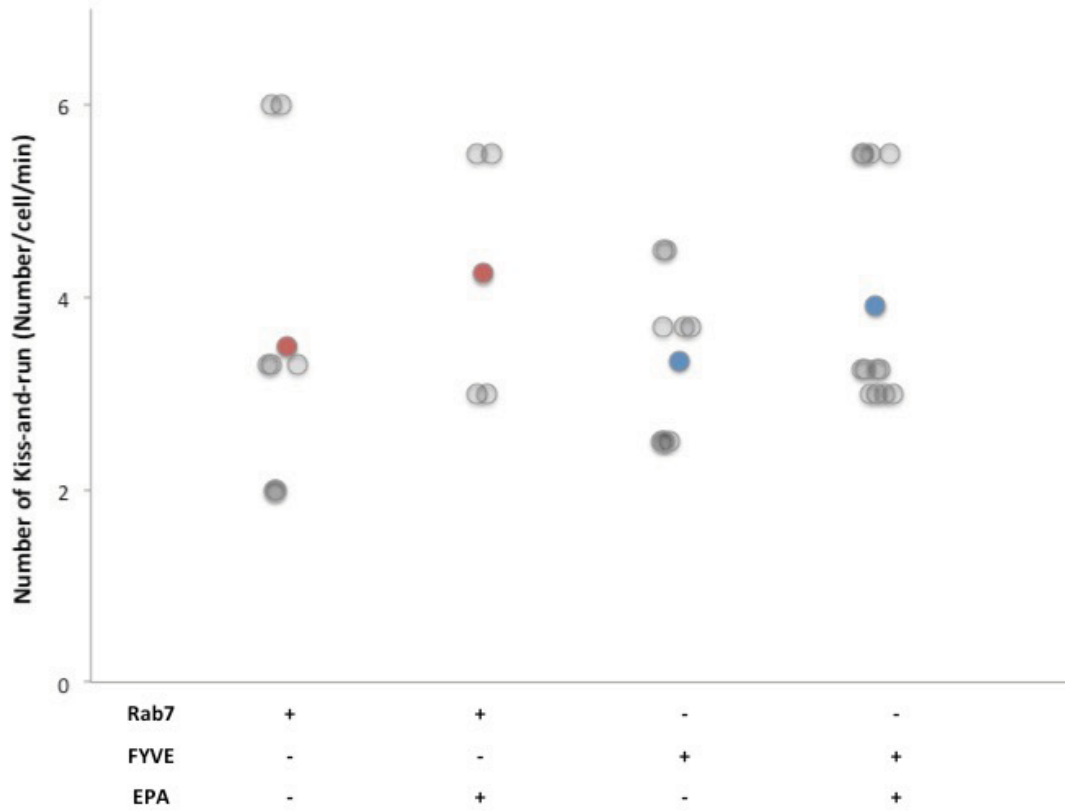


(Figure continues on the next page.)



g.

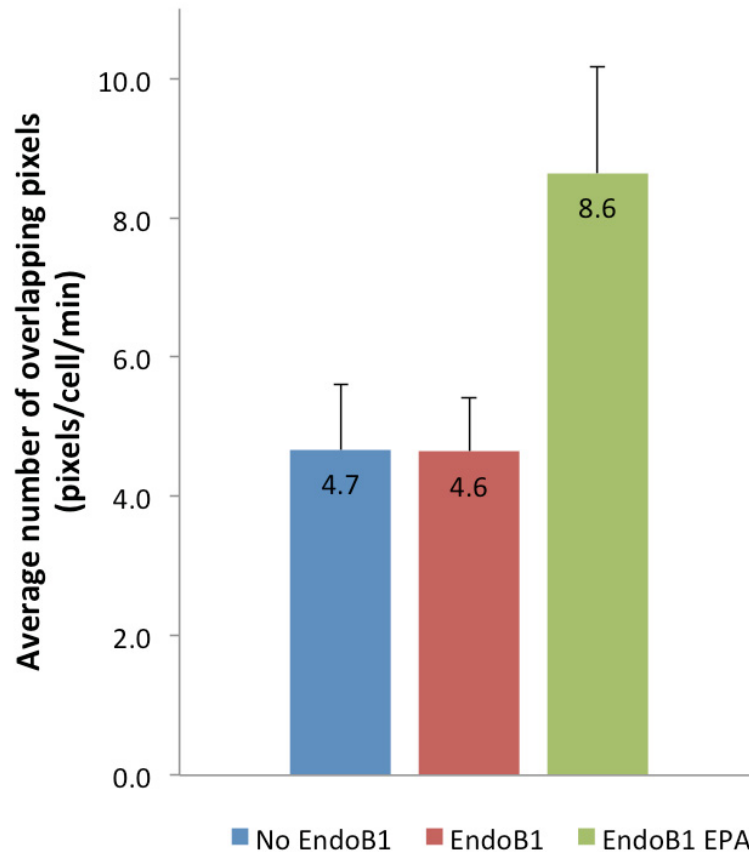


**Figure 4-21:** EPA increases lipid droplet-lysosome association.

- a.** Time-lapse series of OA (0.15mM, 16hours) loaded HeLa cells expressing YFP-Rab7 (1 $\mu$ g, 24hours). EPA was added for 6 hours prior to imaging. Cells were imaged in HEPES supplemented media within 37°C live cell chamber, and each image was captured in 1.25sec interval. LDs are shown in red (Bodipy 558/568). There was an association of Rab7-positive lysosome and the surface of LD (arrow). Evidence of association is shown by the increased intensity at 31.50s and 40.50s, and the two organelles are taken off at 45.00s.
- b.** Time-lapse series of OA loaded HeLa cells expressing mCherry-FYVE (1 $\mu$ g, 24hours). EPA was added for 6 hours prior to imaging. LDs are shown in green (Bodipy 493/503). Putative acidic compartment (highlighted by mCherry-FYVE) associates with LD (arrow) and the two organelles are taken off at 52.50s.
- c.** An average number of overlapping pixels per cell per minute for HeLa cells. Cells were imaged for at least 1 minute. Images were converted to binary and were thresholded from 0-30. Then, thresholded images from LD and Rab7 (or FYVE) channels were overlaid. A number of overlaid pixels was measured, and these values were plotted as a bar graph.

Overlapping pixels represent the association of LD and lysosome. For each group, more than ten cells were quantified.

- d.** A number of Kiss-and-run events per cell per minute for HeLa cells. Images were quantified as in **c**. An average number of overlapping pixels was plotted in function of time. Changes in pixel number greater than the average were considered as ‘kiss’ and the changes lower than the average were considered ‘run.’ Number of Kiss-and-run was recorded for each cell, and these values were plotted as a scatter plot presented here. Coloured dots represent the average. The average number of Kiss-and-run event per cell per min for Rab7, Rab7-EPA, FYVE, and FYVE-EPA cells are 3.49, 4.25, 3.34, and 3.92, respectively.
- e.** Time-lapse series of OA loaded T-REx HeLa cells expressing CFP-Rab7 (1 $\mu$ g, 24hours) and endophilin-EGFP (induced with 500 $\mu$ g/ml tetracycline, not shown). EPA was added for 6 hours prior to imaging. Rab7 is shown in green, and LDs are shown in red (Bodipy 558/568). Rab7-positive lysosome (yellow arrow) and LD (white arrow) move close to each other. Association of the two organelles (white arrow at 43.50s) is observed by the increased signal. Then they have departed from each other shortly after. The background was subtracted from these images by using ImageJ (1.49i) and rolling ball background subtraction of 100 was used.
- f.** A number of Kiss-and-run measured per cell per minute for T-REx HeLa endophilin B1-EGFP cells. EPA (0.4mM, 6hours) was added after rinsing cells once with PBS. Number of Kiss-and-run was measured as described in **d**. Value marked by a triangle is considered an outlier because it is greater than average  $\pm 2$ \*(standard deviation). Average number of Kiss-and-run per cell per min for no EndoB1-Rab7, EndoB1-Rab7, and EndoB1-Rab7-EPA are 2.22, 2.20, and 2.98, respectively.
- g.** An average number of overlapping pixels per cell per minute for T-REx HeLa cells. Cells were imaged for at least 1 minute. All cells were transfected with Rab7, and expression of endophilin B1 was induced for the last two groups. Images were processed as in **c**. A number of overlaid pixels was plotted as a bar graph. Overlapping pixels represent the association of LD and lysosome. For each group, more than ten cells were quantified.

In order to confirm that endophilin B1 binds with proteins known for the direct LD-lysosome interaction, Bio-ID analysis was performed. Bio-ID, an approach described by Roux et al., is a high-throughput analysis of protein binding partners, and it is suitable for the detection of low abundance protein and transient interactions (Roux et al., 2012). To begin, endophilin B1-BirA construct was stably transfected into tetracycline inducible HeLa cells. In these cells, endophilin B1-BirA behaves the same way as endophilin B1-EGFP because upon EPA induction,

endophilin B1-BirA translocates to LD (Fig. 4-22a). In the same tetracycline system, FLAG-BirA does not behave the same as endophilin B1-BirA (Fig. 4-22b).

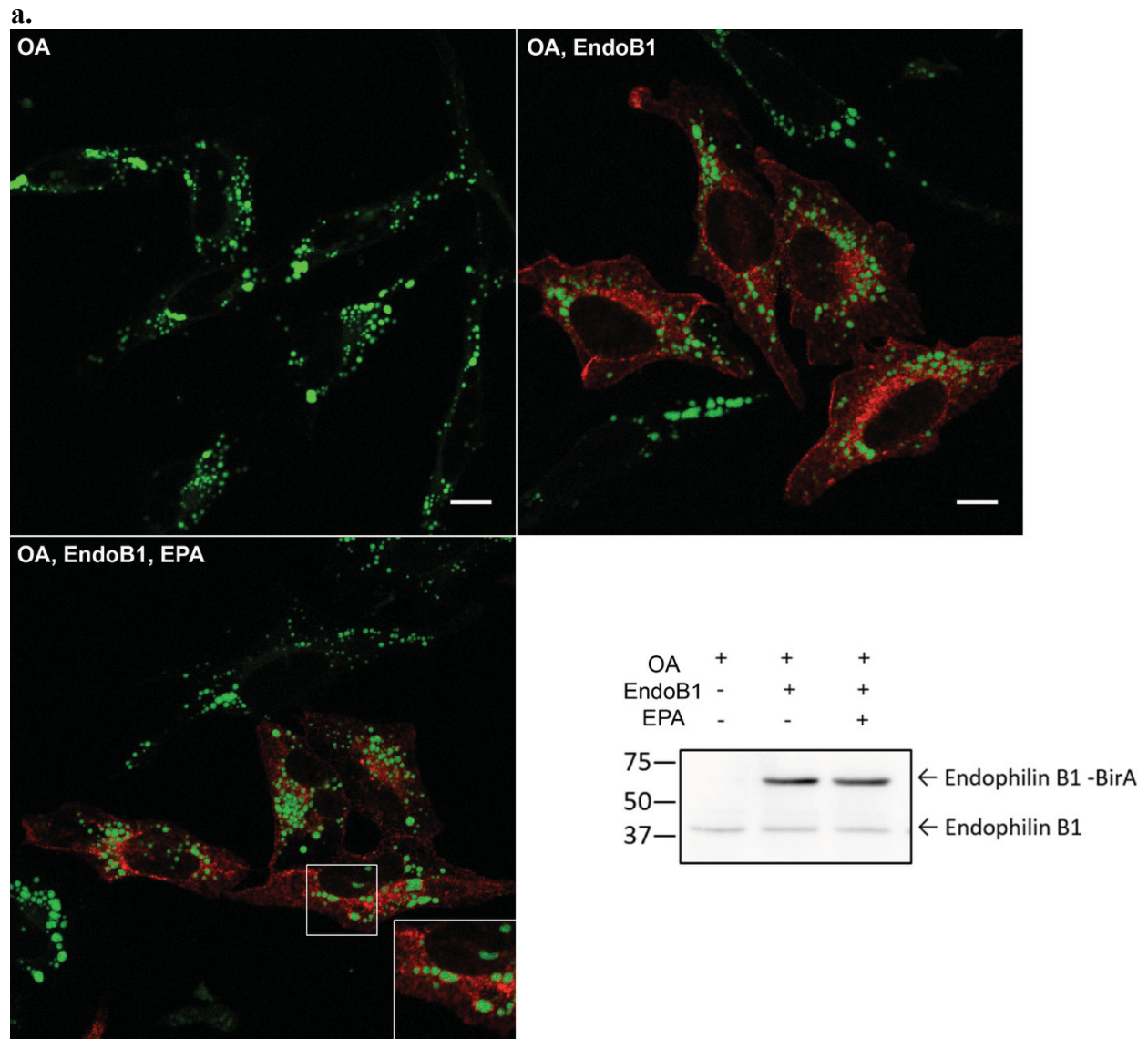
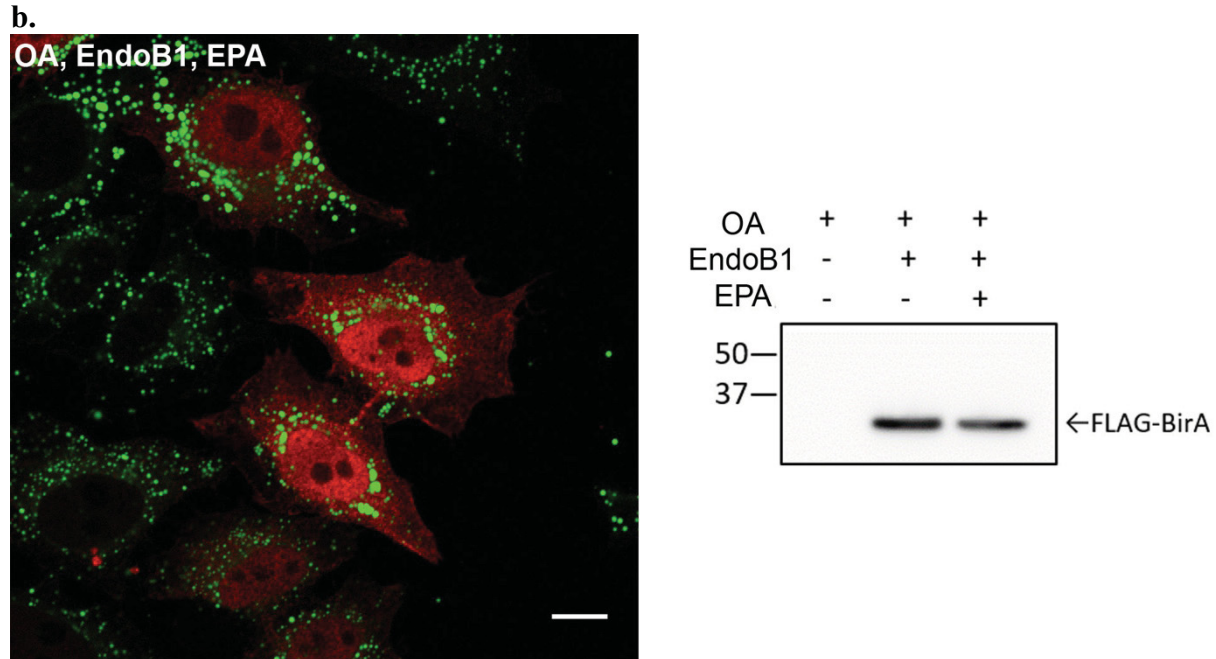


(Figure continues on the next page.)



**c.**

<u>Retromer-related proteins</u>	<u>Motor proteins</u>	<u>Clathrin-related proteins</u>
Vps35	DYNLL1	AP1B1
Vps26A	DYNLT1	AP1G1
SNX1	DYNC1LI1	AP2A1
SNX2	DYNC1I2	AP2A2
SNX4	DYNC1LI2	AP2B1
SNX6		AP2M1
TBC1D5		AP3B1
<u>Lysosome-related proteins</u>	<u>Exosome-related proteins</u>	AP3D1
BLOC1S2	SDCBP	AP3M1
BLOC1S3	PDCD6IP	AP3S1
ARL8B	HNRNPA2B1	

**Figure 4-22:** Interacting partners of endophilin B1 in EPA mediated lipophagy.

- a.** T-REx HeLa cells inducibly expressing endophilin B1-BirA construct. Endophilin B1-BirA behaves the same as endophilin B1-EGFP because it moves to LD after EPA incubation. Western blot probed with endophilin B1 antibody shows the expression of the construct and endogenous endophilin B1. Scale bar is 10 $\mu$ m.
- b.** T-REx HeLa cells inducibly expressing FLAG-BirA construct. This serves as a control for BirA. FLAG-BirA does not behave as endophilin B1-EGFP as it does not translocate to LD in the presence of EPA. Western blot probed with FLAG antibody shows the expression of the construct. Scale bar is 10 $\mu$ m.

- c. Potential interactors of endophilin B1 identified by Bio-ID. Bio-ID identified retromer-related proteins, lysosome-related proteins, motor proteins, exosome-related proteins, and clathrin-related proteins.

From Bio-ID experiment, a number of candidates have been identified: proteins involved in CDP-choline pathway, endocytosis, mitochondrial function, SNAREs, BLOC, retromer, and PIK3C2 $\beta$ . Identification of cytidylyltransferase supports that endophilin B1 plays a role in membrane fission. Similarly, it agrees with our results shown in Fig. 4-3 and previously shown functions of endophilin B1 in membrane tubulation (Farsad et al., 2001; Rostovtseva et al., 2009). Identification of SNAREs and BLOC supports the role of endophilin B1 and EPA in the Kiss-and-run lipophagy (See Discussion 5.2.4.).

One protein, PIK3C2 $\beta$ , came to our interest because it was never seen in Bio-ID of other proteins that our laboratory works on. PIK3C2 $\beta$ , as a member of PI3K family, is recruited to a membrane where it catalyzes the synthesis of PtdIns3P. Sorting nexins (SNX) bind to PtdIns3P, and several SNXs (SNX1, 2, 5, 6) were detected along with members of Vps trimer (Vps26 and Vps 29), and TBC1D5. These proteins make up retromer complex, which is used to mediate endosome-TGN transport. It is plausible that endophilin B1 binds to PIK3C2 $\beta$ , and also participates in retromer carrier formation by binding to SNX1/2, Vps26, and Vps29. Or, it is possible that endophilin B1 binds to TBC1D5 to balance between retromer formation and autophagy induction because TBC1D5 has been implicated as a switch for autophagy (Popovic et al., 2012).

Subunits of a motor protein dynein, which acts in intracellular transport, were detected. Similarly, members of BLOC complex and Arl8b, proteins involved in the lysosomal movement, have been detected. Identification of these proteins suggests that endophilin B1 may also be physically engaged in the lysosomal movement.

Interestingly, Bio-ID experiment identified proteins that are involved in exosome assembly. Exosomes are extracellular vesicles secreted by a variety of cell types, and their role has been suggested in intracellular communication (Raposo and Stoorvogel, 2013). Exosomes enable transfer of membranes, cytosolic proteins, lipids, and RNAs between cells, and they require series of proteins to coordinate their assembly (Raposo and Stoorvogel, 2013). In particular, key proteins for membrane transport, SDCBP (also known as syntenin), and its partner PDCD6IP (also known as ALIX) have been identified in the Bio-ID (Fig. 22c). SDCBP is a multifunctional adaptor for trafficking of transmembrane proteins, and PDCD6IP participates in budding and abscission processes (Baietti et al., 2012). Additionally, PDCD6IP binds to endophilin in the C-terminus (Baietti et al., 2012). HNRNPA2B1, a nuclear ribonucleoprotein involved in sorting of miRNA into exosome (Villarroya-Beltri et al., 2013), has also been identified (Fig. 4-22c). These results suggest that endophilin B1 may be involved in exosome assembly, and it may be contributing to the assembly through introducing curvature to membranes.

Bio-ID experiment identified possible interactions of endophilin B1. Due to its sensitive nature, weak or transient interactions are also detected. Therefore, possible candidates identified from the Bio-ID results are preliminary, and careful observation may open new doors in endophilin B1's functional elucidation (See Discussion **5.2.4**).

## **Chapter 5: Discussions**

## **5.1. Development of tools to understand how Golgi maintains its homeostasis**

In this thesis, a fusion antibody was fully characterized. Fusion antibody accurately represents the behavior of endogenous Golgi-resident enzyme. Results from this study can help understand how endogenous Golgi enzymes traverse the Golgi and how the movement of these enzymes contribute to maintaining structural homeostasis of the Golgi. Furthermore, this work also presented potentials to use fusion antibody for monitoring protein internalization. Other applications are envisaged.

### **5.1.1 Full characterization and advantages of fusion antibody**

A fusion antibody was generated from taking the variable fragment of a monoclonal antibody and adding a fluorescent tag, and its use and characteristics have been fully examined. It is expressed in various cellular systems, recognizes respective antigen, and goes through the secretory pathway. Furthermore, conditioned media and affinity purified fusion antibodies can recognize antigens of non-transfected cells. They truly represent endogenous glycosylation enzymes *in vivo* without affecting the steady-state distribution of enzymes. Advantages of fusion antibody over monoclonal antibody include the following: 1) it can fluorescently monitor Golgi enzyme within fusion antibody expressing cell *in vivo*; 2) it is recombinantly expressed from cDNA, so it can be more easily manipulated than exogenously applied antibody; and 3) since it is made with single-chain-variable-fragment only, size (including fluorescent tag) is significantly smaller (around 58kDa) than IgG (~150kDa) and secondary antibody; 4) Fusion antibody

behaves as a biosynthetic cargo that is expressed and goes through the early secretory pathway, but it also acts a probe that illuminates the location of endogenous Golgi enzyme; 5) expressing fusion antibody (transiently, stably or tetracycline-inducibly) does not affect cell viability or cause ER stress; Therefore, compared to traditional immunofluorescence method that requires primary antibody and secondary antibody tagged with a fluorophore, fusion antibody can overcome the issues of antigen inaccessibility, and it will illuminate the most precise location of the enzyme in the secretory pathway.

Although fusion antibodies were characterized in terms of their antigen recognition and they represent the behavior of endogenous Golgi enzymes, they may not be accurate tools to study the activity of Golgi-resident enzymes. This is because the activity of Golgi-resident enzyme was not tested upon fusion antibody binding. In order to confirm whether fusion antibody affects the activity of GalT, cells can be transfected with FSAB-GalT (or FSAB-GalT expression can be induced with tetracycline in T-REx Hek293 cells). From the transfected cells' lysate, the rate of [<sup>3</sup>H]-UDP-galactose transferred to ovomucoid can be measured. Here, ovomucoid, trypsin inhibitor, is used as an acceptor for radioactive galactose. To assay the enzymatic activity, the whole cell lysate can be mixed with sodium cacodylate buffer, which contains ovomucoid, beta-mercaptoethanol, Triton X-100, ATP, MnCl<sub>2</sub>, UDP-galactose, and [<sup>3</sup>H]-UDP-galactose. After 30minute incubation, the reaction can be terminated by adding ice-cold phosphotungstic acid/HCl. Samples can be centrifuged to remove unbound [<sup>3</sup>H]-UDP-galactose, and the resulting pellet can be solubilized by 2M Tris and 1% SDS before radioactivity (dissociation per minute, dpm) can be measured. From the dpm, the amount of galactose transferred per hour can be calculated. If this value in fusion antibody transfected cells is lower than non-transfected cells, then the activity of GalT is affected by fusion antibody.

### **5.1.2. Potential to use fusion antibody to highlight another cells' antigen**

To verify the specificity of the fusion antibody, one of the experiments performed was to work with conditioned media. Cells that express fusion antibody also secrete fusion antibody to the media, which we call conditioned media. By using the conditioned media as an antibody, antigen in non-transfected cells was highlighted. This experiment did not only confirm that fusion antibody was made specifically for its respective antigen, but also showed that highly specific, a monoclonal-like antibody can be harvested from conditioned media. Similarly, fusion antibody could be affinity purified, and eluate from this experiment maintains the characteristics fusion antibody: it is fluorescent, and it recognizes respective antigen (Fig. 3-10). Furthermore, fusion antibody is tagged with a fluorophore itself, so there is no need to utilize secondary antibody: eliminating the need for secondary antibody reduces the significant distance from an antigen to a fluorophore that is normally attached to the secondary antibody. This is an advantage that will be extremely valuable for visualizing contents within minutely sized COPI vesicles. Previously, two laboratories with prestigious electron microscopy techniques produced opposite findings, even when both labs used the same probe and method. Although both groups used the same antibody against MannII for immune-EM, one group showed that MannII was incorporated in peri-Golgi vesicles (Martínez-Menárguez et al., 2001) while the other group revealed the opposite (Cosson et al., 2002). One explanation for the discrepancy is a relatively long distance between antigen and a colloidal-gold that is conjugated to a secondary antibody, and this distance may have misled the distribution of MannII within small structures like COPI vesicles (30-50nm). Since fusion antibody eliminates a need for a secondary antibody, it will significantly reduce this type of artifact.

In order to accurately determine the size of fusion antibody at the nanometer level, we can perform dynamic light scattering assay. Affinity purified fusion antibody can be shined by direct light, and the angles of light scattering can be measured. The rationale is that the smaller the particle, the smaller will be the angle of the scattered light. Proteins of known nanometer size can be used as a standard, so that size of fusion antibody can be determined empirically. Similarly, affinity purified fusion antibody can be prepared for EM by rotary shadowing or negative stain. By observing the fusion antibody by EM, diameter of fusion antibody molecule can be resolved at the nanometer level. The advantage of this method is that we can also determine the shape of a fusion antibody as well.

### **5.1.3. Fusion antibody as a tool to study protein internalization**

Series of experiments conducted with the affinity purified fusion antibody revealed that fusion antibody could be used as a tool to study protein internalization: Affinity purified EGFP-FSAB-GalT was internalized in non-transfected, live cells, and it colocalized with endogenous GalT in Golgi (Fig. 3-11, 3-12). This observation suggested that GalT is present on PM. Indeed, it is present on plasma membranes of different cell types where it plays a role in gamete recognition (Miller et al., 1992), cell-to-ECM interaction (Steffgen et al., 2002), and metastasis (Zhu et al., 2005). Furthermore, examination of long-, short-, and phosphorylation mutant-GalT showed that GalT might have differential localization depending on the presence of the cytosolic tail. This is because the amount of fusion antibody internalization was different when it was added to these cells (Fig. 3-13). Short form of GalT had the most internalized fusion antibody, suggesting that short form of GalT may be the one present on PM. Although the long form of

GalT was shown to be localized in PM (Hathaway et al., 2003), it is plausible that both short and long form are present and only the short form dynamically cycles between PM and Golgi.

In order to confirm the hypothesis that GalT cycles between plasma membrane (PM) and Golgi/endosome/lysosome compartment, more experiments must be done to ensure the internalized fusion antibody represents the GalT's itinerary from the PM. In this thesis, whole cell lysates were used for Western blot analysis, and this only highlighted the internalized fusion antibody, and it does not necessarily mean that GalT traveled internally from the PM along with the fusion antibody. To address this concern, fusion antibody must be co-immunoprecipitated with GalT in a native condition. If fusion antibody co-immunoprecipitated with GalT, then this GalT may be representative of cell surface GalT that cycled back to the cell interior. Since there is not a significant amount of fusion antibody internalized under normal conditions (Fig. 3-13) and the turnover of GalT at PM is unknown, bafilomycin A may be added.

As for the mechanism of internalization, whole cell lysate has been analyzed by density gradient and cell surface GalT was shown to be in the same fraction as lipid rafts (Hathaway et al., 2003). However, the exact molecular mechanism of how GalT travels to the cell surface and back to the cell interior has not been investigated.

Additionally, GalT may be presented to cell surface before being degraded by the lysosomal pathway. This is because the amount of fusion antibody uptake is different, and the amount of internalization is greater in the presence of lysosomal inhibitor bafilomycin A1 (Fig. 3-13). We determined that fusion antibody was not internalized by random, bulk uptake because non-specific  $\alpha$ -rabbit IgG (H+L) Alexa 568 did not travel inside of the cell (Fig. 3-11). From this

observation, we can safely deduce that internalization was not triggered by fluorophore or immunoglobulin.

However, conclusions should be drawn carefully because a number of assumptions were made: We assumed that fusion antibody remained tightly bound to cell surface GalT and that it followed the trajectory of the cell surface GalT. Similarly, we assumed that the internalization of EGFP represents uptake of entire fusion antibody molecule, and internalized fusion antibody was intact. It is probable that EGFP has been detached from the fusion antibody during the uptake process, and it has been taken up alone. Although fusion antibody was tandem affinity purified by His and FLAG tag, we did not verify if EGFP remained bound to the fusion antibody. To confirm whether fusion antibody was intact, the eluate from tandem affinity purification may be analyzed by Western blot against EGFP. Since the eluate was able to highlight GalT in non-transfected cells and colocalize with monoclonal GalT antibody, the antigen recognition was confirmed. In this experiment, GalT was highlighted with EGFP-FSAB-GalT, so EGFP of the affinity purified fusion antibody was intact. So if EGFP or any other parts of the fusion antibody has fallen, it would be during the uptake process. Additionally, it is plausible that the conformation of fusion antibody was disturbed by the purification method or by low pH of endosome or lysosome. In order to test whether or not exposure to lower pH dissociates fusion antibody, affinity purified fusion antibody can be resuspended in various pH ranging from 4.5 (pH of endosome). Then, the fusion antibody can be analyzed by Coomassie blue stained SDS-PAGE or Western blot probed by EGFP and FLAG.

Interestingly, bafilomycin A1 treated cells revealed greater internalization of the fusion antibody. In order to understand why fusion antibody uptake increased with bafilomycin A1, we have to consider the possibility as to why and when lysosome degrades GalT. One possibility is

that GalT is presented on the cell surface, and then become internalized for lysosomal degradation: this may be a way to get rid of old GalT. According to the cisternal maturation model, Golgi is under a constant turnover where it is taken apart at the *trans* side, and constituents are trafficked to the *cis*- Golgi in a retrograde direction. For any reason, GalT may have not entered the retrograde trafficking, continued the secretory pathway, and eventually reached to PM. Any mislocalized Golgi protein that escaped this transport may be degraded by the lysosome, supported by the bafilomycin A1 experiment (Fig. 3-13). Indeed, lysosomal acid phosphatase (LAP) has been shown to be transported from the Golgi to PM, eventually to the lysosome (Braun et al., 1989). Newly synthesized LAP from Golgi travels to the PM where it gets rapidly endocytosed by a mechanism that decreases upon reduced temperature, chloroquine, NH<sub>4</sub>Cl or primaquine (Braun et al., 1989).

It is possible that the journey of GalT from Golgi to PM, and to lysosome is a way to degrade defective GalT. In order to test this possibility, we can test whether or not defective GalT is transported to the cell surface. Similar to determining enzymatic activity of GalT in fusion antibody transfected cells, cell surface GalT's activity can be measured. Instead of preparing whole cell lysate, we can work with cell surface GalT without lysing cells. To do this, T-REx Hek293 cells can be washed once with warm PBS, and ice-cold PBS can be added directly onto cells before cells are being scraped carefully. To detach cells, trypsin may not be used since it can deactivate proteins of the cell surface. Similarly, EDTA may not be used because GalT enzymatic activity is inhibited (Fleischer et al., 1969).

For cell surface GalT to travel back to Golgi, it is plausible that retromer complex is involved. Retromer complex is a protein complex that mediates retrograde transport of transmembrane proteins from endosomes to TGN, and it is comprised of sorting nexins (SNX,

membrane-binding coat subcomplex), and Vps trimer consists of Vps26, Vps29, and Vps35. After endocytosed into an endosome, Vps trimer associates with cargos located at endosomal membrane. Here, Rab7-GTP would be involved. SNX-BAR subcomplex (comprised of SNX1/2), upon dimerization, senses the curved membrane and its nucleation will introduce more curvature, and this will eventually induce tubule formation. Finally, matured retromer tubule undergoes scission by dynamin, and Vps trimer and SNX-BAR subcomplex are taken off upon GTP hydrolysis of Rab7. Now, the released tubule is transported to TGN by dynein motor protein. Clathrin adaptors are involved in this process because Shiga toxin B-subunit and transferrin receptor accumulate in endosomes in clathrin-depleted cells (Popoff et al., 2007). However, the introduction of dominant-negative clathrin or knockdown of clathrin did not affect retromer tubulation by SNX-BARs (McGough and Cullen, 2013). If cell surface GalT travels to Golgi, it will be endocytosed, shuttled to TGN by retromer, and it will travel to trans-Golgi cisterna by COPI retrograde vesicles. In our observation, however, internalized fusion antibody seemed to occupy the lysosomal region, as it appeared juxta-Golgi (Fig. 3-12). In order to test whether or not GalT has traveled to Golgi by retromer complex, it can be immuno-precipitated with Vps trimers. As well, its association with ESCRT can be examined for the possible itinerary to the lysosome.

#### **5.1.4. Visualization of glycosyltransferases with fusion antibody**

To visualize the Golgi enzymes *in vivo*, fusion antibody will be introduced to GRAB technique (see section 1.2.7.a) (in collaboration with Dr. Julia Fernandez-Rodriguez, University of Gothenburg, Sweden). GRAB technique utilizes free radicals generated upon EGFP or

mTurquoise excitation, and these can be used to precipitate 3,3' diaminobenzidine hexahydrate (DAB) into visible and highly localized precipitates when viewed at the ultrastructural level (Grabnbauer et al., 2005). The density of the DAB product is linear to the initial fluorescence exhibited by the fluorophore (Grabnbauer et al., 2005). Previously, EGFP-GalNacT2 was shown to be incorporated into budding COPI vesicles by using GRAB and EM tomography, (Grabnbauer et al., 2005). However, the disadvantage of the GRAB method is that it relies on overexpressed protein, and this can inevitably affect stoichiometric ratios and true steady-state distribution. To overcome possible issues of over-expressing antigens (i.e. those of Golgi-resident glycosylation enzymes), we have to develop a readily detectable probe that can accurately represent the location of endogenous Golgi glycosylation enzyme. The fusion antibody fulfills this requirement because, after proper expression in mammalian cells, it reflects endogenous Golgi enzyme at its true steady state distribution. Additionally, it can overcome the issues of antigen inaccessibility, which was highlighted in previous studies (See section 1.1.6). Therefore, images in two and three dimensions obtained from combining GRAB with fusion antibody will precisely reveal the ultrastructural location of the Golgi-resident enzyme. Since it first begins at the light microscopy level, retention and recycling of corresponding Golgi-resident glycosyltransferases *in vivo* can be visualized.

### **5.1.5. Fusion antibody as a biosynthetic cargo and a Golgi-resident protein**

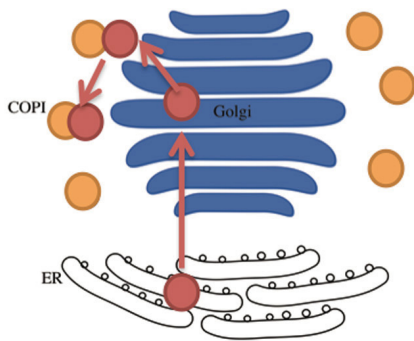
After being expressed, fusion antibody goes through the secretory pathway, traverses the Golgi, and recognizes the Golgi-resident enzymes by acting as a probe. However, when its

respective glycosyltransferase is absent, it will be a biosynthetic protein that simply passes through the early secretory pathway.

Therefore, the fusion antibody has dual roles: it is a probe that illuminates the location of its respective antigen (i.e. either GalNacT2 or GalT), but it also behaves as a biosynthetic cargo that goes through the early secretory pathway. Consequently, its localization either in Golgi cisternae or COPI vesicle (or tubules) will provide answers to clarify the early secretory pathway. The following figure demonstrates how fusion antibody can help understand the early secretory pathway.

## Cisternal Maturation Model

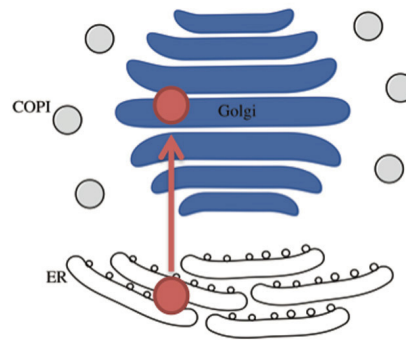
PM



### When antigen is present (WT)

Golgi-resident enzymes (vesicles)  
Fusion antibodies (vesicles)

PM

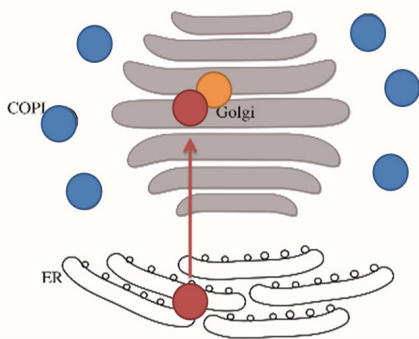


### When antigen is absent (KO)

Vesicles will be devoid of the enzymes  
Fusion antibodies (cisternae)

## Vesicular Transport Model

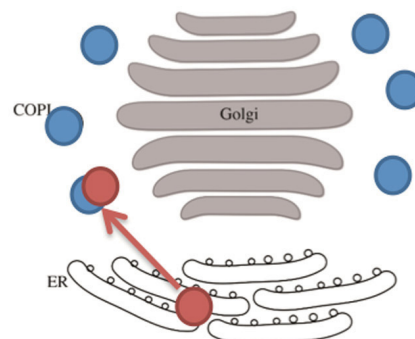
PM



### When antigen is present (WT)

Biosynthetic protein (vesicle)  
Golgi-resident enzymes (cisternae)  
Fusion antibodies (cisternae)

PM



### When antigen is absent (KO)

Biosynthetic protein (vesicle)  
Fusion antibody (vesicle)

● Fusion antibody

● Antigen (Golgi-resident proteins)

● Biosynthetic protein

(Figure legend continues on the next page.)

**Figure 5-1:** Expected observations in the secretory pathway

Localization of fusion antibody will be different depending on the Golgi model and presence of the antigen (Golgi-resident enzyme). See texts for details.

Given this unique characteristic of the fusion antibody, I expect that the behavior of the fusion antibody will be different depending on which of the two Golgi models holds true (Fig. 5-1). Based on VTM, biosynthetic proteins are transported from one cisterna to the next by COPI vesicles, and their glycosylation is performed by Golgi-resident enzymes within stationary cisternae. Therefore, when fusion antibody binds to Golgi enzyme, it will be contained within cisternae. Contrarily, CMPM suggests that Golgi enzyme is packaged into COPI vesicles (or tubules) for retrograde transport. Therefore, according to CMPM, the fusion antibody will follow Golgi-resident enzyme, and it will be found within COPI vesicle (or tubules). Alternatively, in an environment where the fusion antibody's antigen (i.e. Golgi-resident enzyme) is absent, the observation will change. In this case, fusion antibody will no longer act as a probe that highlights Golgi-resident enzyme. Instead, it will be a biosynthetic protein that goes through the secretory pathway. According to VTM, which suggests that biosynthetic proteins are packaged into transport vesicles, fusion antibody will be found within COPI vesicles (or tubules). In accordance with the CMPM, vesicles are going to be devoid of the fusion antibody. Therefore, fusion antibody will stay in the cisternae.

In order to carry out this experiment, glycosylation enzyme must be completely knocked out. The previous siRNA-mediated GalT KD did not result in sufficient KD level. Therefore, we need to generate GalT knockout cell lines by CRISPR/Cas genome editing system.

After proper expression and optimization, results of this experiment will be analyzed by the GRAB method. In place of EGFP tagged Golgi-resident enzyme (Grabenbauer et al., 2005), the fusion antibody will be highlighting the location of endogenous Golgi enzyme. Also, mTurquoise fusion antibody will be used in place of EGFP because this dye generates more free radicals that are useful for DAB precipitation (Goedhart et al., 2010). These mTurquoise tagged fusion antibody has already been incorporated into tetracycline inducible system, as this will facilitate modulation of fusion antibody expression. In addition to T-REx Hek 293 cells, T-REx HeLa cells have also been generated to express the fusion antibody inducibly. The advantage of T-REx HeLa cells over Hek293 is that HeLa cells are more adherent, and they withstand sample preparation steps. To carry out this experiment, fusion antibody expression will be induced by tetracycline. Next, CHX will be added to remove residual fusion antibody from the ER and to remove unbound fusion antibody. After this, subcellular localization of the fusion antibody will be analyzed by the modified GRAB.

## **5.2. Functional elucidation of endophilin B1 in specialized LD breakdown**

### **5.2.1. Endophilin B1 participates in lipid droplet breakdown**

Work presented in this thesis demonstrates a novel function of endophilin B1 in lipid droplet breakdown, and it provides the first observation that endophilin B1 is present on LD surface. Moreover, the abundance of endophilin B1 in LDs of NAFLD patient livers suggests that endophilin B1 is clinically significant.

The amount of endophilin B1 detected by mass spectrometry seems to correlate with the progression of the disease (Fig. 4-1b): 1.5 folds of NASH livers had a high level of endophilin B1 in their LD fractions, compared to NAFLD livers. Similarly, endophilin B1 was shown to be overexpressed in hepatocellular carcinoma (Fan et al., 2012). However, it may be premature to conclude that high level of endophilin B1 is the biomarker for worsened fatty liver disease because NAFLD is a complicated, multi-causal disease, which develops over a period of decades. To fully determine the state of fatty liver disease, a liver biopsy must be taken for histological assessment.

Perhaps, the presence of endophilin B1 may represent a process of the disease progression or a symptom of the disease. That is, endophilin B1 may be recruited to LDs of advanced fatty liver patients and function in LD breakdown to alleviate the symptom. Work presented in this thesis surely indicate that endophilin B1 functions in lipophagy, particularly of the kiss-and-run type.

In OA treated cells, enhanced endophilin B1 expression has led to a decrease in LD diameter and an increase in LD number (Fig. 4-3). One explanation for this phenotype is that

endophilin B1 causes LD fission. Indeed, unique structures of endophilin B1 and previously shown functions strengthen this argument; Endophilin B1 contains an N-BAR domain that gets inserted into phospholipid membrane, and this action introduces curvature to a membrane. Similarly, membrane binding and tubulating activity of endophilin B1 have been seen on numerous occasions. The *in vitro* experiment of purified endophilin B1 incubated together with Bax and giant unilamellar vesicle (GUV) revealed that endophilin B1 binds to GUV and causes tubulation into smaller liposomes (Rostovtseva et al., 2009). Similarly, endophilin B1 directly binds to the synaptic membrane when incubated with brain cytosol and dynamin (Farsad et al., 2001). Likewise, endophilin B1 has been shown to interact with dynamin that pinches off the neck of vesicles (Farsad et al., 2001). Given these observations, it is possible that endophilin B1 binds to LD and oligomerizes to pinch off LD, leading to LD fission. Indeed, knockdown of endophilin B1 resulted in enlarged and fewer LDs compared to the control condition (Fig. 4-4), and this observation certainly reinforces the possibility of LD fission. However, endophilin B1's function may not be mere LD fission; time course expression of endophilin B1 caused a drastic decrease of cellular TAG compared to non-induced cells (Fig. 4-4). If endophilin B1 functions in LD fission only, the amount of TAG before and after the experiment must be similar (or with and without endophilin B1 overexpression), if not the same (more on this later). However, the substantial consumption of TAG after endophilin B1 expression suggests that endophilin B1 may not only function to cause LD fission, but also in LD breakdown. Surely, endophilin B1 may act to prime LD for lipophagy by causing initial LD fission. Now, smaller LDs may be more favored for lipophagy.

Additional evidence for LD fission may be provided by measuring changes in the level of phosphatidylcholine (PC) or phosphatidylethanolamine (PE) because these are main components

of LD monolayer, and increased fission would require more PC and PE to accommodate increased surface area. Also, if endophilin B1 is seen on tubulated LD surface by electron microscopy, it can undoubtedly reinforce this hypothesis on LD fission. In order to observe the LD fission activity of endophilin B1 in a direct way, it would be efficient to measure the light scattering profile of LDs after incubation with recombinant endophilin B1 *in vitro*. The rationale is that large LDs will cause greater angles of light scattering, whereas smaller LDs will cause less scattering. If endophilin B1 does participate in fission of LDs, a condition with endophilin B1 will cause LD fission and yield less light scattering compared to a condition without endophilin B1. Final results can be negatively stained and confirmed by an electron microscope. Furthermore, increased endophilin B1 expression facilitated LD breakdown (Fig. 4-3) and the loss of endophilin B1 attenuated LD clearance (Fig. 4-4, 4-11, 4-12). This observation, in addition to possible LD fission function, strongly suggests that endophilin B1 is essential for LD breakdown.

### **5.2.2. Endophilin B1 is essential for EPA mediated lipophagy.**

Endophilin B1 is involved in the early stages of macroautophagy, where it binds to UVRAG through SH3 domain and become a part of UVRAG-Beclin1-VPS34 complex (Takahashi et al., 2007). This complex may participate in membrane gathering from the Golgi (Takahashi et al., 2011; He et al., 2013). Given this function of endophilin B1, we enquired about the mechanism of endophilin B1 in the LD breakdown. Initially, endogenous endophilin B1 translocated to LD in the presence of rapamycin and bafilomycin A (Fig. 4-2). Similarly, endophilin B1-EGFP also translocated to LD after an omega-3 fatty acid, EPA treatment (Fig. 4-

6). These observations opened up the possibility that endophilin B1 participates in lipophagy that is triggered by global autophagy signal. However, attenuation of endophilin B1 expression in the presence of Torin1, or EPA has resulted in a surprising conclusion that endophilin B1 acts differently depending on the lipophagy stimuli (Fig. 4-12). Endophilin B1 knockdown indeed blocked EPA mediated lipophagy whereas classical macroautophagy by mTOR block (mTOR inhibited by Torin1) was unaffected. This observation strongly suggests that endophilin B1 does not only act in the mTOR-related classical macroautophagy (and maybe endophilin B1 is dispensable from macroautophagy (Liu et al., 2016)), but also in the EPA mediated lipophagy.

EPA, along with another omega-3 fatty acids such as DHA and ALA, is known to lower elevated TAG levels, and it has been regarded as a health supplement to take every day. Similarly, U.S. Food and Drug Administration stated that EPA might reduce coronary heart disease. Recently, EPA was shown to attenuate oxidative stress in cardiomyocyte by activating autophagic responses (Hsu et al., 2014). Moreover, prolonged incubation with EPA was shown to reduce lipotoxicity (Chen et al., 2015). Although the mechanism of EPA in TAG reduction has not been elucidated extensively, publications mentioned above have shown that prolonged incubation of EPA induces LC3-I to LC3-II conversion, which is a marker for macroautophagy. Similarly, our result on EPA also demonstrated a decrease in the size of LD (Fig. 4-7, 4-8) and reduced the amount of TAG (Fig. 4-9). In EPA-treated cells, endophilin B1 was localized closely with LDs, suggesting that endophilin B1 acts in EPA stimulated lipophagy by being directly associated with LDs (Fig. 4-6). Also, when cells are transfected with mRFP-eGFP-LC3 construct where mRFP is acid-insensitive, and eGFP is acid-sensitive, the number of eGFP disappearance is increased (Fig. 4-11): This observation is indicative of the LC3-positive autophagosome digestion by acidic compartment (such as lysosome). However, EPA mediated autophagy must

be independent of the mTOR-regulated autophagy because under the H<sub>2</sub>O<sub>2</sub> oxidative stress, EPA and autophagy repressor (mTOR enhancer 3-methyladenine) LC3-I was still converted to LC3-II (Hsu et al., 2014). Moreover, in EPA treated endophilin B1 KD cells endogenous LC3 was still around LD (Fig. 4-18b), and in EPA treated endophilin B1-EGFP expressing cells, mCherry-LC3 was not around LD (Fig. 4-6). Similarly, knockdown of Atg5 (an essential protein in the macroautophagy) does not hinder endophilin B1-EPA mediated lipophagy (Fig. 4-14). From these observations, it is possible to formulate a hypothesis that EPA acts in two different ways: under the mTOR inhibition it can trigger macroautophagy indicated by LC3; and under lipid-rich conditions, it triggers lipophagy, which requires endophilin B1. Also, this latter type of lipophagy involves a relationship between the LD and lysosome (Fig. 4-18 and Fig. 4-19). It is plausible that endophilin B1 is a determining factor for EPA mediated lipophagy: excess endophilin B1 (induced T-Rex HeLa endophilin B1-EGFP cells) and EPA favors Kiss-and-run, and with normal (or low) level of endophilin B1 (HeLa cells and uninduced T-Rex HeLa endophilin B1-EGFP cells) macroautophagy is favored.

### **5.2.3. Endophilin B1 mediated lipophagy is distinct from macroautophagy or lipolysis.**

So far, expression of endophilin B1 decreased LD diameter, and those observations suggest that endophilin B1 is involved in lipid breakdown. However, there are many types of lipid breakdown, including lipolysis by lipases, lipophagy through a macroautophagic pathway, and lipophagy through Kiss-and-run. In this study, lipolysis and macroautophagy were blocked

separately and together in the presence of endophilin B1 expression and EPA treatment. Results of these experiments provided clues to investigate the role of endophilin B1 in lipid breakdown.

So far, we have established that endophilin B1 mediated lipophagy in the presence of EPA is different from the macroautophagy. However, there is a possibility that LD breakdown we observed was due to lipases such as ATGL. Therefore, to distinguish the Kiss-and-run lipophagy by endophilin B1 against the lipolysis, Atglistatin was used. Atglistatin is a competitive inhibitor of ATGL, which is an enzyme that triggers a rate-limiting step of TAG breakdown. Therefore, inhibiting ATGL in the presence of endophilin B1 should demonstrate the effect of endophilin B1 in conditions, where TAG hydrolysis by ATGL is blocked. Under the ATGL inhibition, endophilin B1 expression continues to mediate LD lipophagy, and endophilin B1 remains tightly around LD (Fig. 4-15). This phenotype was true even in the absence of Atg5 (Fig. 4-14). At the same time, endophilin B1 remains colocalized with LAMP1, and the number of LAMP1 associated LDs increases (Fig. 4-19). Collectively, these observations strongly suggest that endophilin B1 is compensating for the loss of lipolysis in a mechanism of Kiss-and-run lipophagy.

However, lipid breakdown by ATGL may not only be a simple lipolysis since ATGL requires LC3 for its lipolytic activity in brown adipose tissue (Martinez-Lopez et al., 2016). It was shown that ATGL contains an LC3 interacting region (LIR) that its deletion hinders macroautophagy (Martinez-Lopez et al., 2016). Similarly, in yeast it was shown that OA loading causes autophagy and vacuolar uptake of LDs, and this phenotype was not dependent on Atg1 (autophagy regulator) but dependent on Atg15 (vacuolar lipases) (van Zutphen et al., 2014). Therefore, it is plausible that macroautophagy is also affected in Atglistatin treated cells, which

is probably a reason why LD size increased in EndoB1/EPA/Atglistatin treated cells (Fig. 4-15b, navy bar).

Furthermore, endophilin B1 localizes on LD surface of fatty liver cryosection (Fig. 4-17), there is increased LD association with LAMP1 in conditions, where macroautophagy and lipolysis are blocked (Fig. 4-19). It should be noted, however, that the size of LD can grow indefinitely in cells with lipid metabolism defect (such as in NAFLD patient's hepatocyte) and lysosomes can vary from 0.1~1.0 $\mu$ m in diameter (Lüllmann-Rauch, 2005). Therefore, observation of endophilin B1 on LAMP1-positive LD allowed us to postulate that the lipophagy mediated by endophilin B1 may involve LD-lysosome relationship; Kiss-and-run lipophagy. Transient fusion between LD and lysosome, a characteristic of Kiss-and-run lipophagy, is easily observed in this condition (Fig. 4-17, Fig. 4-18 see arrows, and Fig. 4-19). Endophilin B1-positive LD is in proximity with LAMP1-positive lysosomes, and this occurrence seems exaggerated when both macroautophagy and lipolysis are inhibited (Fig. 4-19). Collectively, endophilin B1 translocates to LD to mediate Kiss-and-run lipophagy, and it may be the last mode of lipophagy when macroautophagy and lipolysis are defective.

### **Mechanism of cellular TAG degradation by endophilin B1**

There are three ways for the TAG to be degraded. One is that fatty acids get cleaved off from the glycerol by triacylglycerol lipase, hormone-sensitive lipase, and monoacylglycerol lipase. These free fatty acids are shuttled to mitochondria for beta-oxidation, which can be measured by the amount of radioactive CO<sub>2</sub> emitted from the cell.

Another fate for fatty acid is to be re-esterified back to TAG by either monoacylglycerol pathway or glycerol-3-phosphate pathway (also called Kennedy pathway). Fatty acid-CoA (Acyl-CoA) may be added to monoacylglycerol by monoacylglycerol acyltransferase (MGAT) to produce diacylglycerol (DAG), which is quickly converted to TAG by diacylglycerol acyltransferase (DGAT). Alternatively, Acyl-CoA may be added to glycerol-3-phosphate by glycerol-3-phosphate acyltransferase (GPAT) to produce lysophosphatidic acid (LPA). The addition of acyl-CoA can continue by 1-acylglycerol-3-phosphate-acyltransferase (AGPAT) and yield phosphatidic acid. The phosphate group is then removed by phosphatidic phosphatase (or Lipin) to form DAG. DAG is then converted to TAG. In this way, fatty acids and TAG are continuously turned over within a cell.

During these fatty acid re-esterification steps, the cell does not discriminate a fatty acid from the radiolabeled one. Therefore, the amount of none-labeled TAG, as well as radiolabeled TAG, may be increased. In Fig. 4-5 and Fig. 4-9, our results only reflect the amount of radiolabeled TAG, and we were able to observe the lipophagic effect of endophilin B1 and EPA. Our result shows a sharp decrease from the beginning to the end without any escalation. Therefore, we can assume that the lipophagic activity of endophilin B1 and EPA overrides the rate at which FA gets re-esterified.

Fatty acids diffuse across phospholipid bilayers (but LD is monolayer). It has been shown that fatty acids spontaneously flip-flop in small and large unilamellar vesicles (from 25nm~100nm) at millisecond range (Kamp et al., 1995). Flip-flop rate depends on FFA structure, vesicle type and free volume within the bilayer (Kampf et al., 2006). Also, FFA transport may be dependent on cell type as adipocyte has a different mechanism of the transport across lipid bilayers (Kampf and Kleinfeld, 2007). FFAs that have been exported are accepted to an external

FFA sink such as BSA. FFA-BSA is then dissociated, and FFA is flip-flopped back into the membrane. This flip-flopping of FFA continues spontaneously, and the rate of OA partitioning may be increased when the membrane strain is increased (Mally et al., 2013). In our experiment, the amount of cellular radioactive triacylglycerol decreased rapidly as endophilin B1 was expressed (Fig. 4-5) and EPA was added (Fig. 4-9). At the same time, extracellular radioactivity increased slowly. Given that FFA spontaneously flip-flops to the extracellular environment and OA's carbon length is favourable for the flip-flop, it is plausible that the extracellular radioactivity reflects the radioactive OA that has been flip-flopped. After radioactive OA loading was finished (24 hours), cells were washed with PBS and tetracycline was added for endophilin B1 induction. This media was analyzed for possible radioactive TAG efflux. Since cells were washed after the OA loading, it is less likely that radioactive OA was carried over from the loading, and therefore the radioactivity from the media would reflect what has been exported from the cell. Similarly, Bio-ID result (Fig. 4-22) suggests that endophilin B1 binds to exosome-related proteins. It is plausible that endophilin B1 and EPA do not only mediate lipophagy in a lipotoxic environment, but also cooperate to push lipids to the extracellular environment. However, the radioactivity of the media normalized by protein concentration was extremely small (189 to 8 times less than cellular radioactivity), so it is unlikely that TAG exocytosis by endophilin B1 is significant, if there is any. Also, when the rest of media was analyzed after resuspending cell debris, there was barely any radioactivity.

In this thesis, the amount of TAG measured by the radioactive OA loading experiment (Fig. 4-5 and Fig. 4-9) was reported as counts per minute (CPM) rather than disintegration per minute (DPM). CPM is a rate of detection events registered by the measuring instrument, not the rate of emission from the source of radiation. Therefore, it is not an absolute measurement of the

radiation strength. DPM, on the other hand, is a rate of atomic disintegration event at the source of radiation, and this value can be presented as Curie or Becquerel. In order to convert CPM to DPM, counting efficiency by the instrument must be considered. In this experiment, however, all the samples were measured at the same time using the same instrument. Hence, we assumed that counting efficiencies of all the samples were the same, eliminating the need to convert CPM to DPM. Similarly, the goal of the experiment was to observe whether endophilin B1 expression decreases cellular TAG compared to the control. Therefore, the comparison between the two conditions by CPM was sufficient.

### **Mechanism of EPA in lipophagy**

To explain the mechanism of EPA in cellular TAG reduction, some pathways have been proposed, and they are mostly owing to the bulky, double-bonded structure of the EPA; EPA contains 20 carbons and five double bonds, and these double bonds introduce high conformational flexibility. The long carbon chain of the EPA can be accommodated in the lipid rafts, where relatively longer fatty acids and proteins reside to form a functional network. However, high flexibility in the chain hinders the acyl chain packing and molecular order within the rafts (Shaikh, 2012). In fact, EPA and other Omega-3 fatty acids have low affinity for cholesterol and saturated acyl-chains, and this consequently forces cholesterol to move outside of the rafts. Since saturated acyl chains and cholesterol are critical for maintaining the rafts, deletion of these lipids disturbs the rafts and causes raft proteins to be moved outside of the rafts. For example, CXCR4, a chemokine receptor that normally resides in the raft, was displaced off the membrane upon incubation with EPA and DHA, and this affected the organization of rafts

(Altenburg and Siddiqui, 2009). It is plausible that signals mediated by the rafts are also disturbed by the disorganization (Shaikh, 2012), and these signals may include gene expression for LD breakdown.

Similarly, EPA may directly alter gene expression. N-3 PUFA and fatty acids are ligands for PPAR $\alpha$ , peroxisome proliferator-activated receptor alpha. Activation of PPAR $\alpha$  induces gene expression, and it is plausible that transcription of genes involved in LD breakdown is enhanced. Indeed, prolonged exposure to EPA or DHA (0.1mM for 36hours) resulted in alteration of genes that are directly regulated by PPAR $\alpha$  (Fernández-Alvarez et al., 2011): it lowered mRNA level of SREBP1c (sterol regulatory element-binding protein, involved in synthesis of fatty acids and sterols) and increased LXR (liver X receptor; it regulates cholesterol, fatty acid, and glucose homeostasis) (Chen et al., 2015). When hepatocytes were incubated with free fatty acids and either EPA or DHA, genes related to lipid metabolism, such as ChREBP (carbohydrate-response element-binding protein) and SCD1 (stearoyl-CoA desaturase 1) were down-regulated (Chen et al., 2015).

While EPA presumably results in alteration of gene expression through PPARs, the effect of EPA seen in this thesis is after 4-8 hours. This time frame is very short to have a tremendous change in the gene transcription and protein translation. Therefore, EPA would also mediate changes that respond more quickly, such as GTPase activity, phosphorylation behavior, or direct impact on LD content. Highly flexible acyl chains of EPA make EPA hard to be packaged into TAG. Therefore, EPA may not be easily incorporated into TAG, and TAG made with EPA may not be stable. Consequently, EPA would be tossed around from one place to another, and it may become accumulated in the intracellular environment. To cope with the increased level of lipids, a cell would have to initiate LD breakdown mechanisms such as lipolysis or lipophagy.

An alternative mechanism is that the membrane perturbation by EPA could happen to LD membrane. Indeed, EPA is inserted directly into LD, as shown by McIntosh and colleagues: When fluorescent analog of EPA was added into a cell for 3 hours at 1.25mM concentration, it was seen at LD (McIntosh et al., 2010). In membrane that contains high curvature, such as LD, EPA would not be packed well with the rest of phospholipids. It is likely that this disturbance creates some signal (either physically causing fission or indirect signal) for the LD breakdown. LD comes in proximity with a number of organelles such as mitochondria, so it is plausible that TAG from LD is directly shunted to mitochondria for beta-oxidation. Since endophilin B1 is indispensable for EPA mediated lipophagy and endophilin B1 localizes specifically to LD upon EPA treatment, it is plausible that endophilin B1 primes LD for EPA mediated lipophagy. Notably, endophilin B1 may bind to EPA-positive LD (Fig. 5-2 B, C). Now, endophilin B1-positive LDs may be ready for Kiss-and-run, which will help release energy quickly. In order to visualize this further, endophilin B1 must co-localize with a fluorescent analog of EPA on LD surface, and the LDs that participate in Kiss-and-run must have endophilin B1 and EPA on their surfaces. Moreover, endophilin B's membrane bending activity may have a direct impact on EPA mediated Kiss-and-run lipophagy (Fig. 5-2 C).

#### **5.2.4. Role of endophilin B1 in Kiss-and-run lipophagy**

In this thesis, we have demonstrated that endophilin B1 and EPA trigger Kiss-and-run lipophagy, which brings LD and lysosome together. This transient docking of lysosome to the LD surface was seen in live cells (Fig. 4-21). The interaction between the Rab7-positive lysosomes and LDs seems brief in nature: Lysosomes and LDs docks for a short period, and then

they eventually depart from each other (Fig. 4-21). Schroeder and colleagues demonstrated the Kiss-and-run lipophagy by showing LAMP1-positive lysosome was recruited to Rab7-positive sub-domains of LDs (Schroeder et al., 2015). Moreover, direct contact between lysosome and LD membrane was visualized by mRFP-eGFP-PLIN2, an acid-insensitive mRFP and acid-sensitive eGFP probe that localizes on LD membrane. When lysosome contacted LD, red-green-PLIN2 turned red, and this was an indication that the two organelles indeed fused their membranes through 'kiss' (Schroeder et al., 2015). By doing these experiments, Schroeder and colleagues demonstrated Kiss-and-run accurately. In order to further confirm that endophilin B1 and EPA regulates Kiss-and-run lipophagy, utilizing LAMP1 and mRFP-eGFP-PLIN2 constructs is necessary because these will indeed highlight LD and the contact site between the two organelles. Since the encounter between the two organelles is brief in nature, it would not be feasible to co-precipitate them but to observe their movement by microscopy. To visualize the association of the two organelles better, it would be helpful to slow down the movement of the organelles by utilizing microtubule depolymerization drug nocodazole, or by lowering the temperature, which slows down the microtubule assembly. Indeed, it has been shown that Rab7 drives movement of vesicles (such as phagosomes, LDs, and lysosomes) through microtubules: centripetal direction with its adaptor RILP, and centrifugal direction with another adaptor FYCO1 (FYVE and coiled-coil domain-containing 1) (Pankiv et al., 2010). LDs also move through microtubules. For movement towards microtubule organizing center (MTOC), dynein motor is used with Halo, a specific adaptor to LD. For movements towards cell periphery, kinesin1 motor is connected to Halo, which acts in a complex with Klar and LSD2 (Shubeita et al., 2008). Klar is a regulatory protein, and it is coordinated by LSD2, which a perilipin like protein. LSD2 is responsible for regulating lipid homeostasis, and it also coordinates Klar. It is a

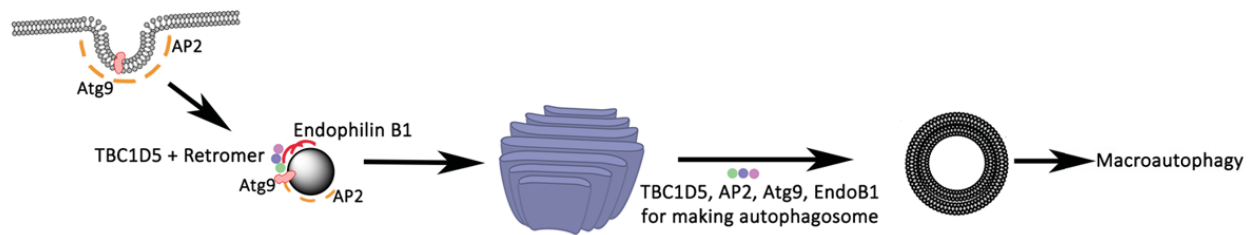
central player in the LD motion. LDs tend to oscillate even in steady-state cells (Walther et al., 2012), and these factors may be constitutively working at an opposite direction. In our live cell imaging, both LD and lysosome showed movement toward each other (Fig. 4-21). Therefore, it was difficult to determine which protein motors or adaptors that EPA targets the most, if it does. Nonetheless, Shubeita and colleagues demonstrated that having higher copy numbers of motor protein does not affect the velocity of LD transport (Shubeita et al., 2008).

Certainly, transient docking of lysosome to the LD surface may provide a quicker release of LD contents because there is no need for autophagosome formation (Schroeder et al., 2015). This process may certainly be less energy-costly. However, the mechanism, in which the two organelles comprised of a phospholipid bilayer and a phospholipid monolayer fusing very quickly and departing is unknown. During 'kiss,' lipids from LD must be liberated into lysosomal lumen. For LD and lysosome to 'run,' the two organelles must be separated quickly. Technically, hydrophobic lipids within LD cannot be released into the lysosomal lumen that is aqueous. Therefore, lipids released from LD must be encased by phospholipid monolayer: Hydrophilic head groups face aqueous lumen whereas hydrophobic tails face LD lipids. After this lipid particle surrounded by phospholipid monolayer is released into the lysosomal lumen, lipases, and different enzymes can metabolize phospholipids and enclosed lipid content. Therefore, during a brief encounter, LD must be budded off and released quickly into lysosomal lumen. The region of membrane tubulation may be a site where endophilin B1 functions (Fig. 5-2C) because endophilin B1 bends and tubulates membranes, and it can cause fission of vesicle by working with dynamin (Sundborger et al., 2011). Membrane budding and sampling of LD content must occur for the Kiss-and-run, and this explains why the presence of endophilin B1 is obligatory (Fig. 4-12, 4-13, 4-18). In order to test the hypothesis for endophilin B1's membrane

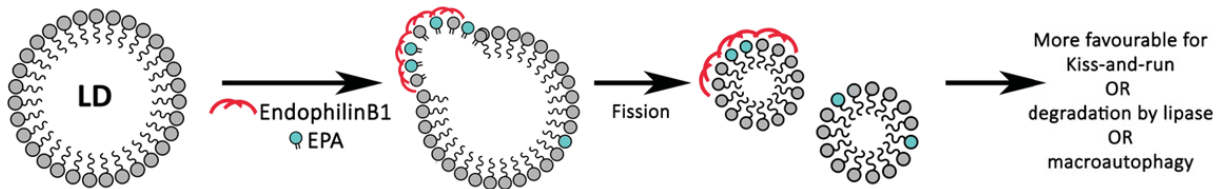
tubulation in EPA mediated Kiss-and-run, it would be best to utilize electron microscopy and capture the budding event where endophilin B1 is around the bud.

Similarly, how the two organelles are brought together for the Kiss-and-run lipophagy has not been elucidated fully. Yet, some proteins that govern the movement of lysosome and LD may be involved. For example, BORC complex, a multi-subunit complex involved in lysosomal positioning, recruits a small GTPase, Arl8b to the lysosome and is held in place (Pu et al., 2015). Subsequently, BORC couples lysosome to kinesin motor, so it becomes plus-end microtubule-directed (Pu et al., 2015). Later, SKIP and kinesin are recruited to this site, and they ultimately move lysosome towards LD (Pu et al., 2015), and this is probably where RAB7-positive domains within LD makes contact with lysosomes. Endophilin B1 may be interacting with these components, as indicated by Bio-ID experiment (Fig. 4-22).

### A. Endophilin B1 in macroautophagy



### B. Endophilin B1 in LD Fission



### C. Endophilin B1 in Kiss-and-run

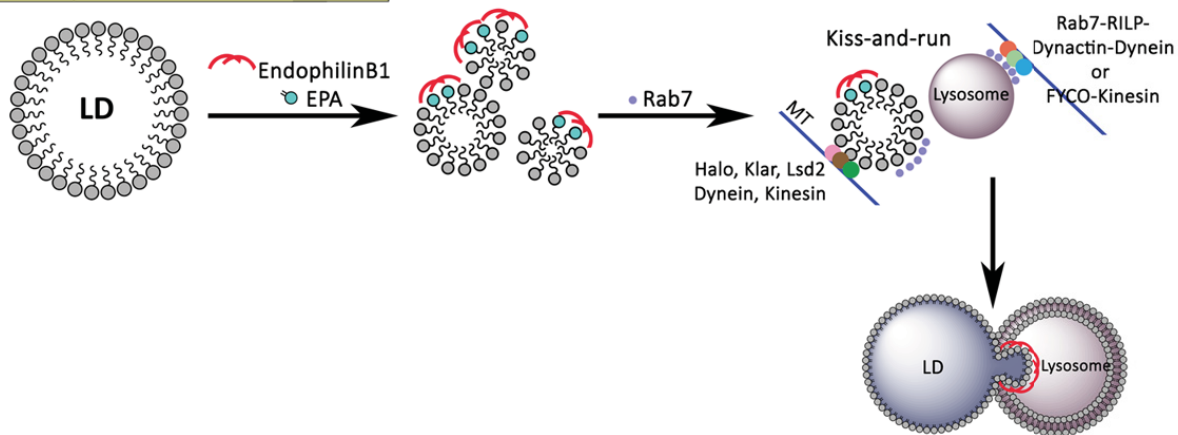


**Figure 5-2:** Possible mechanisms of endophilin B1

**A.** Endophilin B1's role in macroautophagy. Atg9 is endocytosed by AP2. This Atg9-positive endosome is trafficked to Golgi by a mechanism dependent on retromer, TBC1D5, and endophilinB1 (because KD of endophilin B1 or AP2 retains Atg9 to plasma membrane). Then, endophilin B1 tubulates Atg9-positive Golgi membrane to make autophagosome. This mechanism requires AP2 since AP2 KD keeps Atg9 to TGN. Endophilin B1's interaction with AP2, Atg9, retromer, and TBC1D5 supports this hypothesis.

**B.** Endophilin B1 in LD fission. Endophilin B1 causes fission of LD, and this may be facilitated by insertion of EPA-containing TAG into LD monolayer. It is plausible that endophilin B1 directly binds to EPA-containing TAG. Now smaller LDs may be favourable for Kiss-and-run, lipolysis, or macroautophagy.

**C.** Endophilin B1 in Kiss-and-run. Smaller LDs generated by endophilin B1 may undergo Kiss-and-run when Rab7 is recruited. LD and lysosome may be brought together through actions of Halo, Klar, Lsd2, dynein, and kinesin (for LD), and Rab7-RILP-dynactin-dynein or FYCO-kinesin (for lysosome). When the two organelles are brought together, endophilin B1 may cause

tubulation of LD to aid in the sampling of LD contents into lysosomal lumen.

### **Potential interactors of endophilin B1**

Bio-ID provides a high-throughput screening of physiologically relevant protein interactions, and it is based on BirA, a promiscuous biotin ligase that biotinylates proximal proteins (Roux et al., 2013). Biotinylated proteins are subsequently isolated by biotin-affinity purification, and they are identified by mass spectrometry. Weak or transient interactions can be detected, and therefore it provides a list of candidate interactors for the protein of interest (Roux et al., 2013). From Endophilin B1's Bio-ID experiment (Fig. 4-22), a number of known and novel interactors has been identified. Endophilin family of proteins are known to be involved in clathrin-dependent endocytosis, clathrin-independent endocytosis (FEME), maintenance of mitochondrial membranes, and macroautophagy. Therefore, it was not surprising to detect clathrin complex subunits, mitochondrial membrane proteins, and Atg9. However, several protein complexes detected were unanticipated: Retromer subunits, PIK3C2 $\beta$ , BLOC/BORC complex subunits, and exosome-related proteins.

Retromer is a protein complex that functions in retrograde transport of transmembrane proteins from endosomes to the *trans*-Golgi network (TGN). It is also shown to mediate endosome-to-PM transport for protein recycling. Retromer complex is comprised of SNXs (sorting nexins), and Vps trimer (Vps26, Vps29, Vps35). SNX1/2 makes one component of the SNX subcomplex, and SNX5/6 is a candidate for the other (Hong et al., 2009). In particular, SNX1/2 interacts with membranes that contain PtdIns3P or PtdIns(3,5)P<sub>2</sub> (Cozier et al., 2002), and it is a component of SNX-BAR sub-complex that causes membrane deformation. From endophilin B1's Bio-ID experiment, SNX 1, 2, 5, 6, Vps26 and Vps29 were detected. TBC1D5, a

two-LIRs (LC3 Interacting Region) containing protein, was also detected. TBC1D5 binds to Vps29 through one of its two LIRs, and this binding can be titrated out by the addition of LC3 (Popovic et al., 2012). Therefore, TBC1D5 may be a molecular switch between endosome and autophagosome (Goold et al., 2013). In addition, retromer complex is shown to be required for autophagy because knockdown of retromer subunits lowered autophagic activity (Dengjel et al., 2012). Also, TBC1D5 and AP2 complex play important regulatory roles to translocate Atg9 containing vesicles towards sites of autophagosome formation (Popovic et al., 2012). In plasma membrane, Atg9, an essential protein for autophagosome formation (Webber et al., 2007), goes into AP2-positive clathrin-coated pits (and endophilin B1 may be found here) (Popovic and Dikic, 2014). Then, the endocytosed Atg9-positive endosome traffics to Golgi apparatus through a process, which is dependent on TBC1D5 and retromer (Popovic and Dikic, 2014). This trafficking of Atg9 to TGN requires endophilin B1 since KD of endophilin B1 abolishes it (Takahashi et al., 2011). Then, endophilin B1 is also necessary for tubulation of Atg9-positive TGN to form autophagosome because endoB1 KD eliminates this process (Takahashi et al., 2011; He et al., 2013). As well, AP2 must be involved in this trafficking because AP2 KD during autophagy induction retains Atg9 in TGN (Popovic and Dikic, 2014). AP2 subunits were identified in endophilin B1's Bio-ID. In addition, TBC1D5 KD results in mislocalization of Atg9 into late endosome during autophagy induction (Popovic and Dikic, 2014). PI3KC2b produces PI3P, to which retromer subunits (SNX1/2) have an affinity, so its interaction with endophilin B1 confirms the involvement of retromer-TBC1D5 in this process. Also, it is plausible that endophilin B1 firstly binds to PIK3C2 $\beta$ , and it links retromer and autophagic machinery through Atg9 by cooperating with TBC1D5. Endophilin B1's mechanism in macroautophagy is summarized in Fig. 5-2 A.

In endophilin B1's Bio-ID, members of BLOC complex, subunits of dynein motor, and LAMTOR 1/2 were detected, and the detection level was higher in cells treated with EPA. BLOC complex is required for biogenesis of lysosome-related organelles, and its function has been suggested in the cargo-specific trafficking from endosomes to melanocytes, the lysosome-related organelles (Setty et al., 2007). Setty and colleagues proposed that BLOC-1, a subunit of BLOC complex, interacts with syntaxin 13 and SNAP23/25, and this will lead to fusion of lysosome-related organelles (Setty et al., 2007). BLOC complex is comprised of 8 subunits including BLOC-1S, BLOC-2S, snapin, BLOC-3, cappuccino, muted, dysbindin, and pallidin (Pu et al., 2015). The first three members are also components of BORC (BLOC-one-related complex) which is a multi-subunit complex that regulates lysosomal positioning (Pu et al., 2015). It has been shown that BORC recruits Arl8b to lysosomal membrane and couples it to SKIP-kinesin-1 complex, which will drive movement of lysosome towards the cell periphery (Pu et al., 2015). Dynein facilitates translocation of late endosomes, lysosomes and autophagosomes towards perinuclear region together with dynactin,  $\beta$ III spectrin, and RILP-Rab7-ORP1L (Johansson et al., 2007; Pu et al., 2015). In particular, Rab7 has been shown as a key regulator of LD-lysosome interactions (Schroeder et al., 2015). LAMTOR is a multimeric complex that regulates activation of mTORC1 kinase at the lysosomal membrane (Bar-Peled et al., 2012; Efeyan et al., 2012). Inactivation of mTOR leads to deinhibition of ULK1, and this directly stimulates autophagosome formation (Velikkakath et al., 2012). The mTOR inhibition also causes nuclear translocation of TFEB, which subsequently enhances lysosomal activity (Efeyan et al., 2012).

Identification of BLOC/BORC complex, dynein subunits, and LAMTOR supports that endophilin B1 and EPA must be involved in the lysosomal movement. As well, endophilin B1 is

essential for LD-LAMP1 association in the presence of EPA (Fig. 4-18), and endophilin B1 is in the same compartment as Rab7, the central mediator of Kiss-and-run lipophagy (Fig. 4-20). Also, endophilin B1 and EPA, not endophilin B1 alone, increases the number of Kiss-and-run (Fig. 4-21). Collectively, these observations support that endophilin B1 plays a critical role in Kiss-and-run lipophagy, perhaps by directly priming LD (Fig. 5-2 B) or by balancing macroautophagy and Kiss-and-run (Fig. 5-2 A, C). Endophilin B1's Bio-ID experiment did not identify CGI-58 or perilipin1, so regulation of lipophagy by endophilin B1 does not work through manipulating perilipin 1 (protective coat of LD). In support of this, endophilin B1 co-localizes partially with perilipin1 on a fatty liver tissue (Fig. 4-1d).

Identification of exosome-related proteins in endophilin B1's Bio-ID experiment confirms its involvement in exosome formation. Exosome formation requires inward budding of multivesicular body (MVB) membrane, and this process is regulated by syndecan-SDCBP-PDCD6IP (Baietti et al., 2012). MVBs with intraluminal vesicles (ILVs) formed in this way travel to the cell membrane and open up to release ILVs as exosomes, which are then pinocytosed (or phagocytosed) by target cells (Feng et al., 2010; Raposo and Stoorvogel, 2013). Bio-ID results, which identified SDCBP and PDCD6IP as endophilin B1's potential partner, are assured since binding of endophilin A to PDCD6IP was already shown in the literature (Baietti et al., 2012; Mercier et al., 2016). However, endophilin B1 mediated lipophagy did not yield significant TAG secretion (Fig. 4-5, 4-9), and this observation suggests that endophilin B1 is not involved in lipid exocytosis. Endophilin B1 might be specifically involved in miRNA exocytosis, as it was proposed to interact with HNRNPA2B1 (Fig. 4-22c). HNRNPA2B1 is a nuclear ribonucleoprotein involved in sorting of miRNA into exosome (Villarroya-Beltri et al., 2013). After sumoylated, it binds to EXOmotif and enters the ILV (Villarroya-Beltri et al., 2013). Given

endophilin B1's function in other systems, it may contribute to exosome assembly through introducing curvature to membranes.

Bio-ID results confirm endophilin B1's previously known interactors and pathways. In addition, it identifies candidate proteins that endophilin B1 may interact with, and it opens doors to novel pathways for endophilin B1. Since endophilin B1 may be involved in many different processes, results obtained from Bio-ID experiment must be analyzed carefully, and hypothesis must be formulated based on comprehensive understanding of multiple cellular processes. Subsequently, candidate interactors of endophilin B1 must be confirmed by various other methods such as co-immunoprecipitation.

In summary, endophilin B1 is involved in different stages of lipophagy: 1) macroautophagy by mediating transport of Atg9 via retromer complex to Golgi, and then forming autophagosome by utilizing Golgi membranes with Atg9; 2) fission of LD in the presence or absence of EPA. In short hours of EPA treatment (4-8hours), EPA introduces perturbation of LD membrane, and endophilin B1 directly binds to LD and causes fission. 3) Finally, endophilin B1 may directly cause deformation of LD at lysosomal contact site, which is crucial for the sampling of LD content.

## **Chapter 6: General conclusions**

In this thesis, we developed tools to understand how Golgi maintains its homeostasis and elucidated functions of novel lipid droplet protein in a specialized lipid droplet turnover.

A prediction of the CPM is that, via COPI vesicles, Golgi resident enzymes retrograde to earlier cisternae as matured cisternae are pushed forward. Therefore, visualization of Golgi resident enzymes in and around COPI vesicles holds the key to the long debated topic of intra-Golgi transport. So far, previous fluorescence, immuno-EM, and correlative imaging provided limited structural details during observation of small vesicular structures. At the same time, localization of native enzymes has not been analyzed at their undisturbed stoichiometric ratio. The *in vivo* correlative photo-oxidation microscopy integrates specificity of fusion antibodies against native enzymes and capacity to reveal detailed spatial information from the photo-oxidative product. I believe this *in vivo* photo-oxidation microscopy and the new generation of an antibody-based probe will reveal the ultrastructural location of the Golgi enzymes and provide fundamental information required to establish the mechanism of intra-Golgi transport firmly.

We provide new insights into the lipophagic pathway that involves close interactions between lysosomes and LDs. Endophilin B1 appears to be a fundamental component in this Kiss-and-run lipophagy that is facilitated by omega-3 fatty acid, EPA. Endophilin B1 is indispensable for Kiss-and-run, and it may serve as the last tool for lipophagy when macroautophagy and lipolysis machinery are defective. Lipophagic effect of endophilin B1 highlighted in this thesis may also provide answers for facilitating lipid breakdown in metabolic diseases such as Non-Alcoholic Fatty Liver Disease. There is no known treatment or preventative measure whose efficacy does not depend on dietary or fitness interventions. Therefore, speeding up lipid liberation by non-invasive yet effective methods involving

endophilin B1 will not only prevent the disease progression but also result in higher efficacy than existing methods.

## **Chapter 7: References**

- Altenburg, J.D., and R. a Siddiqui. 2009. Omega-3 polyunsaturated fatty acids down-modulate CXCR4 expression and function in MDA-MB-231 breast cancer cells. *Mol. Cancer Res.* 7:1013–20.
- Antonny, B., S. Beraud-Dufour, P. Chardin, and M. Chabre. 1997. N-terminal hydrophobic residues of the G-protein ADP-ribosylation factor-1 insert into membrane phospholipids upon GDP to GTP exchange. *Biochemistry.* 36:4675–4684.
- Appenzeller-Herzog, C., and H.-P. Hauri. 2006. The ER-Golgi intermediate compartment (ERGIC): in search of its identity and function. *J. Cell Sci.* 119:2173–83.
- Appenzeller, C., H. Andersson, F. Kappeler, and H.-P. Hauri. 1999. The lectin ERGIC-53 is a cargo transport receptor for glycoproteins. *Nat. Cell Biol. Biol.* 1:330–334.
- Asp, L., F. Kartberg, J. Fernandez-rodriguez, M. Smedh, M. Elsnér, F. Laporte, K.A. Jansen, J.A. Valentijn, A.J. Koster, J.J.M. Bergeron, and T. Nilsson. 2009. Early Stages of Golgi Vesicle and Tubule Formation Require Diacylglycerol. 20:780–790.
- Asp, L., and T. Nilsson. 2008. Golgi gets wired up. *Nat. Cell Biol.* 10:885–887.
- Baffy, G., E.M. Brunt, and S.H. Caldwell. 2012. Hepatocellular carcinoma in non-alcoholic fatty liver disease: An emerging menace. *J. Hepatol.* 56:1384–1391.
- Baietti, M.F., Z. Zhang, E. Mortier, A. Melchior, G. Degeest, A. Geeraerts, Y. Ivarsson, F. Depoortere, C. Coomans, E. Vermeiren, P. Zimmermann, and G. David. 2012. Syndecan–syntenin–ALIX regulates the biogenesis of exosomes. *Nat. Cell Biol.* 14:677–685.
- Bąkowska-Zywicka, K., and A. Tyczewska. 2009. Ribophagy - The novel degradation system of the ribosome. *Biotechnologia.* 99–103.
- Balch, W.E., W.G. Dunphy, W.A. Braell, and J.E. Rothman. 1984. Reconstitution of the transport of protein between successive compartments of the golgi measured by the coupled incorporation of N-acetylglucosamine. *Cell.* 39:405–416.
- Bandyopadhyay, U., S. Kaushik, L. Varticovski, and A.M. Cuervo. 2008. The chaperone-mediated autophagy receptor organizes in dynamic protein complexes at the lysosomal

membrane. *Mol. Cell. Biol.* 28:5747–5763.

Bar-Peled, L., L.D. Schweitzer, R. Zoncu, and D.M. Sabatini. 2012. Ragulator is a GEF for the rag GTPases that signal amino acid levels to mTORC1. *Cell.* 150:1196–1208.

Barlowe, C. 2003. Signals for COPII-dependent export from the ER: what's the ticket out? *Trends Cell Biol.* 13:295–300.

Barlowe, C., L. Orci, T. Yeung, M. Hosobuchi, S. Hamamoto, N. Salama, M.F. Rexach, M. Ravazzola, M. Amherdt, and R. Schekman. 1994. COPII: A membrane coat formed by sec proteins that drive vesicle budding from the endoplasmic reticulum. *Cell.* 77:895–907.

Beck, R., S. Prinz, P. Diestelkötter-Bachert, S. Röhling, F. Adolf, K. Hoehner, S. Welsch, P. Ronchi, B. Brügger, J.A.G. Briggs, and F. Wieland. 2011. Coatamer and dimeric ADP ribosylation factor 1 promote distinct steps in membrane scission. *J. Cell Biol.* 194:765–77.

Beller, M., C. Sztalryd, N. Southall, B. M, H. Jackle, D. Auld, and B. Oliver. 2008. COPI Complex Is a Regulator of Lipid Homeostasis. *PLoS Biol.* 6:2530–2549.

Ben-Tekaya, H., K. Miura, R. Pepperkok, and H.-P. Hauri. 2005. Live imaging of bidirectional traffic from the ERGIC. *J. Cell Sci.* 118:357–367.

Bentley, M., H. Decker, J. Luisi, and G. Banker. 2015. A novel assay reveals preferential binding between Rabs, kinesins, and specific endosomal subpopulations. *J. Cell Biol.* 208:273–81.

Berger, E.C., K. Crimm, T. Bachi, H. Bosshart, R. Kleene, and M. Watzel. 1993. Double Immunofluorescent Staining of d , 6 Monensin-Treated Cells : Evidence for Different Colgi Compartments ? *J. Cell. Biochem.* 52:275–288.

Bermak, J.C., M. Li, C. Bullock, P. Weingarten, and Q.-Y. Zhou. 2002. Interaction of gamma-COP with a transport motif in the D1 receptor C-terminus. *Eur. J. Cell Biol.* 81:77–85.

Béthune, J., M. Kol, J. Hoffmann, I. Reckmann, B. Brügger, and F. Wieland. 2006. Coatamer, the coat protein of COPI transport vesicles, discriminates endoplasmic reticulum residents from p24 proteins. *Mol. Cell. Biol.* 26:8011–21.

Bickford, L.C., E. Mossessova, and J. Goldberg. 2004. A structural view of the COPII vesicle

coat. *Curr. Opin. Struct. Biol.* 14:147–153.

Bigay, J., J.-F. Casella, G. Drin, B. Mesmin, and B. Antonny. 2005. ArfGAP1 responds to membrane curvature through the folding of a lipid packing sensor motif. *EMBO J.* 24:2244–53.

Bonfanti, L., A.A. Mironov, J.A. Martínez-Menárguez, O. Martella, A. Fusella, M. Baldassarre, R. Buccione, H.J. Geuze, A.A. Mironov, and A. Luini. 1998. Procollagen traverses the Golgi stack without leaving the lumen of cisternae: Evidence for cisternal maturation. *Cell.* 95:993–1003.

Boström, P., L. Andersson, M. Rutberg, J. Perman, U. Lidberg, B.R. Johansson, J. Fernandez-Rodriguez, J. Ericson, T. Nilsson, J. Borén, and S.-O. Olofsson. 2007. SNARE proteins mediate fusion between cytosolic lipid droplets and are implicated in insulin sensitivity. *Nat. Cell Biol.* 9:1286–1293.

Boström, P., M. Rutberg, J. Ericsson, P. Holmdahl, L. Andersson, M.A. Frohman, J. Borén, and S.O. Olofsson. 2005. Cytosolic lipid droplets increase in size by microtubule-dependent complex formation. *Arterioscler. Thromb. Vasc. Biol.* 25:1945–1951.

Boucrot, E., A.P. a Ferreira, L. Almeida-souza, S. Debard, Y. Vallis, G. Howard, L. Bertot, N. Sauvonnet, and H.T. McMahon. 2014. Endophilin marks and controls a clathrin-independent endocytic pathway. *Nature.* 517:460–465.

Braun, M., A. Waheed, and K. von Figura. 1989. Lysosomal acid phosphatase is transported to lysosomes via the cell surface. *EMBO J.* 8:3633–3640.

Bremser, M., W. Nickel, M. Schweikert, M. Ravazzola, M. Amherdt, C.A. Hughes, T.H. Söllner, J.E. Rothman, and F.T. Wieland. 1999. Coupling of Coat Assembly and Vesicle Budding to Packaging of Putative Cargo Receptors. *Cell.* 96:495–506.

Chen, Y., C. Xu, T. Yan, C. Yu, and Y. Li. 2015. Omega 3 Fatty Acids Reverse Lipotoxicity through Induction of Autophagy in Non-alcoholic Fatty Liver Disease. *Nutrition.*

Cosson, P., M. Amherdt, J.E. Rothman, and L. Orci. 2002. A resident Golgi protein is excluded from peri-Golgi vesicles in NRK cells. *Proc. Natl. Acad. Sci. U. S. A.* 99:12831–4.

- Cosson, P., Y. Lefkir, C. Démollière, and F. Letourneur. 1998. New COP1-binding motifs involved in ER retrieval. *EMBO J.* 17:6863–6870.
- Cosson, P., and F. Letourneur. 1994. Coatamer interaction with di-lysine endoplasmic reticulum retention motifs. *Science.* 263:1629–1631.
- Cozier, G.E., J. Carlton, A.H. McGregor, P.A. Gleeson, R.D. Teasdale, H. Mellor, and P.J. Cullen. 2002. The phox homology (PX) domain-dependent, 3-phosphoinositide-mediated association of sorting nexin-1 with an early sorting endosomal compartment is required for its ability to regulate epidermal growth factor receptor degradation. *J. Biol. Chem.* 277:48730–6.
- Cuervo, a M., and J.F. Dice. 1996. A receptor for the selective uptake and degradation of proteins by lysosomes. *Science.* 273:501–503.
- Cui, H., G.S. Ayton, and G. a. Voth. 2009. Membrane binding by the endophilin N-BAR domain. *Biophys. J.* 97:2746–2753.
- Dahan, S., J.P. Ahluwalia, L. Wong, B.I. Posner, and J.J.M. Bergeron. 1994. Concentration of intracellular hepatic apolipoprotein E in Golgi apparatus saccular distensions and endosomes. *J. Cell Biol.* 127:1859–1869.
- Dalen, K.T., K. Schoonjans, S.M. Ulven, M.S. Weedon-Fekjaer, T.G. Bentzen, H. Koutnikova, J. Auwerx, and H.I. Nebb. 2004. Adipose Tissue Expression of the Lipid Droplet Associating Proteins S3-12 and Perilipin Is Controlled by Peroxisome Proliferator-Activated Receptor gamma. *Diabetes.* 53:1243–1252.
- Dengjel, J., M. Høyer-Hansen, M.M.O.M. Nielsen, T. Eisenberg, L.M. Harder, S. Schandorff, T. Farkas, T. Kirkegaard, A.C. Becker, S. Schroeder, K. Vanselow, E. Lundberg, M.M.O.M. Nielsen, A.R. Kristensen, V. Akimov, J. Bunkenborg, F. Madeo, M. Jäätelä, J.S. Andersen, M. Hoyer-Hansen, M.M.O.M. Nielsen, T. Eisenberg, L.M. Harder, S. Schandorff, T. Farkas, T. Kirkegaard, A.C. Becker, S. Schroeder, K. Vanselow, E. Lundberg, M.M.O.M. Nielsen, A.R. Kristensen, V. Akimov, J. Bunkenborg, F. Madeo, M. Jaattela, and J.S. Andersen. 2012. Identification of Autophagosome-associated Proteins and Regulators by Quantitative Proteomic Analysis and Genetic Screens. *Mol. Cell. Proteomics.* 11:M111.014035-M111.014035.

- Diao, J., R. Liu, Y. Rong, M. Zhao, J. Zhang, Y. Lai, Q. Zhou, L.M. Wilz, J. Li, S. Vivona, R.A. Pfuetzner, A.T. Brunger, and Q. Zhong. 2015. ATG14 promotes membrane tethering and fusion of autophagosomes to endolysosomes. *Nature*. 520:563–566.
- Ding, J., V.A. Segarra, S. Chen, H. Cai, S.K. Lemmon, and S. Ferro-Novick. 2015. Auxilin facilitates membrane traffic in the early secretory pathway. *Mol. Biol. Cell*. 27:1–36.
- Dominguez, M., K. Dejgaard, J. Füllekrug, S. Dahan, A. Fazel, J.P. Paccaud, D.Y. Thomas, J.J.M. Bergeron, and T. Nilsson. 1998. gp25L/emp24/p24 protein family members of the cis-Golgi network bind both COP I and II coatomer. *J. Cell Biol.* 140:751–765.
- Dowman, J.K., J.W. Tomlinson, and P.N. Newsome. 2010. Pathogenesis of non-alcoholic fatty liver disease. *QJM*. 103:71–83.
- Dupont, N., S. Chauhan, J. Arko-Mensah, E.F. Castillo, A. Masedunskas, R. Weigert, H. Robenek, T. Proikas-Cezanne, and V. Deretic. 2014. Neutral lipid stores and lipase PNPLA5 contribute to autophagosome biogenesis. *Curr. Biol*. 24:609–620.
- Efeyan, A., R. Zoncu, and D.M. Sabatini. 2012. Amino acids and mTORC1: from lysosomes to disease. *Trends Mol. Med*.
- Emr, S., B.S. Glick, A.D. Linstedt, J. Lippincott-Schwartz, A. Luini, V. Malhotra, B.J. Marsh, A. Nakano, S.R. Pfeffer, C. Rabouille, J.E. Rothman, G. Warren, F.T.W. 2009. Journeys through the Golgi—taking stock in a new era. *J. Cell Biol.* 187:449–453.
- Eugster, A., G. Frigerio, M. Dale, and R. Duden. 2004. The alpha- and beta'-COP WD40 domains mediate cargo-selective interactions with distinct di-lysine motifs. *Mol. Biol. Cell*. 15:1011–1023.
- Evan, G.I., G.K. Lewis, G. Ramsay, and J.M. Bishop. 1985. Isolation of monoclonal antibodies specific for human c-myc proto-oncogene product. *Mol. Cell. Biol.* 5:3610–3616.
- Fan, R., Y. Miao, X. Shan, H. Qian, C. Song, G. Wu, Y. Chen, and W. Zha. 2012. Bif-1 is overexpressed in hepatocellular carcinoma and correlates with shortened patient survival. *Oncol. Lett.* 3:851–854.

- Farsad, K., N. Ringstad, K. Takei, S.R. Floyd, K. Rose, and P. De Camilli. 2001. Generation of high curvature membranes mediated by direct endophilin bilayer interactions. *J. Cell Biol.* 155:193–200.
- Fei, W., H. Wang, X. Fu, C. Bielby, and H. Yang. 2009. Conditions of endoplasmic reticulum stress stimulate lipid droplet formation in *Saccharomyces cerevisiae*. *Biochem. J.* 424:61–7.
- Feng, D., W.L. Zhao, Y.Y. Ye, X.C. Bai, R.Q. Liu, L.F. Chang, Q. Zhou, and S.F. Sui. 2010. Cellular internalization of exosomes occurs through phagocytosis. *Traffic.* 11:675–687.
- Fernández-Alvarez, A., M.S. Alvarez, R. Gonzalez, C. Cucarella, J. Muntané, and M. Casado. 2011. Human SREBP1c expression in liver is directly regulated by peroxisome proliferator-activated receptor alpha (PPARalpha). *J. Biol. Chem.* 286:21466–77.
- Fleischer, B., S. Fleischer, and H. Ozawa. 1969. Isolation and characterization of Golgi membranes from bovine liver. *J. Cell Biol.* 43:59–79.
- Fossati, M., S.F. Colombo, and N. Borgese. 2014. A positive signal prevents secretory membrane cargo from recycling between the Golgi and the ER. *EMBO J.* 33:1–18.
- Fujioka, Y., N.N. Noda, H. Nakatogawa, Y. Ohsumi, and F. Inagaki. 2010. Dimeric coiled-coil structure of *saccharomyces cerevisiae* Atg16 and its functional significance in autophagy. *J. Biol. Chem.* 285:1508–1515.
- Fujiwara, T., K. Oda, S. Yokotas, A. Takatsukig, and Y. Ikeharan. 1988. Brefeldin A Causes Disassembly of the Golgi Complex and Accumulation of Secretory Proteins in the Endoplasmic Reticulum. 263:18545–18552.
- Futai, E., S. Hamamoto, L. Orci, and R. Schekman. 2004. GTP/GDP exchange by Sec12p enables COPII vesicle bud formation on synthetic liposomes. *EMBO J.* 23:4286–4296.
- Gad, H., P. Löw, E. Zotova, L. Brodin, and O. Shupliakov. 1998. Dissociation between Ca<sup>2+</sup>-triggered synaptic vesicle exocytosis and clathrin-mediated endocytosis at a central synapse. *Neuron.* 21:607–616.
- Gad, H., N. Ringstad, P. Löw, O. Kjaerulff, J. Gustafsson, M. Wenk, G. Di Paolo, Y. Nemoto, J.

Crun, M.H. Ellisman, P. De Camilli, O. Shupliakov, and L. Brodin. 2000. Fission and uncoating of synaptic clathrin-coated vesicles are perturbed by disruption of interactions with the SH3 domain of endophilin. *Neuron*. 27:301–312.

Gallop, J.L., P.J. Butler, and H.T. McMahon. 2005. Endophilin and CtBP/BARS are not acyl transferases in endocytosis or Golgi fission. *Nature*. 438:675–678.

Gallop, J.L., C.C. Jao, H.M. Kent, P.J.G. Butler, P.R. Evans, R. Langen, and H.T. McMahon. 2006. Mechanism of endophilin N-BAR domain-mediated membrane curvature. *EMBO J*. 25:2898–2910.

Gandotra, S., K. Lim, A. Girousse, V. Saudek, S. O’Rahilly, and D.B. Savage. 2011. Human frame shift mutations affecting the carboxyl terminus of perilipin increase lipolysis by failing to sequester the adipose triglyceride lipase (ATGL) coactivator AB-hydrolase-containing 5 (ABHD5). *J. Biol. Chem*. 286:34998–5006.

Gannon, J., J.J.M. Bergeron, and T. Nilsson. 2011. Golgi and related vesicle proteomics: Simplify to identify. *Cold Spring Harb. Perspect. Biol*. 3.

Gannon, J., J. Fernandez-Rodriguez, H. Alamri, S.B. Feng, F. Kalantari, S. Negi, A.H.Y. Wong, A. Mazur, L. Asp, A. Fazel, A. Salman, A. Lazaris, P. Metrakos, J.J.M. Bergeron, and T. Nilsson. 2014. ARFGAP1 is dynamically associated with lipid droplets in hepatocytes. *PLoS One*. 9:1–12.

Gao, J., and G. Serrero. 1999. Adipose differentiation related protein (ADRP) expressed in transfected COS-7 cells selectively stimulates long chain fatty acid uptake. *J. Biol. Chem*. 274:16825–16830.

Gao, J., H. Ye, and G. Serrero. 2000. Stimulation of adipose differentiation related protein (ADRP) expression in adipocyte precursors by long-chain fatty acids. *J. Cell. Physiol*. 182:297–302.

Giachino, C., E. Lantelme, L. Lanzetti, S. Saccone, G. Bella Valle, and N. Migone. 1997. A novel SH3-containing human gene family preferentially expressed in the central nervous system. *Genomics*. 41:427–434.

Gilchrist, A., C.E. Au, J. Hiding, A.W. Bell, J. Fernandez-Rodriguez, S. Lesimple, H. Nagaya, L.

- Roy, S.J.C. Gosline, M. Hallett, J. Paiement, R.E. Kearney, T. Nilsson, and J.J.M. Bergeron. 2006a. Quantitative proteomics analysis of the secretory pathway (Supplemental Data). *Cell*. 127:1265–81.
- Gilchrist, A., C.E. Au, J. Hiding, A.W. Bell, J. Fernandez-Rodriguez, S. Lesimple, H. Nagaya, L. Roy, S.J.C. Gosline, M. Hallett, J. Paiement, R.E. Kearney, T. Nilsson, and J.J.M. Bergeron. 2006b. Quantitative proteomics analysis of the secretory pathway. *Cell*. 127:1265–81.
- Girod, a, B. Storrie, J.C. Simpson, L. Johannes, B. Goud, L.M. Roberts, J.M. Lord, T. Nilsson, and R. Pepperkok. 1999. Evidence for a COP-I-independent transport route from the Golgi complex to the endoplasmic reticulum. *Nat. Cell Biol.* 1:423–430.
- Goedhart, J., L. van Weeren, M.A. Hink, N.O.E. Vischer, K. Jalink, and T.W.J. Gadella. 2010. Bright cyan fluorescent protein variants identified by fluorescence lifetime screening. *Nat. Methods*. 7:137–9.
- Goold, R., C. McKinnon, S. Rabbanian, J. Collinge, G. Schiavo, and S.J. Tabrizi. 2013. Alternative fates of newly formed PrPSc upon prion conversion on the plasma membrane. *J. Cell Sci.* 126:3552–62.
- Grabenbauer, M., W.J.C. Geerts, J. Fernandez-Rodriguez, A. Hoenger, A.J. Koster, and T. Nilsson. 2005. Correlative microscopy and electron tomography of GFP through photooxidation. *Nat. Methods*. 2:857–862.
- Granneman, J.G., H.P.H. Moore, E.P. Mottillo, Z. Zhu, and L. Zhou. 2011. Interactions of Perilipin-5 (Plin5) with adipose triglyceride lipase. *J. Biol. Chem.* 286:5126–5135.
- Grasse, P.P. 1957. [Ultrastructure, polarity and reproduction of Golgi apparatus.]. *C R Hebd Seances Acad Sci.* 245:1278–1281.
- Griffiths, G. 2000. Gut thoughts on the Golgi complex. *Traffic*. 1:738–45.
- Guo, Y., K.R. Cordes, R. V Farese, and T.C. Walther. 2009. Lipid droplets at a glance. *J. Cell Sci.* 122:749–52.
- Guo, Y., T.C. Walther, M. Rao, N. Stuurman, G. Goshima, K. Terayama, J.S. Wong, R.D. Vale,

- P. Walter, and R. V Farese. 2008. Functional genomic screen reveals genes involved in lipid droplet formation and utilization. *Nature*. 453:657–661.
- Ha, K.D., B.A. Clarke, and W.J. Brown. 2012. Regulation of the Golgi complex by phospholipid remodeling enzymes. *Biochim. Biophys. Acta - Mol. Cell Biol. Lipids*. 1821:1078–1088.
- Hanada, T., N.N. Noda, Y. Satomi, Y. Ichimura, Y. Fujioka, T. Takao, F. Inagaki, and Y. Ohsumi. 2007. The Atg12-Atg5 Conjugate Has a Novel E3-like Activity for Protein Lipidation in Autophagy. *J. Biol. Chem*. 282:37298–37302.
- Hapala, I., E. Marza, and T. Ferreira. 2011. Is fat so bad? Modulation of endoplasmic reticulum stress by lipid droplet formation. *Biol. Cell*. 103:271–285.
- Hathaway, H.J., S.C. Evans, D.H. Dubois, C.I. Foote, B.H. Elder, and B.D. Shur. 2003. Mutational analysis of the cytoplasmic domain of beta1,4-galactosyltransferase I: influence of phosphorylation on cell surface expression. *J. Cell Sci*. 116:4319–30.
- Hauke, V. 2015. On the endocytosis rollercoaster. *Nature*. 517:10–11.
- Hauri, H.P., F. Kappeler, H. Andersson, and C. Appenzeller. 2000. ERGIC-53 and traffic in the secretory pathway. *J. Cell Sci*. 113 ( Pt 4:587–596.
- Hauri, H.P., and a Schweizer. 1992. The endoplasmic reticulum-Golgi intermediate compartment. *Curr. Opin. Cell Biol*. 4:600–608.
- He, C., and D.J. Klionsky. 2009. Regulation mechanisms and signaling pathways of autophagy. *Annu. Rev. Genet*. 43:67–93.
- He, S., D. Ni, B. Ma, J.-H. Lee, T. Zhang, I. Ghosalli, S.D. Pirooz, Z. Zhao, N. Bharatham, B. Li, S. Oh, W.-H. Lee, Y. Takahashi, H.-G. Wang, A. Minassian, P. Feng, V. Deretic, R. Pepperkok, M. Tagaya, H.S. Yoon, and C. Liang. 2013. PtdIns(3)P-bound UVRAG coordinates Golgi-ER retrograde and Atg9 transport by differential interactions with the ER tether and the beclin 1 complex. *Nat. Cell Biol*.
- Helms, J.B., and J.E. Rothman. 1992. Inhibition by brefeldin A of a Golgi membrane enzyme that catalyses exchange of guanine nucleotide bound to ARF. *Nature*. 360:352–354.

- Hong, Z., Y. Yang, C. Zhang, Y. Niu, K. Li, X. Zhao, and J.-J. Liu. 2009. The retromer component SNX6 interacts with dynactin p150Glued and mediates endosome-to-TGN transport. *Cell Res.* 19:1334–1349.
- Hosseini, K., and T. Saeed. 2011. Non-alcoholic steatohepatitis: An update in pathophysiology, diagnosis and therapy. *Hepat. Mon.* 2011:74–85.
- Hsu, H.C., C.Y. Chen, C.H. Chiang, and M.F. Chen. 2014. Eicosapentaenoic acid attenuated oxidative stress-induced cardiomyoblast apoptosis by activating adaptive autophagy. *Eur. J. Nutr.* 53:541–547.
- Hsu, J.-W., L.-C. Chang, L.-T. Jang, C.-F. Huang, and F.-J.S. Lee. 2013. The N-terminus of Vps74p is essential for the retention of glycosyltransferases in the Golgi but not for the modulation of apical polarized growth in *Saccharomyces cerevisiae*. *PLoS One.* 8:e74715.
- Imamura, M., T. Inoguchi, S. Ikuyama, S. Taniguchi, K. Kobayashi, N. Nakashima, and H. Nawata. 2002. ADRP stimulates lipid accumulation and lipid droplet formation in murine fibroblasts. *Am. J. Physiol. Endocrinol. Metab.* 283:E775–E783.
- Jamieson, J.D., and G.E. Palade. 1968. Intracellular transport of secretory proteins in the pancreatic exocrine cell. IV. Metabolic requirements. *J. Cell Biol.* 39:589–603.
- Jenkins, B., H. Decker, M. Bentley, J. Luisi, and G. Banker. 2012. A novel split kinesin assay identifies motor proteins that interact with distinct vesicle populations. *J. Cell Biol.* 198:749–761.
- Jiang, P., T. Nishimura, Y. Sakamaki, E. Itakura, T. Hatta, T. Natsume, and N. Mizushima. 2014. The HOPS complex mediates autophagosome-lysosome fusion through interaction with syntaxin 17. *Mol. Biol. Cell.* 25:1327–37.
- Johansson, M., N. Rocha, W. Zwart, I. Jordens, L. Janssen, C. Kuijl, V.M. Olkkonen, and J. Neefjes. 2007. Activation of endosomal dynein motors by stepwise assembly of Rab7-RILP-p150Glued, ORP1L, and the receptor betaIII spectrin. *J. Cell Biol.* 176:459–71.
- Kaiser, C.A., and R. Schekman. 1990. Distinct sets of SEC genes govern transport vesicle formation and fusion early in the secretory pathway. *Cell.* 61:723–733.

- Kalantari, F., J.J.M. Bergeron, and T. Nilsson. 2010. Biogenesis of lipid droplets--how cells get fatter. *Mol. Membr. Biol.* 27:462–468.
- Kamp, F., D. Zakim, F. Zhang, N. Noy, and J. a Hamilton. 1995. Fatty acid flip-flop in phospholipid bilayers is extremely fast. *Biochemistry.* 34:11928–11937.
- Kampf, J.P., D. Cupp, and A.M. Kleinfeld. 2006. Different mechanisms of free fatty acid flip-flop and dissociation revealed by temperature and molecular species dependence of transport across lipid vesicles. *J. Biol. Chem.* 281:21566–21574.
- Kampf, J.P., and A.M. Kleinfeld. 2007. Is membrane transport of FFA mediated by lipid, protein, or both? An unknown protein mediates free fatty acid transport across the adipocyte plasma membrane. *Physiology (Bethesda).* 22:7–14.
- Kappeler, F., D.R.C. Klopfenstein, M. Foguet, J.-P. Paccard, and H.-P. Hauri. 1997. The Recycling of ERGIC-53 in the Early Secretory Pathway. *J. Biol. Chem.* 272:31801–31808.
- Karbowski, M., S.Y. Jeong, and R.J. Youle. 2004. Endophilin B1 is required for the maintenance of mitochondrial morphology. *J. Cell Biol.* 166:1027–1039.
- Kartberg, F., L. Asp, S.Y. Dejgaard, M. Smedh, J. Fernandez-Rodriguez, T. Nilsson, and J.F. Presley. 2010. ARFGAP2 and ARFGAP3 are essential for COPI coat assembly on the Golgi membrane of living cells. *J. Biol. Chem.* 285:36709–20.
- Kaushik, S., and A.M. Cuervo. 2008. Chaperone-mediated autophagy. *Methods Mol. Biol.* 445:227–244.
- Kawano, J., S. Ide, T. Oinuma, and T. Suganuma. 1994. A protein-specific monoclonal antibody to rat liver beta 1-->4 galactosyltransferase and its application to immunohistochemistry. *J. Histochem. Cytochem.* 42:363–369.
- Kershaw, E.E., J.K. Hamm, L.A.W. Verhagen, O. Peroni, M. Katic, and J.S. Flier. 2006. Adipose triglyceride lipase: Function, regulation by insulin, and comparison with adiponutrin. *Diabetes.* 55:148–157.
- Khaminets, A., T. Heinrich, M. Mari, A.K. Huebner, M. Akutsu, P. Grumati, L. Liebmann, S.

- Nietzsche, I. Katona, J. Weis, F. Reggiori, I. Kurth, and C.A. Hübner. 2015. Regulation of endoplasmic reticulum turnover by FAM134B-mediated selective autophagy. *Nature*. 522:359–62.
- Kiššova, I., B. Salin, J. Schaeffer, S. Bhatia, S. Manon, and N. Camougrand. 2007. Selective and non-selective autophagic degradation of mitochondria in yeast. *Autophagy*. 3:329–336.
- Kokame, K., K.L. Agarwal, H. Kato, and T. Miyata. 2000. Herp, a new ubiquitin-like membrane protein induced by endoplasmic reticulum stress. *J. Biol. Chem.* 275:32846–32853.
- Kubli, D.A., and Å.B. Gustafsson. 2012. Mitochondria and mitophagy: The yin and yang of cell death control. *Circ. Res.* 111:1208–1221.
- Kuma, A., N. Mizushima, N. Ishihara, and Y. Ohsumi. 2002. Formation of the approximately 350-kDa Apg12-Apg5-Apg16 multimeric complex, mediated by Apg16 oligomerization, is essential for autophagy in yeast. *J. Biol. Chem.* 277:18619–18625.
- Lanoix, J., J. Ouwendijk, C.C. Lin, a Stark, H.D. Love, J. Ostermann, and T. Nilsson. 1999. GTP hydrolysis by arf-1 mediates sorting and concentration of Golgi resident enzymes into functional COP I vesicles. *EMBO J.* 18:4935–48.
- Lanoix, J., J. Ouwendijk, A. Stark, E. Szafer, D. Cassel, K. Dejgaard, and M. Weiss. 2001. Sorting of Golgi resident proteins into different subpopulations of COPI vesicles: a role for ArfGAP1. *J. Cell Biol.* 155:1199–1212.
- Lavieu, G., H. Zheng, and J.E. Rothman. 2013. Stapled Golgi cisternae remain in place as cargo passes through the stack. *Elife*. 2:e00558.
- Lee, B., J. Zhu, N.E. Wolins, J.X. Cheng, and K.K. Buhman. 2009. Differential association of adipophilin and TIP47 proteins with cytoplasmic lipid droplets in mouse enterocytes during dietary fat absorption. *Biochim. Biophys. Acta - Mol. Cell Biol. Lipids*. 1791:1173–1180.
- Lee, J.-S., R. Mendez, H.H. Heng, Z.-Q. Yang, and K. Zhang. 2012. Pharmacological ER stress promotes hepatic lipogenesis and lipid droplet formation. *Am. J. Transl. Res.* 4:102–13.
- Lee, S.A., R. Eyeson, M.L. Cheever, J. Geng, V. V Verkhusha, C. Burd, M. Overduin, and T.G.

- Kutateladze. 2005a. Targeting of the FYVE domain to endosomal membranes is regulated by a histidine switch. *Proc. Natl. Acad. Sci. U. S. A.* 102:13052–13057.
- Lee, S.Y., J.-S. Yang, W. Hong, R.T. Premont, and V.W. Hsu. 2005b. ARFGAP1 plays a central role in coupling COPI cargo sorting with vesicle formation. *J. Cell Biol.* 168:281–90.
- Li, W.W., J. Li, and J.K. Bao. 2012. Microautophagy: Lesser-known self-eating. *Cell. Mol. Life Sci.* 69:1125–1136.
- Liu, Y., R.A. Kahn, and J.H. Prestegard. 2010. Dynamic structure of membrane-anchored Arf\*GTP. *Nat. Struct. Mol. Biol.* 17:876–81.
- Liu, Y., Y. Takahashi, N. Desai, J. Zhang, J.M. Serfass, Y.-G. Shi, C.J. Lynch, and H.-G. Wang. 2016. Bif-1 deficiency impairs lipid homeostasis and causes obesity accompanied by insulin resistance. *Sci. Rep.* 6:20453.
- Long, A.P., A.K. Mannes Schmidt, B. VerBrugge, M.R. Dortch, S.C. Minkin, K.E. Prater, J.P. Biggerstaff, J.R. Dunlap, and P. Dalhaimer. 2012. Lipid droplet de novo formation and fission are linked to the cell cycle in fission yeast. *Traffic.* 13:705–14.
- Losev, E., C. a Reinke, J. Jellen, D.E. Strongin, B.J. Bevis, and B.S. Glick. 2006. Golgi maturation visualized in living yeast. *Nature.* 441:1002–1006.
- Lüllmann-Rauch, R. 2005. History and Morphology of the Lysosome. *In* Lysosomes. Springer US, Boston, MA. 1–16.
- Machado, M., P. Marques-Vidal, and H. Cortez-Pinto. 2006. Hepatic histology in obese patients undergoing bariatric surgery. *J. Hepatol.* 45:600–606.
- Madiyalakan, R., C.F. Piskorz, M.S. Piver, and K.L. Matta. 1987. Serum beta-(1----4)-galactosyltransferase activity with synthetic low molecular weight acceptor in human ovarian cancer. *Eur. J. Cancer Clin. Oncol.* 23:901–906.
- Majeed, W., S. Liu, and B. Storrie. 2014. Distinct Sets of Rab6 Effectors Contribute to ZW10- and COG-Dependent Golgi Homeostasis. *Traffic.* 15:630–647.
- Mally, M., P. Peterlin, and S. Svetina. 2013. Partitioning of Oleic Acid into Phosphatidylcholine

Membranes Is Amplified by Strain. *J. Phys. Chem. B.* 117:12086–12094.

Malsam, J., A. Satoh, L. Pelletier, and G. Warren. 2005. Golgin tethers define subpopulations of COPI vesicles. *Science.* 307:1095–8.

Mancias, J.D., and J. Goldberg. 2008. Structural basis of cargo membrane protein discrimination by the human COPII coat machinery. *EMBO J.* 27:2918–28.

Marcinkiewicz, A., D. Gauthier, A. Garcia, and D.L. Brasaemle. 2006. The phosphorylation of serine 492 of perilipin a directs lipid droplet fragmentation and dispersion. *J. Biol. Chem.* 281:11901–9.

Margariti, A., H. Li, T. Chen, D. Martin, G. Vizcay-Barrena, S. Alam, E. Karamariti, Q. Xiao, A. Zampetaki, Z. Zhang, W. Wang, Z. Jiang, C. Gao, B. Ma, Y.G. Chen, G. Cockerill, Y. Hu, Q. Xu, and L. Zeng. 2013. XBP1 mRNA splicing triggers an autophagic response in endothelial cells through BECLIN-1 transcriptional activation. *J. Biol. Chem.* 288:859–872.

Martin, S., and R.G. Parton. 2006. Lipid droplets: a unified view of a dynamic organelle. *Nat. Rev. Mol. Cell Biol.* 7:373–378.

Martínez-Alonso, E., J. Ballesta, and J.A. Martínez-Menárguez. 2007. Low-temperature-induced Golgi tubules are transient membranes enriched in molecules regulating intra-Golgi transport. *Traffic.* 8:359–368.

Martínez-Alonso, E., G. Egea, J. Ballesta, and J. a Martínez-Menárguez. 2005. Structure and dynamics of the Golgi complex at 15 degrees C: low temperature induces the formation of Golgi-derived tubules. *Traffic.* 6:32–44.

Martinez-Alonso, E., M. Tomas, and J.A. Martinez-Menarguez. 2013. Morpho-functional architecture of the Golgi complex of neuroendocrine cells. *Front. Endocrinol. (Lausanne).* 4:1–12.

Martinez-Lopez, N., M. Garcia-Macia, S. Sahu, F. Cecconi, G.J. Schwartz, R. Singh Correspondence, D. Athonvarangkul, E. Liebling, P. Merlo, and R. Singh. 2016. Autophagy in the CNS and Periphery Coordinate Lipophagy and Lipolysis in the Brown Adipose Tissue and Liver.

- Martinez-Menarguez, J.A., H.J. Geuze, and J. Ballesta. 1996. Identification of two types of beta-COP vesicles in the Golgi complex of rat spermatids. *Eur. J. Cell Biol.* 71:137–143.
- Martínez-Menárguez, J.A., R. Prekeris, V.M.J. Oorschot, R. Scheller, J.W. Slot, H.J. Geuze, and J. Klumperman. 2001. Peri-Golgi vesicles contain retrograde but not anterograde proteins consistent with the cisternal progression model of intra-Golgi transport. *J. Cell Biol.* 155:1213–1224.
- Masuda, M., S. Takeda, M. Sone, T. Ohki, H. Mori, Y. Kamioka, and N. Mochizuki. 2006a. Endophilin BAR domain drives membrane curvature by two newly identified structure-based mechanisms. *EMBO J.* 25:2889–2897.
- Masuda, M., S. Takeda, M. Sone, T. Ohki, H. Mori, Y. Kamioka, and N. Mochizuki. 2006b. Endophilin BAR domain drives membrane curvature by two newly identified structure-based mechanisms. *EMBO J.* 25:2889–2897.
- Matsuura-Tokita, K., M. Takeuchi, A. Ichihara, K. Mikuriya, and A. Nakano. 2006. Live imaging of yeast Golgi cisternal maturation. *Nature.* 441:1007–1010.
- Mayer, N., M. Schweiger, M. Romauch, G.F. Grabner, T.O. Eichmann, E. Fuchs, J. Ivkovic, C. Heier, I. Mrak, A. Lass, G. Höfler, C. Fledelius, R. Zechner, R. Zimmermann, and R. Breinbauer. 2013. Development of small-molecule inhibitors targeting adipose triglyceride lipase. *Nat. Chem. Biol.* 9:785–7.
- McGough, I.J., and P.J. Cullen. 2013. Clathrin is not required for SNX-BAR-retromer-mediated carrier formation. *J. Cell Sci.* 126:45–52.
- McIntosh, A.L., H. Huang, B.P. Atshaves, E. Wellberg, D. V Kuklev, W.L. Smith, A.B. Kier, and F. Schroeder. 2010. Fluorescent n-3 and n-6 very long chain polyunsaturated fatty acids: three-photon imaging in living cells expressing liver fatty acid-binding protein. *J. Biol. Chem.* 285:18693–708.
- Meiblitzer-Ruppitsch, C., M. Vetterlein, H. Stangl, S. Maier, J. Neumüller, M. Freissmuth, M. Pavelka, and A. Ellinger. 2008. Electron microscopic visualization of fluorescent signals in cellular compartments and organelles by means of DAB-photoconversion. *Histochem. Cell Biol.*

130:407–19.

Melkonian, M., B. Becker, and D. Becker. 1991. Scale formation in algae. *J. Electron Microsc. Tech.* 17:165–78.

Mercier, V., M.H. Laporte, O. Destaing, B. Blot, C.M. Blouin, K. Pernet-Gallay, C. Chatellard, Y. Saoudi, C. Albiges-Rizo, C. Lamaze, S. Fraboulet, A. Petiot, and R. Sadoul. 2016. ALG-2 interacting protein-X (Alix) is essential for clathrin-independent endocytosis and signaling. *Sci. Rep.* 6:26986.

Michelsen, K., H. Yuan, and B. Schwappach. 2005. Hide and run. Arginine-based endoplasmic-reticulum-sorting motifs in the assembly of heteromultimeric membrane proteins. *EMBO Rep.* 6:717–22.

Mijaljica, D., M. Prescott, and R.J. Devenish. 2011. Microautophagy in mammalian cells: Revisiting a 40-year-old conundrum. *Autophagy.* 7:673–682.

Millen, J.I., R. Krick, T. Prick, M. Thumm, and D.S. Goldfarb. 2009. Measuring piecemeal microautophagy of the nucleus in *Saccharomyces cerevisiae*. *Autophagy.* 5:75–81.

Miller, D.J., M.B. Macek, and B.D. Shur. 1992. Complementarity between sperm surface beta-1,4-galactosyltransferase and egg-coat ZP3 mediates sperm-egg binding. *Nature.* 357:589–593.

Milosevic, I., S. Giovedi, X. Lou, A. Raimondi, C. Collesi, H. Shen, S. Paradise, E. O’Toole, S. Ferguson, O. Cremona, and P. De Camilli. 2011. Recruitment of endophilin to clathrin-coated pit necks is required for efficient vesicle uncoating after fission. *Neuron.* 72:587–601.

Mironov, A.A., G. V. Beznoussenko, P. Nicoziani, O. Martella, A. Trucco, H.S. Kweon, D. Di Giandomenico, R.S. Polishchuk, A. Fusella, P. Lupetti, E.G. Berger, W.J.C. Geerts, A.J. Koster, K.N.J. Burger, and A. Luini. 2001. Small cargo proteins and large aggregates can traverse the Golgi by a common mechanism without leaving the lumen of cisternae. *J. Cell Biol.* 155:1225–1238.

Mironov, A., G. V. Beznoussenko, A. Trucco, P. Lupetti, J.D. Smith, W.J.C. Geerts, A.J. Koster, K.N.J. Burger, M.E. Martone, T.J. Deerinck, M.H. Ellisman, and A. Luini. 2003. ER-to-Golgi carriers arise through direct en bloc protrusion and multistage maturation of specialized ER exit

domains. *Dev. Cell.* 5:583–594.

Miserey-Lenkei, S., G. Chalancon, S. Bardin, E. Formstecher, B. Goud, and A. Echard. 2010. Rab and actomyosin-dependent fission of transport vesicles at the Golgi complex. *Nat Cell Biol.* 12:645–654.

Mizushima, N., T. Noda, T. Yoshimori, Y. Tanaka, T. Ishii, M.D. George, D.J. Klionsky, M. Ohsumi, and Y. Ohsumi. 1998. A protein conjugation system essential for autophagy. *Nature.* 395:395–398.

Mizushima, N., A. Yamamoto, M. Hatano, Y. Kobayashi, Y. Kabey, K. Suzuki, T. Tokuhi, Y. Ohsumi, and T. Yoshimori. 2001. Dissection of autophagosome formation using Apg5-deficient mouse embryonic stem cells. *J. Cell Biol.* 152:657–667.

Modregger, J., A.A. Schmidt, B. Ritter, W.B. Huttner, and M. Plomann. 2003. Characterization of endophilin B1b, a brain-specific membrane-associated lysophosphatidic acid acyl transferase with properties distinct from endophilin A1. *J. Biol. Chem.* 278:4160–4167.

Monastyrska, I., and D.J. Klionsky. 2006. Autophagy in organelle homeostasis: Peroxisome turnover. *Mol. Aspects Med.* 27:483–494.

Morriswood, B., and G. Warren. 2013. Stalemate in the Golgi Battle. *Science.* 341:1465–1466.

Oprins, A., R. Duden, T.E. Kreis, H.J. Geuze, and J.W. Slot. 1993. b-COP localizes mainly to the cis-Golgi side in exocrine pancreas. *J. Cell Biol.* 121:49–60.

Orci, L., M. Ravazzola, A. Volchuk, T. Engel, M. Gmachl, M. Amherdt, A. Perrelet, T.H. Sollner, and J.E. Rothman. 2000. Anterograde flow of cargo across the golgi stack potentially mediated via bidirectional “percolating” COPI vesicles. *Proc. Natl. Acad. Sci. U. S. A.* 97:10400–5.

Orci, L., M. Starnes, M. Ravazzola, M. Amherdt, A. Perrelet, T.H. Söllner, and J.E. Rothman. 1997. Bidirectional transport by distinct populations of COPI-coated vesicles. *Cell.* 90:335–349.

Osowski, C.M., and F. Urano. 2011. Measuring ER stress and the unfolded protein response using mammalian tissue culture system. *Methods Enzymol.* 490:71–92.

- Otomo, C., Z. Metlagel, G. Takaesu, and T. Otomo. 2013. Structure of the human ATG12~ATG5 conjugate required for LC3 lipidation in autophagy. *Nat. Struct. Mol. Biol.* 20:59–66.
- Otte, S., and C. Barlowe. 2002. The Erv41p-Erv46p complex: Multiple export signals are required in trans for COPII-dependent transport from the ER. *EMBO J.* 21:6095–6104.
- Pankiv, S., E.A. Alemu, A. Brech, J.A. Bruun, T. Lamark, A. Øvervatn, G. Bjørkøy, and T. Johansen. 2010. FYCO1 is a Rab7 effector that binds to LC3 and PI3P to mediate microtubule plus end - Directed vesicle transport. *J. Cell Biol.* 188:253–269.
- Pankiv, S., T.H. Clausen, T. Lamark, A. Brech, J.A. Bruun, H. Outzen, A. Øvervatn, G. Bjørkøy, and T. Johansen. 2007. p62/SQSTM1 binds directly to Atg8/LC3 to facilitate degradation of ubiquitinated protein aggregates by autophagy\*[S]. *J. Biol. Chem.* 282:24131–24145.
- Park, S.-Y., J.-S. Yang, A.B. Schmider, R.J. Soberman, and V.W. Hsu. 2015. Coordinated regulation of bidirectional COPI transport at the Golgi by CDC42. *Nature.* 521:529–32.
- Patterson, G.H., K. Hirschberg, R.S. Polishchuk, D. Gerlich, R.D. Phair, and J. Lippincott-Schwartz. 2008. Transport through the Golgi apparatus by rapid partitioning within a two-phase membrane system. *Cell.* 133:1055–67.
- Pecot, M.Y., and V. Malhotra. 2006. The Golgi apparatus maintains its organization independent of the endoplasmic reticulum. *Mol. Biol. Cell.* 17:5372–80.
- Peipp, M., D. Saul, K. Barbin, J. Bruenke, S.J. Zunino, M. Niederweis, and G.H. Fey. 2004. Efficient eukaryotic expression of fluorescent scFv fusion proteins directed against CD antigens for FACS applications. *J. Immunol. Methods.* 285:265–280.
- Pelham, H.R., and J.E. Rothman. 2000. The debate about transport in the Golgi--two sides of the same coin? *Cell.* 102:713–719.
- Ploegh, H.L. 2007. A lipid-based model for the creation of an escape hatch from the endoplasmic reticulum. *Nature.* 448:435–438.
- Popoff, V., F. Adolf, B. Brügger, and F. Wieland. 2011. COPI budding within the Golgi stack.

*Cold Spring Harb. Perspect. Biol.* 3:a005231.

Popoff, V., G.A. Mardones, D. Tenza, R. Rojas, C. Lamaze, J.S. Bonifacino, G. Raposo, and L. Johannes. 2007. The retromer complex and clathrin define an early endosomal retrograde exit site. *J. Cell Sci.* 120.

Popovic, D., M. Akutsu, I. Novak, J.W. Harper, C. Behrends, and I. Dikic. 2012. Rab GTPase-activating proteins in autophagy: regulation of endocytic and autophagy pathways by direct binding to human ATG8 modifiers. *Mol. Cell. Biol.* 32:1733–44.

Popovic, D., and I. Dikic. 2014. TBC1D5 and the AP2 complex regulate ATG9 trafficking and initiation of autophagy. *EMBO Rep.* 15:392–401.

Presley, J.F., N.B. Cole, T. a Schroer, K. Hirschberg, K.J. Zaal, and J. Lippincott-Schwartz. 1997. ER-to-Golgi transport visualized in living cells. *Nature.* 389:81–85.

Presley, J.F., T.H. Ward, A.C. Pfeifer, E.D. Siggia, R.D. Phair, and J. Lippincott-Schwartz. 2002. Dissection of COPI and Arf1 dynamics in vivo and role in Golgi membrane transport. *Nature.* 417:187–93.

Pu, J., C. Schindler, R. Jia, M. Jarnik, P. Backlund, and J.S. Bonifacino. 2015. BORC, a Multisubunit Complex that Regulates Lysosome Positioning. *Dev. Cell.* 33:176–188.

Raposo, G., and W. Stoorvogel. 2013. Extracellular vesicles: Exosomes, microvesicles, and friends. *J. Cell Biol.* 200.

Renard, H.-F., M. Simunovic, J. Lemière, E. Boucrot, M.D. Garcia-Castillo, S. Arumugam, V. Chambon, C. Lamaze, C. Wunder, A.K. Kenworthy, A. a. Schmidt, H.T. McMahon, C. Sykes, P. Bassereau, and L. Johannes. 2015. Endophilin-A2 functions in membrane scission in clathrin-independent endocytosis. *Nature.* 517:493–6.

van Rijnsoever, C., V. Oorschot, and J. Klumperman. 2008. Correlative light-electron microscopy (CLEM) combining live-cell imaging and immunolabeling of ultrathin cryosections. *Nat. Methods.* 5:973–80.

Ringstad, N., H. Gad, P. Löw, G. Di Paolo, L. Brodin, O. Shupliakov, and P. De Camilli. 1999.

Endophilin/sh3p4 is required for the transition from early to late stages in clathrin-mediated synaptic vesicle endocytosis. *Neuron*. 24:143–154.

Rizzo, R., S. Parashuraman, P. Mirabelli, C. Puri, J. Lucocq, and A. Luini. 2013. The dynamics of engineered resident proteins in the mammalian Golgi complex relies on cisternal maturation. *J. Cell Biol.* 201:1027–1036.

Robenek, H., S. Lorkowski, M. Schnoor, and D. Troyer. 2005. Spatial integration of TIP47 and adipophilin in macrophage lipid bodies. *J. Biol. Chem.* 280:5789–5794.

Rollins, C.T., V.M. Rivera, D.N. Woolfson, T. Keenan, M. Hatada, S.E. Adams, L.J. Andrade, D. Yaeger, M.R. van Schravendijk, D.A. Holt, M. Gilman, and T. Clackson. 2000. A ligand-reversible dimerization system for controlling protein-protein interactions. *Proc. Natl. Acad. Sci. U. S. A.* 97:7096–101.

Ross, J.A., Y. Chen, J. Müller, B. Barylko, L. Wang, H.B. Banks, J.P. Albanesi, and D.M. Jameson. 2011. Dimeric endophilin A2 stimulates assembly and GTPase activity of dynamin 2. *Biophys. J.* 100:729–737.

Rostovtseva, T.K., H. Boukari, A. Antignani, B. Shiu, S. Banerjee, A. Neutzner, and R.J. Youle. 2009. Bax activates endophilin B1 oligomerization and lipid membrane vesiculation. *J. Biol. Chem.* 284:34390–34399.

Röttger, S., J. White, H.H. Wandall, J.C. Olivo, A. Stark, E.P. Bennett, C. Whitehouse, E.G. Berger, H. Clausen, and T. Nilsson. 1998. Localization of three human polypeptide GalNAc-transferases in HeLa cells suggests initiation of O-linked glycosylation throughout the Golgi apparatus. *J. Cell Sci.* 111 ( Pt 1:45–60.

Roux, K.J., D.I. Kim, and B. Burke. 2013. BioID: A screen for protein-protein interactions. *Curr. Protoc. Protein Sci.* 1–14.

Roux, K.J., D.I. Kim, M. Raida, and B. Burke. 2012. A promiscuous biotin ligase fusion protein identifies proximal and interacting proteins in mammalian cells. *J. Cell Biol.* 196:801–810.

Sahu-Osen, A., G. Montero-Moran, M. Schittmayer, K. Fritz, A. Dinh, Y.-F. Chang, D. McMahon, A. Boeszoermyeni, I. Cornaciu, D. Russell, M. Oberer, G.M. Carman, R. Birner-

- Gruenberger, and D.L. Brasaemle. 2015. CGI-58/ABHD5 is phosphorylated on Ser239 by protein kinase A: control of subcellular localization. *J. Lipid Res.* 56:109–21.
- Samali, A., U. FitzGerald, S. Deegan, and S. Gupta. 2010. Methods for Monitoring Endoplasmic Reticulum Stress and the Unfolded Protein Response. *Int. J. Cell Biol.* 2010:1–11.
- Schaub, B.E., B. Berger, E.G. Berger, and J. Rohrer. 2006. Transition of Galactosyltransferase 1 from Trans-Golgi Cisterna to the Trans-Golgi Network Is Signal Mediated. 17:5153–5162.
- Schlager, S., M. Goeritzer, K. Jandl, R. Frei, N. Vujic, D. Kolb, H. Strohmaier, J. Dorow, T.O. Eichmann, A. Rosenberger, A. Wölfler, A. Lass, E.E. Kershaw, U. Ceglarek, A. Dichlberger, A. Heinemann, and D. Kratky. 2015. Adipose triglyceride lipase acts on neutrophil lipid droplets to regulate substrate availability for lipid mediator synthesis. *J. Leukoc. Biol.* 206:69–78.
- Schmitz, K.R., J. Liu, S. Li, T.G. Setty, C.S. Wood, C.G. Burd, and K.M. Ferguson. 2008. Golgi Localization of Glycosyltransferases Requires a Vps74p Oligomer. *Dev. Cell.* 14:523–534.
- Schröder, B., C. Wrocklage, C. Pan, R. Jäger, B. Kösters, H. Schäfer, H.P. Elsässer, M. Mann, and A. Hasilik. 2007. Integral and associated lysosomal membrane proteins. *Traffic.* 8:1676–1686.
- Schroeder, B., R.J. Schulze, S.G. Weller, A.C. Sletten, C.A. Casey, and M.A. Mcniven. 2015. The Small GTPase Rab7 as a Central Regulator of Hepatocellular Lipophagy. *Hepatology.* 61:1896–1907.
- Schuske, K.R., J.E. Richmond, D.S. Matthies, W.S. Davis, S. Runz, D.A. Rube, A.M. Van Der Blik, and E.M. Jorgensen. 2003. Endophilin is required for synaptic vesicle endocytosis by localizing synaptojanin. *Neuron.* 40:749–762.
- Schweizer, A., J.A. Fransen, K. Matter, T.E. Kreis, L. Ginsel, and H.P. Hauri. 1990. Identification of an intermediate compartment involved in protein transport from endoplasmic reticulum to Golgi apparatus. *Eur J Cell Biol.* 53:185–196.
- Seino, J., L. Wang, Y. Harada, C. Huang, K. Ishii, N. Mizushima, and T. Suzuki. 2013. Basal autophagy is required for the efficient catabolism of sialyloligosaccharides. *J. Biol. Chem.* 288:26898–26907.

Semenza, J.C., K.G. Hardwick, N. Dean, and H.R.B. Pelham. 1990. ERD2, a yeast gene required for the receptor-mediated retrieval of luminal ER proteins from the secretory pathway. *Cell*. 61:1349–1357.

Sengupta, P., P. Satpute-Krishnan, A.Y. Seo, D.T. Burnette, G.H. Patterson, and J. Lippincott-Schwartz. 2015. ER trapping reveals Golgi enzymes continually revisit the ER through a recycling pathway that controls Golgi organization. *Proc. Natl. Acad. Sci. U. S. A.* E6752–E6761.

Serafini, T., L. Orci, M. Amherdt, M. Brunner, R.A. Kahn, and J.E. Rothman. 1991. ADP-ribosylation factor is a subunit of the coat of Golgi-derived COP-coated vesicles: A novel role for a GTP-binding protein. *Cell*. 67:239–253.

Setty, S.R.G., D. Tenza, S.T. Truschel, E. Chou, E. V Sviderskaya, A.C. Theos, M.L. Lamoreux, S.M. Di Pietro, M. Starcevic, D.C. Bennett, E.C. Dell’Angelica, G. Raposo, and M.S. Marks. 2007. BLOC-1 is required for cargo-specific sorting from vacuolar early endosomes toward lysosome-related organelles. *Mol. Biol. Cell*. 18:768–80.

Shaikh, S.R. 2012. Biophysical and biochemical mechanisms by which dietary N-3 polyunsaturated fatty acids from fish oil disrupt membrane lipid rafts☆. *J. Nutr. Biochem*. 23:101–105.

Shintani, T., N. Mizushima, Y. Ogawa, A. Matsuura, T. Noda, and Y. Ohsumi. 1999. Apg10p, a novel protein-conjugating enzyme essential for autophagy in yeast. *EMBO J*. 18:5234–5241.

Shubeita, G.T., S.L. Tran, J. Xu, M. Vershinin, S. Cermelli, S.L. Cotton, M.A. Welte, and S.P. Gross. 2008. Consequences of Motor Copy Number on the Intracellular Transport of Kinesin-1-Driven Lipid Droplets. *Cell*. 135:1098–1107.

Singh, R., S. Kaushik, Y. Wang, Y. Xiang, I. Novak, M. Komatsu, K. Tanaka, A.M. Cuervo, and M.J. Czaja. 2009. Autophagy regulates lipid metabolism. *Nature*.

Smith, R.D., R. Willett, T. Kudlyk, I. Pokrovskaya, A.W. Paton, J.C. Paton, and V. V. Lupashin. 2009. The COG complex, Rab6 and COPI define a novel golgi retrograde trafficking pathway that is exploited by SubAB toxin. *Traffic*. 10:1502–1517.

Söllner, T., M.K. Bennett, S.W. Whiteheart, R.H. Scheller, J.E. Rothman, T. Soellner, M.K.

- Bennett, S.W. Whiteheart, R.H. Scheller, and J.E. Rothman. 1993. A Protein Assembly-Disassembly Pathway In Vitro That May Correspond to Sequential Steps of Synaptic Vesicle Docking, Activation, and Fusion. *Cell*. 75:409–418.
- Soni, K.G., G. a Mardones, R. Sougrat, E. Smirnova, C.L. Jackson, and J.S. Bonifacino. 2009. Coatamer-dependent protein delivery to lipid droplets. *J. Cell Sci.* 122:1834–1841.
- Spiegelhalter, C., V. Tosch, D. Hentsch, M. Koch, P. Kessler, Y. Schwab, and J. Laporte. 2010. From Dynamic Live Cell Imaging to 3D Ultrastructure: Novel Integrated Methods for High Pressure Freezing and Correlative Light-Electron Microscopy. *PLoS One*. 5:12.
- Stanley, P. 2011. Golgi glycosylation. *Cold Spring Harb. Perspect. Biol.* 3:1–13.
- Steffgen, K., K. Dufraux, and H. Hathaway. 2002. Enhanced branching morphogenesis in mammary glands of mice lacking cell surface beta1,4-galactosyltransferase. *Dev. Biol.* 244:114–33.
- Sundborger, A., C. Soderblom, O. Vorontsova, E. Evergren, J.E. Hinshaw, and O. Shupliakov. 2011. An endophilin-dynamin complex promotes budding of clathrin-coated vesicles during synaptic vesicle recycling. *J. Cell Sci.* 124:133–143.
- Suzuki, M., Y. Ohsaki, T. Tatematsu, Y. Shinohara, T. Maeda, J. Cheng, and T. Fujimoto. 2012. Translation inhibitors induce formation of cholesterol ester-rich lipid droplets. *PLoS One*. 7:e42379.
- Takahashi, Y., D. Coppola, N. Matsushita, H.D. Cualing, M. Sun, Y. Sato, C. Liang, J.U. Jung, J.Q. Cheng, J.J. Mulé, W.J. Pledger, and H.-G. Wang. 2007. Bif-1 interacts with Beclin 1 through UVRAG and regulates autophagy and tumorigenesis. *Nat. Cell Biol.* 9:1142–1151.
- Takahashi, Y., C.L. Meyerkord, T. Hori, K. Runkle, T.E. Fox, M. Kester, T.P. Loughran, and H.G. Wang. 2011. Bif-1 regulates Atg9 trafficking by mediating the fission of Golgi membranes during autophagy. *Autophagy*. 7:61–73.
- Takahashi, Y., C.L. Meyerkord, and H.-G. Wang. 2009. Bif-1/endophilin B1: a candidate for crescent driving force in autophagy. *Cell Death Differ.* 16:947–955.

- Tanida, I., N. Mizushima, M. Kiyooka, M. Ohsumi, T. Ueno, Y. Ohsumi, and E. Kominami. 1999. Apg7p/Cvt2p: A novel protein-activating enzyme essential for autophagy. *Mol Biol Cell*. 10:1367–1379.
- Tanigawa, G., L. Orci, M. Amherdt, M. Ravazzola, J.B. Helms, and J.E. Rothman. 1993. Hydrolysis of bound GTP by ARF protein triggers uncoating of golgi-derived COP-coated vesicles. *J. Cell Biol.* 123:1365–1371.
- Thiele, C., and J. Spandl. 2008. Cell biology of lipid droplets. *Curr. Opin. Cell Biol.* 20:378–385.
- Trahey, M., and J.C. Hay. 2010. Transport vesicle uncoating: it's later than you think. *F1000 Biol. Rep.* 6:1–6.
- Tu, L., W.C.S. Tai, L. Chen, and D.K. Banfield. 2008. Signal-mediated dynamic retention of glycosyltransferases in the Golgi. *Science*. 321:404–407.
- Velikkakath, a. K.G., T. Nishimura, E. Oita, N. Ishihara, and N. Mizushima. 2012. Mammalian Atg2 proteins are essential for autophagosome formation and important for regulation of size and distribution of lipid droplets. *Mol. Biol. Cell*. 23:896–909.
- Verstreken, P., O. Kjaerulff, T.E. Lloyd, R. Atkinson, Y. Zhou, I.A. Meinertzhagen, and H.J. Bellen. 2002. Endophilin mutations block clathrin-mediated endocytosis but not neurotransmitter release. *Cell*. 109:101–112.
- Villarroya-Beltri, C., C. Gutiérrez-Vázquez, F. Sánchez-Cabo, D. Pérez-Hernández, J. Vázquez, N. Martín-Cofreces, D.J. Martínez-Herrera, A. Pascual-Montano, M. Mittelbrunn, and F. Sánchez-Madrid. 2013. Sumoylated hnRNPA2B1 controls the sorting of miRNAs into exosomes through binding to specific motifs. *Nat. Commun.* 4:2980.
- Volpicelli-Daley, L.A., Y. Li, C.-J. Zhang, and R.A. Kahn. 2005. Isoform-selective effects of the depletion of ADP-ribosylation factors 1-5 on membrane traffic. *Mol. Biol. Cell*. 16:4495–508.
- Walther, T.C., R. V Farese, and Jr. 2012. Lipid droplets and cellular lipid metabolism. *Annu. Rev. Biochem.* 81:687–714.
- Wang, D.B., T. Uo, C. Kinoshita, B.L. Sopher, R.J. Lee, S.P. Murphy, Y. Kinoshita, G. a Garden,

H.-G. Wang, and R.S. Morrison. 2014. Bax interacting factor-1 promotes survival and mitochondrial elongation in neurons. *J. Neurosci.* 34:2674–83.

Wang, H., M. Bell, U. Sreenevasan, H. Hu, J. Liu, K. Dalen, C. Londos, T. Yamaguchi, M.A. Rizzo, R. Coleman, D. Gong, D. Brasaemle, and C. Sztalryd. 2011. Unique regulation of adipose triglyceride lipase (ATGL) by perilipin 5, a lipid droplet-associated protein. *J. Biol. Chem.* 286:15707–15715.

Waters, M.G., T. Serafini, and J.E. Rothman. 1991. “Coatomer”: a cytosolic protein complex containing subunits of non-clathrin-coated Golgi transport vesicles. *Nature.* 349:248–251.

Watzel, G., R. Bachofner, and E.G. Berger. 1991. Immunocytochemical localization of the Golgi apparatus using protein-specific antibodies to galactosyltransferase. *Eur. J. Cell Biol.* 56:451–458.

Webber, J.L., A.R.J. Young, and S.A. Tooze. 2007. Atg9 trafficking in mammalian cells. *Autophagy.* 3:54–56.

Weering, J.R.T. Van, E. Brown, T.H. Sharp, J. Mantell, P.J. Cullen, and P. Verkade. 2010. Intracellular Membrane Traffic at High Resolution. Elsevier Inc. 619-648 pp.

White, J., L. Johannes, F. Mallard, A. Girod, S. Grill, S. Reinsch, P. Keller, B. Tzschaschel, A. Echard, B. Goud, and E.H.K. Stelzer. 1999. Rab6 coordinates a novel Golgi to ER retrograde transport pathway in live cells. *J. Cell Biol.* 147:743–759.

Yang, J.-S., H. Gad, S.Y. Lee, A. Mironov, L. Zhang, G. V Beznoussenko, C. Valente, G. Turacchio, A.N. Bonsra, G. Du, G. Baldanzi, A. Graziani, S. Bourgoïn, M.A. Frohman, A. Luini, and V.W. Hsu. 2008. A role for phosphatidic acid in COPI vesicle fission yields insights into Golgi maintenance. *Nat. Cell Biol.* 10:1146–53.

Yang, J.-S., S.Y. Lee, S. Spanò, H. Gad, L. Zhang, Z. Nie, M. Bonazzi, D. Corda, A. Luini, and V.W. Hsu. 2005. A role for BARS at the fission step of COPI vesicle formation from Golgi membrane. *EMBO J.* 24:4133–43.

Yang, J.-S., L. Zhang, S.Y. Lee, H. Gad, A. Luini, and V.W. Hsu. 2006. Key components of the fission machinery are interchangeable. *Nat. Cell Biol.* 8:1376–1382.

Zagani, R., W. El-Assaad, I. Gamache, and J.G. Teodoro. 2015. Inhibition of adipose triglyceride lipase (ATGL) by the putative tumor suppressor G0S2 or a small molecule inhibitor attenuates the growth of cancer cells. *Oncotarget*. 6:28282–95.

Zerangue, N., M.J. Malan, S.R. Fried, P.F. Dazin, Y.N. Jan, L.Y. Jan, and B. Schwappach. 2001. Analysis of endoplasmic reticulum trafficking signals by combinatorial screening in mammalian cells. *Proc. Natl. Acad. Sci. U. S. A.* 98:2431–6.

Zhang, C., G. Wang, Z. Zheng, K.R. Maddipati, X. Zhang, G. Dyson, P. Williams, S.A. Duncan, R.J. Kaufman, and K. Zhang. 2012. Endoplasmic reticulum-tethered transcription factor cAMP responsive element-binding protein, hepatocyte specific, regulates hepatic lipogenesis, fatty acid oxidation, and lipolysis upon metabolic stress in mice. *Hepatology*. 55:1070–1082.

Zhu, X., J. Jiang, H. Shen, H. Wang, H. Zong, Z. Li, Y. Yang, Z. Niu, W. Liu, X. Chen, Y. Hu, and J. Gu. 2005. Elevated beta-1,4-galactosyltransferase I in highly metastatic human lung cancer cells: Identification of E1AF as important transcription activator. *J. Biol. Chem.* 280:12503–12516.

van Zutphen, T., V. Todde, R. de Boer, M. Kreim, H.F. Hofbauer, H. Wolinski, M. Veenhuis, I.J. van der Klei, and S.D. Kohlwein. 2014. Lipid droplet autophagy in the yeast *Saccharomyces cerevisiae*. *Mol. Biol. Cell*. 25:290–301.